MEDITERRANEAN ACTION PLAN
MED POL

UNITED NATIONS ENVIRONMENT PROGRAMME

CLIMATIC RESEARCH UNIT, SCHOOL OF ENVIRONMENTAL SCIENCES
UNIVERSITY OF EAST ANGLIA

REGIONAL CHANGES IN CLIMATE IN THE MEDITERRANEAN BASIN DUE TO GLOBAL GREENHOUSE GAS WARMING

J.P. Palutikof, X. Guo, T.M.L. Wigley and J.M. Gregory

Climatic Research Unit
School of Environmental Sciences
University of East Anglia
Norwich NR4 7TJ, U.K.

MAP Technical Reports Series No. 66

UNEP
Athens, 1992

The preparation of this document has been commissioned by the United Nations Environment Programme (UNEP) under project FP/5101-88-01 (2862). The designations employed and the presentation of the material in this document do not imply the expression of any opinion whatsoever on the part of UNEP concerning the legal status of any State, Territory, city or area, or of its authorities, or concerning the delimitation of their frontiers or boundaries. The document contains the views expressed by the Climatic Research Unit of the University of East Anglia and may not necessarily reflect the views of UNEP.

For bibliographic purposes this volume may be cited as:

J.P. Palutikof, X. Guo, T.M.L. Wigley and J.M. Gregory: Regional Changes in Climate in the Mediterranean Basin due to Global Greenhouse Gas Warming. MAP Technical Reports Series No. 66, UNEP, Athens, 1992.

Pour des fins bibliographiques, citer le présent volume comme suit:

J.P. Palutikof, X. Guo, T.M.L. Wigley et J.M. Gregory: Modifications régionales du climat dans le bassin méditerranéen résultant du réchauffement global dû aux gaz à effet de serre. MAP Technical Reports Series No. 66, UNEP, Athens, 1992.

MEDITERRANEAN ACTION PLAN
MED POL

UNITED NATIONS ENVIRONMENT PROGRAMME

CLIMATIC RESEARCH UNIT, SCHOOL OF ENVIRONMENTAL SCIENCES
UNIVERSITY OF EAST ANGLIA

REGIONAL CHANGES IN CLIMATE IN THE MEDITERRANEAN BASIN DUE TO GLOBAL GREENHOUSE GAS WARMING

J.P. Palutikof, X. Guo, T.M.L. Wigley and J.M. Gregory

Climatic Research Unit
School of Environmental Sciences
University of East Anglia
Norwich NR4 7TJ, U.K.

MAP Technical Reports Series No. 66

UNEP
Athens, 1992

This volume is the sixty-sixth issue of the Mediterranean Action Plan Technical Report Series.

This series contains selected reports resulting from the various activities performed within the framework of the components of the Mediterranean Action Plan: Pollution Monitoring and Research Programme (MED POL), Blue Plan, Priority Actions Programme, Specially Protected Areas and Regional Marine Pollution Emergency Response Centre for the Mediterranean Sea.

PREFACE

To assess the environmental problems associated with the potential impact of expected climatic changes on the marine environment and on adjacent coastal areas and to identify suitable policy options and response measures which may mitigate the negative consequences of the expected impacts, the Oceans and Coastal Areas Programme Activity Centre (OCA/PAC) of the United Nations Environment Programme (UNEP), in cooperation with the Intergovernmental Oceanographic Commission (IOC) and several other intergovernmental and non-governmental organisations, launched, co-ordinated and financially supported number of activities, including establishment of regional task teams. By 1990 task teams were established for nine regions covered by UNEP Regional Seas Programme (Mediterranean, Caribbean, South Pacific, East Asian Seas, South Asian Seas, Southeast Pacific, West and Central Africa, Eastern Africa and Kuwait Action Plan Regions). The two initial objectives of the task teams were to prepare regional overviews and site specific case studies on the possible impact of predicted climate change on the ecologic systems as well as on the socio-economic structures and activities of their respective regions, and to assist governments in the identification and implementation of suitable policy options and response measures which may mitigate the negative consequences of the impact. The regional studies were intended to cover the marine environment and adjacent coastal areas influenced by or influencing the marine environment.

The dominant factor in determining changes of climate around the world over the next 50-100 years is expected to be a global warming caused by increasing concentrations of carbon dioxide (CO_2) and other trace gases (e.g. methane (CH_4), nitrous oxide (N_2O), ozone (O_3) and chlorofluorocarbons (CFCs)) in the atmosphere due to human activities. The so-called greenhouse effect exercised by these trace gases is likely to cause increases in global-mean temperature on time scales of decades to centuries, with associated changes in climate in all regions of the world.

The matter of climate change was the main topic of the Second World Climate Conference (Geneva, 1990). The Conference agreed that the international consensus of scientific understanding of climate change points out that without actions to reduce emissions, global warming is predicted to reach 2 to 5 °C over the next century, a rate of change unprecedented in the past 10,000 years. The warming is expected to be accompanied by a sea level rise of 65 ± 35 cm by the end of the next century. There remain uncertainties in the predictions, particularly in regard to the timing, magnitude and regional patterns of climate change.

Changes in climate variables such as precipitation, evaporation, wind patterns and cloudiness will necessarily accompany the above-mentioned changes in the global mean temperature. These changes, however, will differ noticeably from region to region. For assessing regional environmental impacts of climatic changes, global mean values are mainly

of academic interest. Instead, regional scale (or smaller) details of future changes are required not only for temperature but for a variety of climate variables. The present document provides a method for predicting which smaller regional changes in climate variables would occur in the Mediterranean Basin due to global warming and gives results of such predictions. These regional changes in climate may later be used for assessments of likely environmental impacts.

The most important method available today for obtaining information on possible future climates is based on the use of atmospheric General Circulation Models (GCMs). The large-scale GCM results can, for example, be accepted with some confidence as predictions of future climates.

However, for the purpose of predicting future changes in climatic variables at a smaller regional scale, the presently available GCMs have considerable deficiencies basically due to their coarse resolution and highly smoothed orography, in fact they are for these reasons, quite limited in their ability to predict changes in small-scale meteorological variables.

This resolution problem of the GCMs is particularly important in the Mediterranean basin where many of the characteristic features of climate are controlled by meteorological and geographical factors which are of a scale considerably smaller than the grid used in the GCMs. Even with improved-resolution GCMs, it is unlikely that these models will be able to capture the details of climate change in the Mediterranean basin with any fidelity for many years. It is therefore necessary to develop methods of providing smaller scale information from the relatively coarse-resolution output of the present GCMs.

The aim of this project was to apply a statistical approach to establishing the interrelationship between the smaller and the larger scale. By developing regression relationships between local climatic and atmospheric circulation variables in the Mediterranean basin on the one hand and larger-scale general circulation variables on the other, and by using these regressions with current GCMs, the details of possible future climatic conditions were examined.

SUMMARY

One of the most pressing requirements with regard to research into the enhanced greenhouse effect is the need for regional scenarios of climate change. Only on this basis can plans be made to adapt to or ameliorate the effects of the predicted changes. This report presents the results of a two-year study to develop scenarios of future climate change in the Mediterranean Basin. It falls into three sections.

Regional Scenarios of Climate Change

Regional scenarios of mean climate change in the Mediterranean Basin have been developed from the equilibrium response predictions of four General Circulation Models (GCMs). Two methods of construction are used. In the first (Chapter 3), scenarios of the change in temperature, precipitation and mean sea level pressure are produced directly from GCM grid-point output. One problem with this type of scenario is the coarse resolution of the underlying model grid. The GCMs used here have a spatial resolution of several hundreds of kilometres, which is inadequate for many regional climate change studies, especially in areas of high relief. Therefore a second set of sub-grid-scale scenarios (for temperature and precipitation) are presented (Chapter 4), based on the statistical relationship between large-scale climate data and small-scale observations from surface meteorological stations. For both construction methods, the results from the four models are synthesized to produce a single scenario for each climate variable, and are expressed as the change per °C global mean temperature change.

Model Validation

For each GCM simulation of the greenhouse effect, two model runs are performed: the control run and the perturbed run. One useful test of model performance is to compare the results from the control run with present-day climate. This procedure is known as model validation.

The perturbed-run predictions of a model which fails to reproduce adequately the principal features of the present-day circulation and climate must be regarded as less reliable than the predictions of a model which reproduces the present-day climate well. The results from the validation of the performance over the Mediterranean Basin of the four GCMs used in this study are presented in Chapter 2.

Precipitation Extremes

In an area such as the Mediterranean Basin, prone to droughts and floods, it is important to understand how the frequency and severity of precipitation extremes is likely to change because of the enhanced greenhouse effect. GCMs do not produce such information in a form convenient for analysis. It is therefore necessary to adopt an alternative approach to the problem.

In Chapter 5 we present the results of a statistical analysis of precipitation extremes, based on Markov Chain theory. On the basis of this analysis, estimates of the frequency and severity of precipitation extremes in a high greenhouse gas world are obtained.

TABLE OF CONTENTS

LIST OF FIGURES

LIST OF TABLES

ACKNOWLEDGEMENTS

We would like to thank the Meteorological Departments of the following countries for their assistance in obtaining the temperature and precipitation data used for the construction of the sub-grid-scale scenarios presented in this Report:

Algeria
Cyprus
Egypt
France
Greece
Italy
Jordan
Lebanon
Libya
Malta
Morocco
Saudi Arabia
Spain
Syria
Tunisia
Turkey
Yugoslavia

Without their assistance, and that of colleagues in many different countries, this Report could not have been completed. Our thanks to all of them.

CHAPTER 1

INTRODUCTION

In this Report we present the results of a two-year study of potential climate change due to the enhanced greenhouse effect over the Mediterranean Basin. This region is vulnerable to climate change, particularly through changes in rainfall and soil moisture and their impacts on agriculture and domestic and industrial water supply.

1.1 THE PRESENT-DAY CLIMATE OF THE MEDITERRANEAN

In the Köppen classification, a Mediterranean climate is defined as one in which winter rainfall is at least three times the summer rainfall. This is true of almost the whole of the area studied in this Report. Indeed, over much of the Mediterranean, summer rainfall is virtually zero. This strong summer-winter rainfall contrast is echoed by a pronounced seasonal cycle in almost all climate variables.

In July, August and September the region experiences warm, dry conditions linked to the presence of a strong high-pressure ridge extending eastwards from the Azores subtropical anticyclone. Over Egypt, this ridge is displaced southward by a trough extending northwest from the Arabian Gulf towards Greece, which is associated with the Indian summer monsoon trough.

The rainy season commences in mid-October. At this time, the average upper westerlies change from a three-wave to a four-wave pattern on the five-day time scale (Chang, 1972). A trough in this wave pattern is located over Europe, although the exact position is highly variable. Winter is characterized by cyclonic disturbances and low mean pressure in the Mediterranean, with higher pressure to the east associated with the Siberian high. The rainy season continues until around the end of April. However, from the time of the equinox the major features of the upper

circulation move northwards in response to the passage of the Sun. By May, the polar front and the associated strong upper-air westerly flow are sufficiently far north that their influence is removed. The subtropical highs and their associated ridges once more exert their influence and the rainy season ends.

Precipitation is caused mainly by cyclonic disturbances that originate in the Mediterranean Basin. Local orographic effects also play an important role. Very few surface cyclones can be traced back to a source in the Atlantic Ocean. There are four preferred points of origin within the Basin itself, three of which spawn rain-producing depressions. Of these, the most important is the Gulf of Genoa, where depressions form in the lee of the Alps. In the eastern Mediterranean, the preferential locations for the formation of depressions are to the south of Greece and over Cyprus. Atlas Mountain lee depressions, which form in the spring, are seldom associated with rainfall. Rather they are accompanied by hot, dry and windy conditions, particularly when they track eastwards across North Africa into Egypt.

The movement of depressions is not well understood. In the western Mediterranean, depressions are frequently steered along the Mediterranean Front, formed when cold continental air moves over a warmer sea surface. This front is most pronounced in the spring. Fronts formed in the Eastern Mediterranean tend to follow a preferred path either to the northeast or the east.

1.2 CLIMATIC CHANGE OVER THE MEDITERRANEAN BASIN

The Intergovernmental Panel on Climate Change (IPCC) made a special study of Southern Europe and Turkey (35°-50°N and 10°W-45°E). They predicted climate changes over the region as a whole, due to the global warming expected by the year 2030. These results indicate a warming of

about 2°C in winter and 2-3°C in summer. They suggest a small increase in precipitation in winter, but a decrease of 5-15% in summer. Summer soil moisture was predicted to decrease by 15-25% (Mitchell et al., 1990, Table 5.1). IPCC notes that there are large uncertainties associated with these predictions. Because of this, the term "scenario" is often used instead of "prediction".

The problem with the type of prediction presented by the IPCC is that the results are generalized for the whole of the region; yet we know that climate, particularly the spatially-sensitive parameters such as precipitation, varies over distances much smaller than this. Clearly, we must expect climate change to vary over scales smaller than that of the whole of southern Europe and Turkey. In this Report, we present regional scenarios of climate change due to the enhanced greenhouse effect.

1.3 GENERAL CIRCULATION MODELS

The study by the IPCC was based on the results from General Circulation Models (GCMs). These are complex, computer-based models of the atmospheric circulation which have been developed by climatologists from numerical meteorological forecasting models. The standard approach is to run the model with a nominal "pre-industrial" atmospheric CO_2 concentration (the control run) and then to rerun the model with doubled (or sometimes quadrupled) CO_2 (the perturbed run). In both, the models are allowed to reach equilibrium before the results are recorded. This type of model application is therefore known as an equilibrium response prediction (see Cubasch and Cess, 1990, for a review of equilibrium GCM experiments). The results from these types of experiment were used in the IPCC study of the Mediterranean Basin.

For any given CO_2 level, the actual change will lag behind the corresponding equilibrium change for that CO_2 level. However, the pattern

of actual change (at least as a first approximation) will be similar to the equilibrium pattern (scaled down by an appropriate factor. The predicted regional patterns of equilibrium climate change do differ from those that occur if time-dependent predictions are made, where the CO^2 concentration increases gradually through the perturbed run and where the oceans are modelled using ocean GCMs. This is because equilibrium model runs ignore important oceanic processes, not least ocean current changes, differential thermal inertia effects between different parts of the oceans and between land and ocean, and changes in the oceanic thermohaline circulation. However, the differences are relatively small in most regions (and in the Mediterranean Basin in particular), and the complexity of the problem in relation to present-day computing capability casts some doubt on the reliability of these early transient response results. The present study restricts itself, therefore, to the use of results from equilibrium GCM experiments.

Mitchell et al. (1990) present three justifications for equilibrium experiments, which are:

i. they are parsimonious of computer time;

ii. they are easier to compare than time-dependent experiments; and,

iii. apart from areas where the ocean thermal inertia is large, such as the North Atlantic and high southern latitudes, their results can be scaled and used as approximations to the time-dependent response.

This latter point is particularly important. The scenarios presented in this report are based on the difference, at each GCM grid point, between the 2 x CO_2 and the 1 x CO_2 value for a particular climate variable. This difference is then linearly scaled to represent the change expected as the result of a 1°C change in global temperature. Essentially, by expressing the climate change over the Mediterranean as a function of the global temperature change, we are introducing a time dependency into the scenarios. A scenario for any particular future time can be developed

provided that the global mean temperature change at that time can be estimated.

The results from four GCMs developed for climate studies are used in this Report, from the following research institutions:

UK Meteorological Office (UKMO)
Goddard Institute of Space Studies (GISS)
Geophysical Fluid Dynamics Laboratory (GFDL)
Oregon State University (OSU)

The models vary in the way in which they handle the physical equations describing atmospheric behaviour. The UKMO, GISS and OSU GCMs solve these in grid-point form whereas the GFDL model uses a spectral method. All models have a realistic land/ocean distribution and orography (within the constraints of model resolution), all have predicted sea ice and snow, and clouds are calculated in each atmospheric layer in all models.

1.4 STRUCTURE OF THE REPORT

1.4.1 Regional Scenarios of Climate Change

One of the most pressing requirements with regard to research into the greenhouse effect is the need for regional scenarios of climate change. Only on this basis can plans be made to adapt to or ameliorate the effects of the predicted changes. Broad-brush predictions at the global, hemispheric or continental scale are of little use in this planning process.

It is generally recognized that the results from GCMs offer the best potential for the development of regional scenarios of climate change. Equilibrium response predictions for the grid points appropriate to the Mediterranean Basin are available in the Climatic Research Unit for the above four models. These predictions form the basis of the regional scenarios of climate change presented in this Report, as described in Chapters 3 and 4.

In Chapter 3, we examine scenarios produced directly from GCM grid-point output. The results from the four models are synthesized to produce a single scenario for each climate variable. This approach also allows the impact analyst to assess uncertainty by examining inter-model differences and to easily produce a range of scenarios.

One problem with the application of GCMs to the study of climate impacts is the coarse resolution of the model grid. The grid scale of the four models listed above ranges from 4° latitude x 5° longitude (OSU) to 7.83° latitude x 10° longitude (GISS). GCMs, therefore, have a spatial resolution of several hundreds of kilometres, which is inadequate for many regional climate change studies, especially in areas of high relief. In Chapter 4 we present a set of high resolution scenarios, based on the statistical relationship between large-scale climate data and small-scale observations from surface meteorological stations.

1.4.2 Model Validation

As noted above, for each GCM simulation of the greenhouse effect, two model runs are performed: the control run and the perturbed run. One useful test of model performance is to compare the results from the control run, which usually has an atmospheric CO_2 concentration of around 300-330ppmv, with present-day climate. (By "present-day" we usually mean the climate of the last 3-4 decades. The mean CO_2 concentration over this period was around 390ppmv, which is sufficiently close to the value assumed in control run simulations to allow a sensible comparison.) This procedure is known as model validation.

The perturbed-run predictions of a model which fails to reproduce adequately the principal features of the present-day circulation and climate must be regarded as less reliable than the predictions of a model which reproduces the present-day climate well. The results from the

validation of the performance over the Mediterranean Basin of the four GCMs used in this study are presented in Chapter 2.

1.4.3 Precipitation Extremes

In an area such as the Mediterranean Basin, prone to droughts and floods, it is important to understand how the frequency and severity of precipitation extremes is likely to change because of the enhanced greenhouse effect. GCMs do not produce such information in a form convenient for analysis. It is therefore necessary to adopt an alternative approach to the problem.

In Chapter 5 we present the results of a statistical analysis of precipitation extremes, based on Markov Chain theory. On the basis of this analysis, estimates of the frequency and severity of precipitation extremes in a high greenhouse gas world are obtained.

1.4.4 Conclusions

The conclusions of the Report are presented in Chapter 6. The principal results of the study are reviewed and discussed. Particular attention is paid in the discussion to the reliability of the scenarios of climate change. Some of the implications of the changes indicated for the regional economies and ecologies of the area are briefly outlined, although a full discussion of this topic is beyond the expertise of the authors.

The information presented in this Report should provide a useful tool for impact analysts. As such, it forms only the first step in evaluating the implications of the enhanced greenhouse effect for the Mediterranean Basin. Climate models are being continually improved, as are the methods for interpreting model output and using both model and observed data to obtain information at the regional and subregional scales. The scenarios presented in this Report should be refined at regular intervals as these improvements are made.

CHAPTER 2

MODEL VALIDATION

Before we can proceed with the construction of the regional scenarios of climate change, it is important to investigate the reliability of the GCM data on which these scenarios are to be based. This is done through the process of control run validation. As noted in the Introduction, GCMs are normally run for present-day concentrations of CO_2 and for doubled CO_2. We can compare the $1xCO_2$ climatology of the models with observations, in order to assess their ability to simulate present-day climates. Clearly, if a model fails to simulate present-day climates satisfactorily, we must place reduced confidence in its predictions for the future.

Here we have assessed the ability of the models to simulate present-day patterns of sea level pressure and precipitation over the Mediterranean Basin. It is not possible to validate temperature simulations, since control runs use observed temperature as a boundary condition. Atmospheric pressure is a fundamental characteristic of climate: the position and intensity of high and low pressure systems determines the distribution of temperature, precipitation and winds. Therefore, if a GCM is unable to simulate pressure adequately, we must exercise caution in accepting its simulations of other climate parameters. Even if the simulation of variables such as temperature and precipitation is apparently adequate, it may be for the wrong reasons.

The distribution of precipitation is highly variable in both time and space. Indeed, the scale of many rain-producing systems is considerably less than the grid-size of most of the GCMs used to date in climate change studies. Furthermore, the regional patterns of precipitation are strongly influenced by topographic details that are not resolved by these GCMs. We would not, therefore, expect control run simulations of precipitation to succeed except at quite large spatial scales, scales at which precipitation

depends mainly on the broad-scale fluxes of moisture rather than how these fluxes are modified by smaller-scale processes and boundary conditions. In spite of these a priori reasons to expect precipitation change predictions to be relatively poor, we will, in this study of climate change over the Mediterranean Basin, still produce precipitation scenarios, simply because changes in rainfall amount and/or distribution have such important implications for the region. Before proceeding to generate such scenarios, it is important that we investigate the ability of GCMs to simulate precipitation, given this imbalance of scale between the model grid and the rain-producing mechanisms.

2.1 VALIDATION OF PRESSURE

In order to perform the validation of pressure, we have compared the GCM output with a data set of daily mean sea level pressure (MSLP). This was originally compiled from forecasting analysis charts, and is continually updated from the same source by the U.K. Met. Office. In the region of interest, the pressure data are gridded at a resolution of 5° latitude by 10° longitude, as shown in Fig. 2.1 (see Jones, 1987, and Jones et al., 1987, for a full description of this data set).

The grid-point pressure output for the control run of each of the four GCMs was interpolated onto the same grid as the pressure data set. For validation of the control run, we took data for the thirty-year period 1951-80 from the MSLP data set.

As a first step, we examined the spatial correlation between the GCM output and the MSLP data set. For each of the 36 points shown in Fig. 2.1, the mean pressure for 1951-80 was calculated from the MSLP data set for the whole period and for each season: winter (December, January, February), spring (March, April, May), summer (June, July, August), and autumn (September, October, November). The correlation coefficients between the

GCM output and the MSLP data set were then calculated, where the number of cases = the number of grid points = 36. The results are shown in Table 2.1. Already we can see that there are substantial differences in model performance. The best results are obtained from the GISS (surprisingly, given its coarse horizontal resolution) and UKMO models. The GISS GCM has the best annual correlation (0.74). The UKMO model performs particularly well in the summer ($r = 0.94$) and autumn ($r = 0.82$), but returns a correlation of only 0.57 at the annual level owing to its poor performance in winter and spring. The least successful is the OSU model. In spring and autumn, and for the year as a whole, there is actually an inverse (although weak) relationship between observed and modelled pressure. The GFDL model has an overall correlation of 0.48, and one negative seasonal correlation coefficient, in winter.

The spatial distribution was plotted, to determine whether there are any areas in the Mediterranean Basin where the agreement between observed and control-run MSL pressure is particularly weak or strong. The observed patterns, based on the 1951-80 time series, are shown in Fig. 2.2. At the annual level, there is a smooth transition from south-east to north-west across the study region, with a range of about 9mb. In winter, the formation zones of cyclonic disturbances, over the Gulf of Genoa and

Table 2.1 Spatial correlation of GCM output and MSLP data set.

	GFDL	GISS	OSU	UKMO
Annual	0.54	0.74	-0.28	0.57
Winter	-0.17	0.27	-0.05	0.20
Spring	0.57	0.63	-0.24	0.24
Summer	0.65	0.92	0.79	0.94
Autumn	0.53	0.78	-0.45	0.82

Greece, are clearly seen. Pressure rises towards the north-east, indicating the influence of the Siberian anticyclone. Relatively cold conditions over North Africa lead to higher pressure in this region also. The summer pattern is simple, showing a gradual transition from a low pressure trough in the south-east (an extension of the Indian Monsoon system), to higher pressure in the north-west. In spring and autumn, the pressure patterns are transitional between those of winter and summer.

For each of the four models, the control-run pressure distribution and the difference between the control run and observed MSLP have been plotted. The results, for the year and for each season, are shown in Figs. 2.3-2.6.

The results for the GFDL GCM are shown in Fig. 2.3. It should be noted that the pressure values for this model refer not to mean sea level, but to the lowest sigma surface. This does not affect the spatial correlation coefficients of Table 2.1, nor the spatial pattern of control run/observed pressure differences. However, the actual differences cannot be directly compared with those shown in Figs. 2.4-2.6 for the other GCMs. The patterns are consistent throughout. Across the region, pressures are generally too low. The best fit is found in the central Mediterranean Basin, between Tunisia and north-east Libya, and towards the north-western and north-eastern extremities of the study area.

The pressure distribution for the year as a whole in the GISS model (Fig. 2.4) varies from lower pressure in the south of the study area to higher pressure in the north. This is also true of all seasons except winter, when the pattern is ill-defined but shows some tendency to increase towards the north-east. Overall, the control run pressure is again too low, particularly in the south of the region, where the differences rise to over -12mb in summer. The best agreement is found in the winter season.

The OSU model (Fig. 2.5) demonstrates highly variable pressure patterns from season to season, and it is only in summer that these bear close

resemblance to the observed distribution. The winter pattern is the opposite of the observed, varying from low pressure in the north to high pressure over Africa. Overall, pressure tends to be too low. If we examine the map of annual control run/observed MSLP differences, the fit is apparently very good, with differences generally less than -4mb. However, this is due largely to compensating errors arising from the great seasonal variation in the control run pressure patterns, rather than to good model performance. The poorest seasonal performance is seen in winter (when the pressure over most of Europe is over 8mb too low) and autumn (pressure over Europe more than 6mb too low).

The UKMO GCM (Fig. 2.6) shares certain features in common with the OSU model. There is considerable variation in the seasonal pressure patterns, with summer showing the greatest similarity to the observed distribution, and the winter pattern again varying between low pressure in the north of the study region and high pressure in the south. Overall, the performance of the UKMO model is superior to the OSU model, in that the control run/observed MSLP differences are smaller. The performance is particularly impressive in summer and autumn when, throughout the study area, the differences do not exceed 5mb.

In summary, the results of the spatial correlation analysis are confirmed by the pressure distribution maps. The GISS model reproduces the observed pressure patterns most realistically but, in terms of control run/observed pressure differences, the UKMO model is the most successful. The OSU model fails to reproduce the spatial patterns satisfactorily, and the pressure differences are high. It is not possible to compare the GFDL model's absolute performance, because of the differences in variable type (the GFDL pressure values are for the lowest sigma surface in the model, rather than for mean sea level). All models are poor in winter. We note that the GISS performance over the Mediterranean region is not echoed by

its performance over the wider North American-Atlantic-European region, where it is noticeably the worst of the models (see Santer and Wigley, 1990).

2.2 VALIDATION OF PRECIPITATION

Model precipitation has been validated against a gridded data set of land-based precipitation records for the period 1951-80 which has a spatial resolution of 5° latitude x 5° longitude (Hulme, 1991). The GCM precipitation output was interpolated onto the same grid as the precipitation data set. Validation was performed using spatial correlations, basin-scale seasonal cycles and by comparing the absolute values of observed and simulated data.

The spatial correlation coefficients between the GCM and observed grid-point precipitation were calculated. Forty-two grid points were used, giving 42 cases for the computation of the coefficients, as shown in Fig. 2.1. Grid points over the Bay of Biscay, those south of the Atlas Mountains, and those over Saudi Arabia were excluded on the assumption that the rainfall regimes in these areas would be generically different from those of the Mediterranean Basin. The results are shown in Table 2.2. The correlation coefficients vary less than those obtained in the pressure validation exercise, between 0.67 (GISS) and 0.78 (UKMO) at the annual level. No negative coefficients were obtained. There is no consistent trend in the seasonal values: the highest value is for the GFDL GCM in summer (0.82) and the lowest is for the OSU model in the same season (0.36). The UKMO model is best in the autumn, winter and annual correlations, and insignificantly different from the other models in spring.

The Mediterranean Basin has a pronounced and distinctive seasonal cycle of precipitation. A successful model must be able to reproduce this cycle,

Table 2.2 Spatial correlation of GCM control run and observed precipitation.

	GFDL	GISS	OSU	UKMO
Annual	0.75	0.67	0.70	0.78
Winter	0.48	0.67	0.73	0.81
Spring	0.77	0.74	0.75	0.76
Summer	0.82	0.69	0.36	0.61
Autumn	0.64	0.54	0.57	0.73

which is a critical factor in the ecologies and economies of the region. The area was divided into a western and an eastern region, along longitude 15° East. The network of grid points was reduced still further, to be certain of including only those points which experience the same seasonal regime, characteristic of a Mediterranean climate: 12 points were considered in the western basin and 13 in the eastern basin. The mean monthly precipitation was then calculated for each basin.

The seasonal cycles of the GCM control runs and observed precipitation are shown in Fig. 2.7 for the two basins. The observed patterns are broadly similar, with the highest rainfall occurring in December and the lowest in July. The rainy season is more prolonged in the western basin, and the seasonal cycle here is less pronounced than in the eastern basin.

In general, the GCMs tend to overestimate the precipitation total. This is particularly true for the GFDL and UKMO models, and the tendency is more pronounced in the western than in the eastern basin. The seasonal cycle is well reproduced by the GISS and OSU models. The GFDL and UKMO models fail to reproduce the seasonal cycle satisfactorily, and this is particularly the case in the western basin.

The spatial distribution of the absolute amounts of control-run precipitation was next compared with the observed amounts. The observed

patterns, contoured from the gridded precipitation data set for 1951-80, are presented in Fig. 2.8. The winter precipitation field shows the influence of depressions tracking eastwards across the northern Mediterranean, bringing local precipitation maxima (more than 100mm/month) to southern Italy, Greece and eastern Turkey. In spring there is still evidence of tracking depressions producing higher rainfall amounts over southern Italy and northern Turkey. However, by summer the whole of the area south of 40°N is receiving less than 30mm of rainfall per month, and at some grid points there is no rainfall in this season. The influence of the tracking depressions over south-west Italy is reasserted in autumn, with over 110mm/month at two grid points.

The differences between the control run and observed precipitation amounts were expressed as a ratio to facilitate comparison. Because of the large seasonal differences and the very low rainfall totals in summer, it would not be meaningful to assess model performance on the basis of a simple difference. Grid-point values less than 1mm/month were rounded up to 1mm/month.

The spatial patterns are complex. We have therefore summarized the information contained in the maps in Table 2.3, which shows the ratio between the mean control run and mean observed precipitation, the mean being calculated for all 50 grid points. Values close to one indicate the most successful performance. This table confirms the tendency of the models to overestimate precipitation, the only ratio less than one being for the GFDL model in summer. At the annual level, the GFDL GCM produces the most successful result, and the UKMO model the least successful, followed by GISS. The poor results for these two models are due to their failure to simulate the summer drought over the Mediterranean. This deficiency has already been noted in the validation of the seasonal cycles.

Table 2.3 Ratios between GCM control run and observed mean precipitation

	GFDL	GISS	OSU	UKMO
Annual	1.18	1.48	1.23	1.51
Winter	1.19	1.25	1.14	1.02
Spring	1.46	1.66	1.40	1.52
Summer	0.74	2.10	1.09	2.76
Autumn	1.17	1.28	1.29	1.42

The spatial patterns of control run precipitation and of the modelled-to-observed ratios for the GFDL GCM are shown in Fig. 2.9. In all seasons the model distinguishes successfully between the wetter north and the drier south of the study region. However, the north-south contrast is generally too small, as can be seen from the ratios in Fig. 2.9, or by comparing Figs. 2.8 and 2.9. In all seasons the ratios over North Africa are greater than 1.5. The GISS model (Fig. 2.10) performs particularly poorly in terms of modelled-to-observed precipitation ratios in spring and summer: large areas of the study region have ratios greater than 1.5. The OSU GCM (Fig. 2.11) produces a reasonable simulation of precipitation in the transitional seasons of spring and autumn. The autumn results show a precipitation maximum over the central Mediterranean Basin, which coincides approximately with the position of depression tracks. The UKMO model control run simulation of precipitation is shown in Fig. 2.12. This reproduces the seasonal patterns well in spring, summer and autumn, with clear maxima in the areas of cyclone formation and along the preferred depression tracks. The simulation patterns in summer are less successful and, as already noted, the overall rainfall in this season is too high.

We have used four tests of the ability of the models to simulate present-day climate: the spatial correlation of grid-point precipitation, the simulation of the seasonal cycle, the overall ratio between control run

and observed precipitation, and the spatial pattern of the grid-point ratios of modelled to observed precipitation. On this basis, we are unable to select one model which consistently out-performs the others. The poorest results are for the GISS model, which does badly on all four tests. The OSU model simulates the seasonal cycle well, and the overall ratio between control run and observed rainfall is low. However, the spatial correlation is poor and the patterns of control run precipitation are substantially different from the observed. The UKMO model has the highest spatial correlation of the four GCMs, and simulates the spatial patterns most effectively. On the other hand, it fails to reproduce the seasonal cycle adequately, and has the highest ratio between control run and observed precipitation. The GFDL model has the second highest spatial correlation, and the patterns of precipitation are reasonably well simulated. The seasonal cycle is good, and it has the lowest ratio between control run and observed rainfall.

2.3. CONCLUSIONS

In this chapter, model validation has been performed using two climate variables: mean sea level pressure and precipitation. On the MSLP tests, the most realistic models were the UKMO and GISS GCMs. The GFDL model produced the best simulation of precipitation. The precipitation results, especially the inter-model differences, should be treated cautiously since they are not consistent with the MSLP results. One should be particularly wary when a good seasonal precipitation simulation occurs in conjunction with a poor MSLP simulation.

It is of interest to note the improvements in model performance which can be obtained by increasing the grid resolution of the model. The UKMO model has been run with an enhanced resolution of 2.5° latitude by 3.75° longitude (as opposed to the 5° x 7.5° resolution of the model used above).

Table 2.4 Control run performance of the UKMO and UKMO2 GCMs

	Spatial Correlation		Overall Ratios	
	UKMO2	UKMO	UKMO2	UKMO
Annual	0.81	0.78	0.95	1.51
Winter	0.66	0.81	1.03	1.02
Spring	0.76	0.76	0.92	1.52
Summer	0.88	0.61	1.04	2.76
Autumn	0.75	0.73	0.86	1.42

This model simulation (referred to as UKMO2 below) produces a significant improvement in performance, even though in other respects the model specification remains broadly the same. We present here the results for the validation of precipitation. In Table 2.4 we show the spatial correlations and overall ratios for the UKMO and UKMO2 GCMs. The seasonal cycle, compared to the other models, is presented in Fig. 2.13, and the spatial patterns of control run precipitation are shown in Fig. 2.14. Although permission has been granted by the U.K. Met. Office to use this model run for validation purposes, we do not have permission to use the perturbed run results in this study.

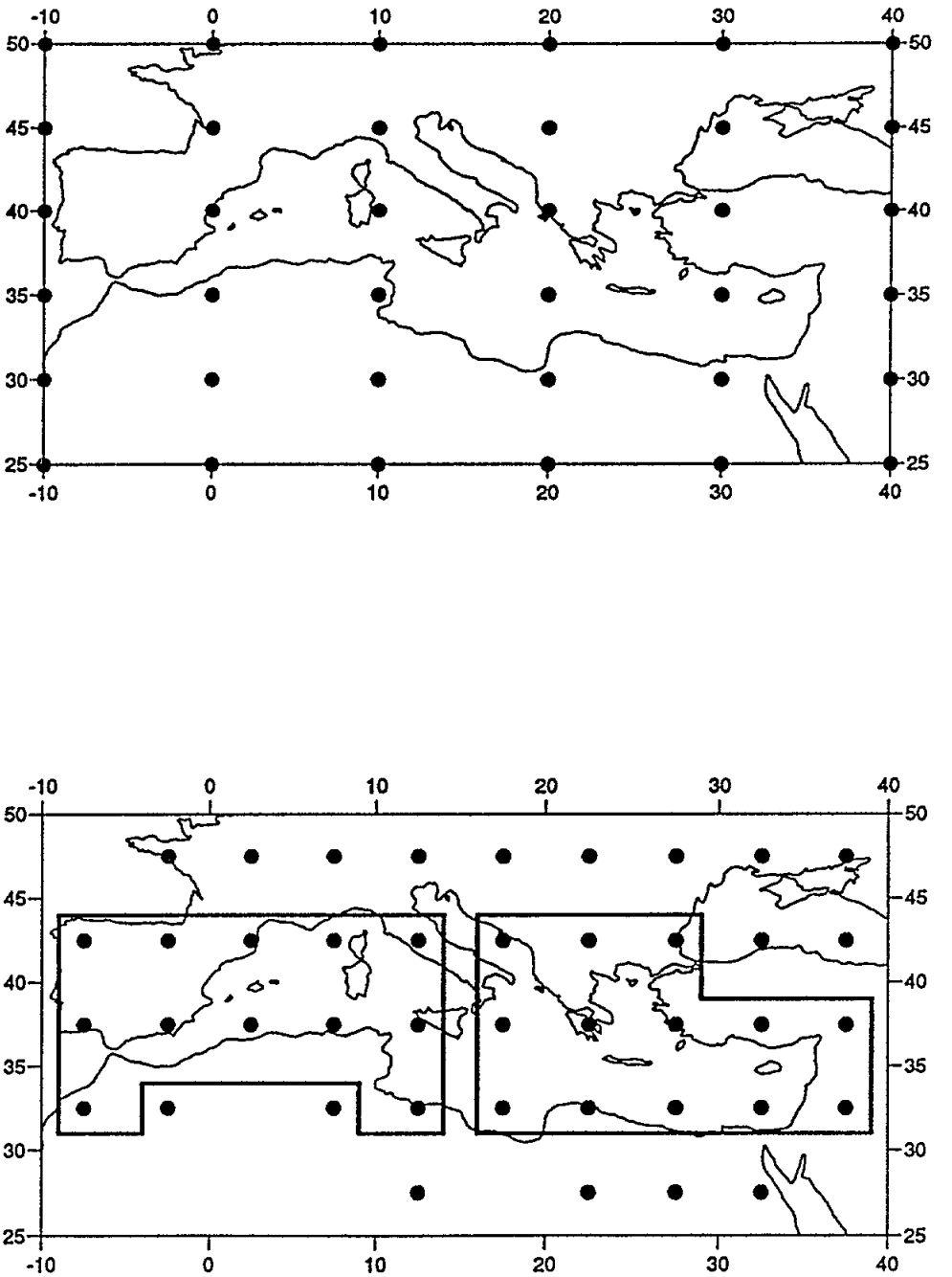

Fig. 2.1 Location of grid points for mean sea level pressure data set (above) and land-based precipitation data set (below)

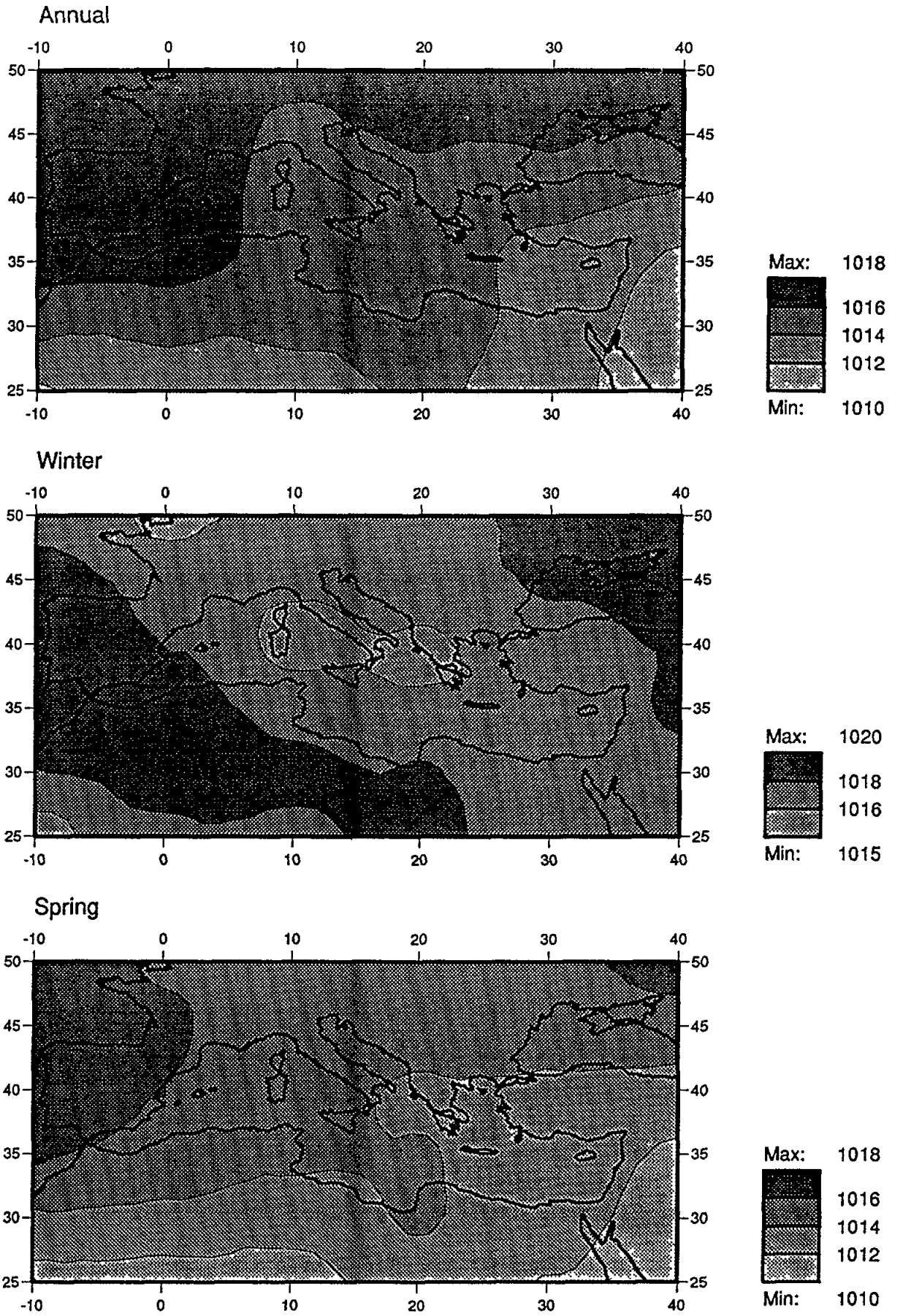

Fig. 2.2 Observed MSLP pressure (mb)

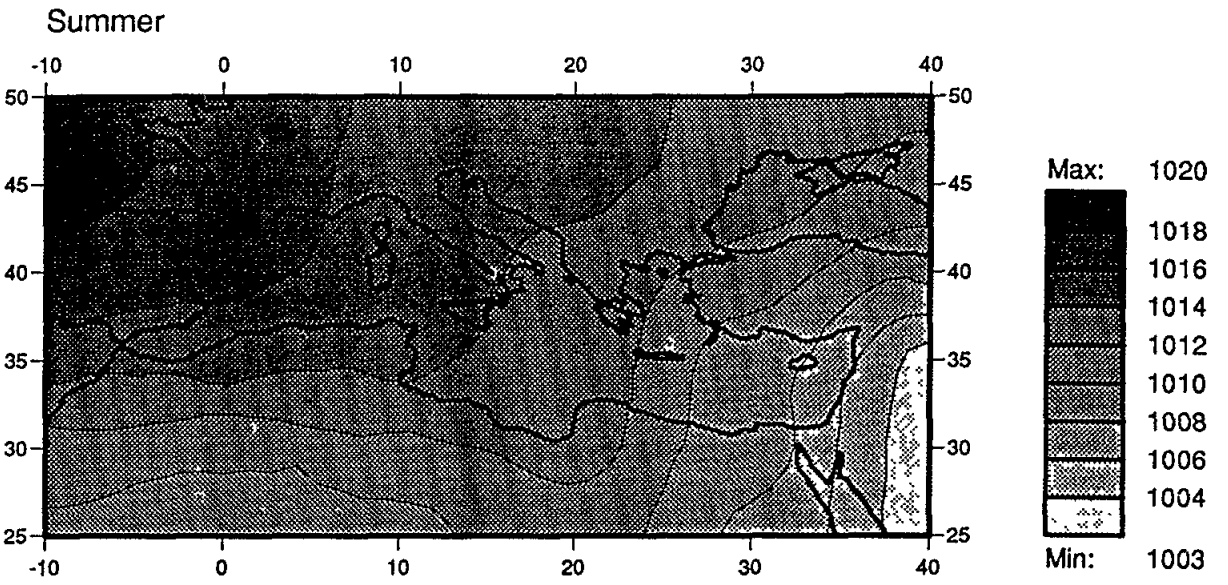
Summer
-10
0
10
20
30
40
50
45
40
35
30
25
Max: 1020
1018
1016
1014
1012
1010
1008
1006
1004
Min: 1003

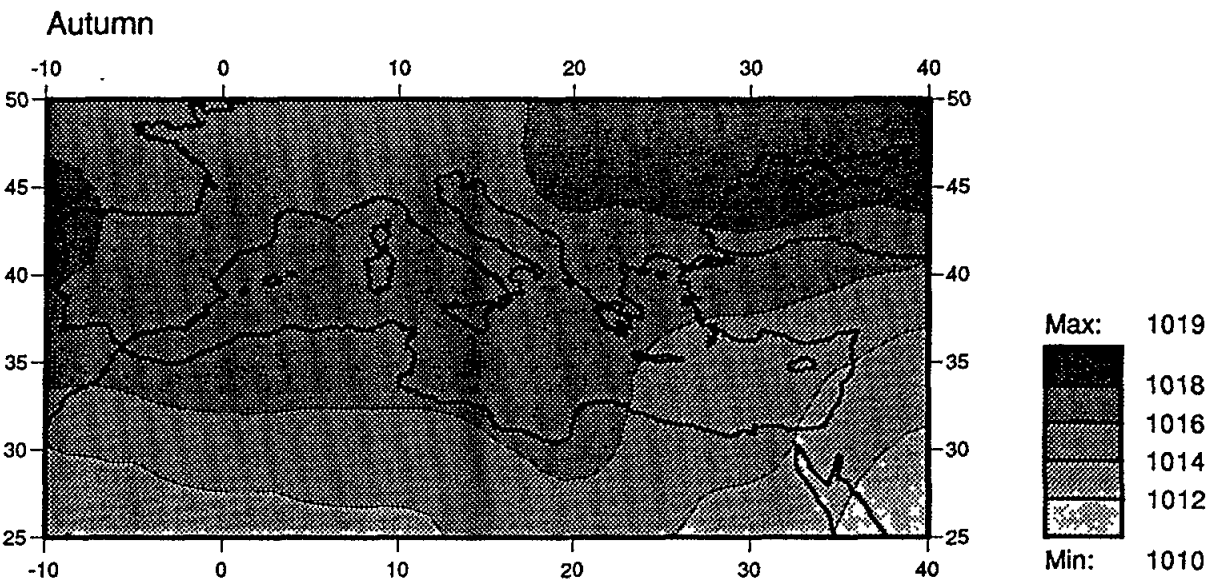
Autumn
-10
0
10
20
30
40
50
45
40
35
30
25
Max: 1019
1018
1016
1014
1012
Min: 1010

Fig. 2.2 cont.

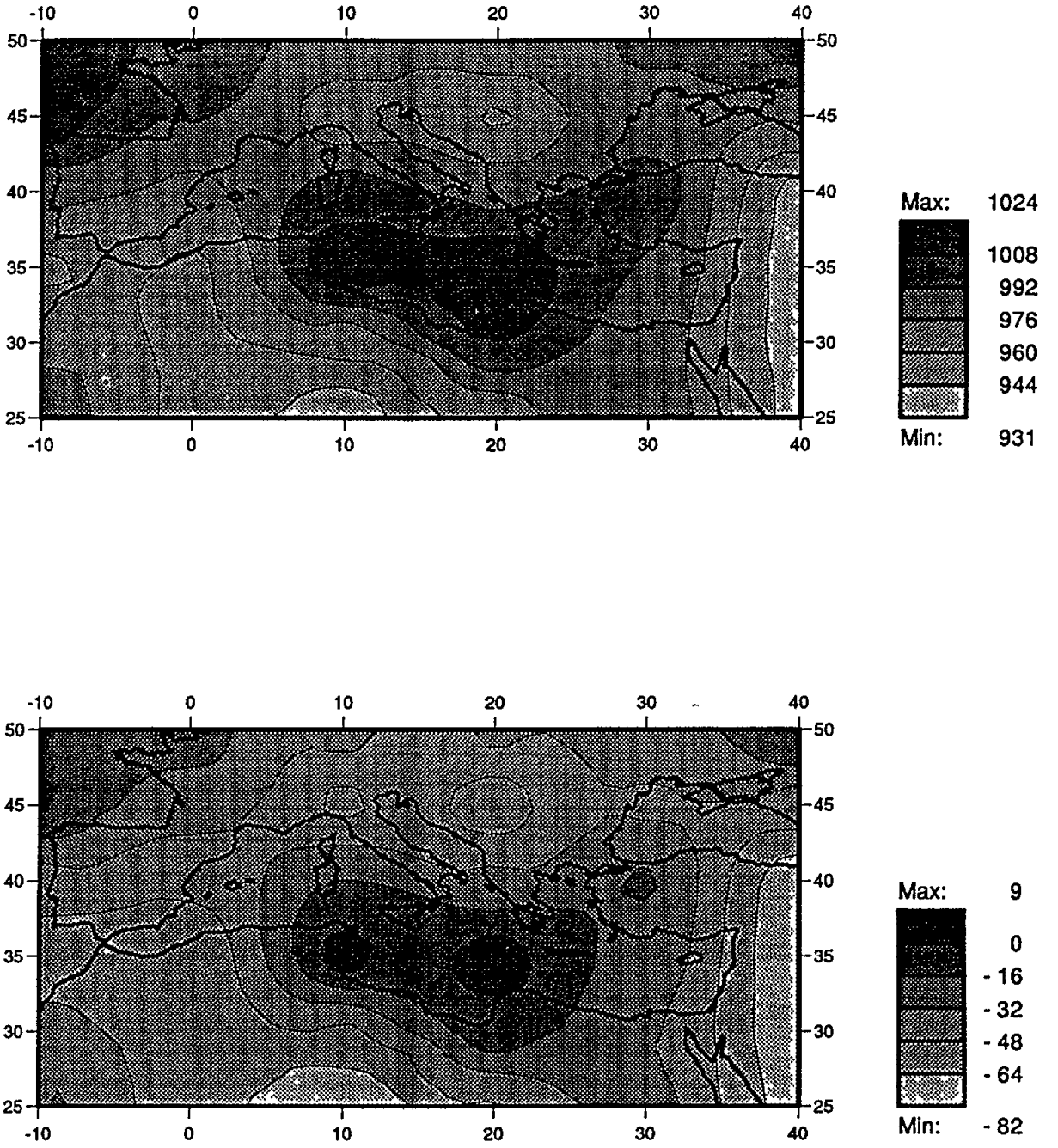

Fig. 2.3 Annual MSLP control run (above) and control/observed differences (below) in mb: GFDL GCM

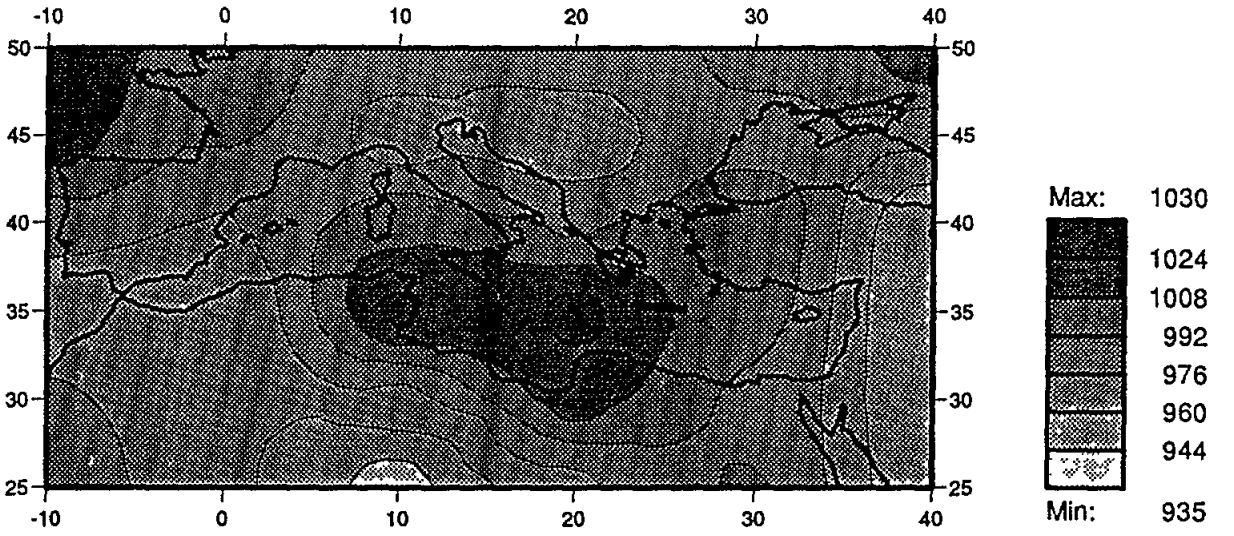

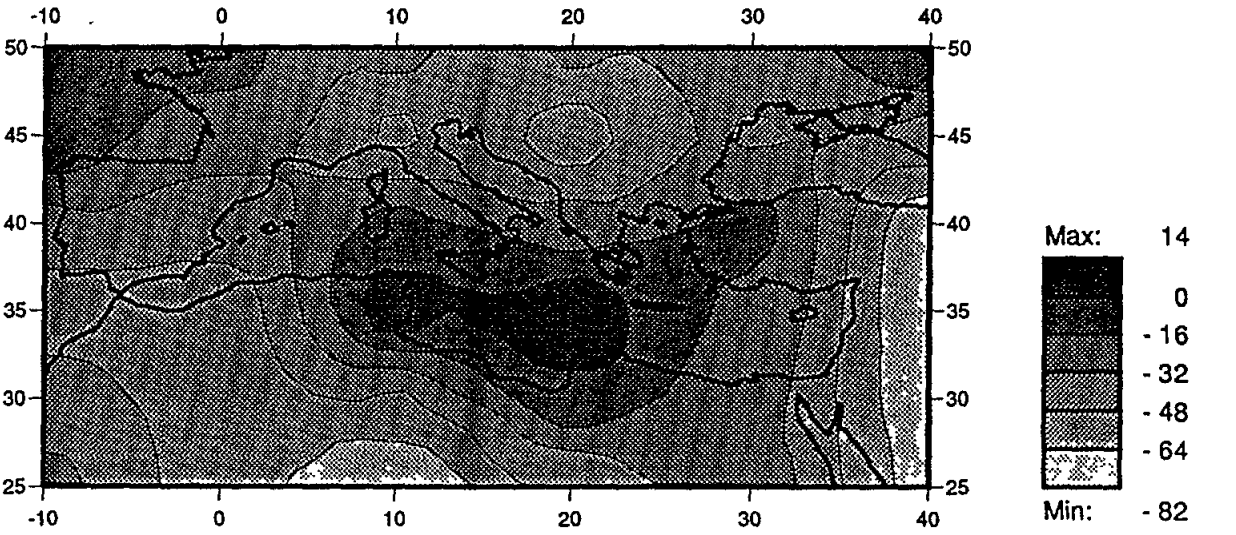

Fig. 2.3 cont. Winter MSLP control run (above) and control/observed differences (below) in mb: GFDL GCM

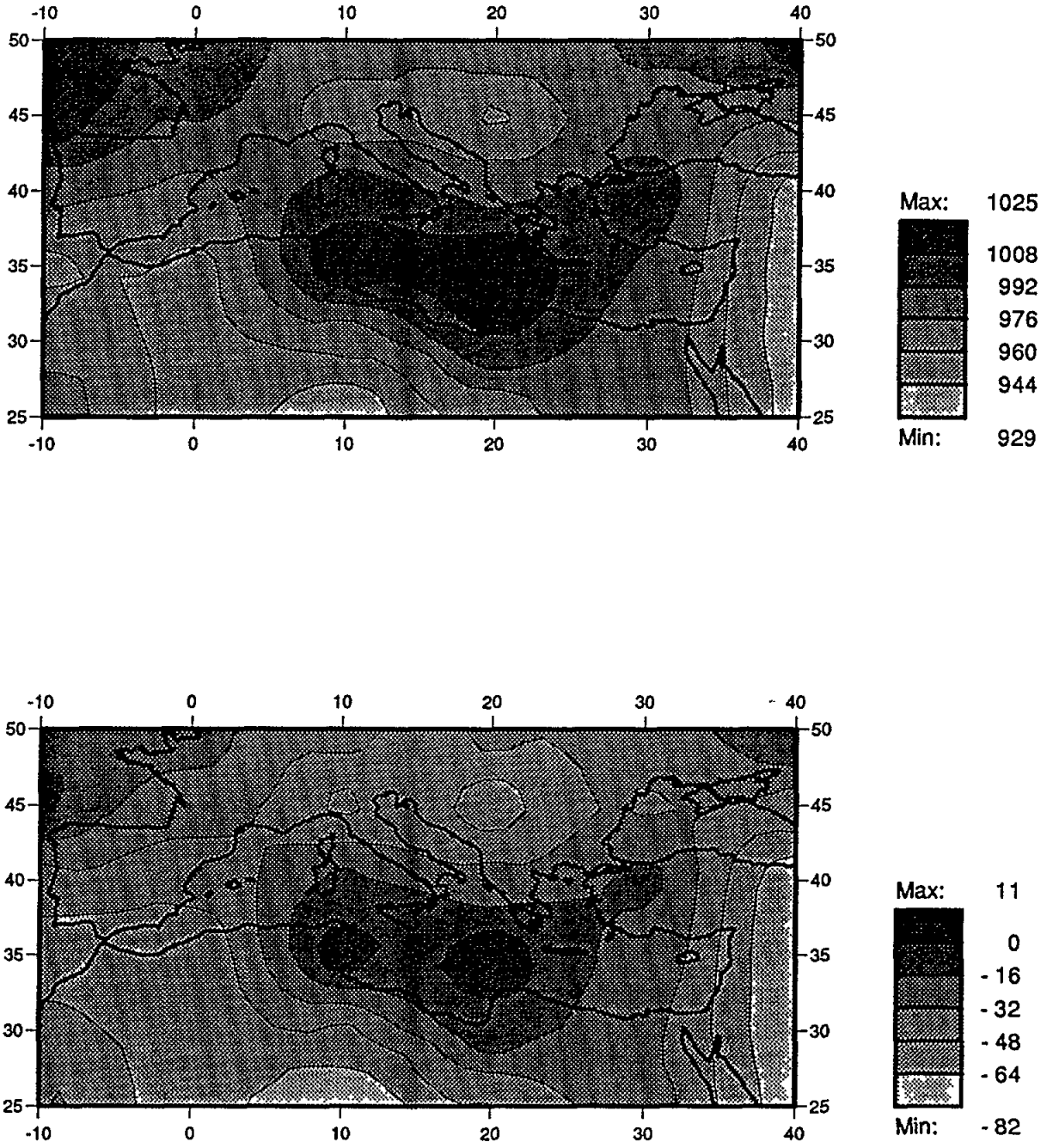

Fig. 2.3 cont. Spring MSLP control run (above) and control/observed differences (below) in mb: GFDL GCM

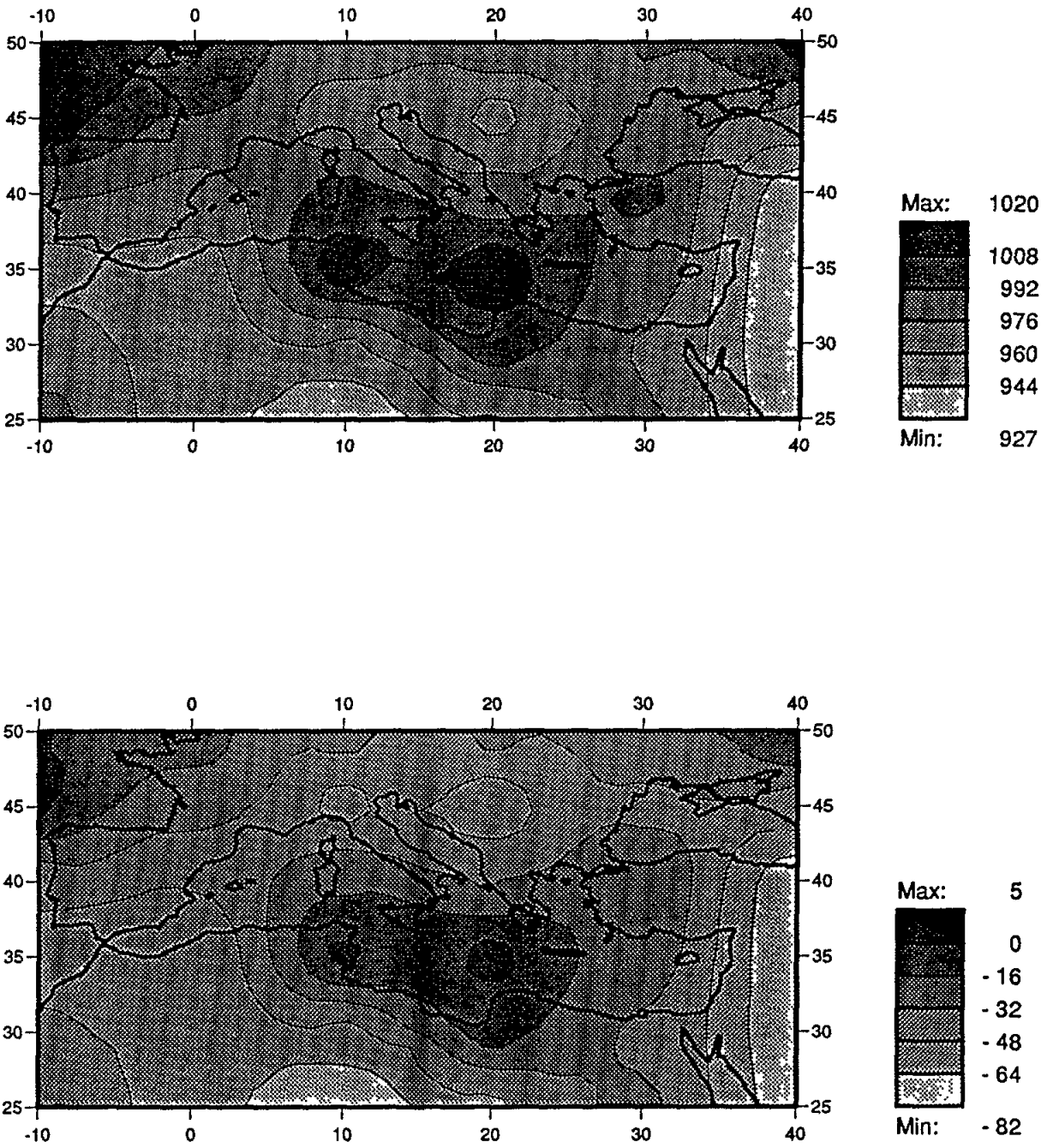

Fig. 2.3 cont. Summer MSLP control run (above) and control/observed differences (below) in mb: GFDL GCM

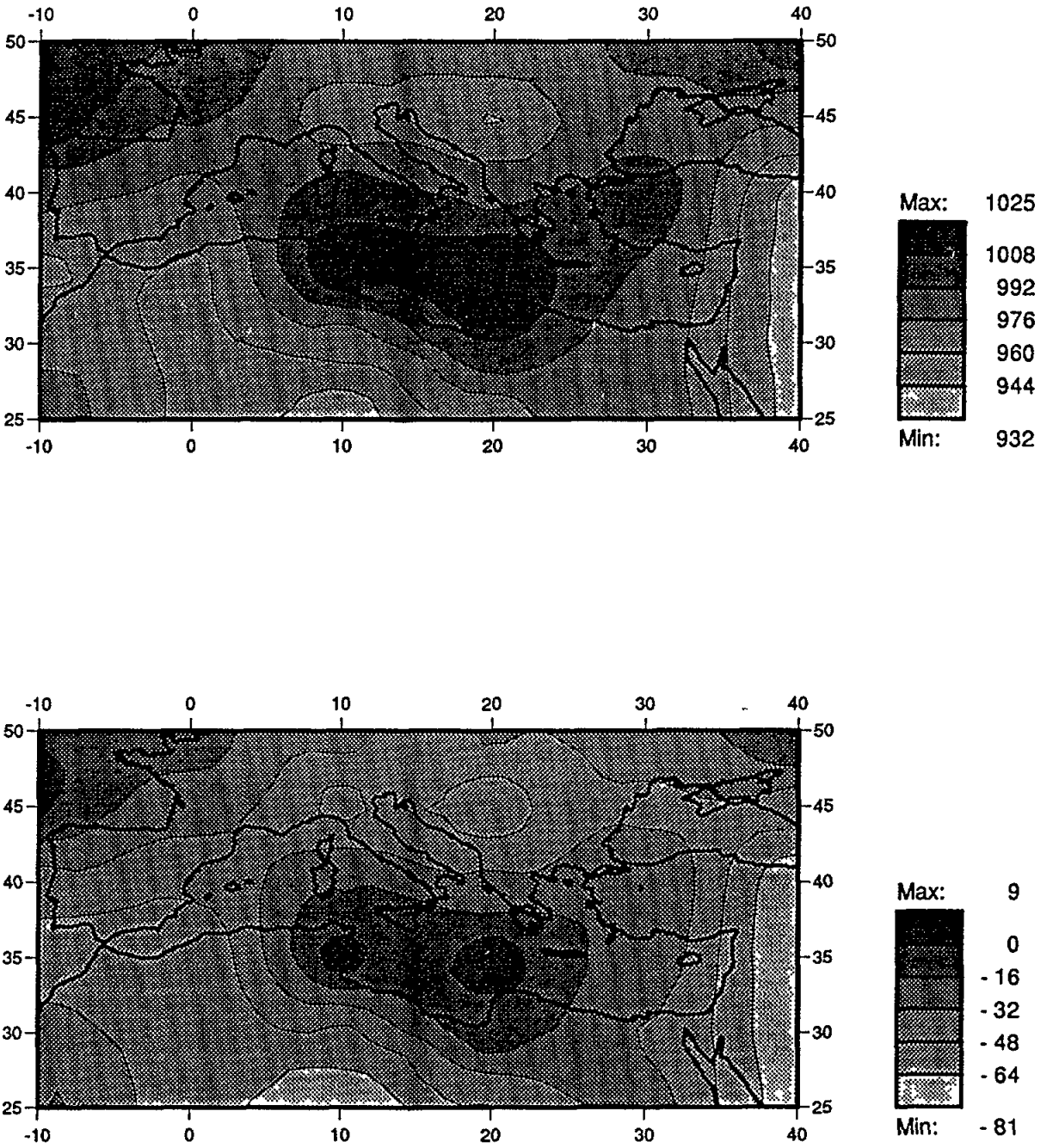

Fig. 2.3 cont. Autumn MSLP control run (above) and control/observed differences (below) in mb: GFDL GCM

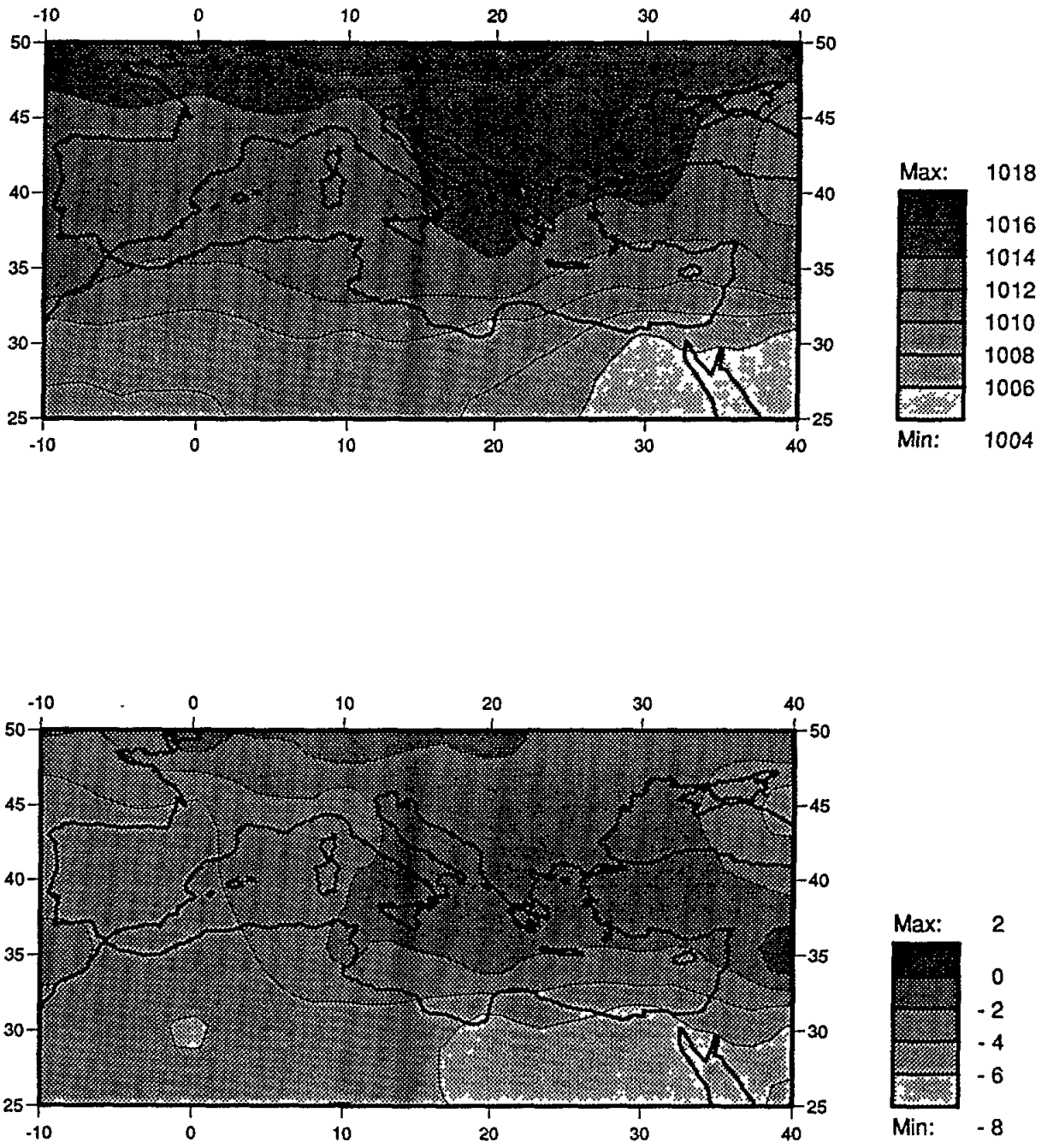

Fig. 2.4 Annual MSLP control run (above) and control/observed differences (below) in mb: GISS GCM

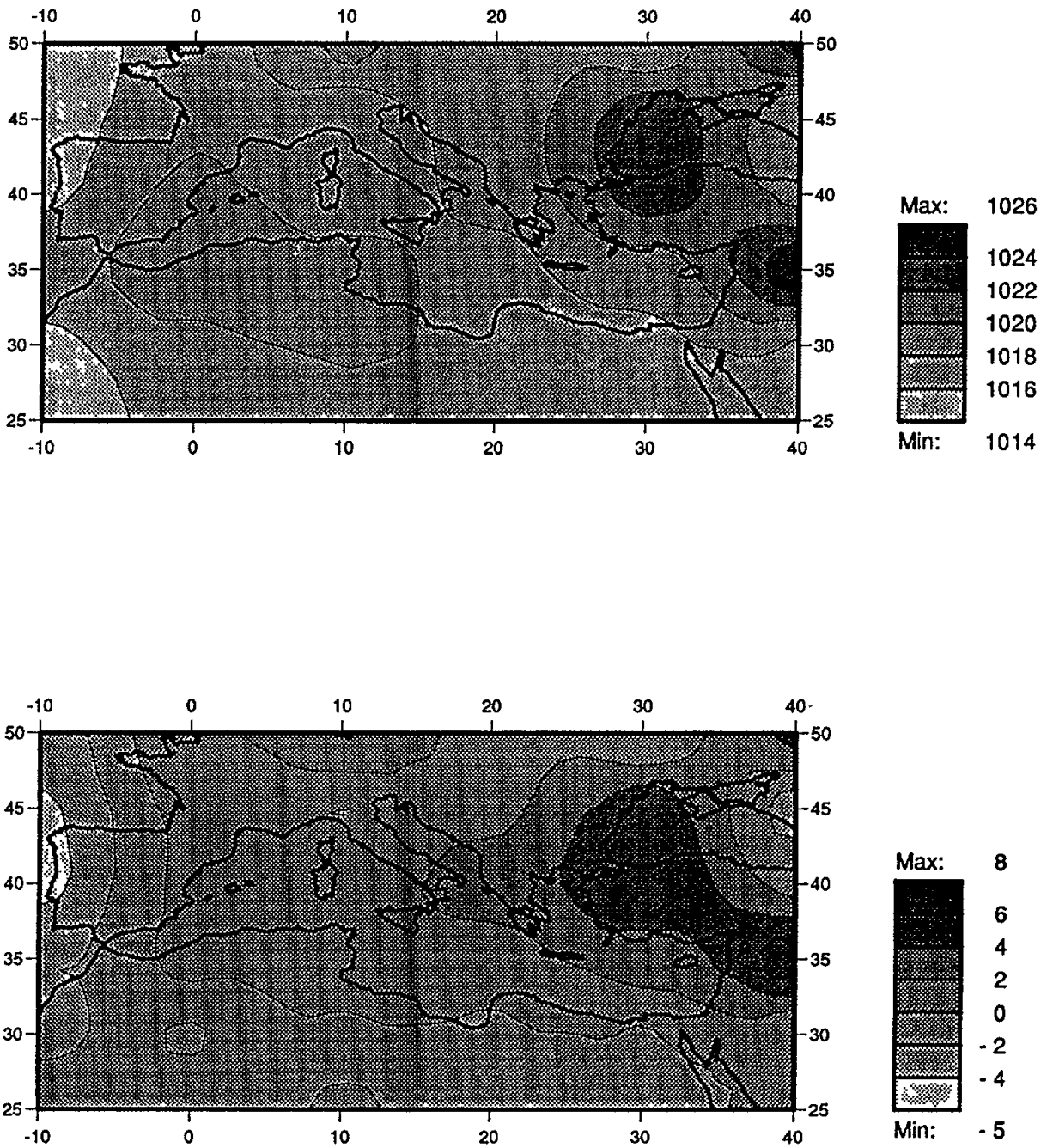

Fig. 2.4 cont. Winter MSLP control run (above) and control/observed differences (below) in mb: GISS GCM

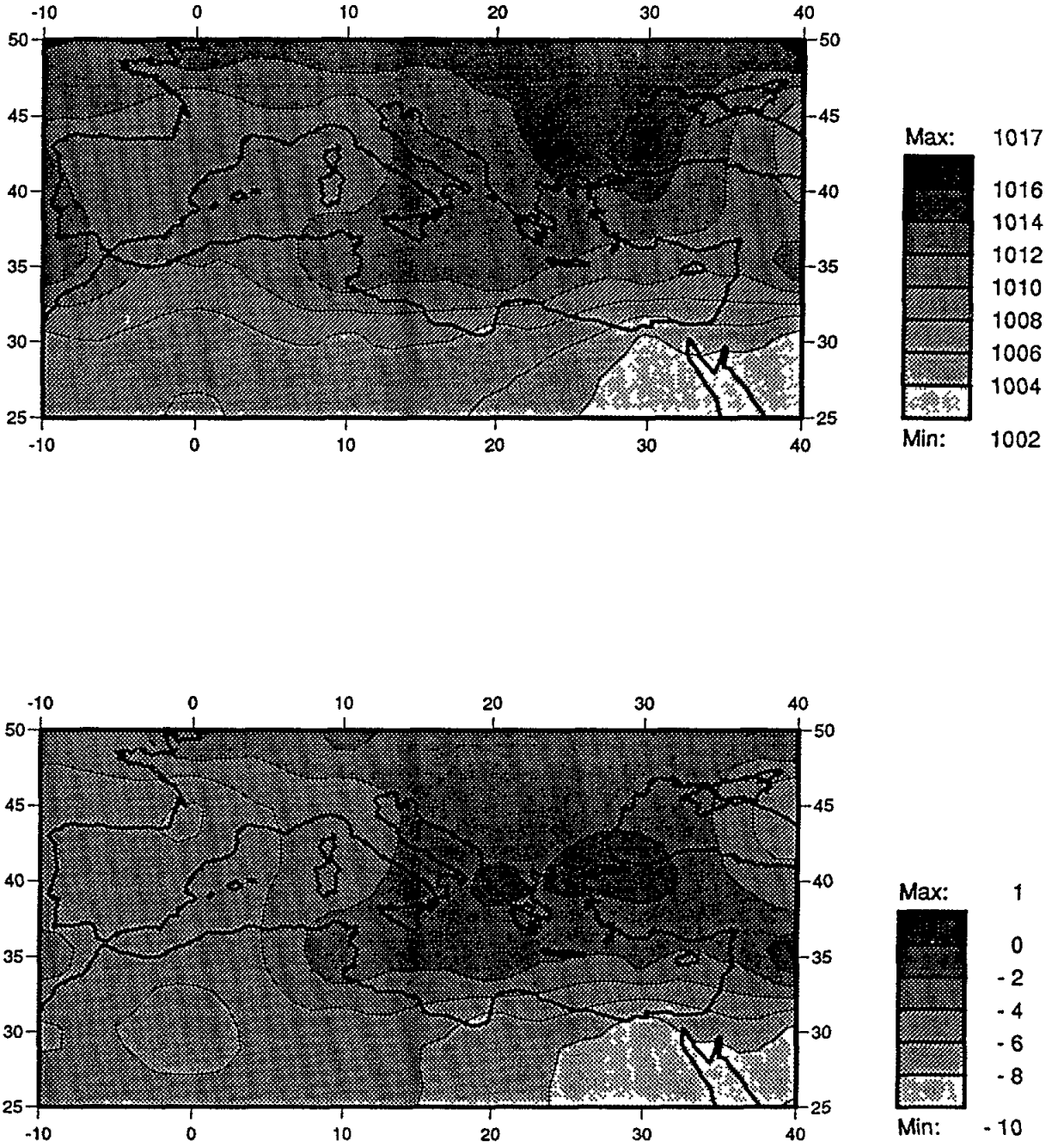

Fig. 2.4 cont. Spring MSLP control run (above) and control/observed differences (below) in mb: GISS GCM

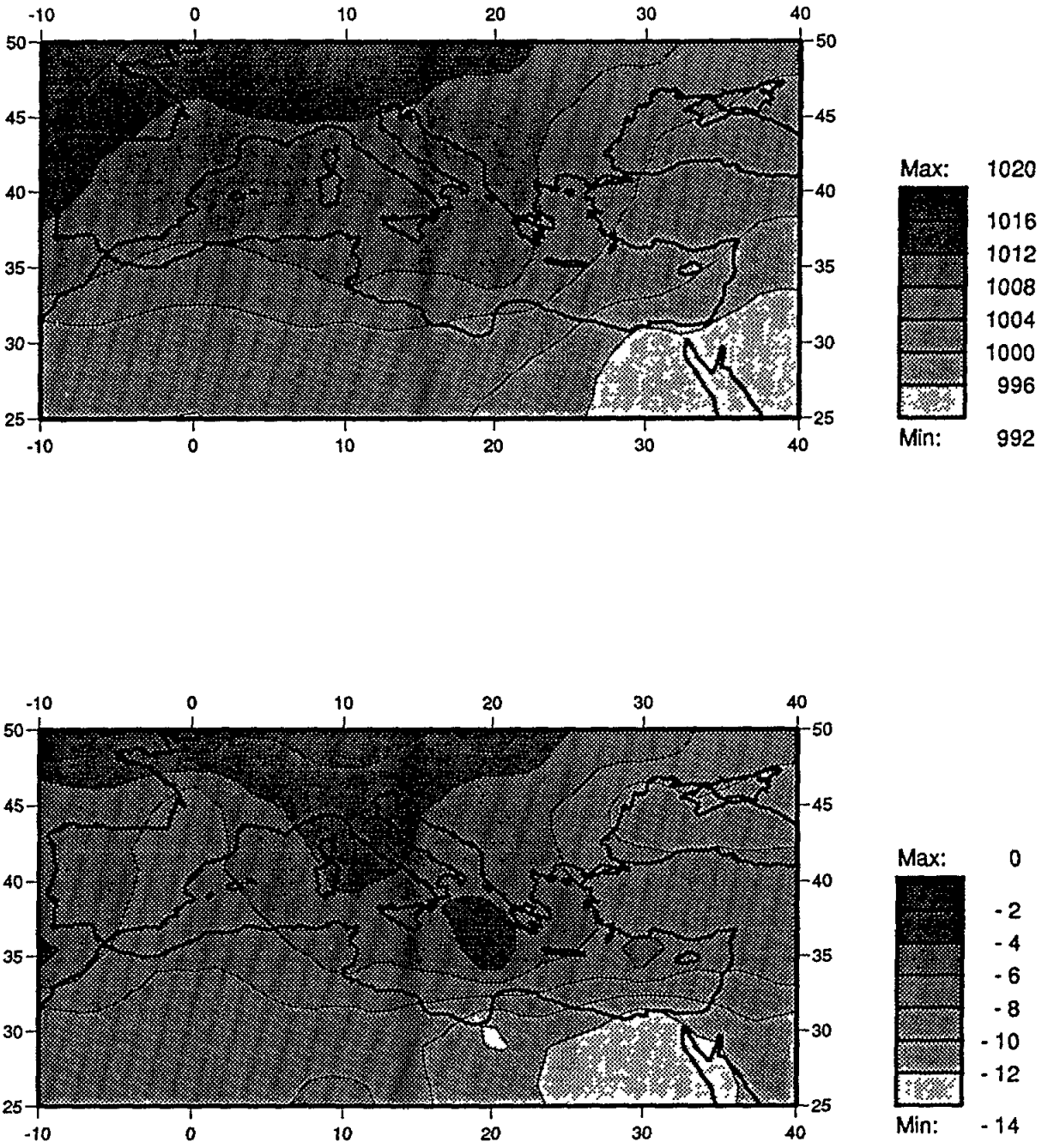

Fig. 2.4 cont. Summer MSLP control run (above) and control/observed differences (below) in mb: GISS GCM

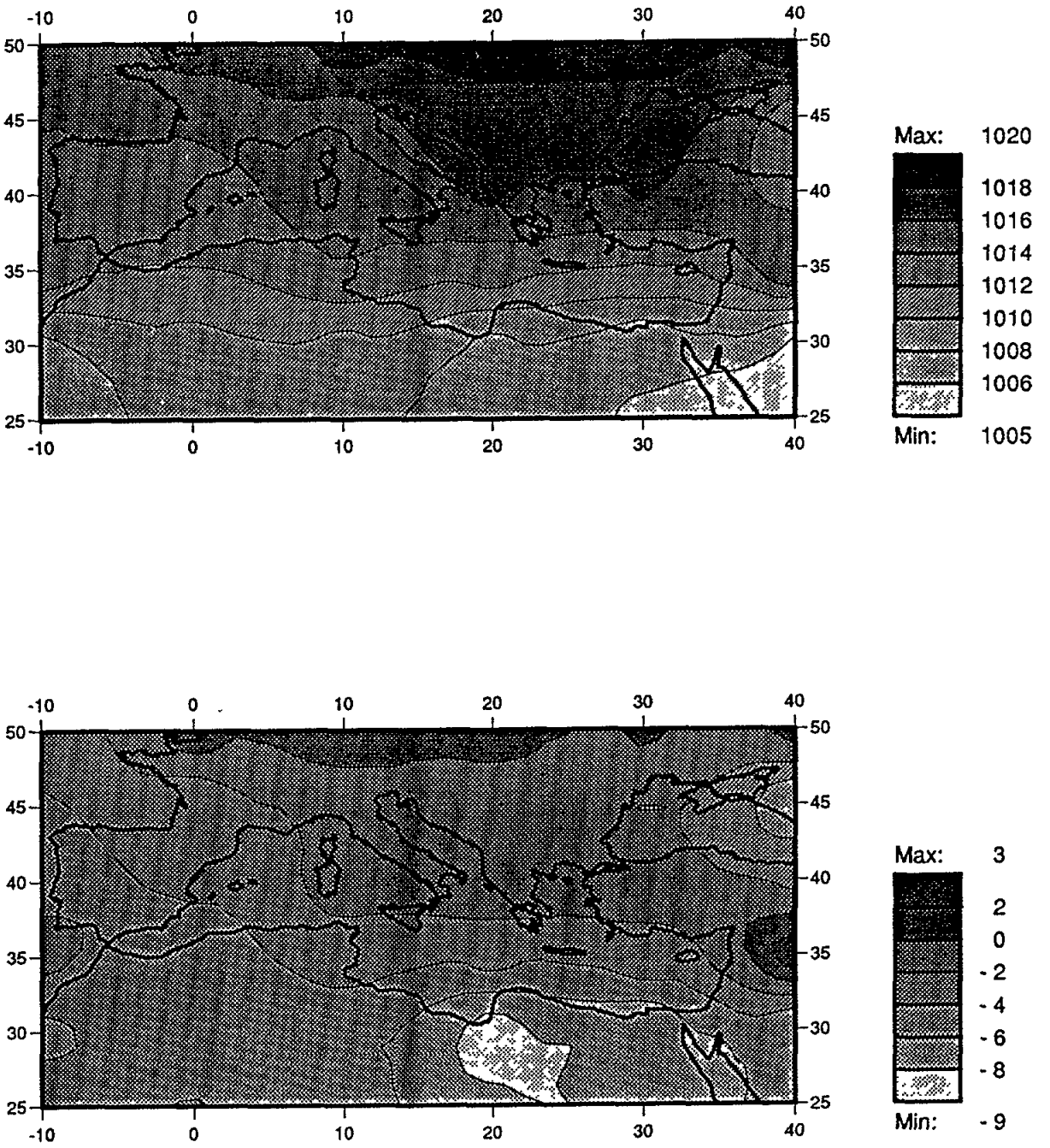

Fig. 2.4 cont. Autumn MSLP control run (above) and control/observed differences (below) in mb: GISS GCM

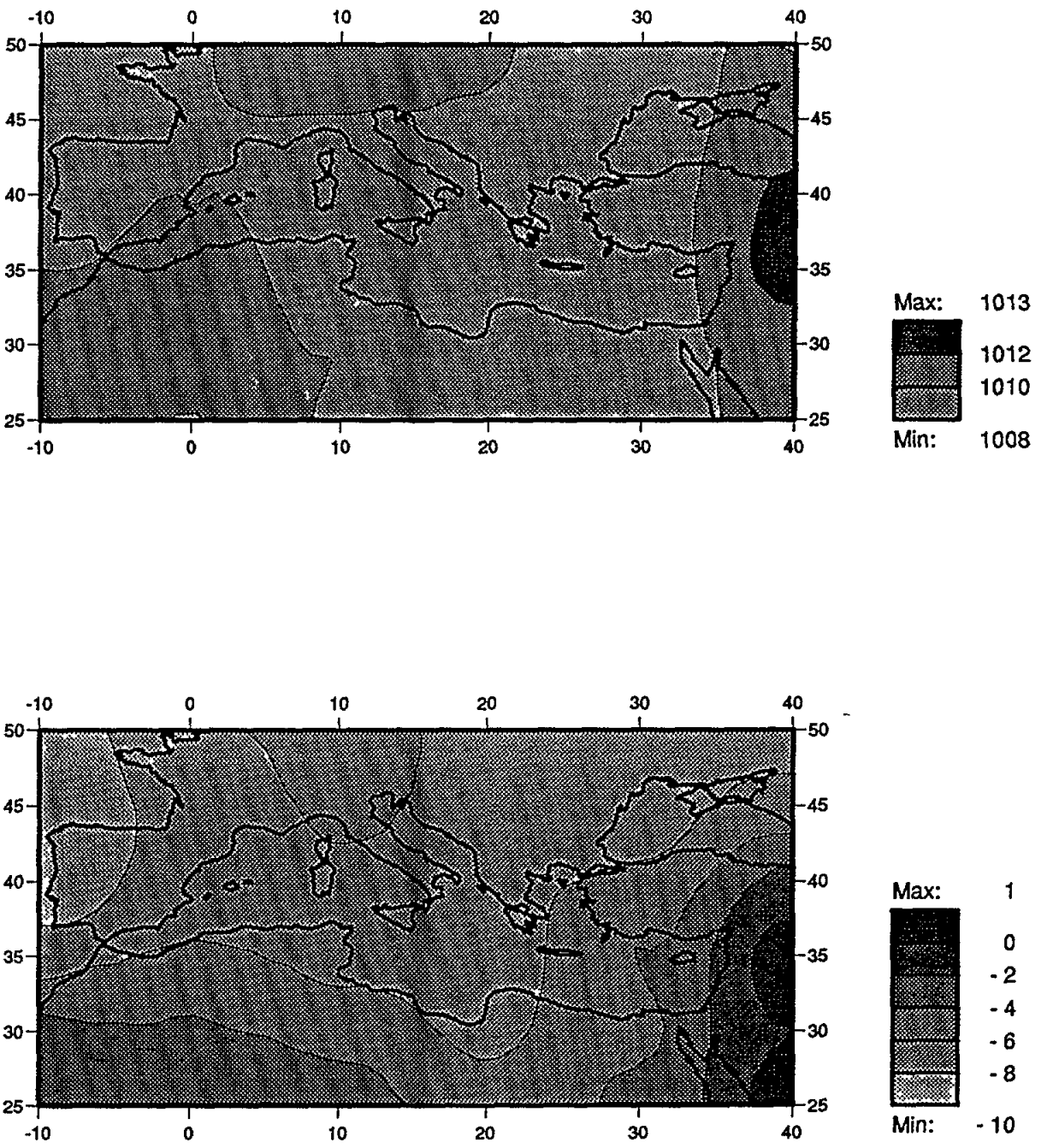

Fig. 2.5 Annual MSLP control run (above) and control/observed differences (below) in mb: OSU GCM

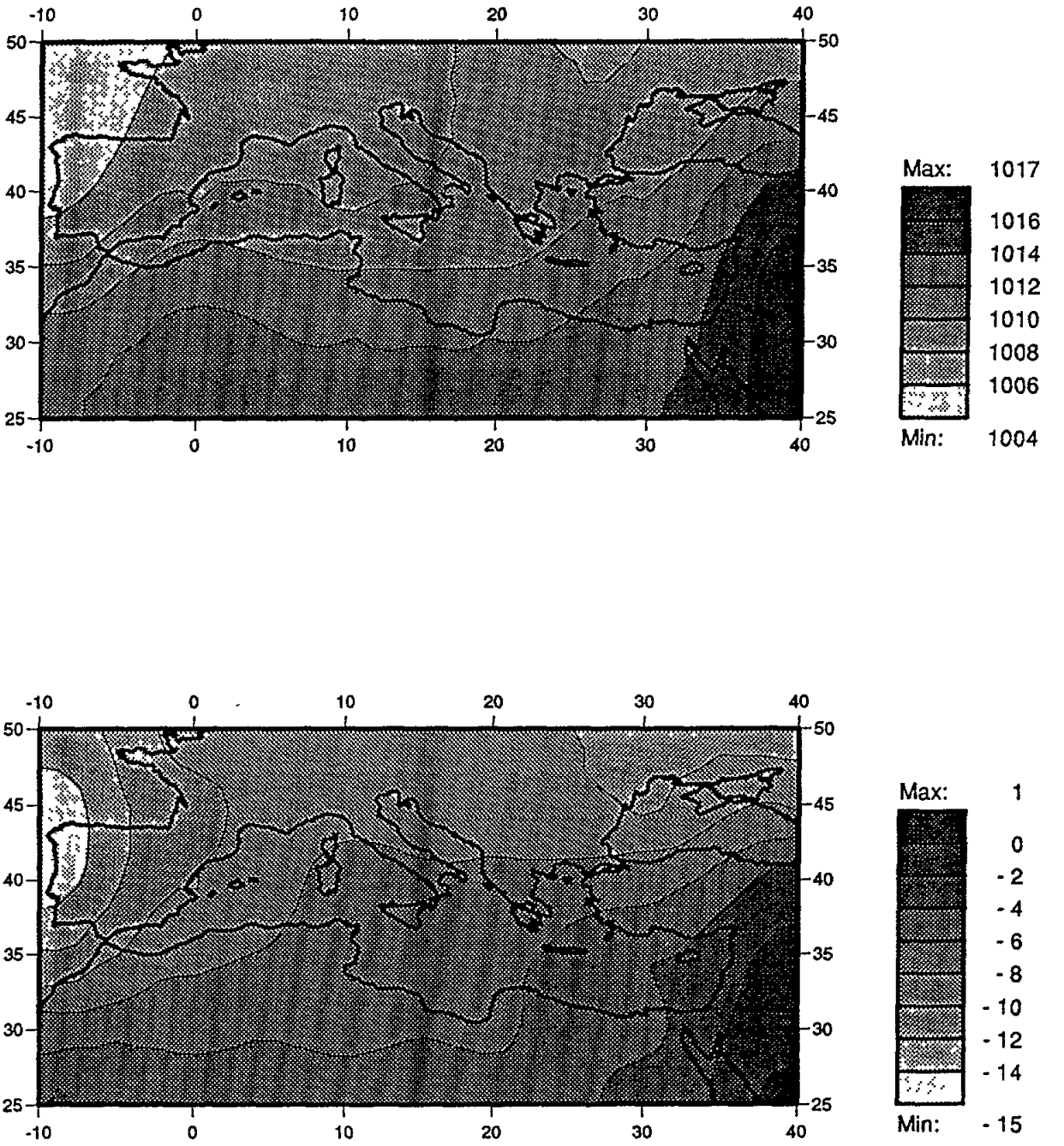

Fig. 2.5 cont. Winter MSLP control run (above) and control/observed differences (below) in mb: OSU GCM

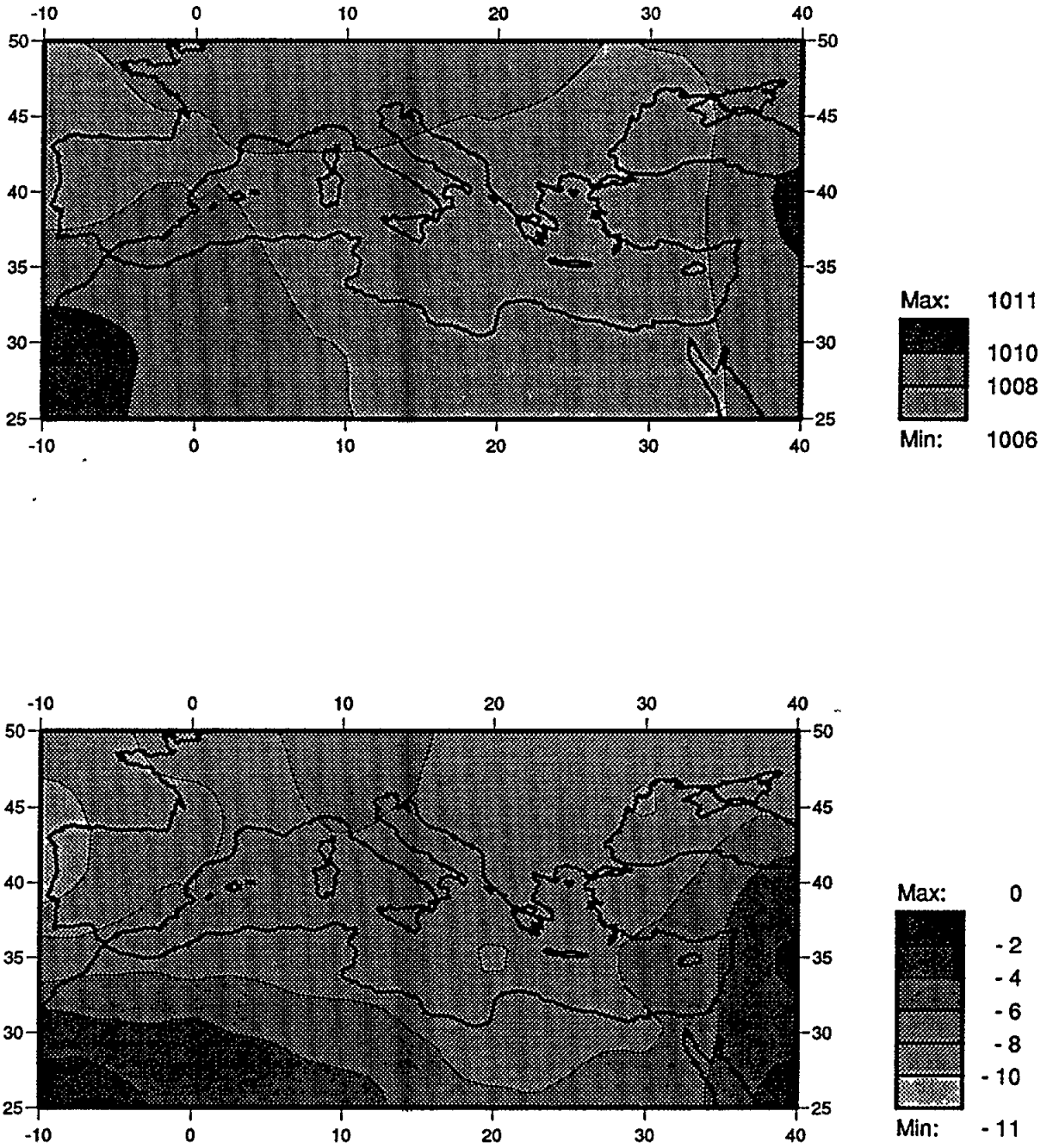

Fig. 2.5 cont. Spring MSLP control run (above) and control/observed differences (below) in mb: OSU GCM

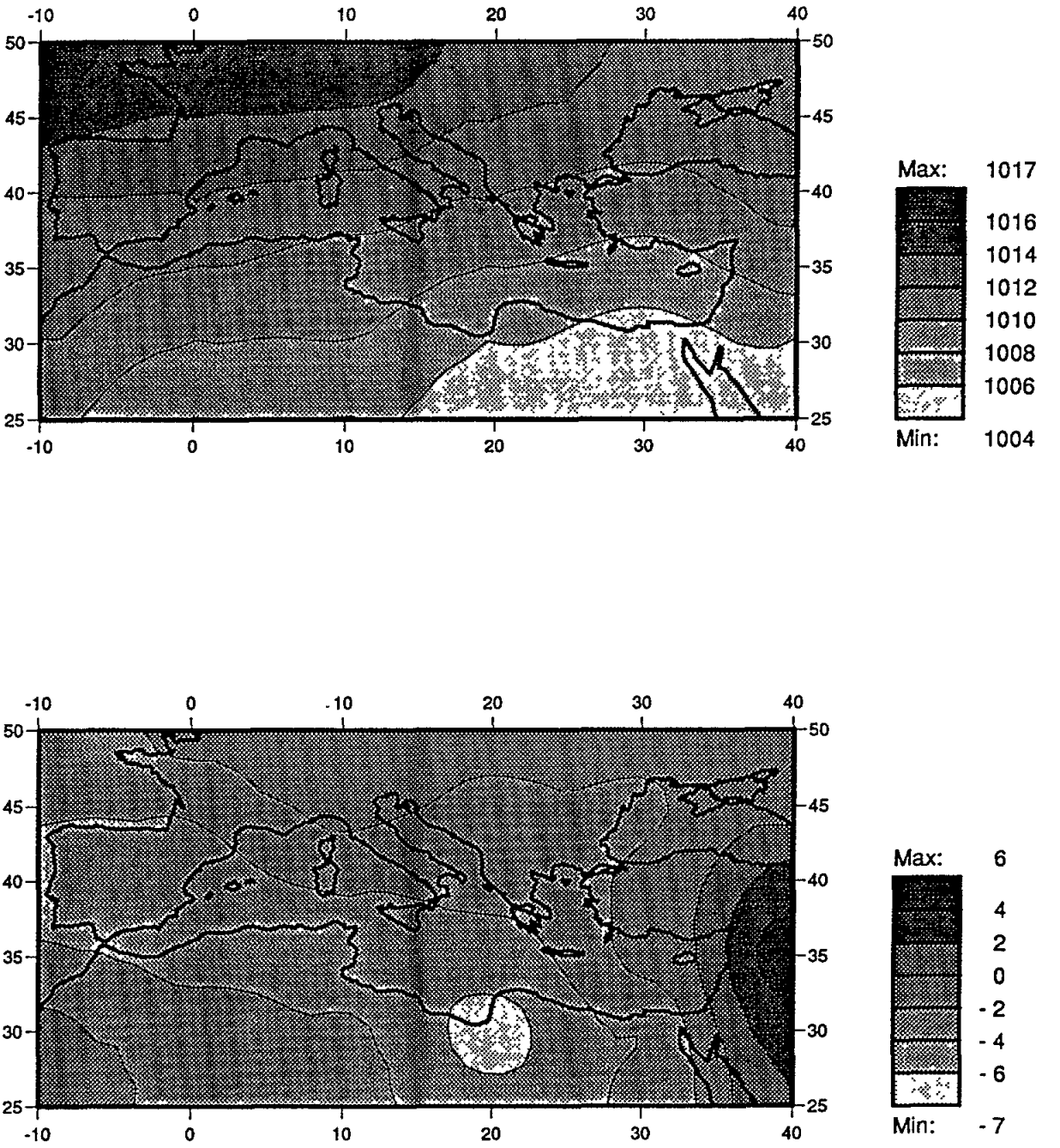

Fig. 2.5 cont. Summer MSLP control run (above) and control/observed differences (below) in mb: OSU GCM

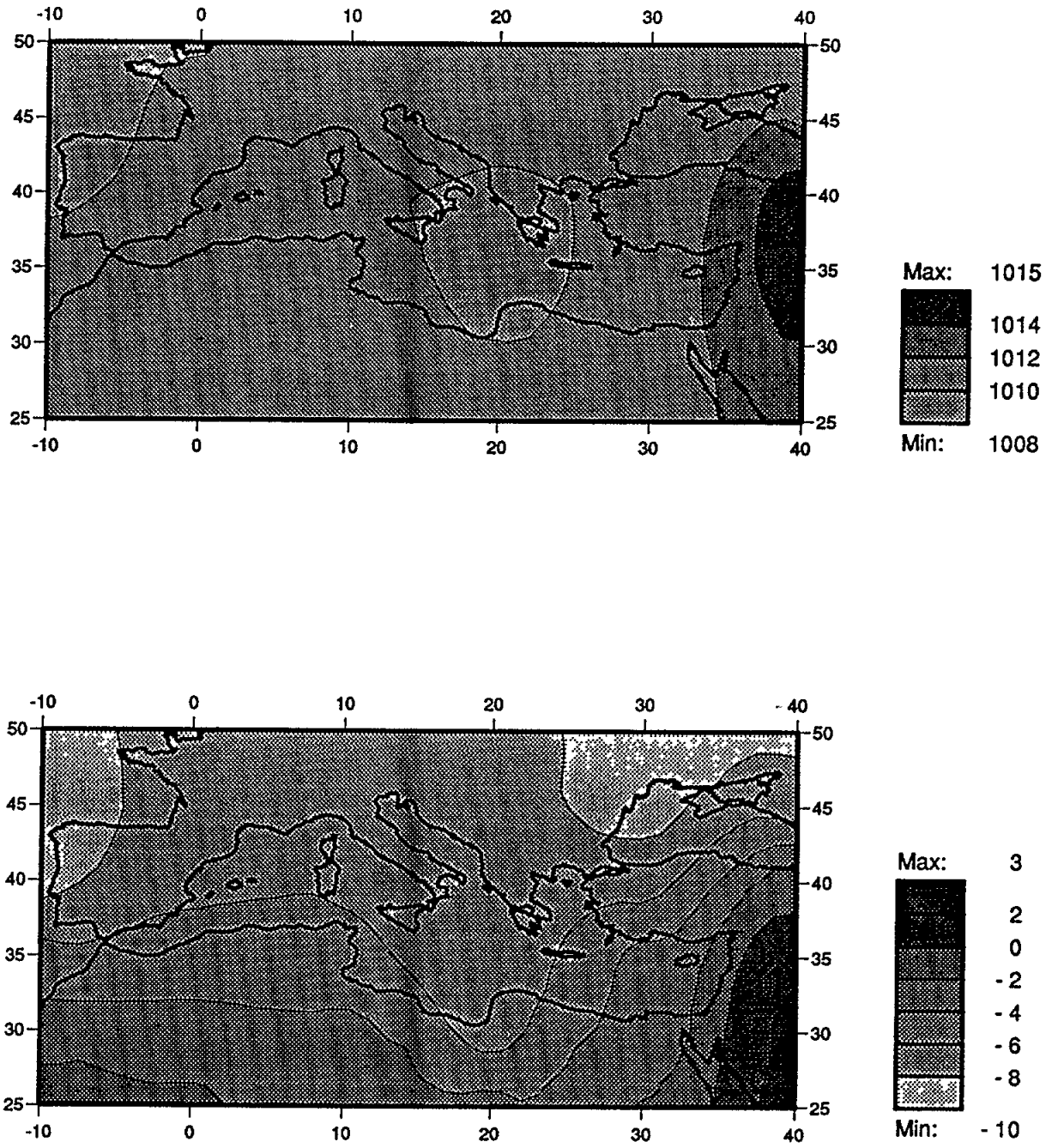

Fig. 2.5 cont. Autumn MSLP control run (above) and control/observed differences (below) in mb: OSU GCM

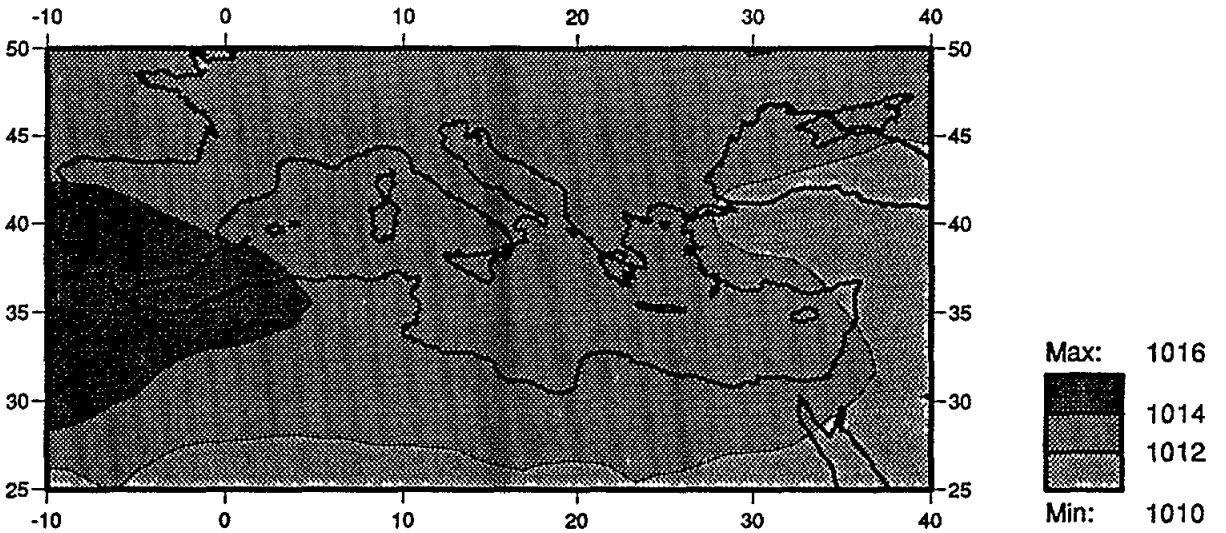

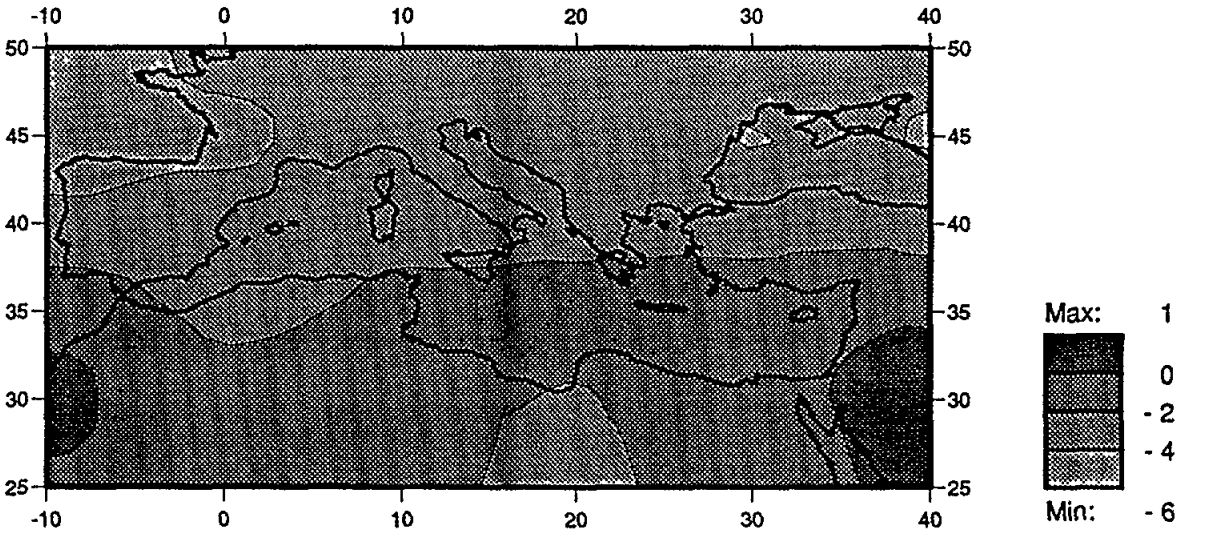

Fig. 2.6 Annual MSLP control run (above) and control/observed differences (below) in mb: UKMO GCM

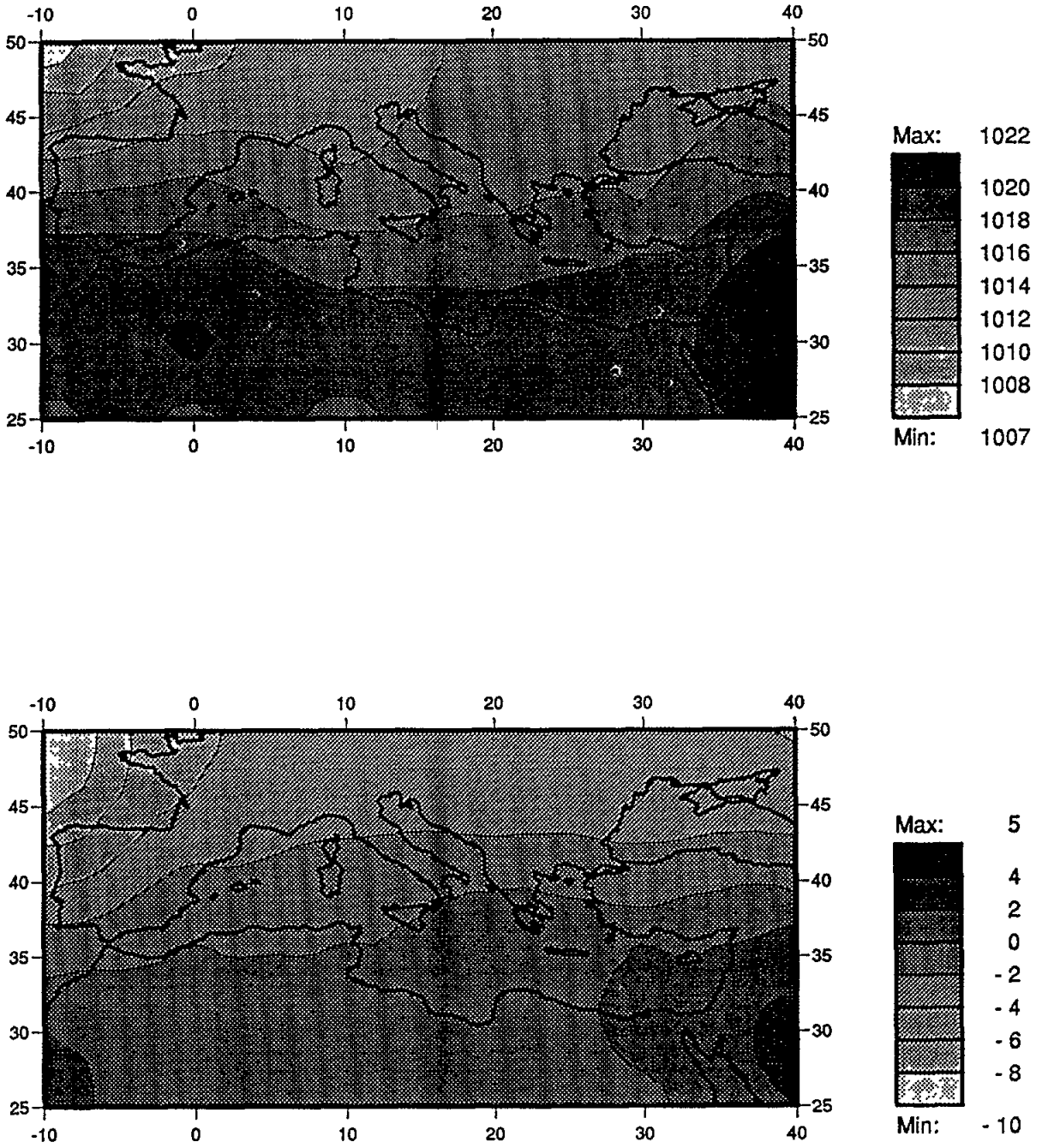

Fig. 2.6 cont. Winter MSLP control run (above) and control/observed differences (below) in mb: UKMO GCM

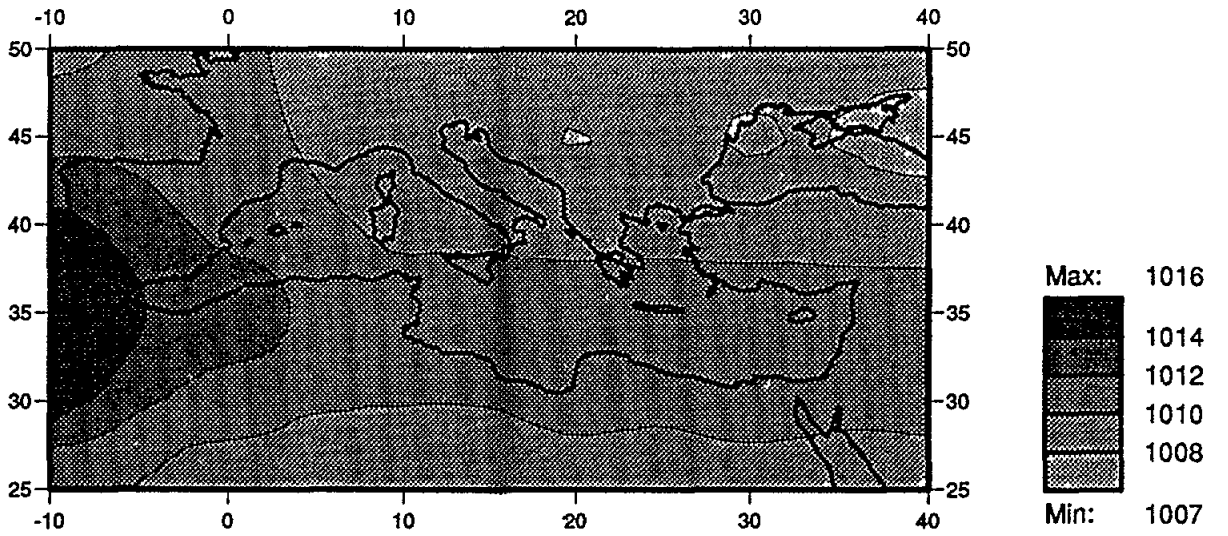

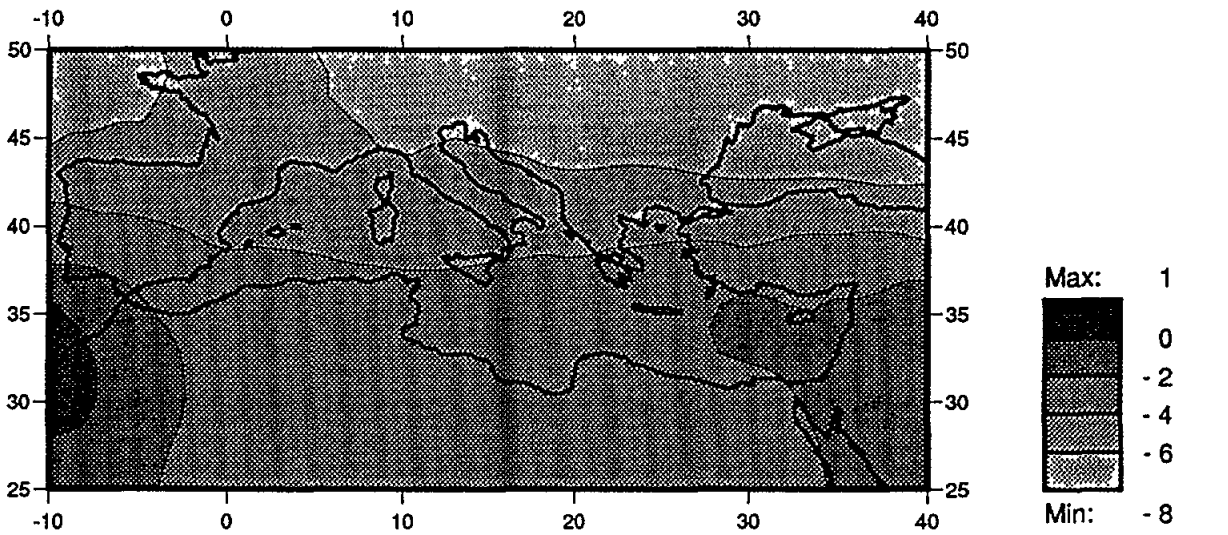

Fig. 2.6 cont. Spring MSLP control run (above) and control/observed differences (below) in mb: UKMO GCM

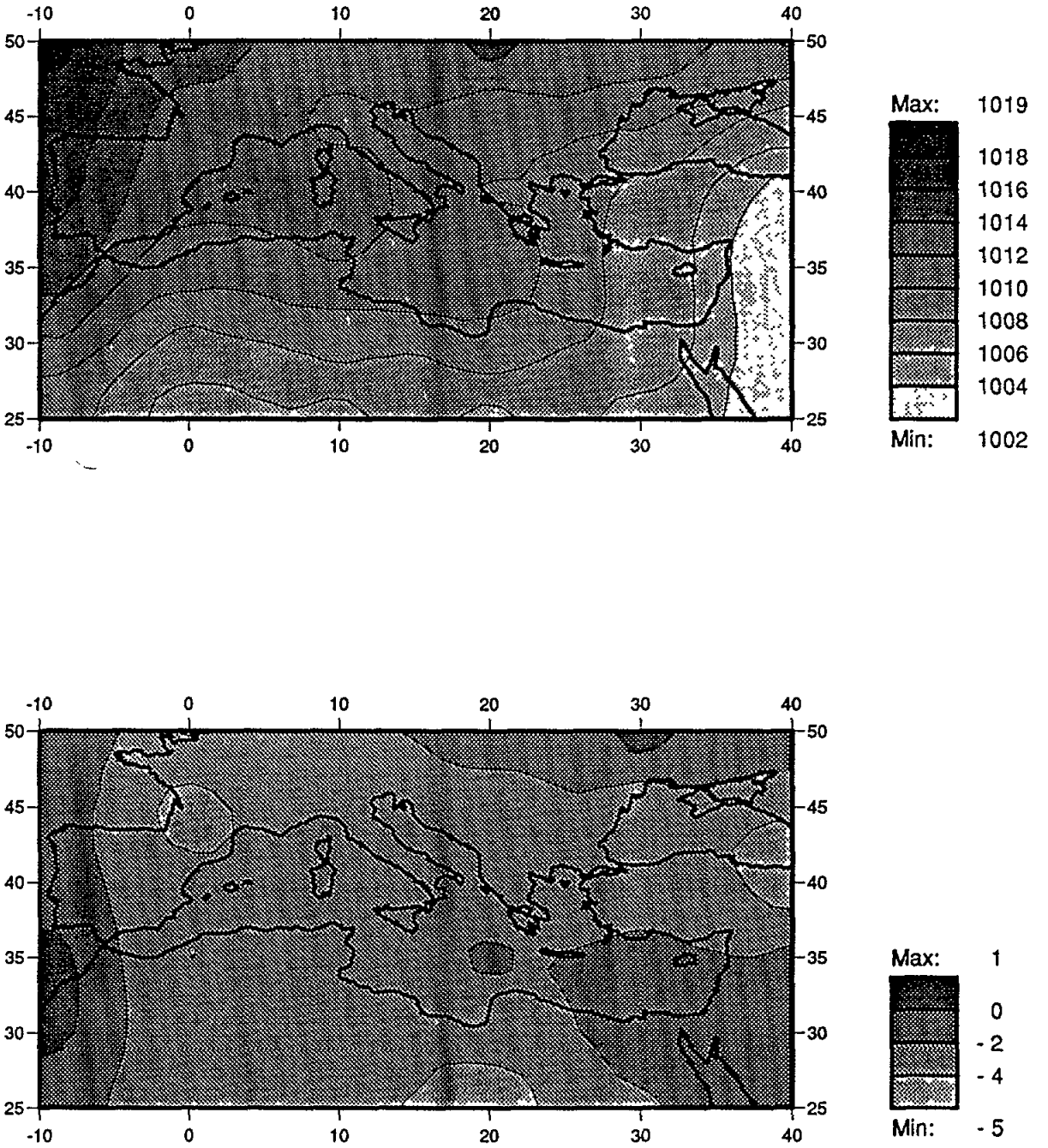

Fig. 2.6 cont. Summer MSLP control run (above) and control/observed differences (below) in mb: UKMO GCM

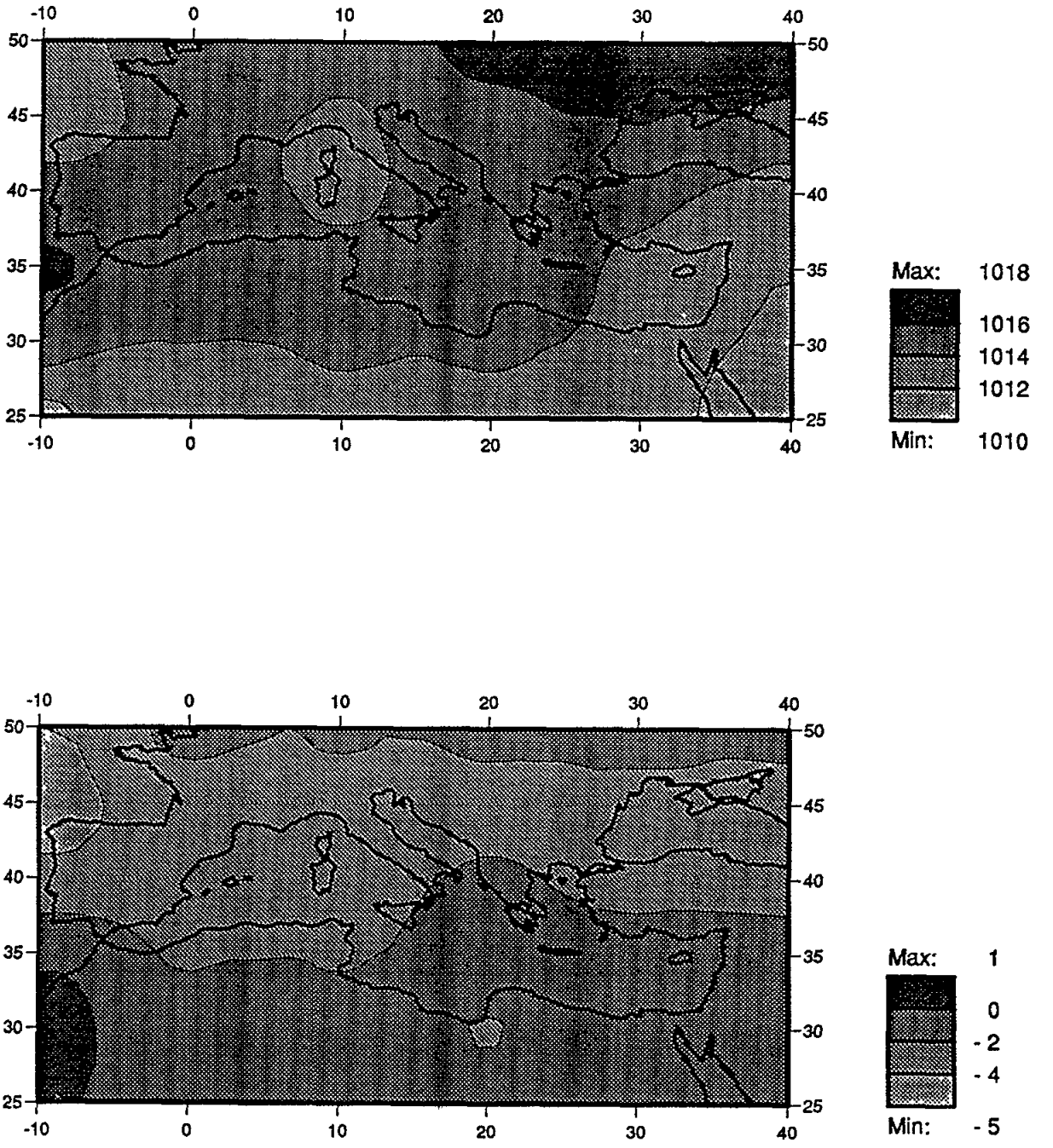

Fig. 2.6 cont. Autumn MSLP control run (above) and control/observed differences (below) in mb: UKMO GCM

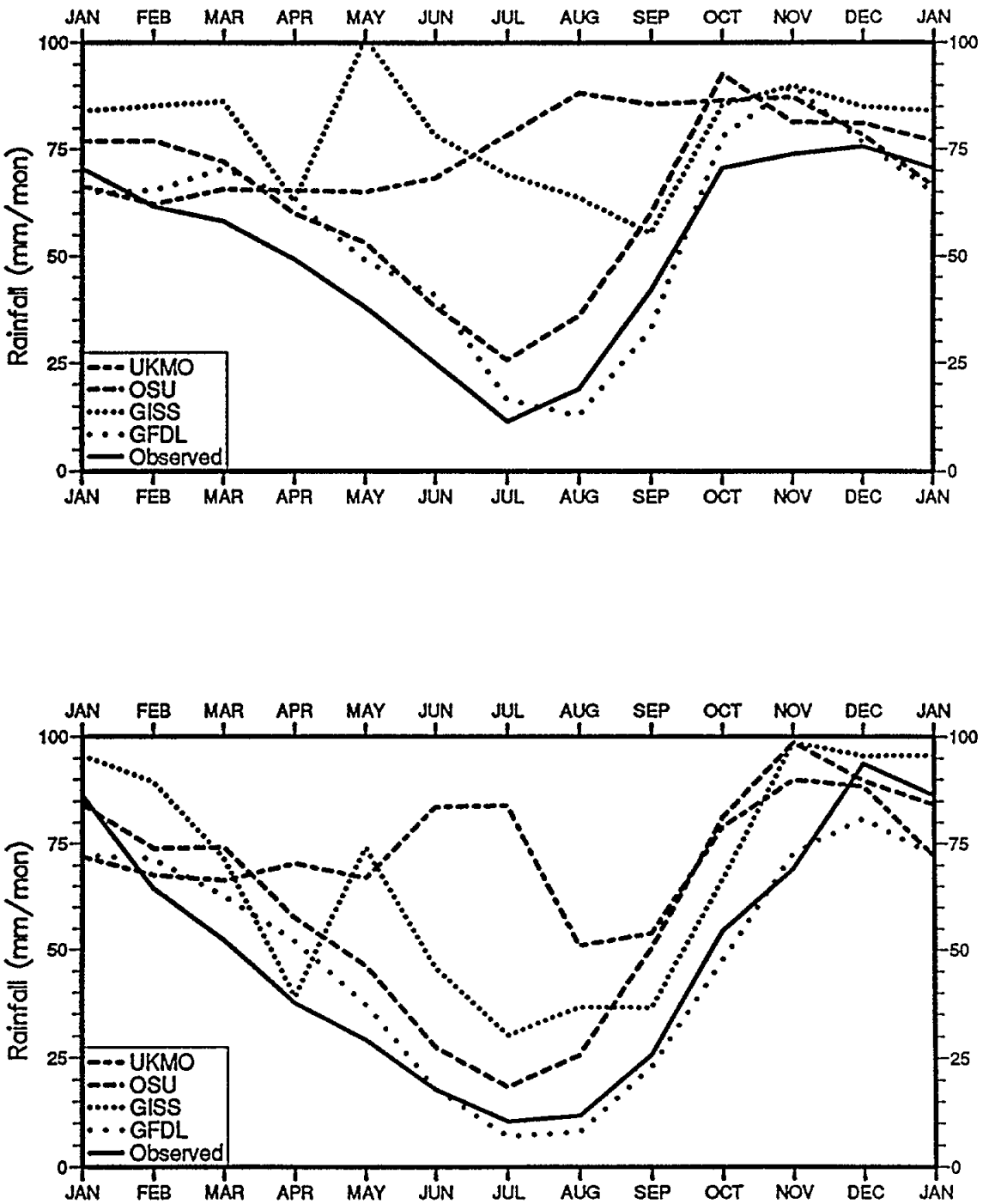

Fig. 2.7 Seasonal cycle of observed and control run precipitation in the western (above) and eastern (below) Mediterranean Basin

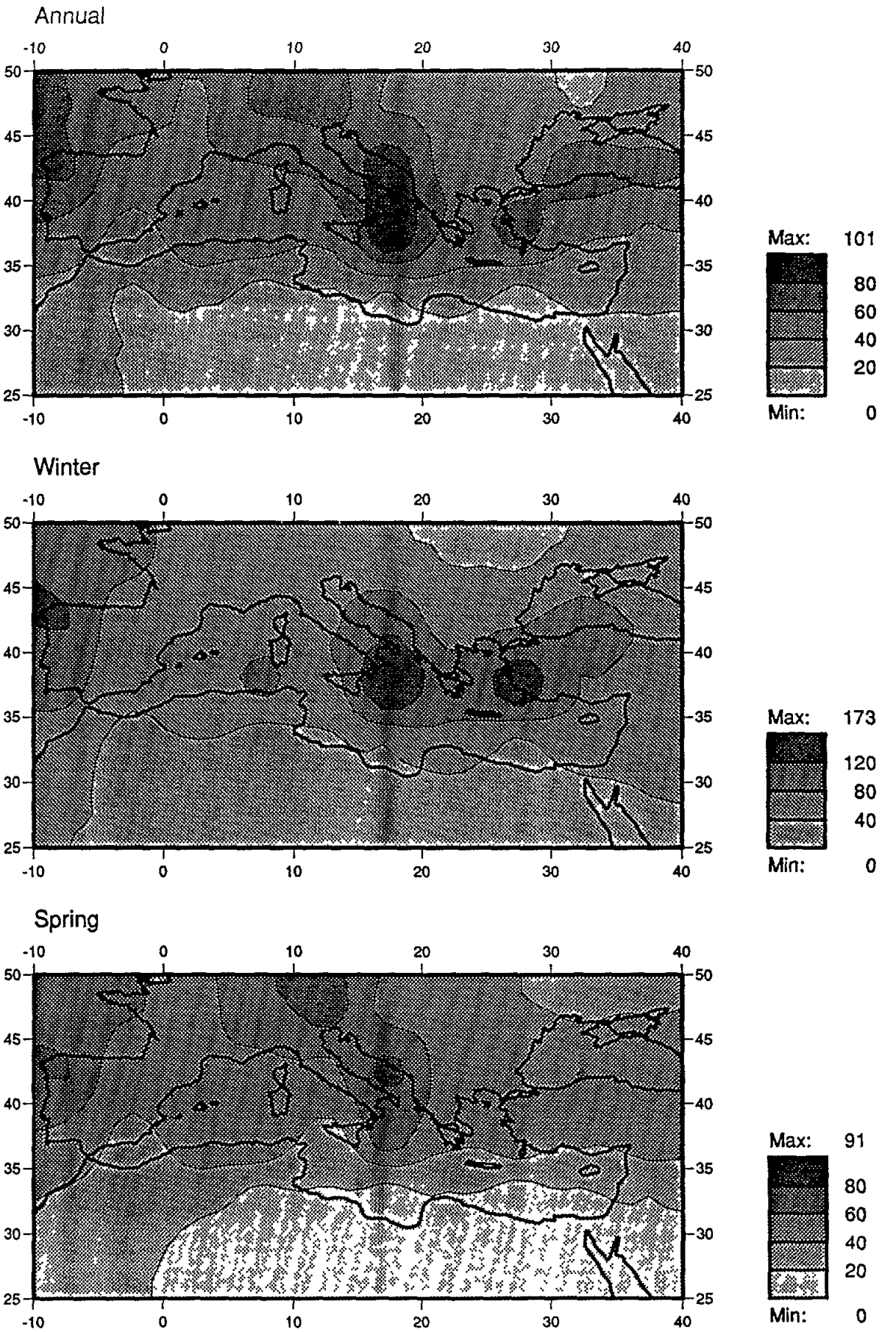

Fig. 2.8 Observed precipitation (mm/month)

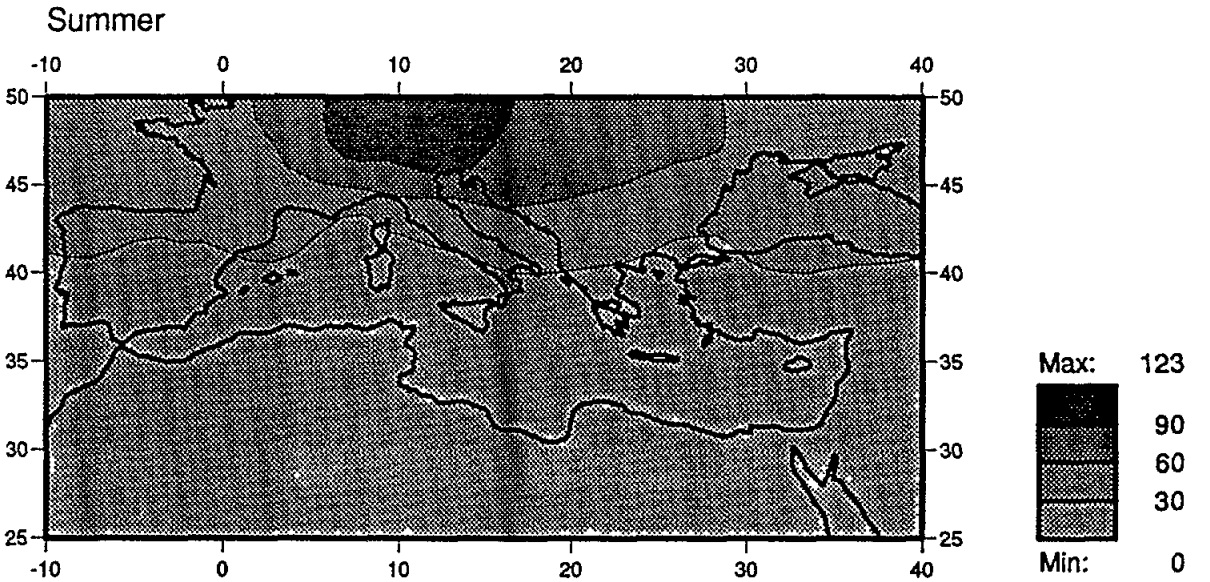
Summer
-10
0
10
20
30
40
50
45
40
35
30
25
Max: 123
90
60
30
Min: 0

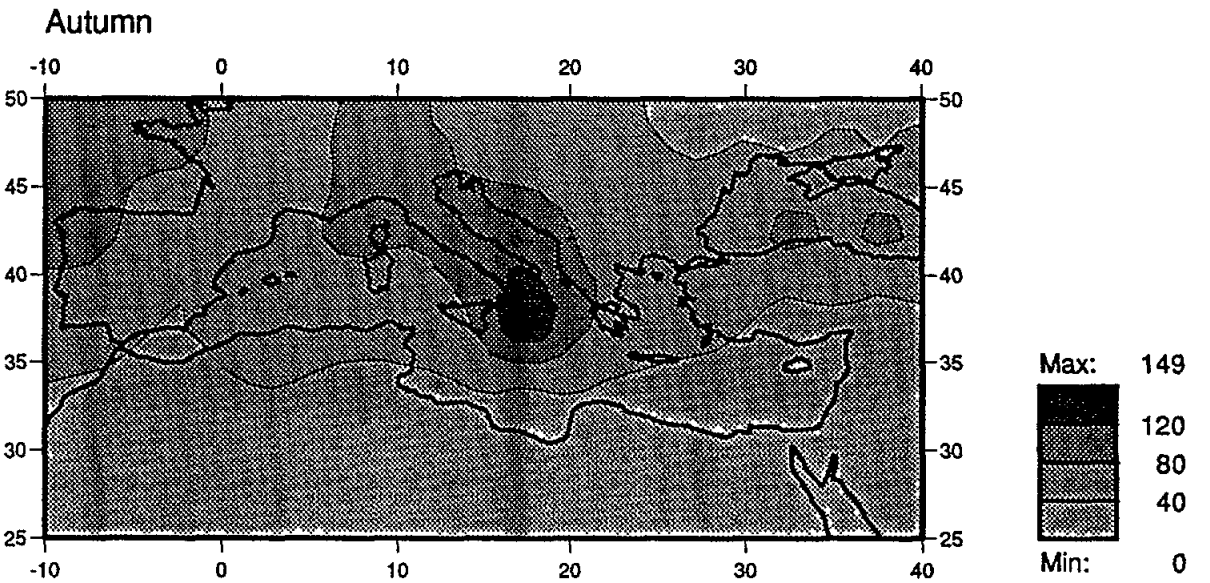
Autumn
-10
0
10
20
30
40
50
45
40
35
30
25
Max: 149
120
80
40
Min: 0

Fig. 2.8 cont.

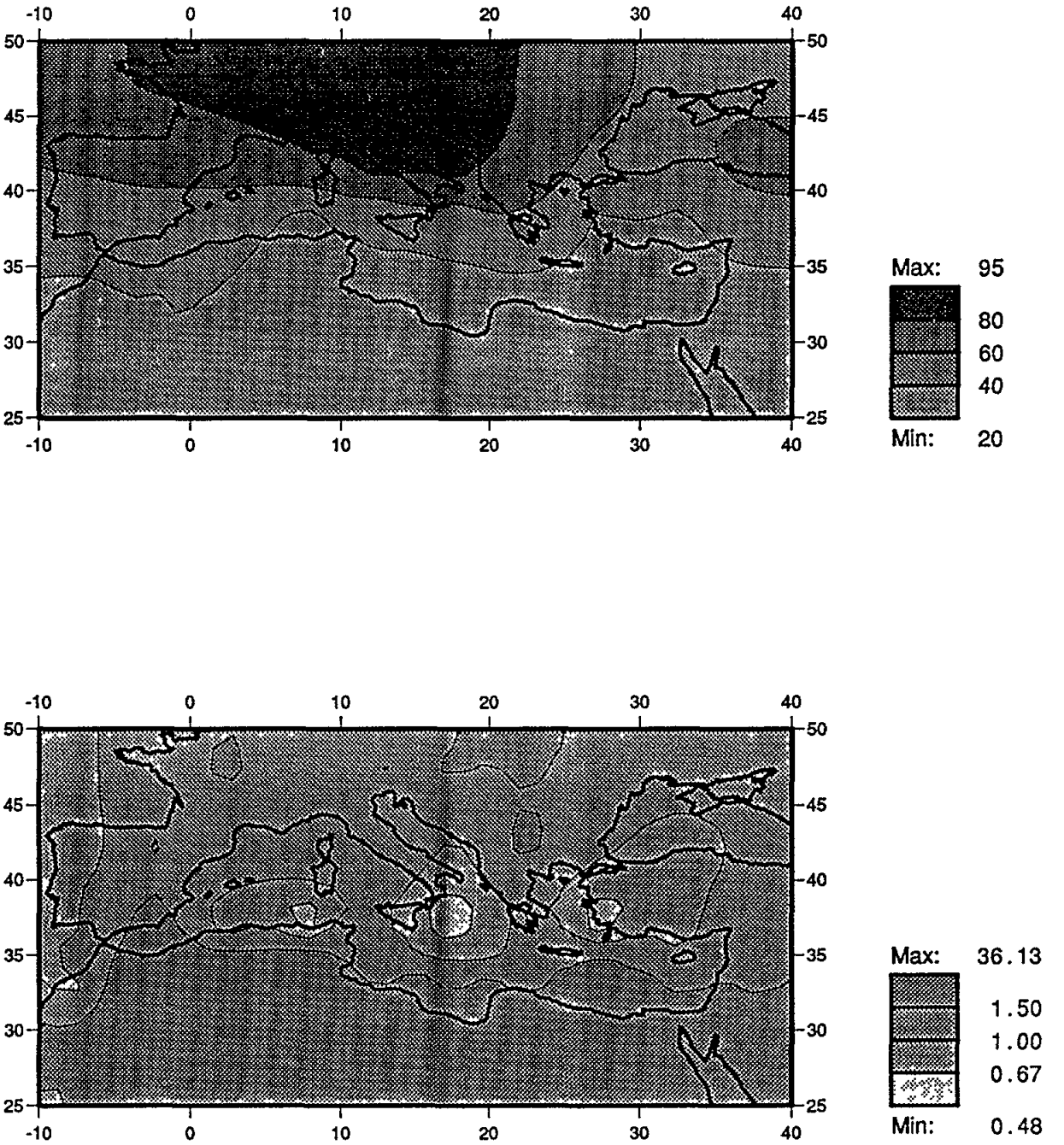

Fig. 2.9 Annual control run precipitation (above, mm/month) and modelled-to-observed precipitation ratios (below): GFDL GCM

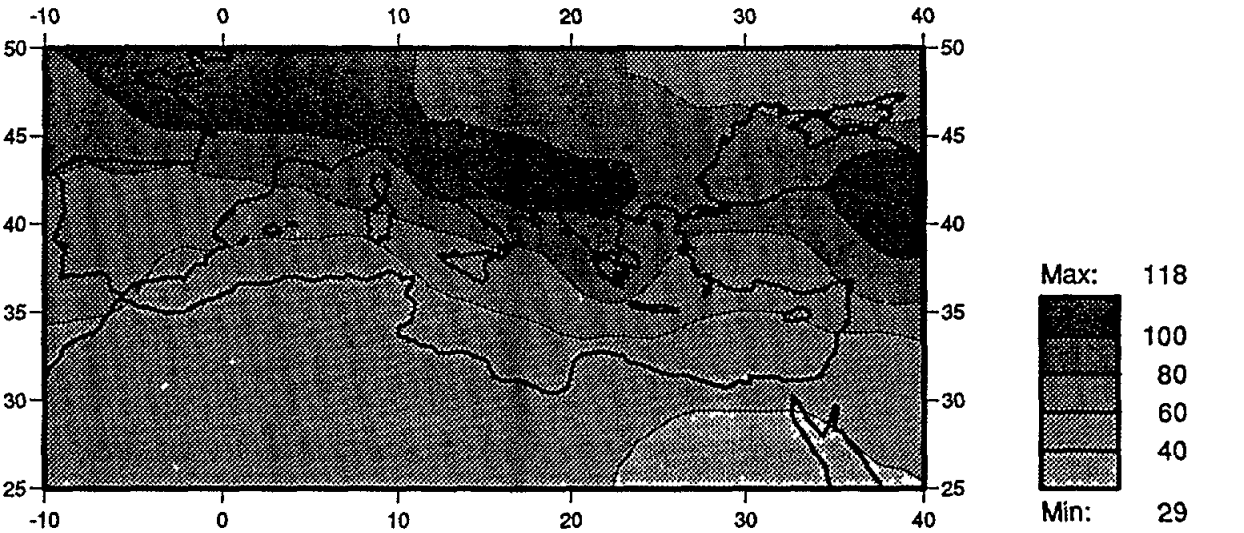

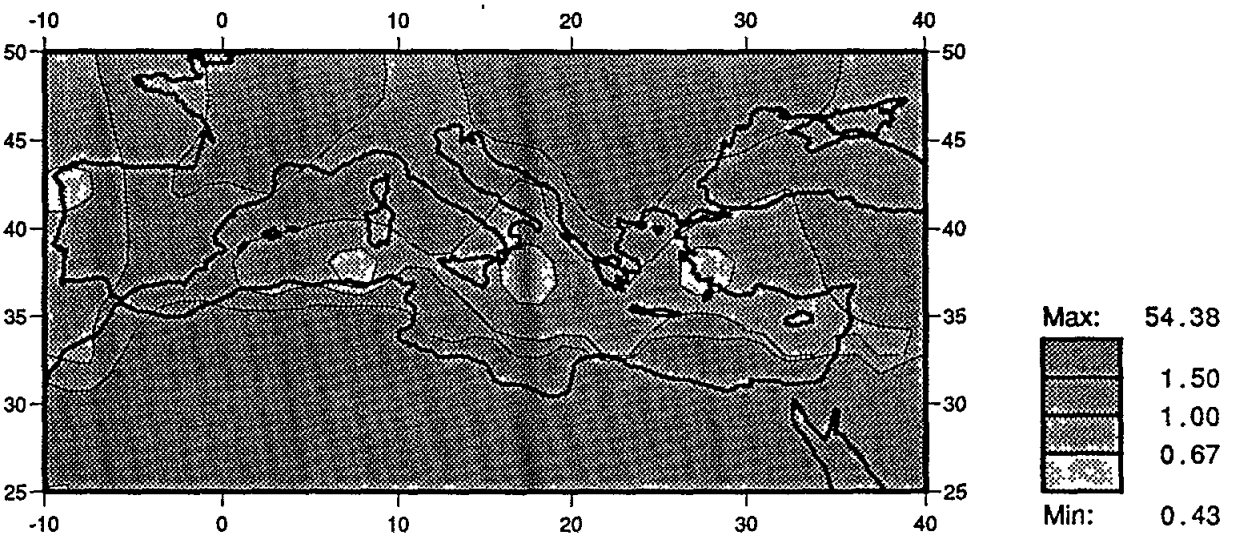

Fig. 2.9 cont. Winter control run precipitation (above, mm/month) and modelled-to-observed precipitation ratios (below): GFDL GCM

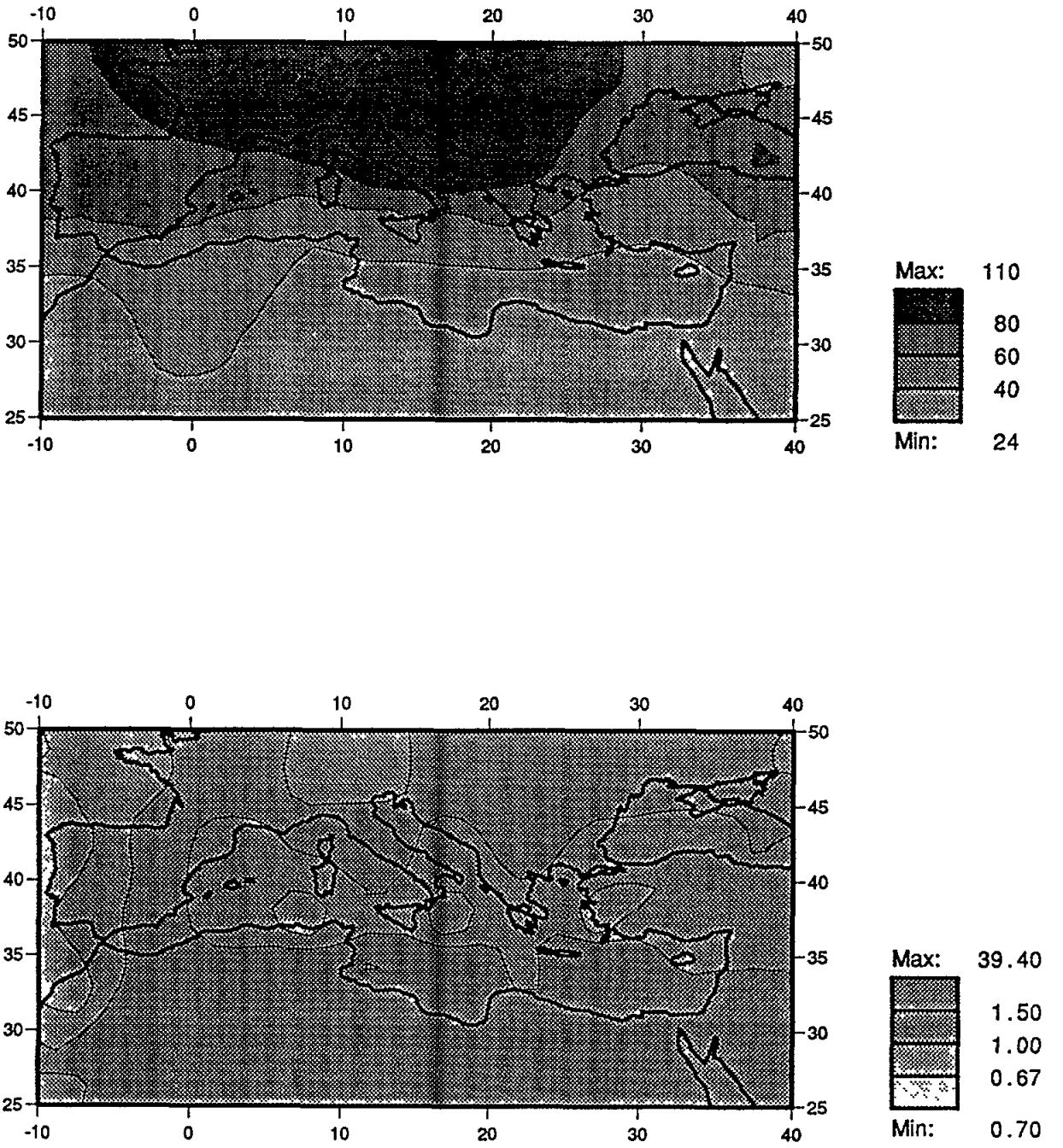

Fig. 2.9 cont. Spring control run precipitation (above, mm/month) and modelled-to-observed precipitation ratios (below): GFDL GCM

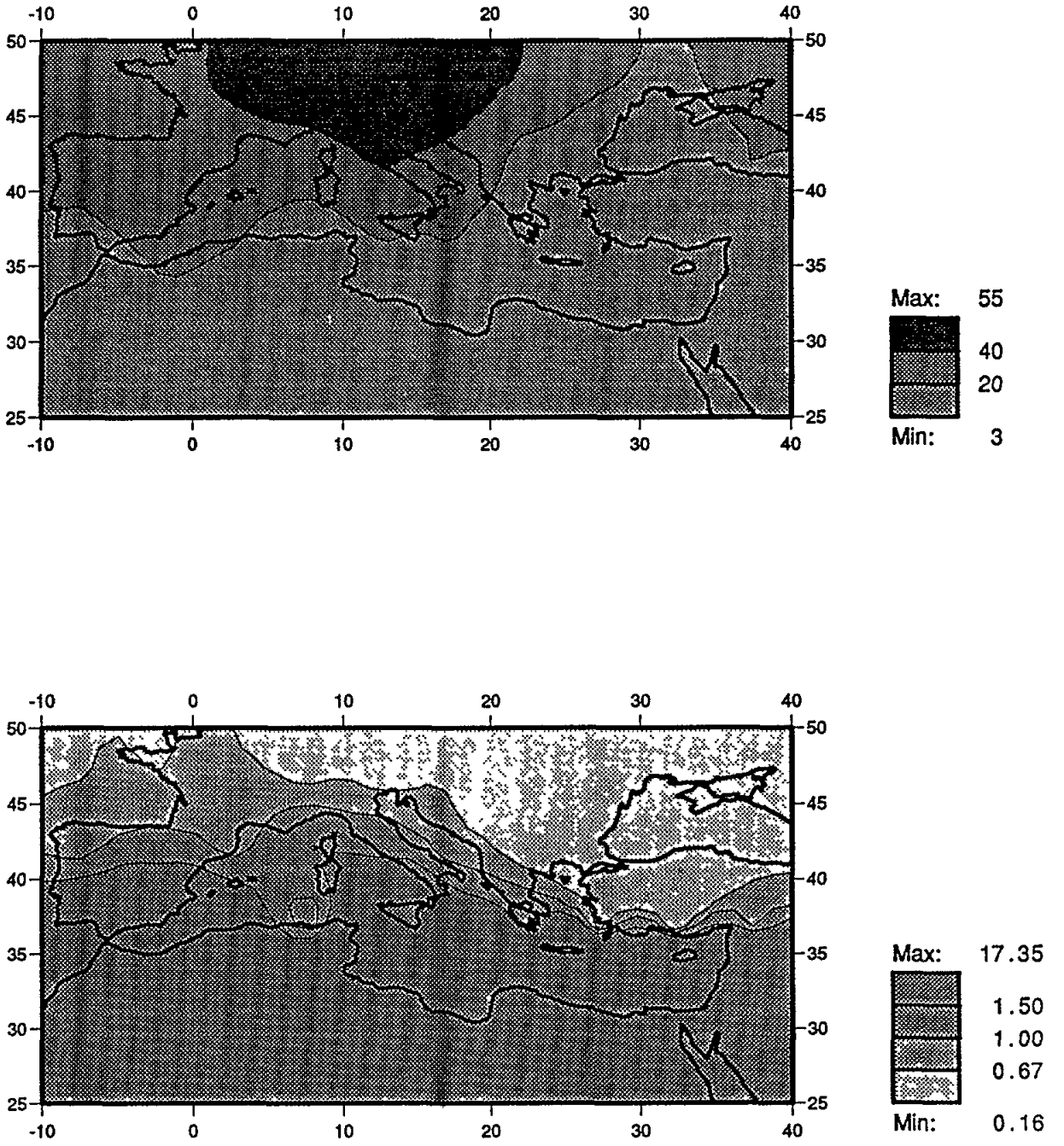

Fig. 2.9 cont. Summer control run precipitation (above, mm/month) and modelled-to-observed precipitation ratios (below): GFDL GCM

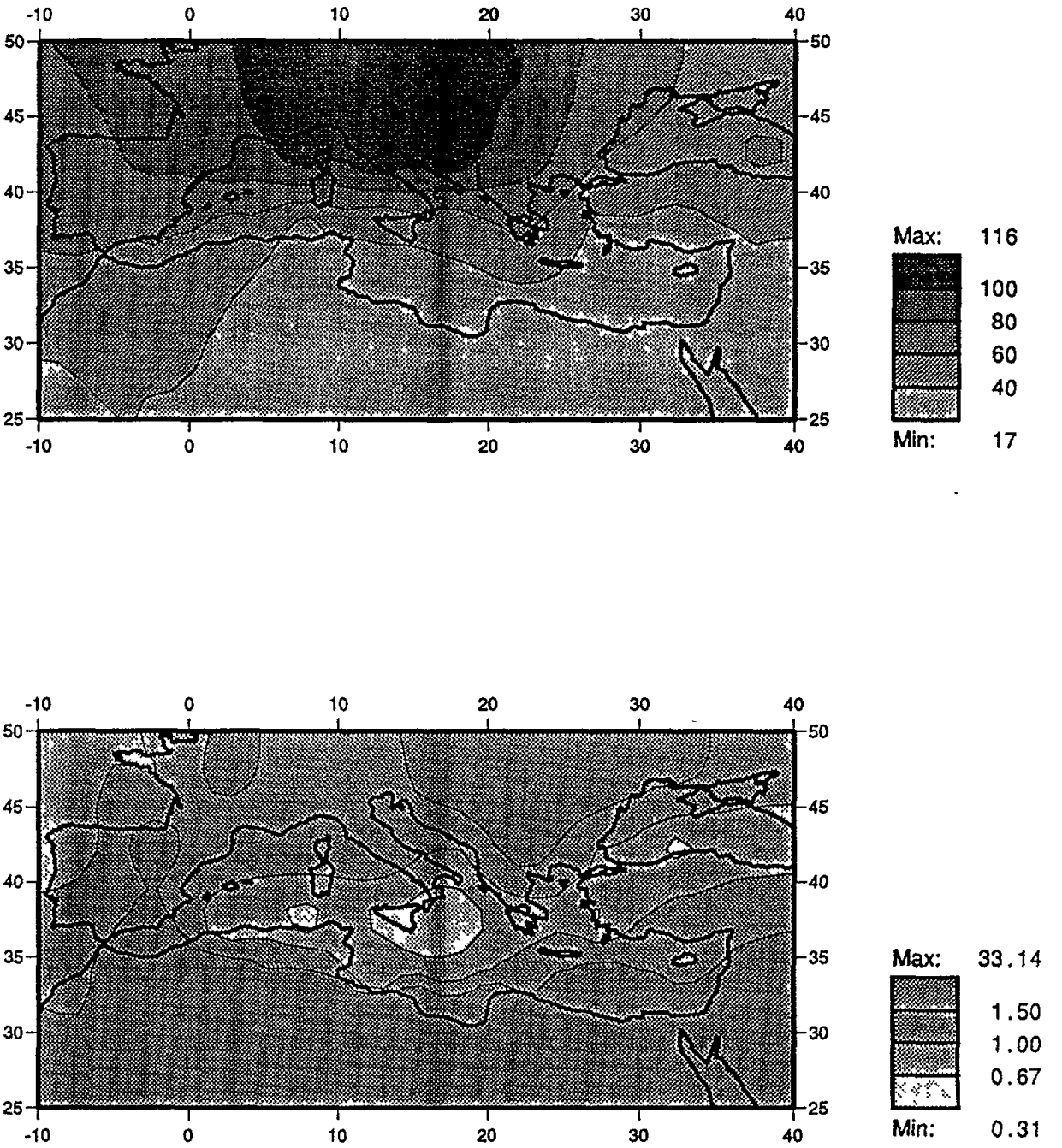

Fig. 2.9 *cont.* Autumn control run precipitation (above, mm/month) and modelled-to-observed precipitation ratios (below): GFDL GCM

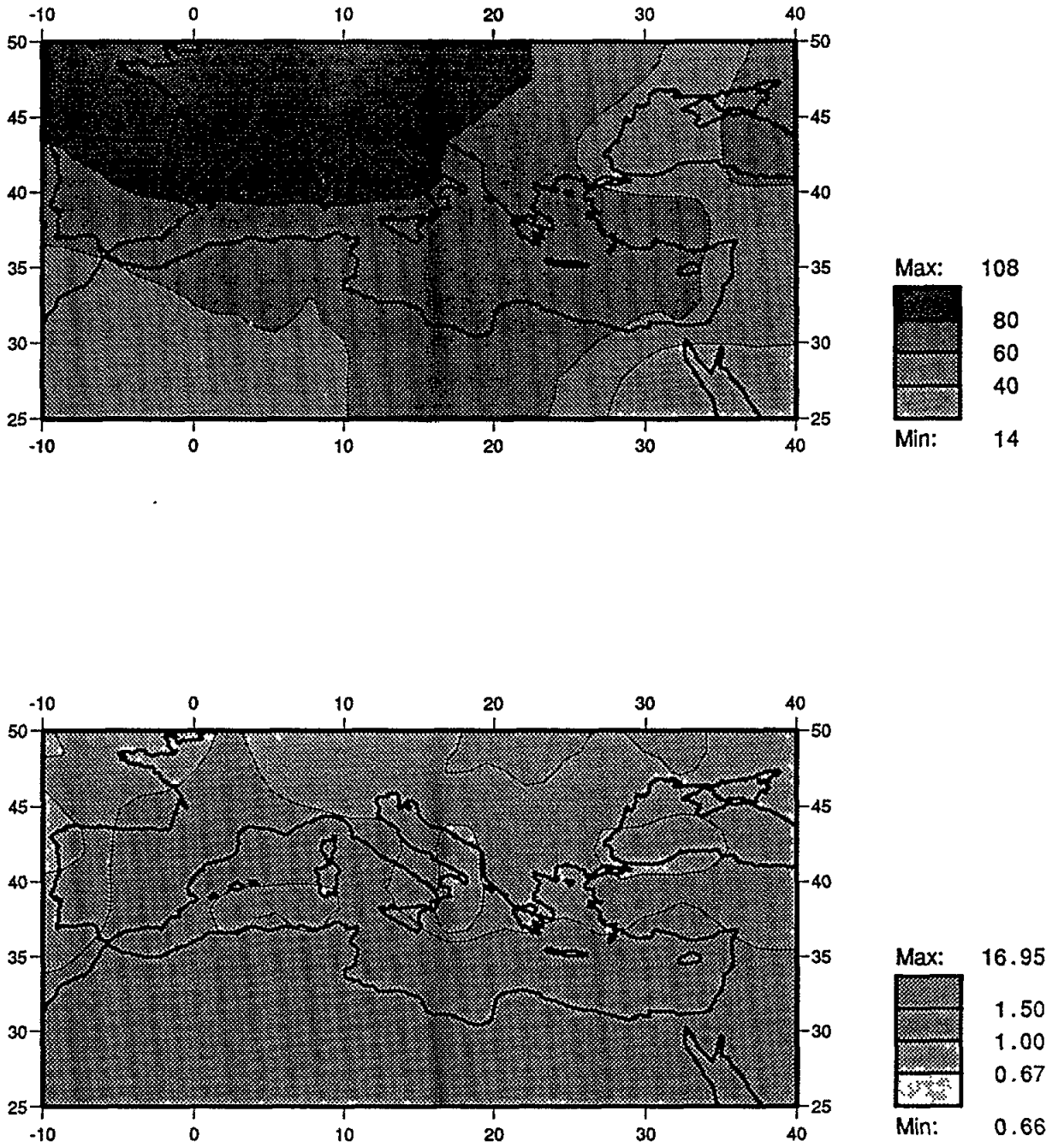

Fig. 2.10 Annual control run precipitation (above, mm/month) and modelled-to-observed precipitation ratios (below): GISS GCM

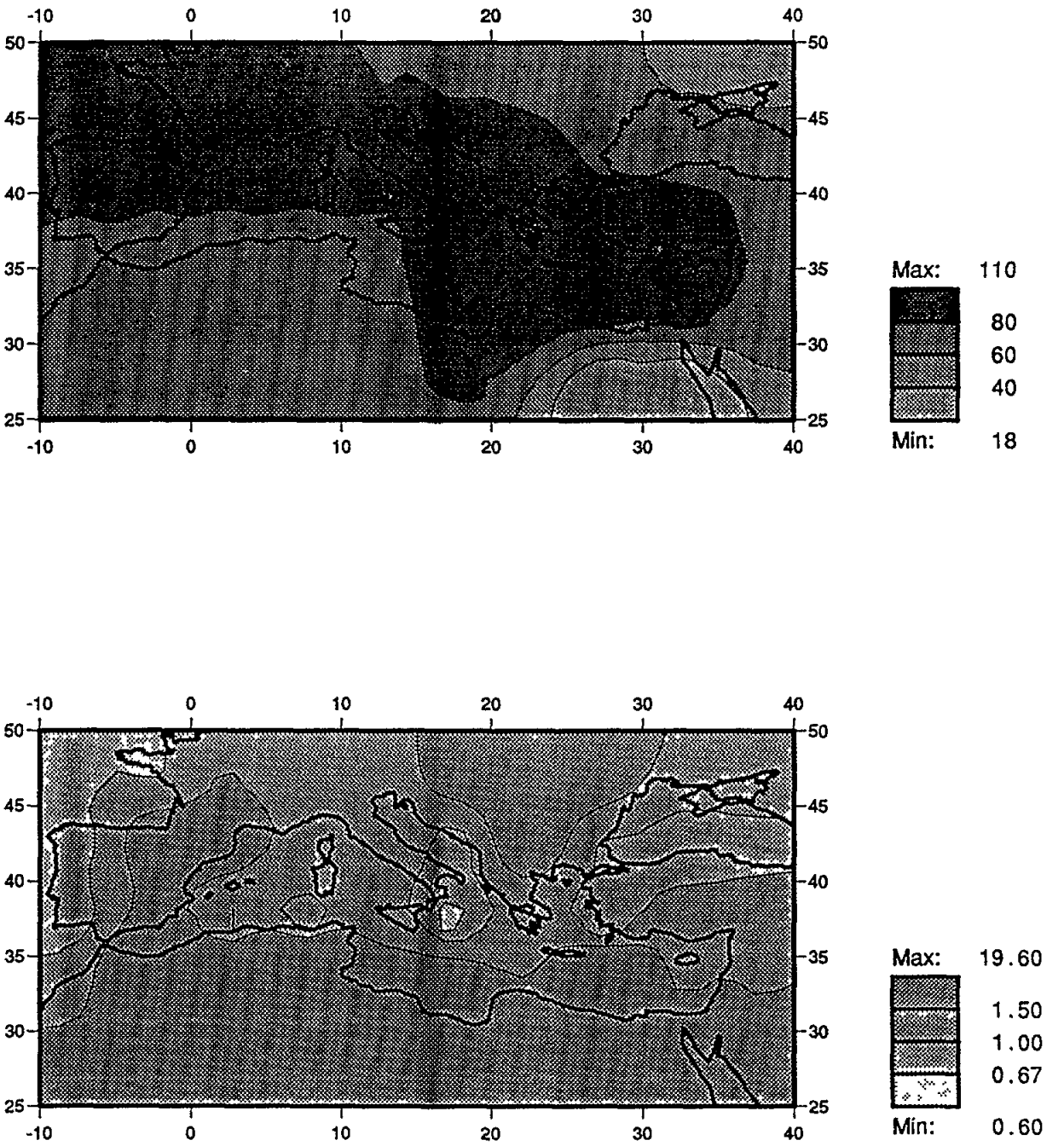

Fig. 2.10 cont. Winter control run precipitation (above, mm/month) and modelled-to-observed precipitation ratios (below): GISS GCM

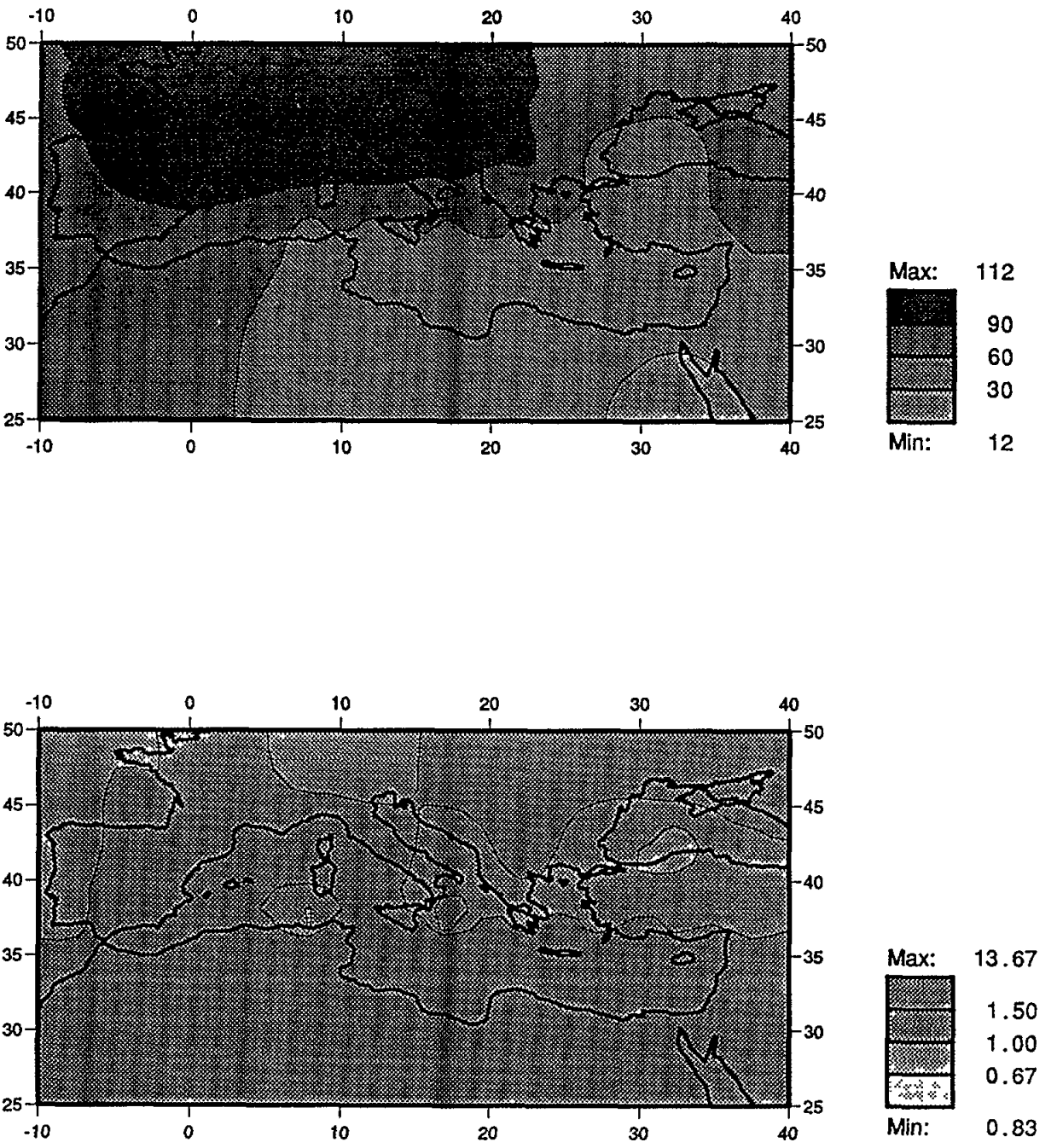

Fig. 2.10 cont. Spring control run precipitation (above, mm/month) and modelled-to-observed precipitation ratios (below): GISS GCM

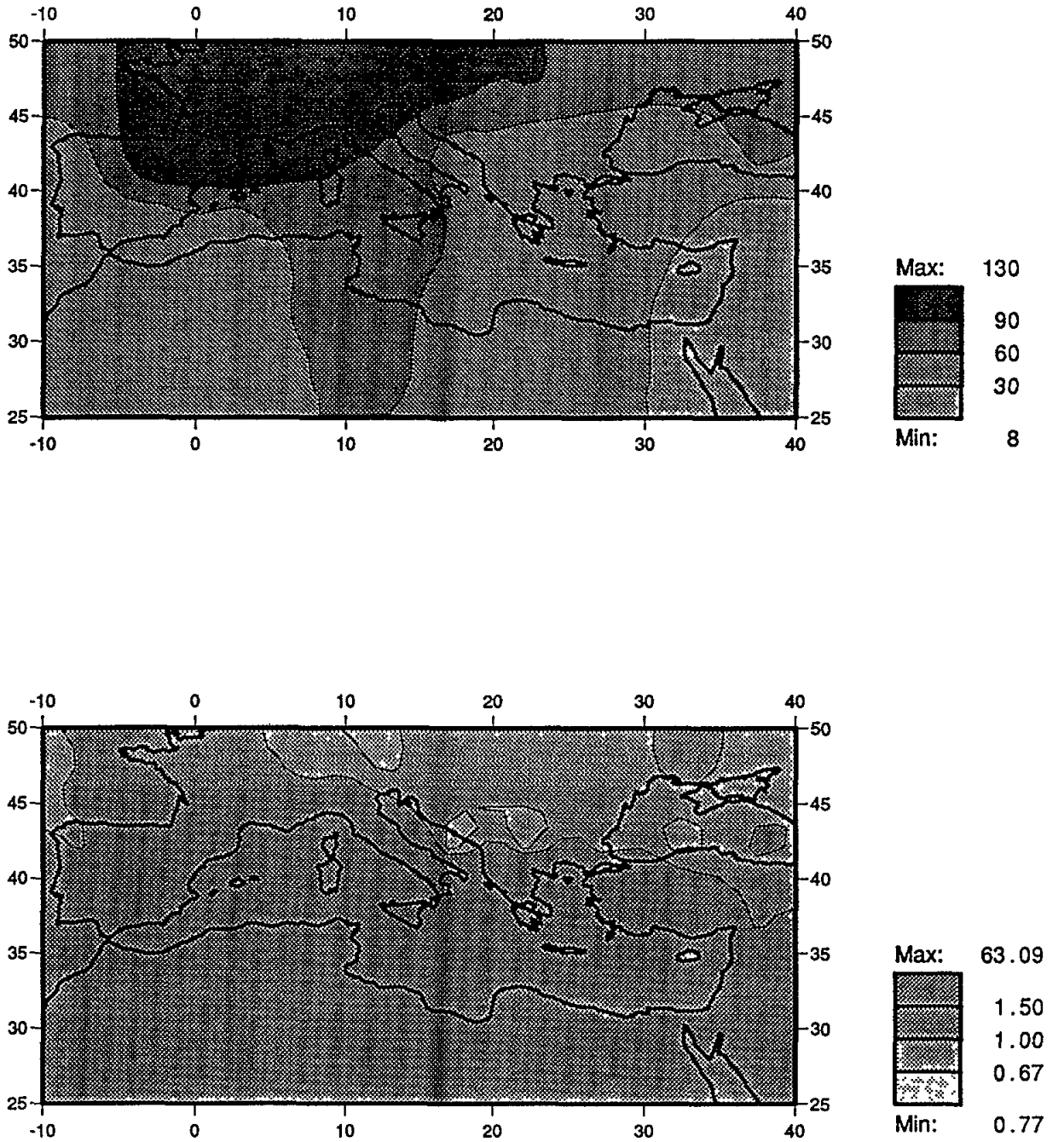

Fig. 2.10 cont. Summer control run precipitation (above, mm/month) and modelled-to-observed precipitation ratios (below): GISS GCM

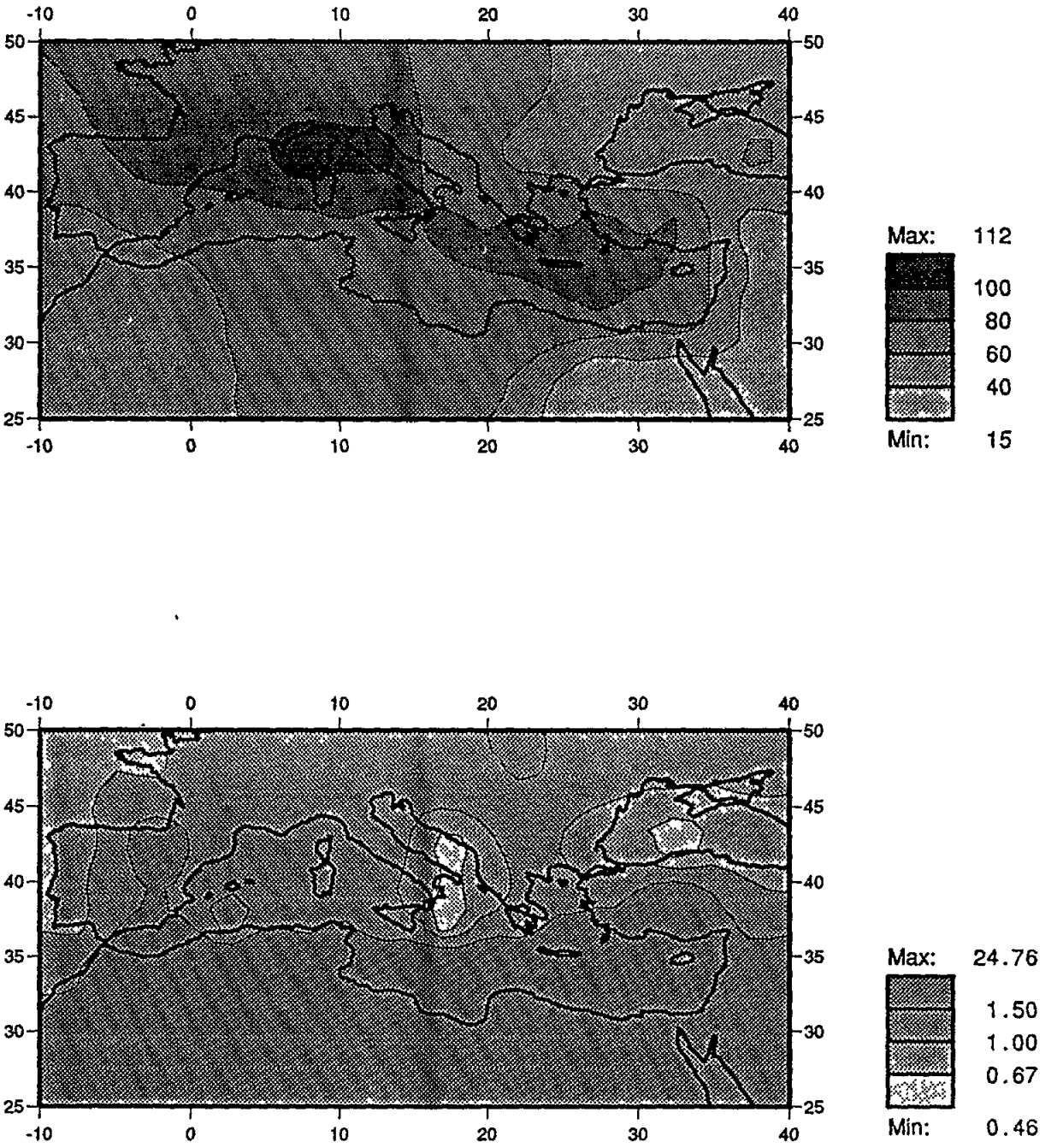

Fig. 2.10 cont. Autumn control run precipitation (above, mm/month) and modelled-to-observed precipitation ratios (below): GISS GCM

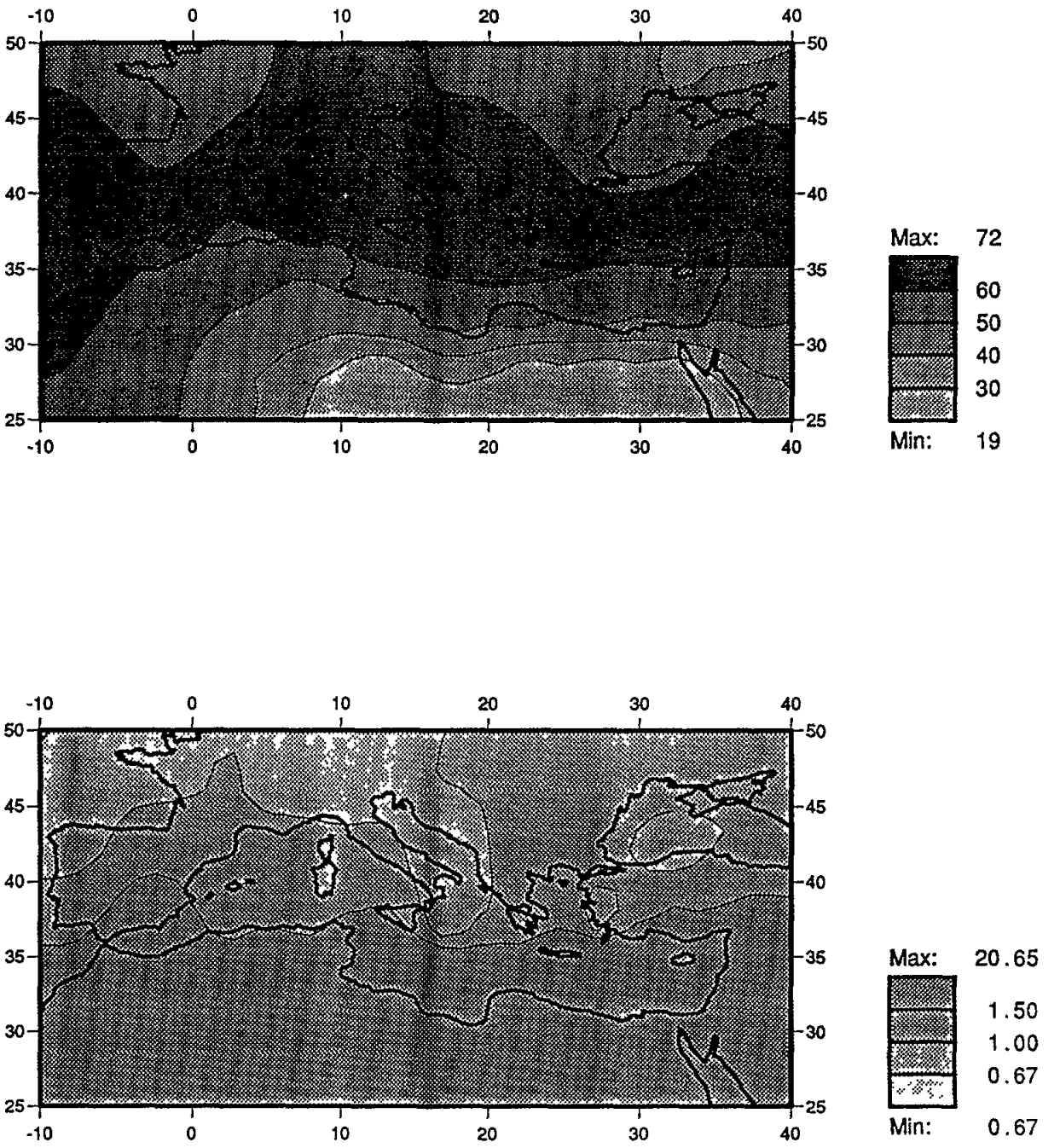

Fig. 2.11 Annual control run precipitation (above, mm/month) and modelled-to-observed precipitation ratios (below): OSU GCM

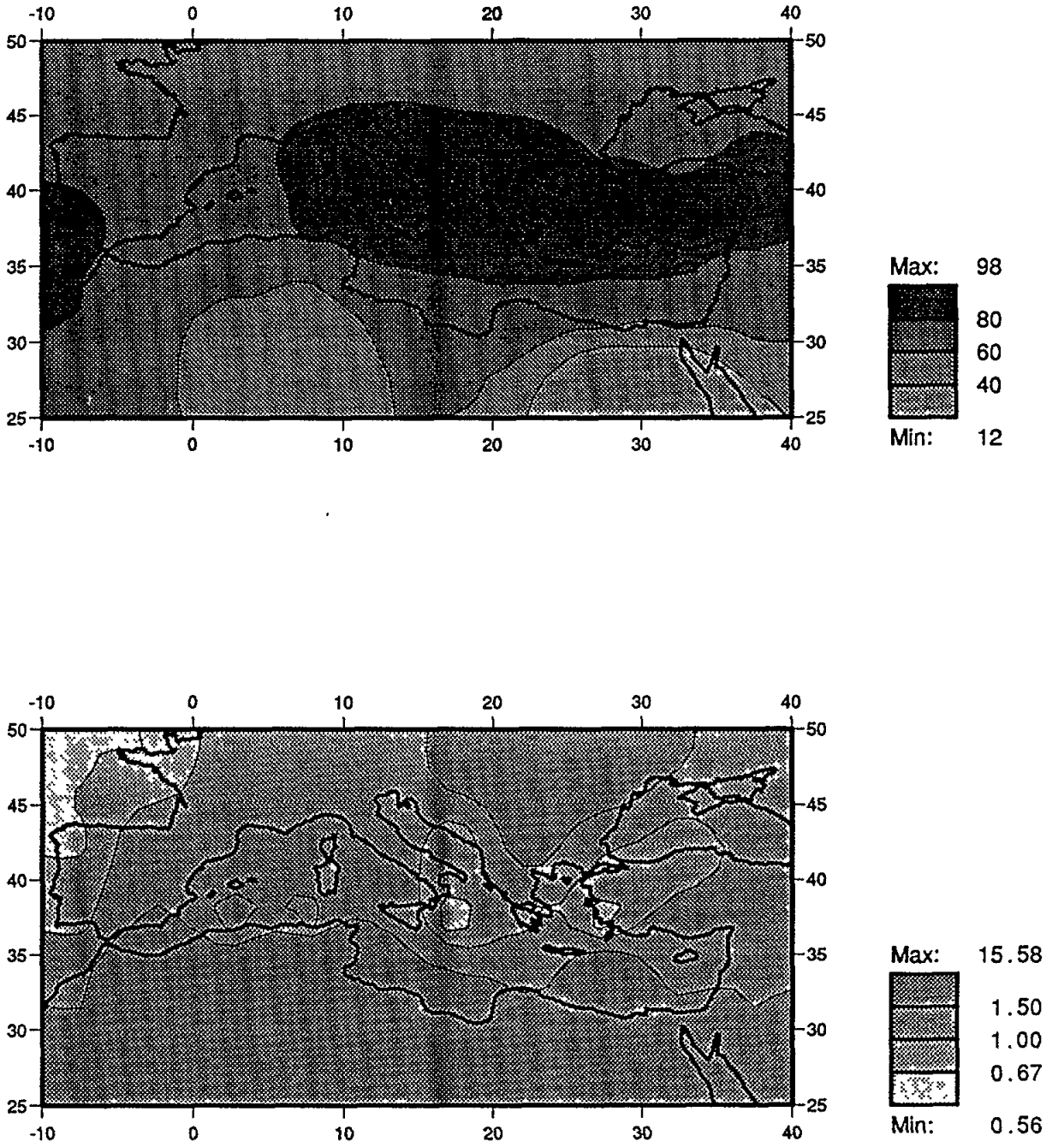

Fig. 2.11 cont. Winter control run precipitation (above, mm/month) and modelled-to-observed precipitation ratios (below): OSU GCM

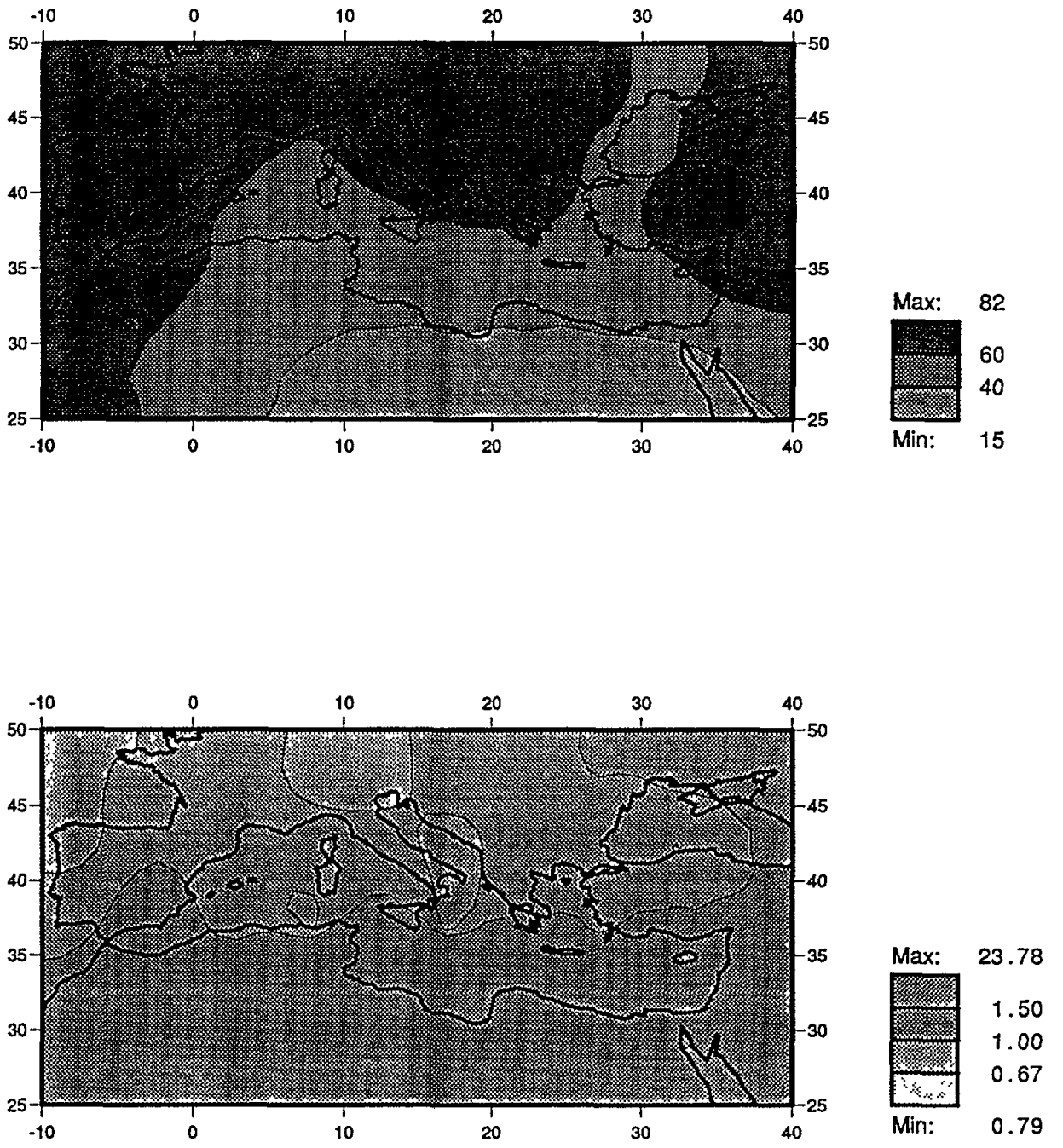

Fig. 2.11 cont. Spring control run precipitation (above, mm/month) and modelled-to-observed precipitation ratios (below): OSU GCM

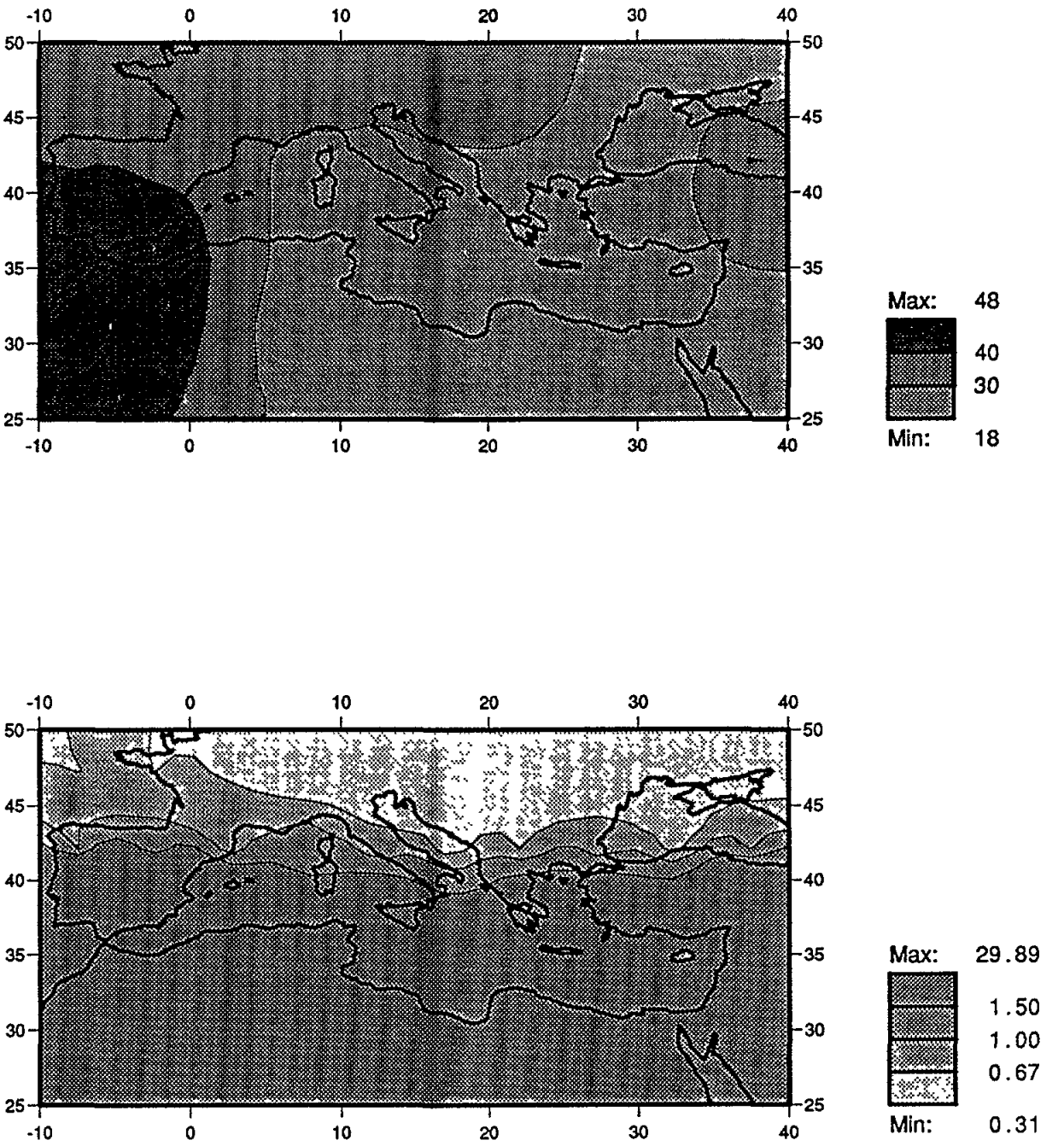

Fig. 2.11 cont. Summer control run precipitation (above, mm/month) and modelled-to-observed precipitation ratios (below): OSU GCM

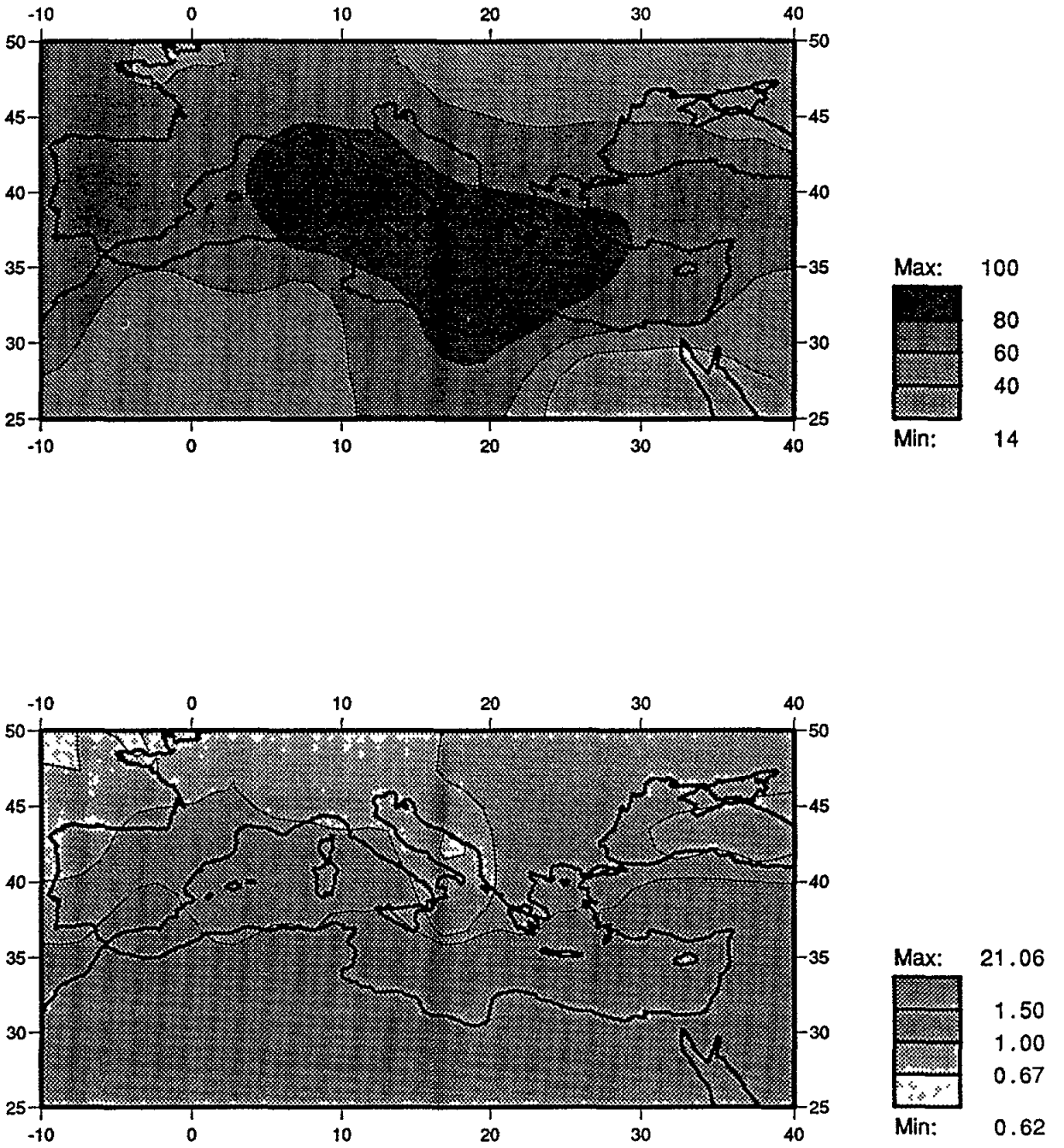

Fig. 2.11 cont. Autumn control run precipitation (above, mm/month) and modelled-to-observed precipitation ratios (below): OSU GCM

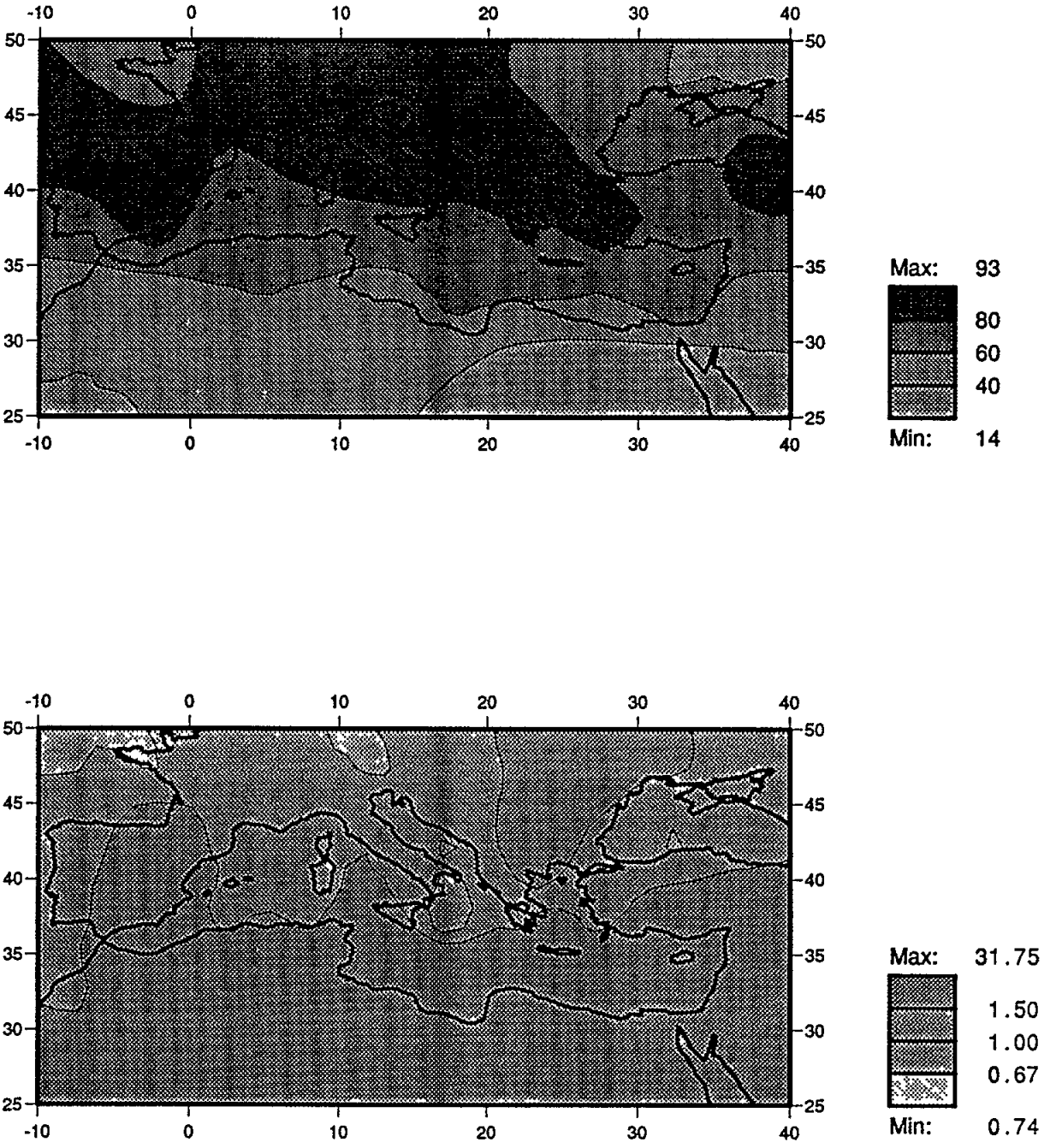

Fig. 2.12 Annual control run precipitation (above, mm/month) and modelled-to-observed precipitation ratios (below) UKMO GCM

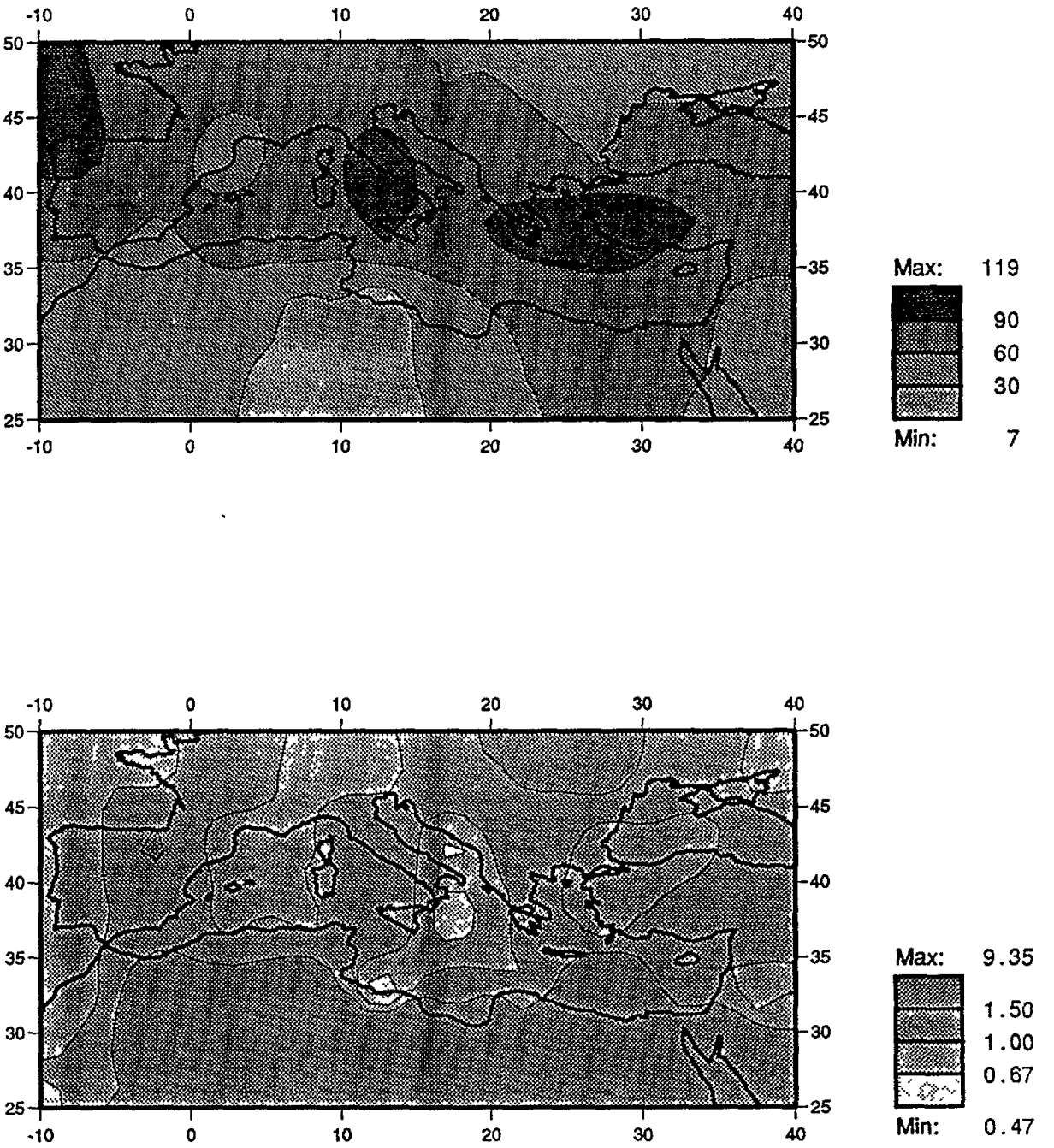

Fig. 2.12 cont. Winter control run precipitation (above, mm/month) and modelled-to-observed precipitation ratios (below): UKMO GCM

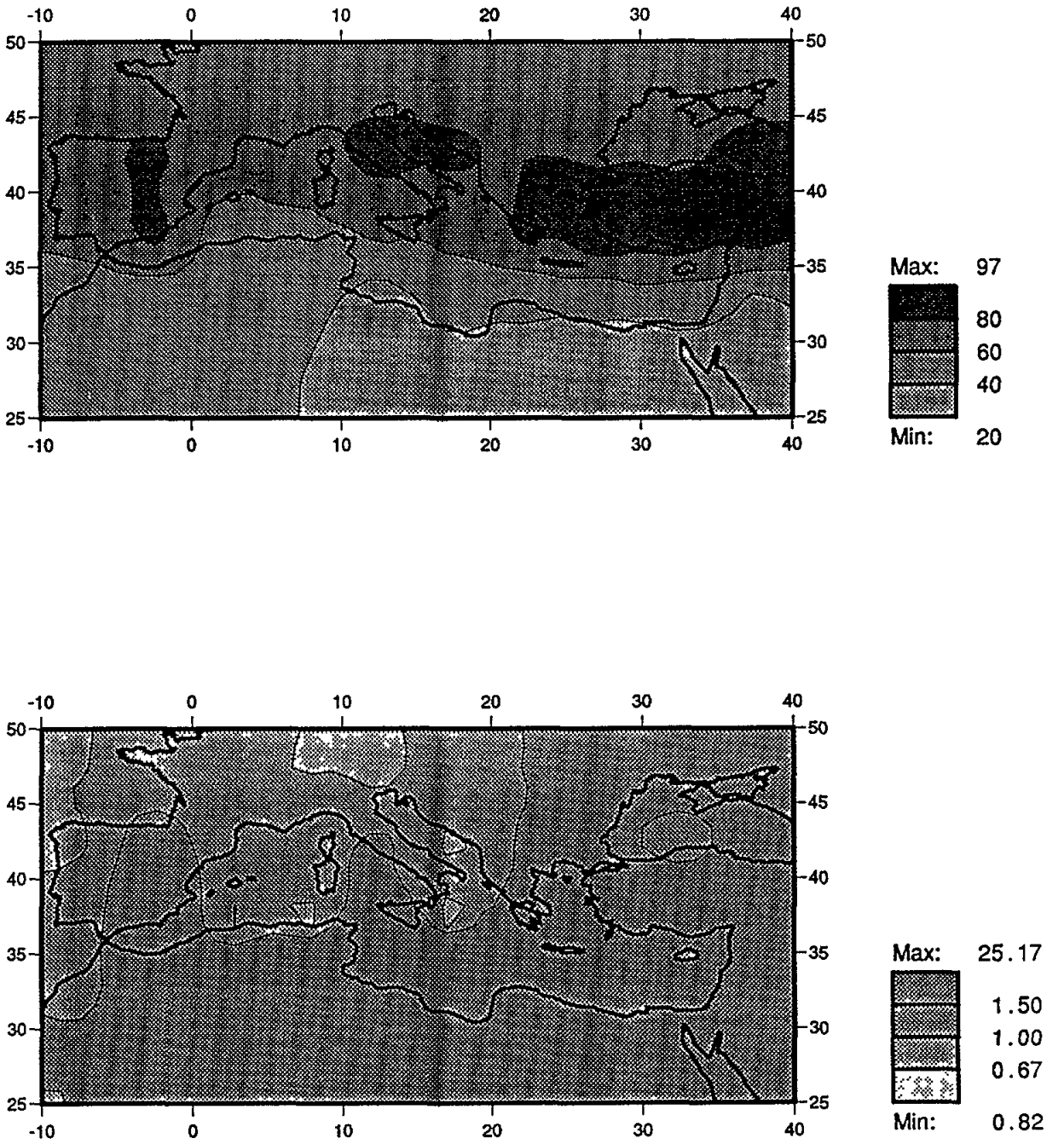

Fig. 2.12 cont. Spring control run precipitation (above, mm/month) and modelled-to-observed precipitation ratios (below): UKMO GCM

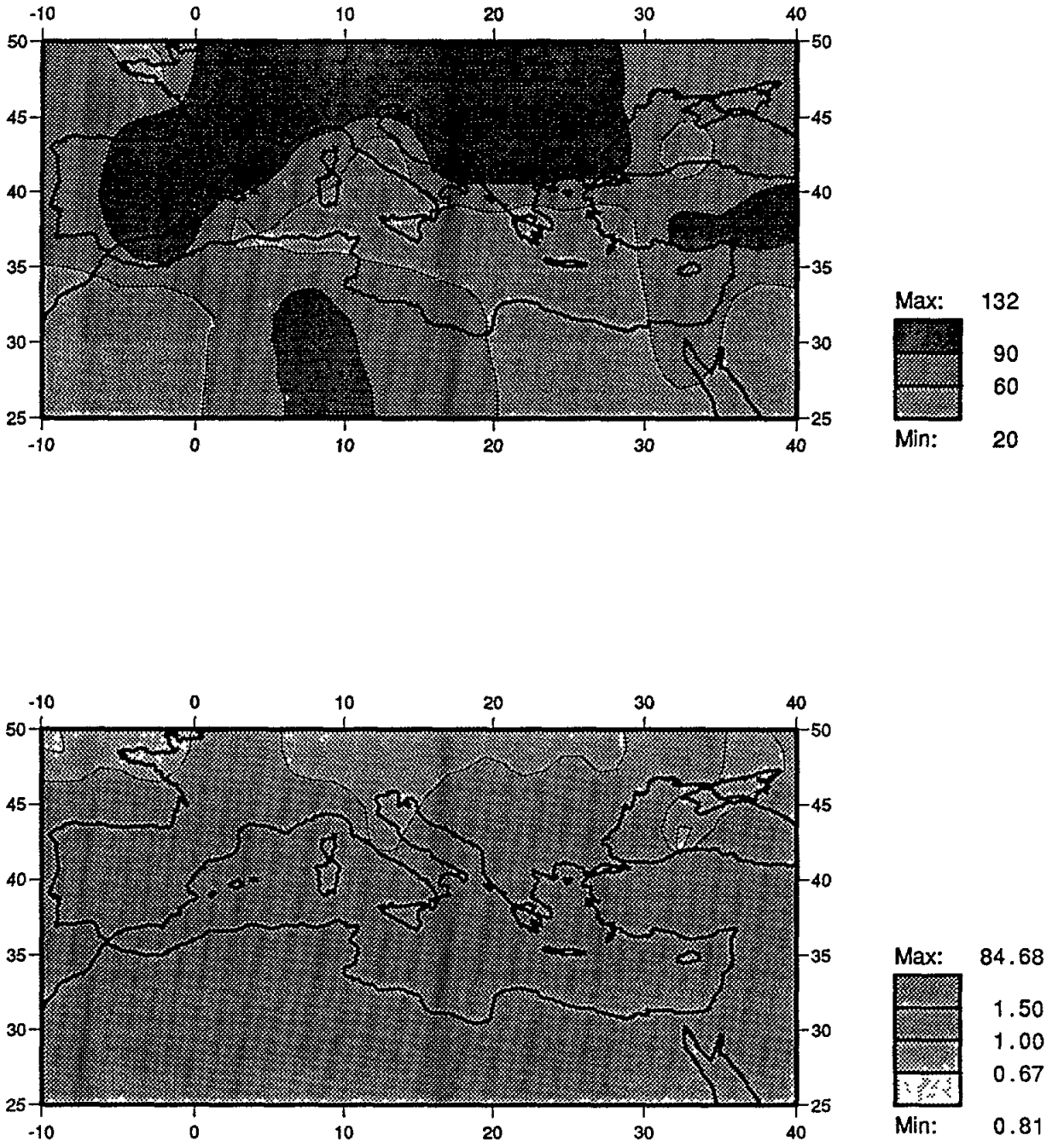

Fig. 2.12 cont. Summer control run precipitation (above, mm/month) and modelled-to-observed precipitation ratios (below): UKMO GCM

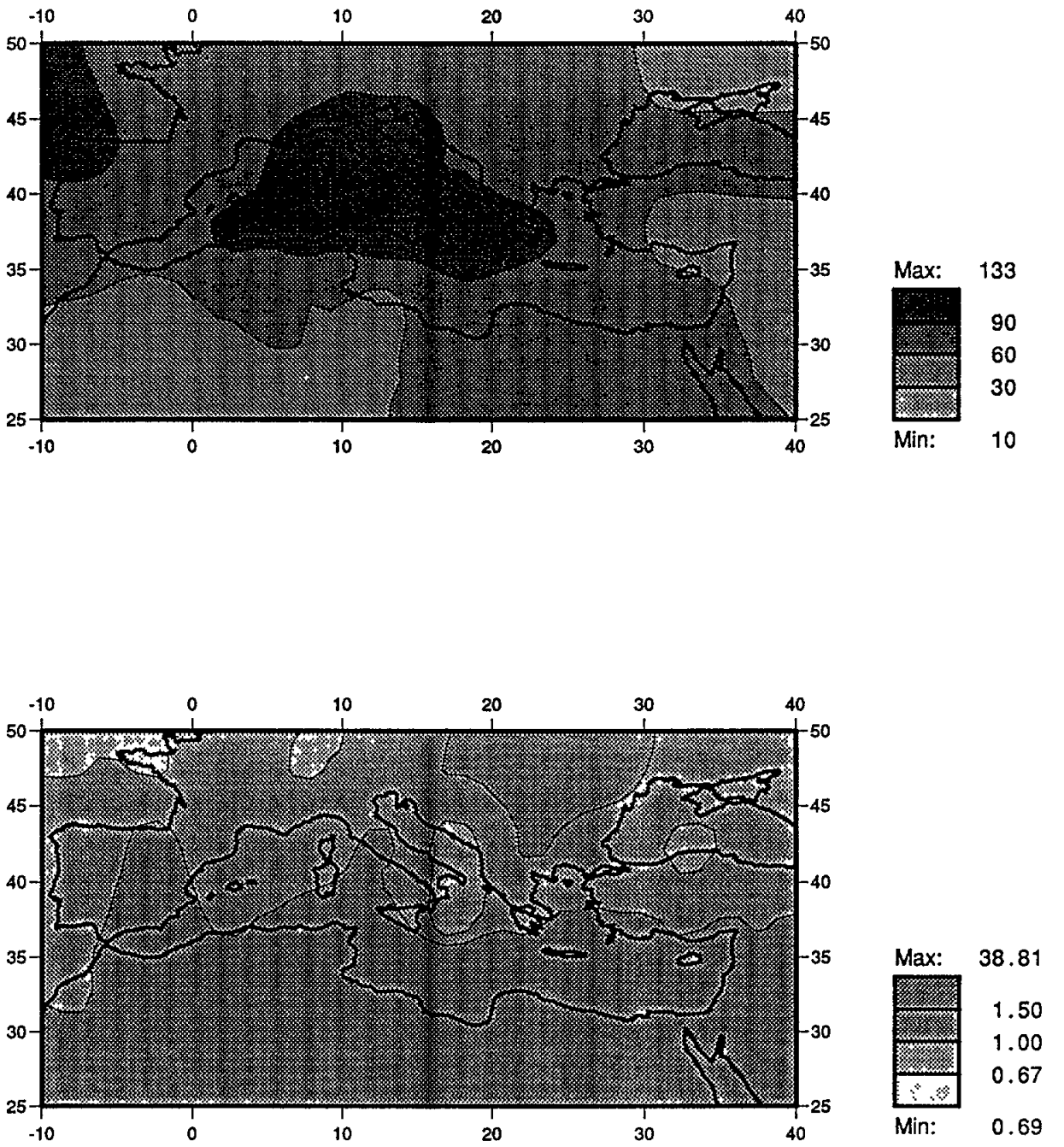

Fig. 2.12 cont. Autumn control run precipitation (above, mm/month) and modelled-to-observed precipitation ratios (below): UKMO GCM

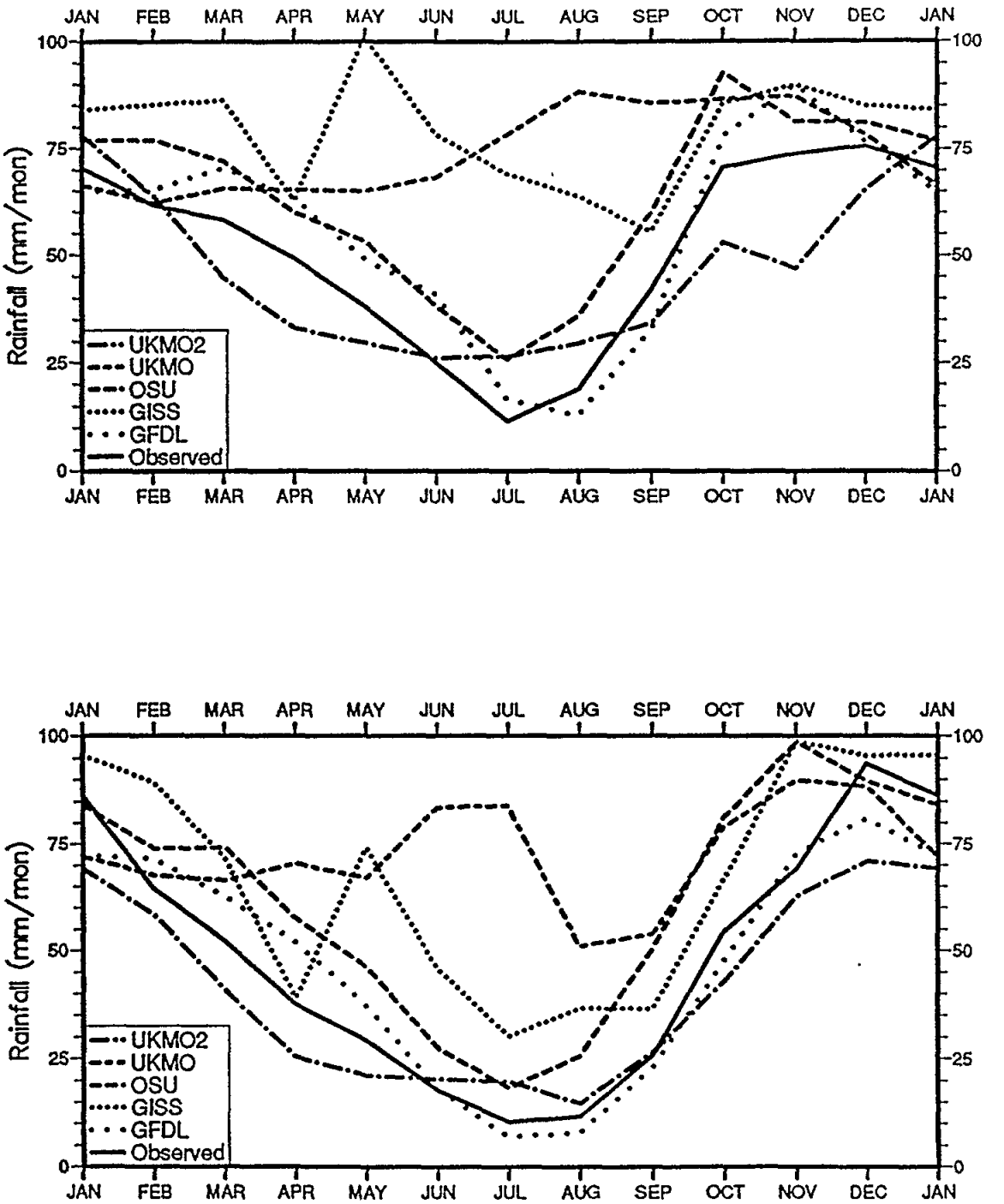

Fig. 2.13 Seasonal cycle of observed and control run precipitation in the western (above) and eastern (below) Mediterranean Basin, including the results for UKMO2

CHAPTER 3

COMPOSITE GCM SCENARIOS

In this chapter we develop and discuss scenarios based directly on the grid-point output from GCMs. The four models used are those already discussed in Section 1.3: the GFDL, GISS, OSU and UKMO GCMs. Details of some relevant model properties are given in Table 3.1. The climate variables considered are temperature, precipitation and MSL pressure.

Table 3.1 Characteristics of the four GCMs

	GFDL	GISS	OSU	UKMO
Horizontal resolution (lat. x long.)	4.44° x 7.5°	7.83° x 10.0°	4.0° x 5.0°	5.0° x 7.5°
Base 1xCO2 (ppmv)	300	315	326	323
Equil. temp.*(°C)	4.0	4.2	2.8	5.2
Precip. change*(%)	8.7	11.0	7.8	15.0
Reference	Wetherald & Manabe, 1986	Hansen et al., 1984	Schlesinger & Zhao, 1989	Wilson & Mitchell 1987

* Global-mean values

It was established in the previous chapter that no single GCM can be identified as being consistently better than the others at simulating current climate. This being the case, there is little merit in presenting scenarios based on only one model. Presentation of scenarios for each of the four models individually would avoid the issue, but this would leave the task of deciding which model is the 'best' and/or of synthesizing the information to obtain a best estimate to the impact analyst. We have therefore adopted the approach of Wigley et al. (1992), whereby the

information from the four models is combined into a single scenario for each variable.

3.1 TEMPERATURE SCENARIOS

3.1.1 Method of Construction

The simplest temperature scenario which utilizes results from all four models is the unweighted model average change in surface air temperature due to increased atmospheric CO_2. First, the temperature output from each GCM is interpolated on to a common grid of resolution 5° latitude by 10° longitude. Then, the difference between the perturbed run ($2xCO_2$) and the control run ($1xCO_2$) temperature is found at each grid point for each model. Finally, the average temperature change for each grid point is calculated. This procedure may be expressed mathematically as:

$$\Delta\bar{T} = \frac{1}{n} \sum_{i=1}^{n} \Delta T_i$$

where $\Delta\bar{T}$ is the model-average temperature change for each grid point, ΔT_i is the temperature change for the i-th model, and n = 4 is the number of models.

The problem with presenting the temperature scenarios in this form is that the results may be biased by the different equilibrium responses of the individual models. Reference to Table 3.1 shows that the global warming due to $2xCO_2$ for the four GCMs ranges between 2.8°C for the OSU model and 5.2°C for the UKMO model. We would therefore expect that the warming indicated by the UKMO GCM for the Mediterranean Basin will be greater than that suggested by the OSU model, even though the sensitivity of the region to climate change when compared to the global sensitivity might be the same.

To produce temperature scenarios which are independent of this bias, the temperature change for each model at each grid point was first divided by the equilibrium (global annual) temperature change for that model, prior to the calculation of the four-model average. For each grid point, this produces a 'standardized' model average temperature change per °C global change. If $\Delta\overline{T}^*$ is the standardized model average and $\Delta T_{eq(i)}$ is the equilibrium temperature change, this may be expressed as:

$$\Delta\overline{T}^* = \frac{1}{n} \sum_{i=1}^{n} (\Delta T_i / \Delta T_{eq(i)})$$

There are two reasons why the standardized scenarios are superior to the simple model average. First, the results capture the patterns of temperature change without being biased by the different model equilibrium sensitivities. Second, by expressing the temperature change over the Mediterranean as a function of the global temperature change, we can introduce a time dimension into the scenarios. A scenario for any particular future time can be developed provided that the global mean temperature change at that time can be estimated (see Houghton et al., 1990, for a discussion of such estimates). The validity of this approach depends on the assumption that the equilibrium and transient patterns of climate change are similar (see Section 1.3 for a brief discussion of the difference between the equilibrium and transient response). There is still considerable scientific debate surrounding this issue.

In order to assess reliability of the standardized patterns of change, upper and lower confidence limits, *tu* and *tl*, representing the 90% confidence intervals, have been placed on the scenarios. This has been done by calculating the standard deviation, s, of the distribution of the standardized temperature changes at each grid point. The confidence limits are given by:

$$tu = \Delta\bar{T}^* + 1.64s$$

$$tl = \Delta\bar{T}^* - 1.64s$$

On the assumption that different model results are a random sample from the true population of temperature changes (an assumption that is made here as a practical measure; it is difficult to make on *a priori* grounds), there is a 90% probability that the actual temperature change will lie within these two limits, and a 10% probability that it will lie outside these limits, either above (5% probability) or below (5% probability).

3.1.2 The Results

The annual and seasonal temperature change scenarios are presented in Fig. 3.1-3.5. Each scenario is accompanied by maps showing the spatial distribution of *tu* and *tl*.

The annual map (Fig. 3.1) indicates that temperature changes will be least over the Mediterranean Sea and the adjoining coastlines of Italy, Greece and North Africa. Here, the sensitivity is less than the global level. However, elsewhere in the study region the sensitivity exceeds the global figure, rising to a relative value of over 1.3 in the extreme north-east.

At the seasonal level, the sensitivity over the Mediterranean Sea and the adjacent coastline is always below the global level. In winter (Fig. 3.2) the low sensitivity region extends westwards to cover Spain. Highest sensitivities are found in the south-east of the study region, over 1.3. The spring season (Fig. 3.3) shows the greatest extent of sensitivities less than the global level, covering almost the whole of Spain, France and Italy as well as the Mediterranean Sea and much of the adjoining coast. Maximum relative sensitivities are shown in the summer (Fig. 3.4). Much of the study region west of 5°E has values greater than 1.3, and the area of sensitivity less than one is much restricted. In contrast, autumn (Fig. 3.5) shows the lowest seasonal sensitivity over the region as a whole. The

maximum ratio between grid-point and global temperature change is only 1.24.

In summary, we can say that, on the basis of the model results, for much of the area immediately adjoining the Mediterranean Sea, the temperature changes due to the enhanced greenhouse effect in each season should be similar to the global, annual-mean change.

3.2 PRECIPITATION SCENARIOS

3.2.1 Method of Construction

As noted in the chapter on validation, it is not meaningful to express the model change in precipitation in terms of a simple difference, because of the great contrasts in seasonal amounts. For each grid point and each model, the $2xCO_2$ minus $1xCO_2$ precipitation has been expressed as a percentage of the control run precipitation. The percentage change was then divided by the equilibrium temperature increase for that model. Finally, the results from the four models were used to calculate a mean standardized precipitation change (p in units of % per °C global-mean warming) for that grid point. Mathematically, this has the form:

$$p = (1/n) \sum_{i=1}^{n} 100 \, [(P_i(2xCO_2) - P_i(1xCO_2)) \, / \, P_i(1xCO_2)] \, / \, \Delta T_{eq(i)}$$

where P_i denotes the absolute precipitation. The upper and lower 90% confidence limits, pu and pl, were calculated for each grid point using the distribution of the standardized precipitation changes for the four models.

3.2.2 The Results

The annual and seasonal maps of the mean standardized precipitation changes p are presented in Figs. 3.6-3.10. The spatial patterns of pu and pl are also shown. Assuming that the GCM output results are a random

sample from a true population, there is a 90% probability that the mean standardized precipitation change will fall within these limits.

For most of the region, and for most of the year, the standardized change scenarios indicate that precipitation will increase because of the greenhouse effect. The important exception to this statement is the summer season, when a reduction in rainfall is suggested for the whole region except parts of North Africa. The decrease is predicted to be as much as 6%/°C. A more restricted area of reduced rainfall is also indicated in spring. The greatest changes are shown to occur in spring and summer.

For the year as a whole (Fig. 3.6), the mean standardized precipitation change for the central Mediterranean Basin is small, in the range -1 to +2%/°C. Larger increases are predicted for the northern and southern peripheries of the study region, rising to as much as 4%/°C.

In winter (Fig. 3.7) the model results indicate that most of the region should experience a slight increase in precipitation. Over the eastern and northern Mediterranean this should be in the region of 2-3%/°C, rising to over 3%/°C in some areas. The only area of reduced precipitation lies over southern Italy and the adjacent parts of North Africa. The changes do not exceed -2%/°C. The changes in spring are much greater (Fig. 3.8). A decrease is indicated for much of the eastern Mediterranean and the North African coast of the western Mediterranean. Most land areas north of the Mediterranean should experience higher rainfall, except for southern Greece and Turkey. Summer patterns indicate the greatest spatial extent and severity of drying (Fig. 3.9). The western Mediterranean, central Turkey and Cyprus are indicated to experience lower rainfall, by as much as 6%/°C. The models suggest a slight increase over the central Mediterranean. Autumn precipitation (Fig. 3.10) is predicted to increase over almost the entire study region, with the greatest changes occurring over southern and western areas.

It is of interest to study the 90% confidence limit maps for precipitation in some detail. The model-average maps, for example, suggest that winter should be a time of increased precipitation. However, inspection of Fig. 3.7 shows that the lower confidence limit is, for much of the study area, a negative value, indicating a decrease in precipitation. To illustrate this point further, we can take the example of grid point 35°N by 20°E. Here, the model-average change is +2.6%/°C. However, the upper and lower 90% confidence limits are, respectively, +7.8%/°C and -2.6%/°C. In terms of probabilities, therefore, we can only say that there is a 90% probability that the winter precipitation change at this grid point will lie between +7.8%/°C and -2.6%/°C; in other words. although the "best guess" may be for an increase in precipitation, there is still a significant probability that precipitation will decrease. The summer model-average map indicates lower rainfall at this grid point, but the map of *pu* shows that there is a strong probability that this decrease may be very small or that there may be an increase. These results arise from the very wide distribution of the individual model results for precipitation change, and they graphically identify the very high degree of uncertainty associated with all precipitation scenarios.

3.3 MSL PRESSURE SCENARIOS

3.3.1 Method of Construction

The pressure scenarios have been constructed in the same way as the temperature scenarios. That is, the pressure change for each model at each grid point was first divided by the equilibrium temperature change for that model, and then a four-model average was calculated. This gives a standardized model-average pressure change per °C global temperature change. The results, with the 90% upper and lower confidence limits, are shown in Figs. 3.11-3.15.

3.3.2 The Results

At the annual level, the model average suggests a slight decrease in MSL pressure over the whole region, of no more than 0.3mb/°C (Fig. 3.11). Inspection of the seasonal maps indicates that this pattern is repeated throughout the year, except in winter. The winter season shows increased pressure over the whole of the Mediterranean Basin: only the fringes of the study area display negative values (Fig. 3.12). However, the increases are small, not exceeding 0.2mb/°C.

Because the model mean pressure changes are small, the 90% confidence limit maps are opposite in sign over much of the area. For example, the annual 90% upper confidence limit map has only a small percentage of its area which is not positive in sign, whereas the annual lower confidence limit map indicates lower pressure in most places. We are therefore unable to say with any certainty in what direction MSL pressure is expected to change in a high greenhouse gas world. It appears probable, however, on the basis of the model evidence, that the changes will be small. The model-average changes are much less than the normal interannual variability of MSLP.

3.4 CONCLUSIONS

Temperature changes due to the greenhouse effect over the area immediately adjoining the Mediterranean Sea, on the basis of the models used in this study, are likely to be similar to the global, annual-mean change. The effect on precipitation is expected to be an increase in autumn and winter, but a decrease in summer and, particularly in the eastern Mediterranean, in spring also. The mean change was, in winter, around +3%/°C and, in summer, around -3%/°C. MSLP changes are unlikely to be large, and will probably be well within the range of present-day natural variability.

It is of interest to compare these results with those obtained for the IPCC high-resolution equilibrium model runs for Southern Europe (Mitchell et al., 1990, Table 5.1; Cubasch and Cess, 1990, Table 3.2a). Three models were employed: the UKMO and GFDL GCMs (earlier, low resolution, results from which are used in this study) and the National Center for Atmospheric Research GCM. The results were scaled to a global-mean warming of 1.8°C, the warming expected to have occurred by the year 2030. The predicted change in precipitation ranged between zero and +10% in the winter, and between -5% and -15% in the summer. For the winter season, our results are very much in accord with the IPCC findings. For summer, the IPCC results indicate a rather greater decrease in rainfall than we obtained. However, the overall agreement is encouraging.

In interpreting the precipitation scenarios it is most important to bear in mind the position of the upper and lower 90% confidence limits. Where the model-average precipitation change is shown to be positive, the lower 90% confidence limit is generally negative, and vice versa. Our confidence in the model scenarios of precipitation change must therefore be low, and this view is supported by the IPCC Report in the discussion of their Mediterranean scenarios (Mitchell et al., 1990).

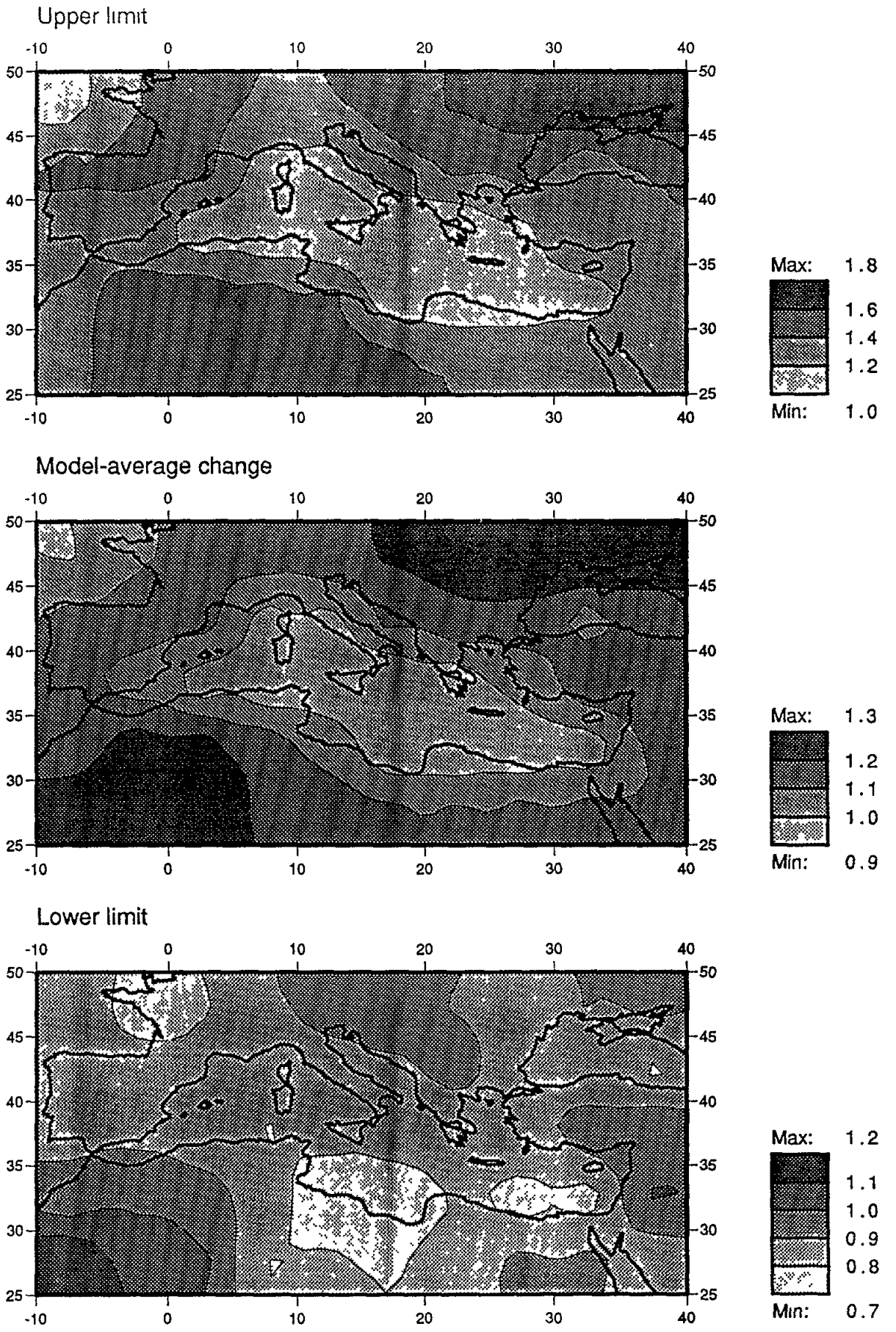

Fig. 3.1 Annual standardized model-average temperature change per ^{o}C global change, shown with the upper (above) and lower (below) 90% confidence limits (^{o}C)

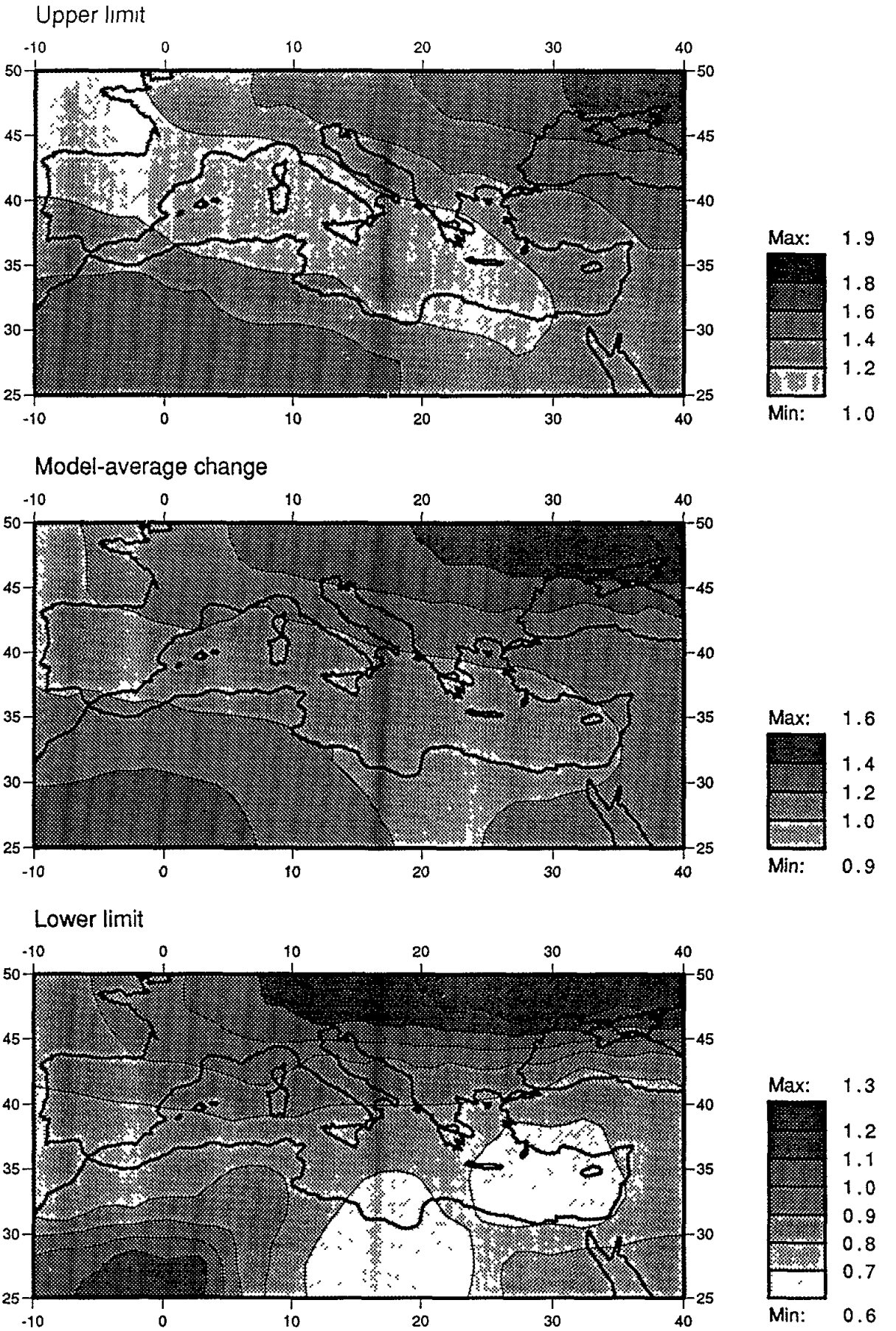

Fig. 3.2 Winter standardized model-average temperature change per °C global change, shown with the upper (above) and lower (below) 90% confidence limits (°C)

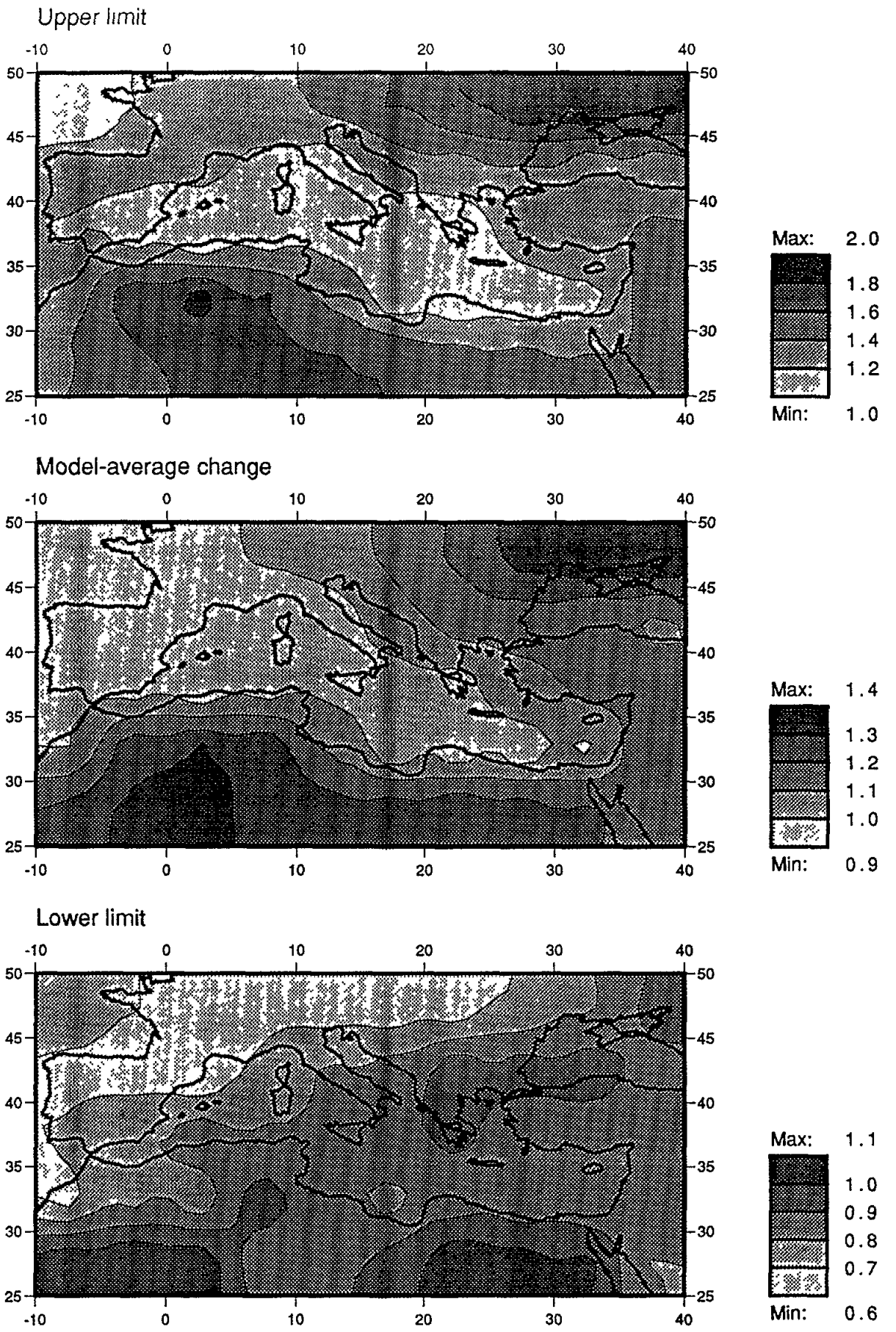

Fig. 3.3 Spring standardized model-average temperature change per ^{o}C global change, shown with the upper (above) and lower (below) 90% confidence limits (^{o}C)

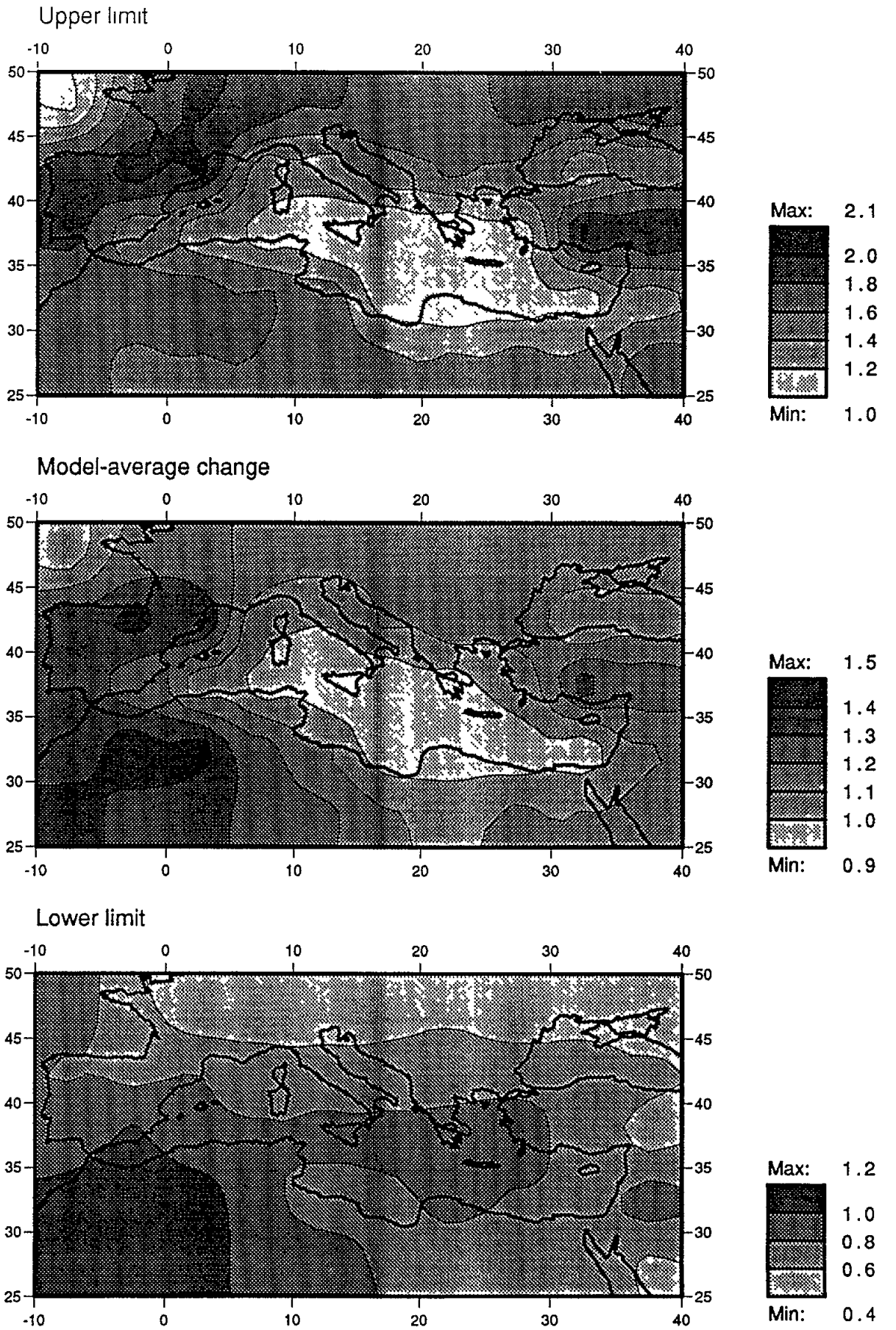

Fig. 3.4 Summer standardized model-average temperature change per ^{o}C global change, shown with the upper (above) and lower (below) 90% confidence limits (^{o}C)

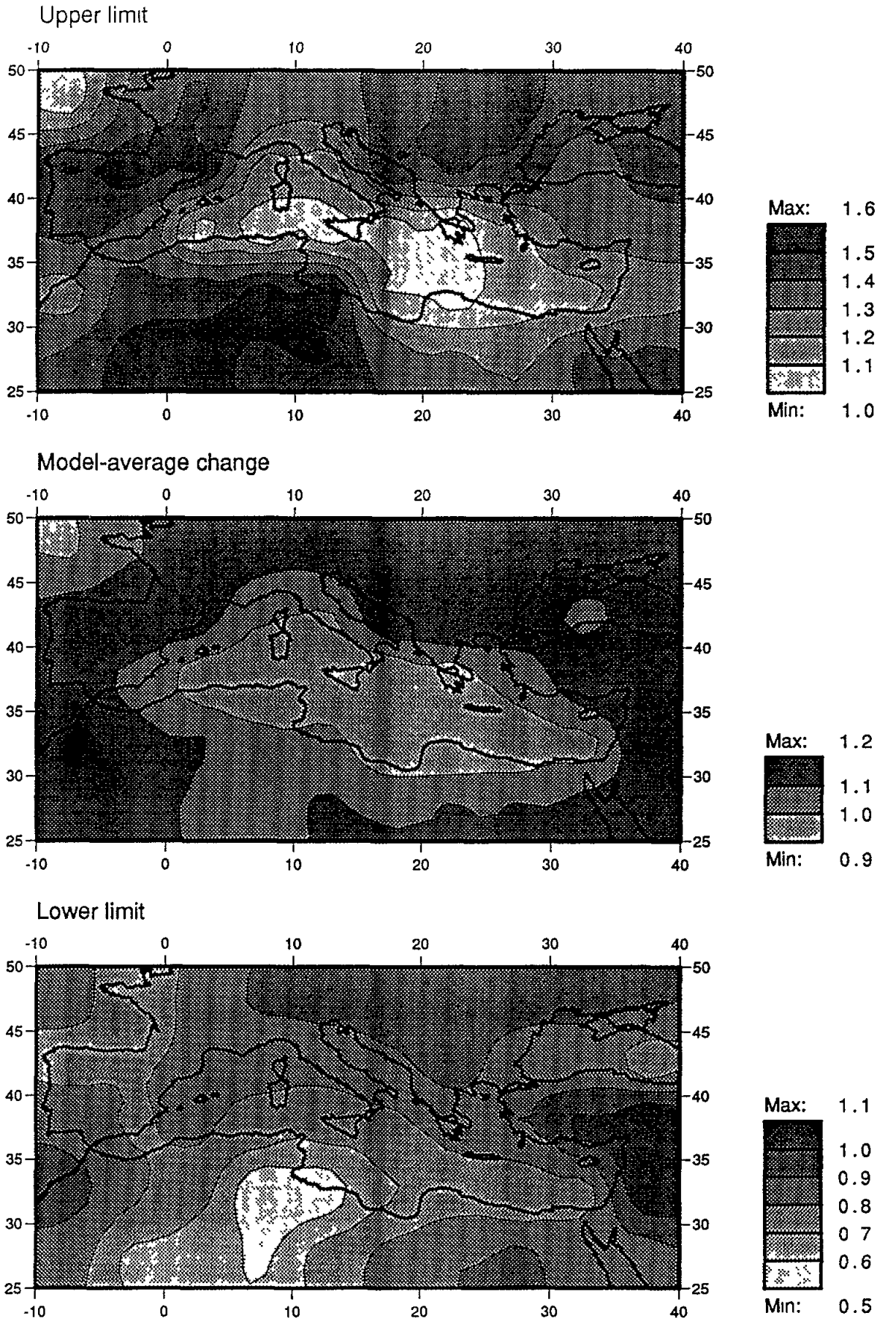

Fig. 3.5 Autumn standardized model-average temperature change per ^{o}C global change, shown with the upper (above) and lower (below) 90% confidence limits (^{o}C)

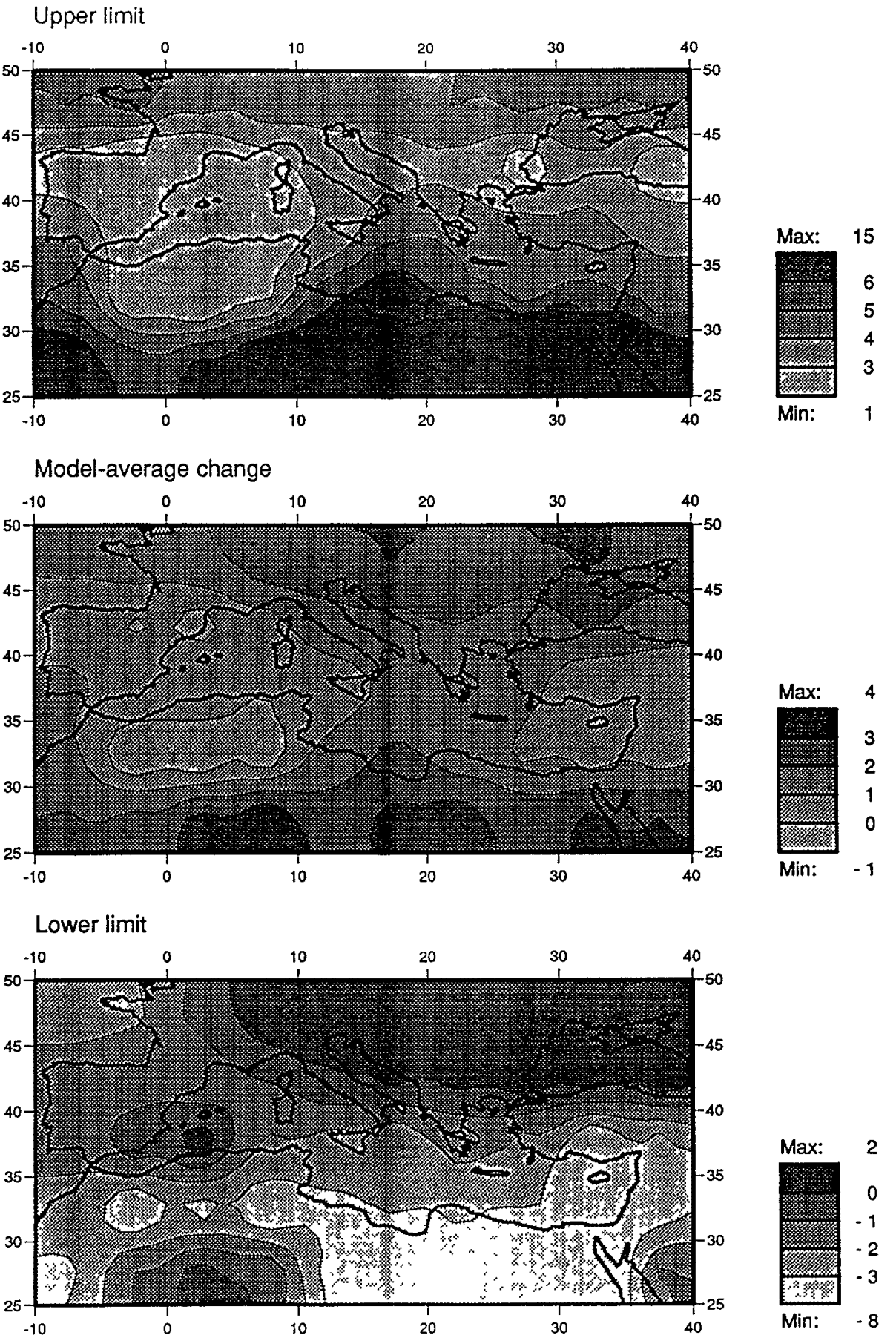

Fig. 3.6 Annual standardized model-average precipitation change in % per °C global change, shown with the upper (above) and lower (below) 90% confidence limits

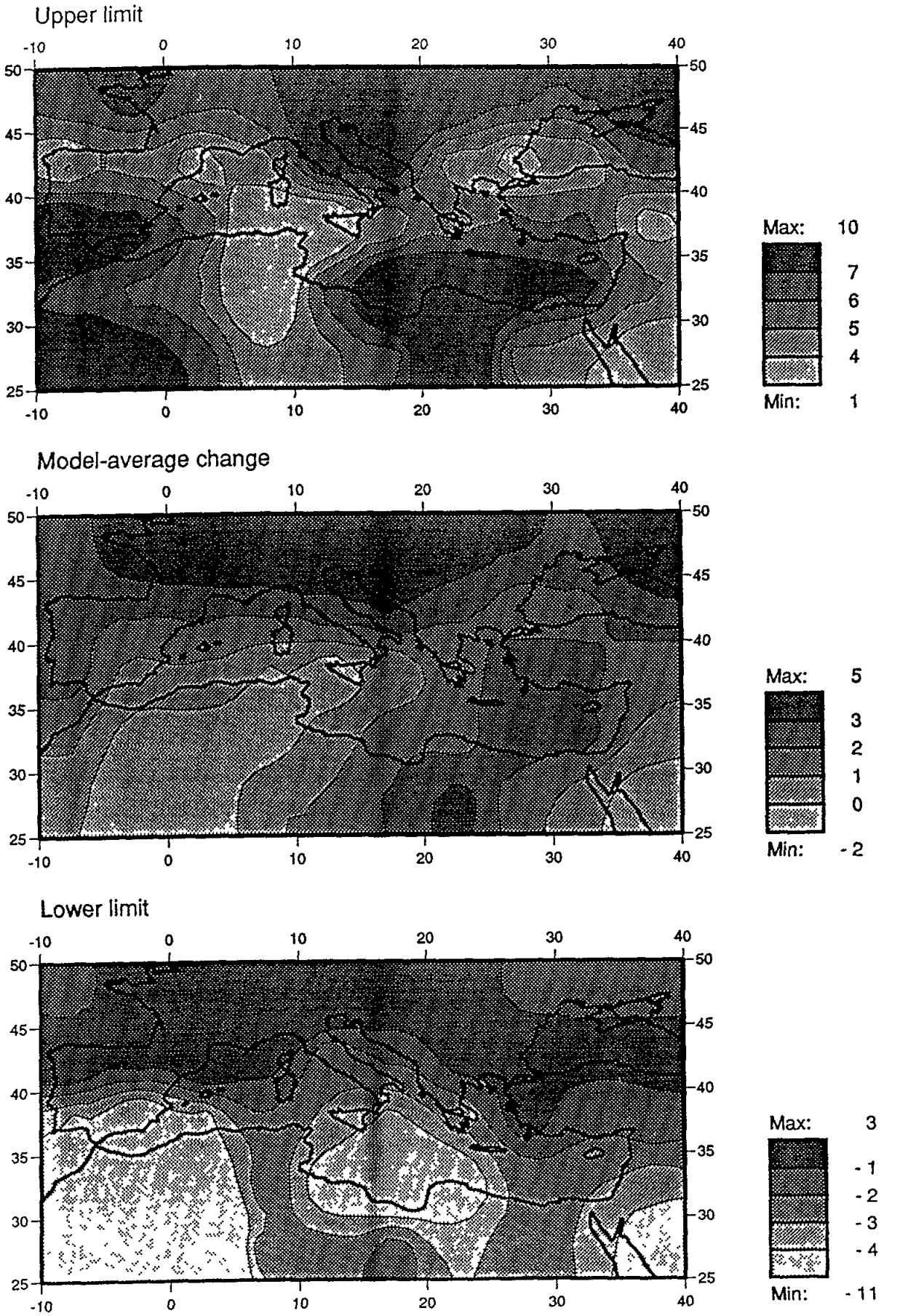

Fig. 3.7 Winter standardized model-average precipitation change in % per °C global change, shown with the upper (above) and lower (below) 90% confidence limits

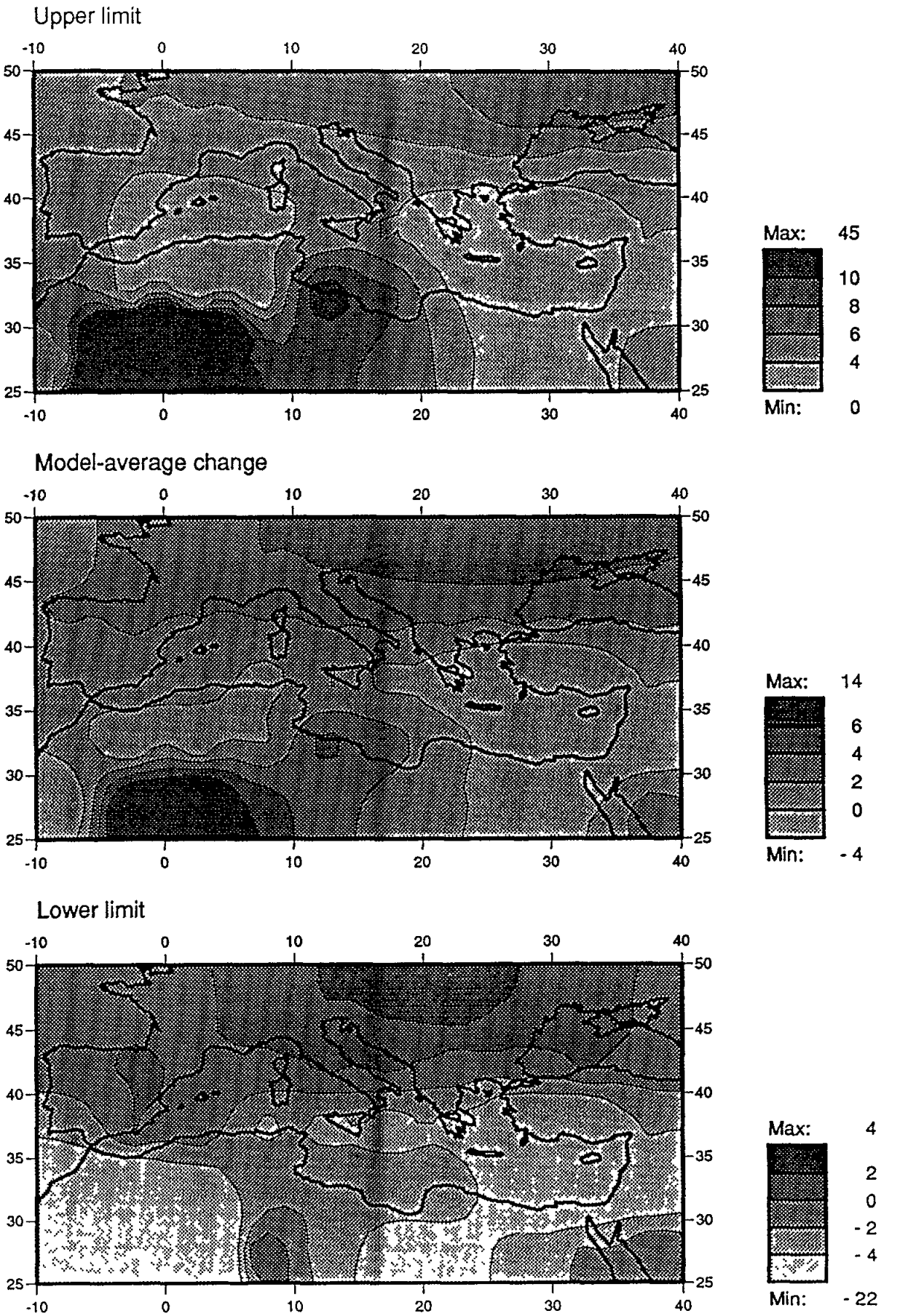

Fig. 3.8 Spring standardized model-average precipitation change in % per ^{o}C global change, shown with the upper (above) and lower (below) 90% confidence limits

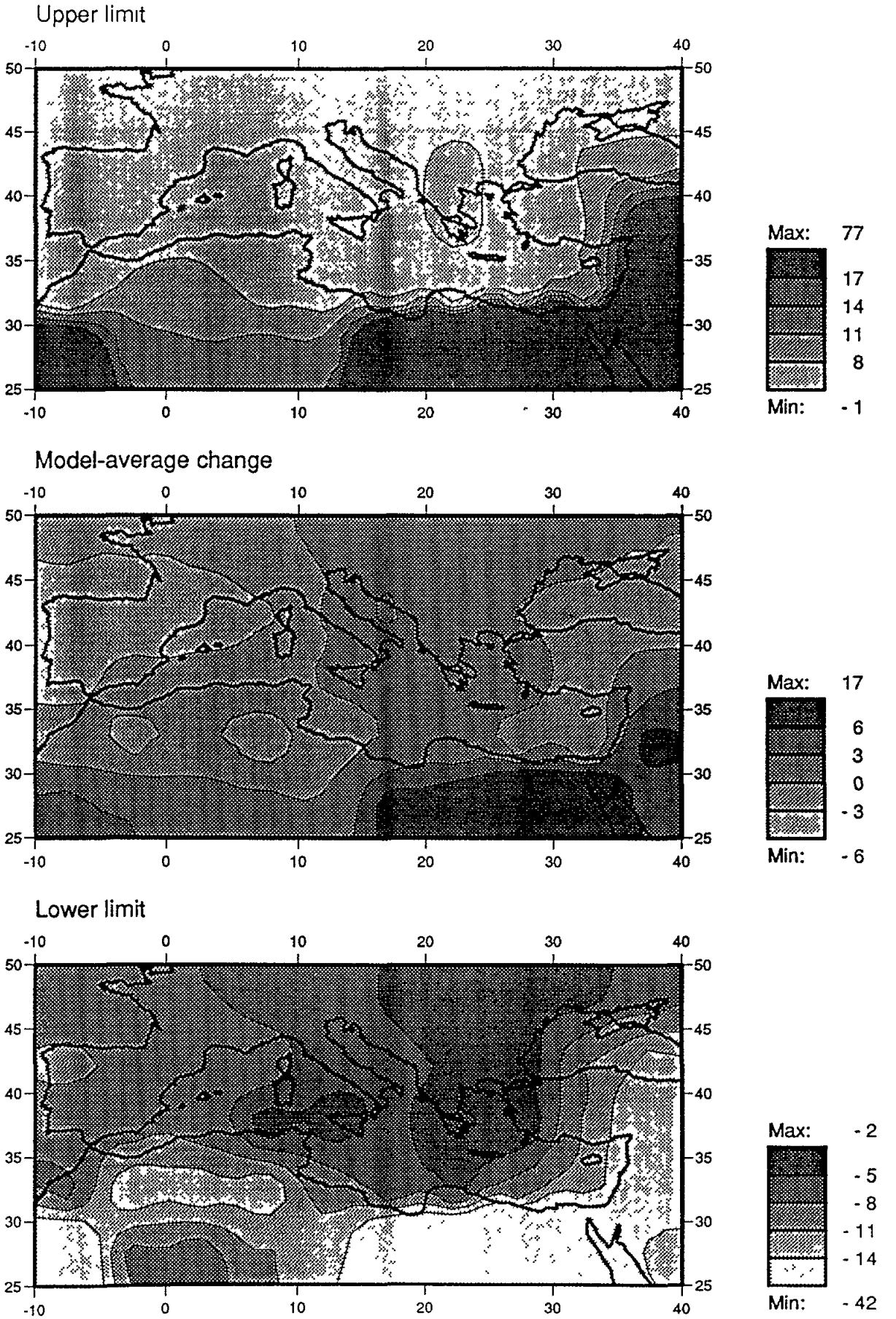

Fig. 3.9 Summer standardized model-average precipitation change in % per °C global change, shown with the upper (above) and lower (below) 90% confidence limits

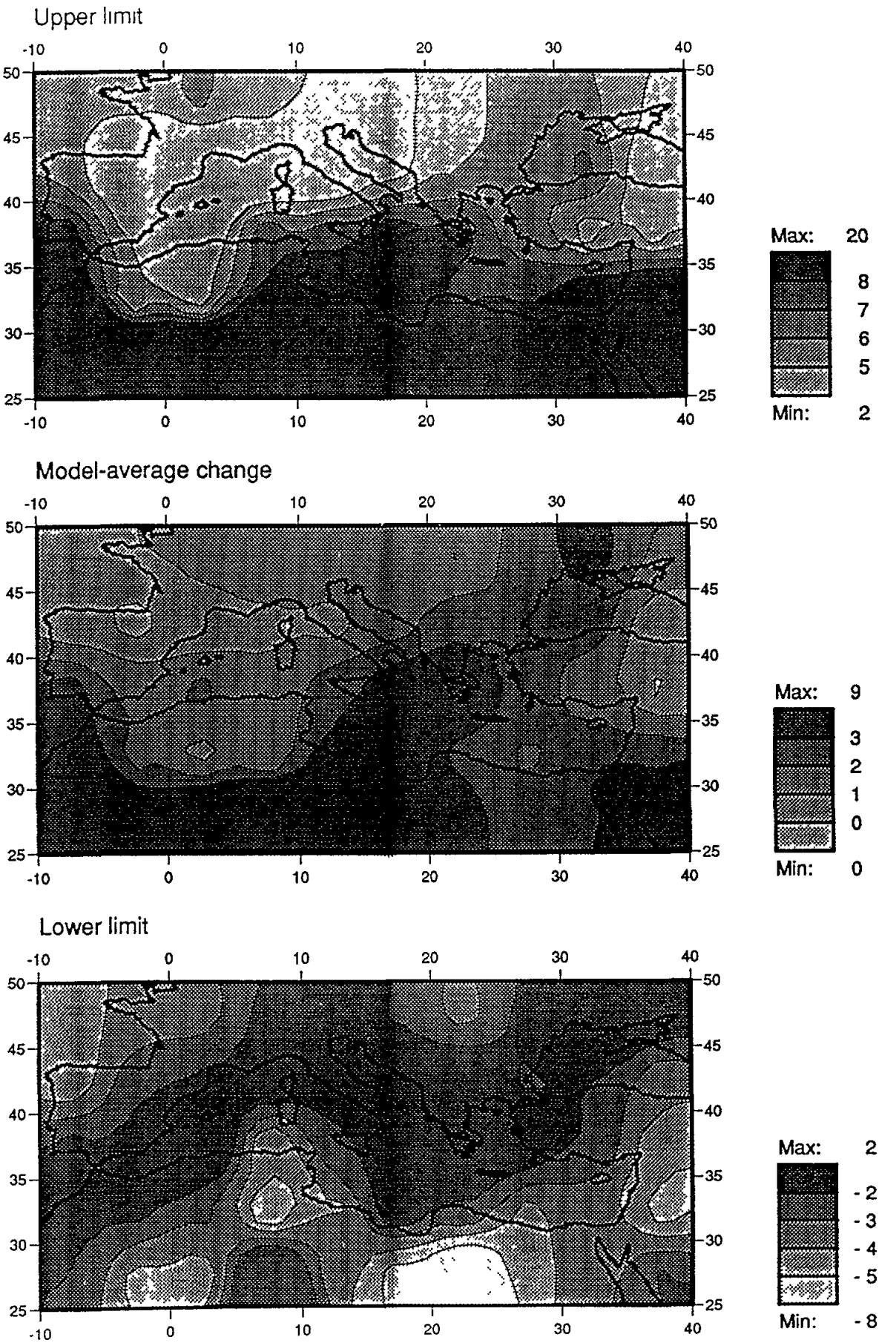

Fig. 3.10 Autumn standardized model-average precipitation change in % per ^{o}C global change, shown with the upper (above) and lower (below) 90% confidence limits

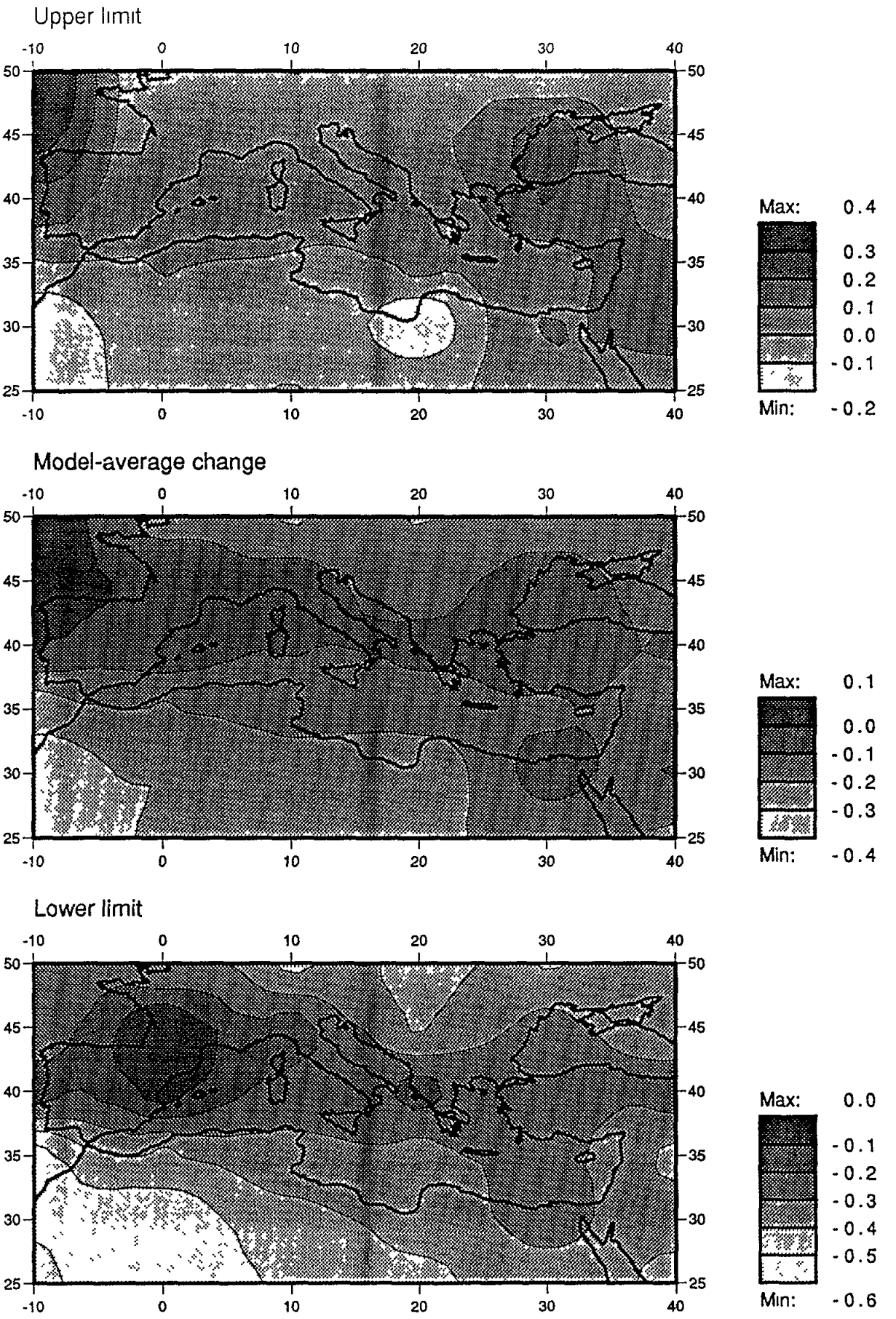

Fig. 3.11 Annual standardized model-average MSL pressure change per ^{o}C global change, shown with the upper (above) and lower (below) 90% confidence limits (mb)

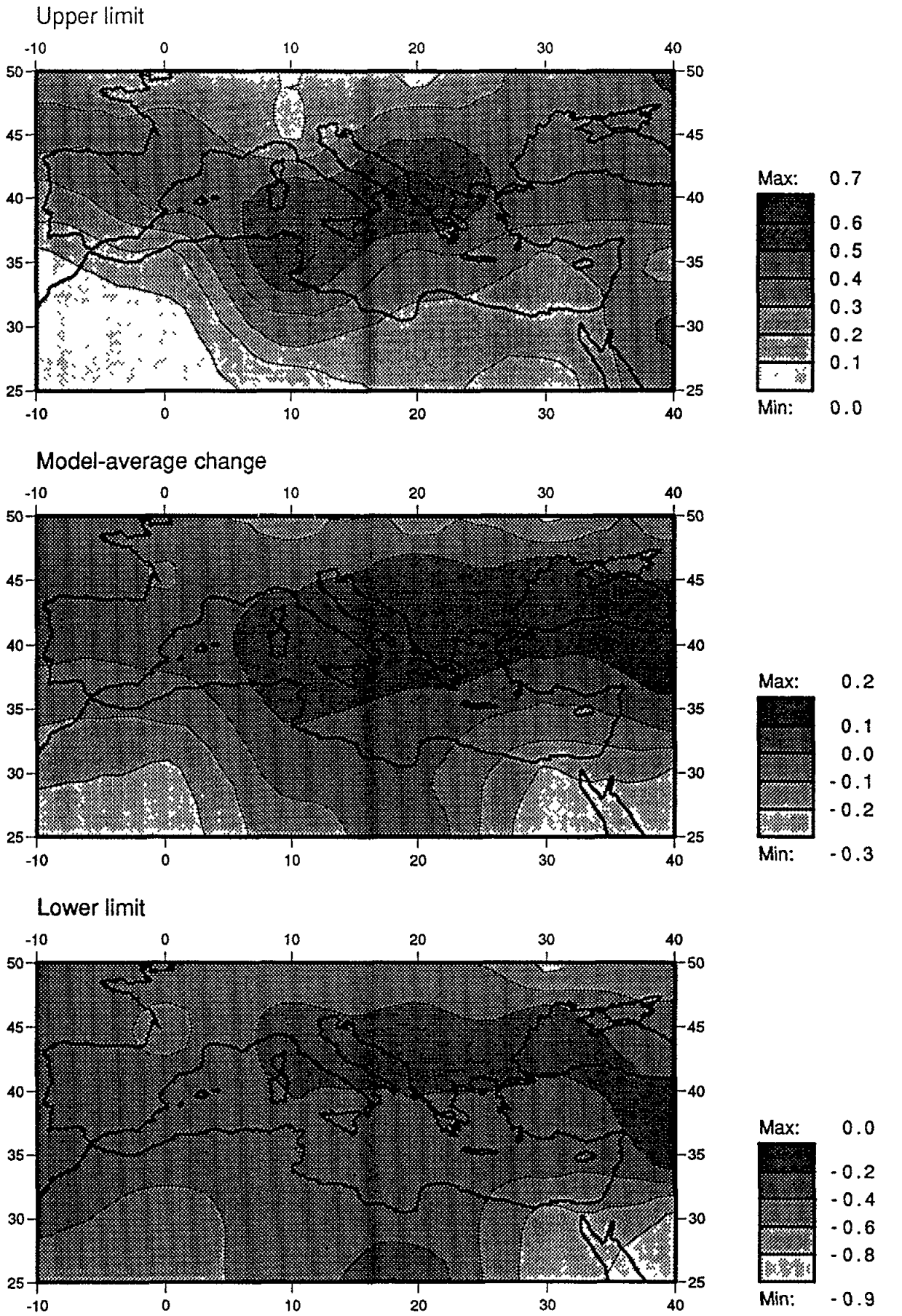

Fig. 3.12 Winter standardized model-average MSL pressure change per ^{o}C global change, shown with the upper (above) and lower (below) 90% confidence limits (mb)

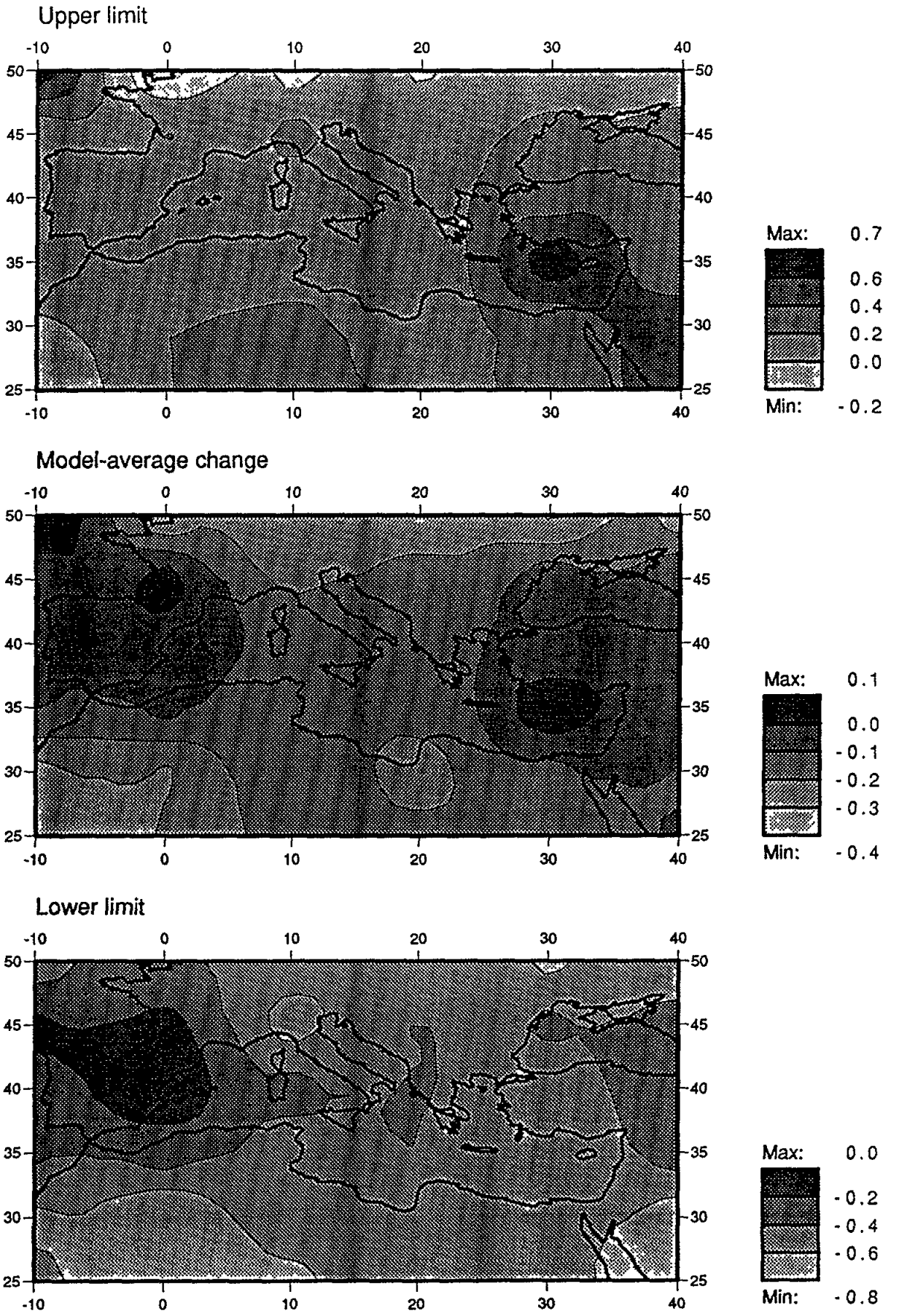

Fig. 3.13 Spring standardized model-average MSL pressure change per ^{o}C global change, shown with the upper (above) and lower (below) 90% confidence limits (mb)

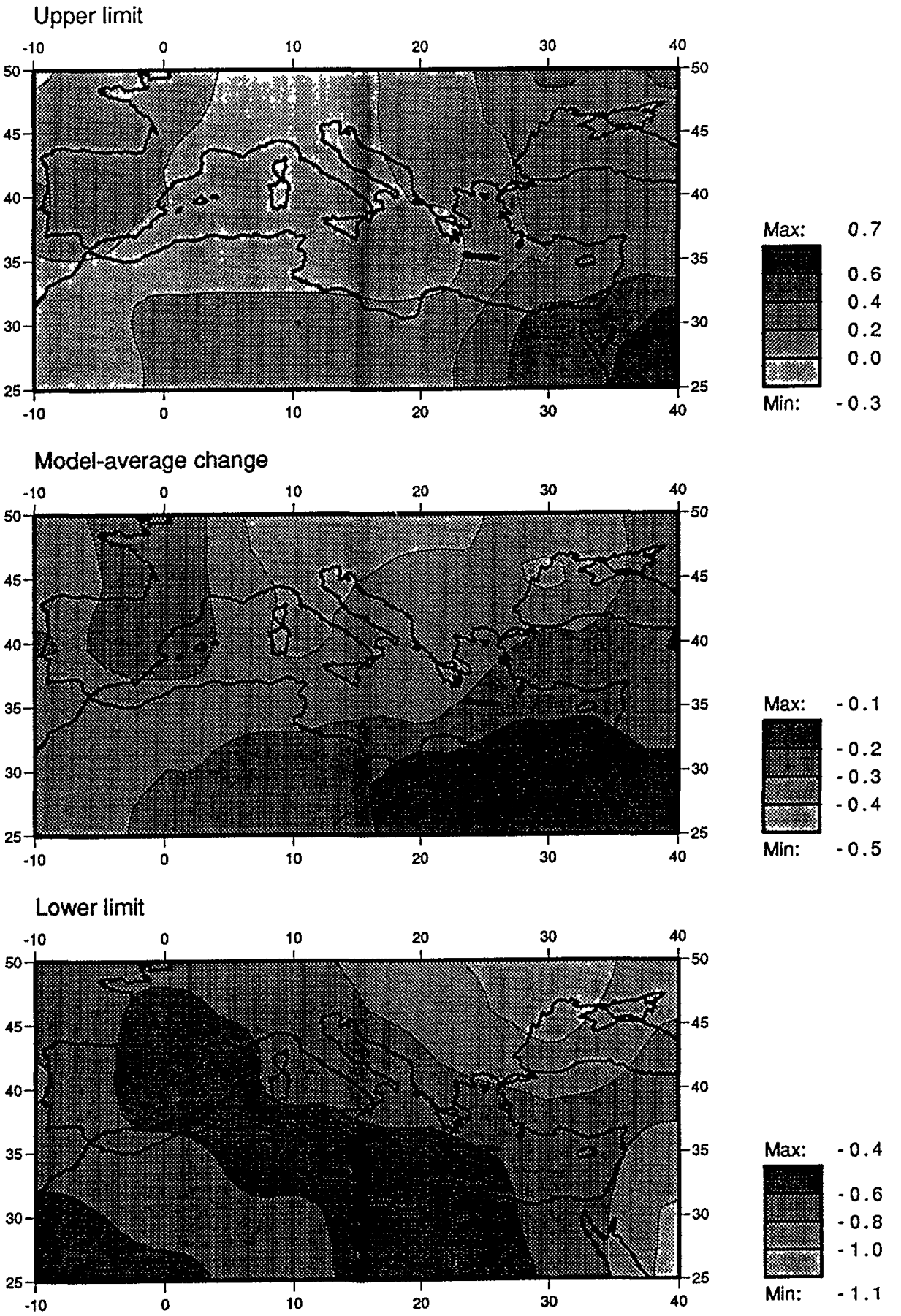

Fig. 3.14 Summer standardized model-average MSL pressure change per ^{o}C global change, shown with the upper (above) and lower (below) 90% confidence limits (mb)

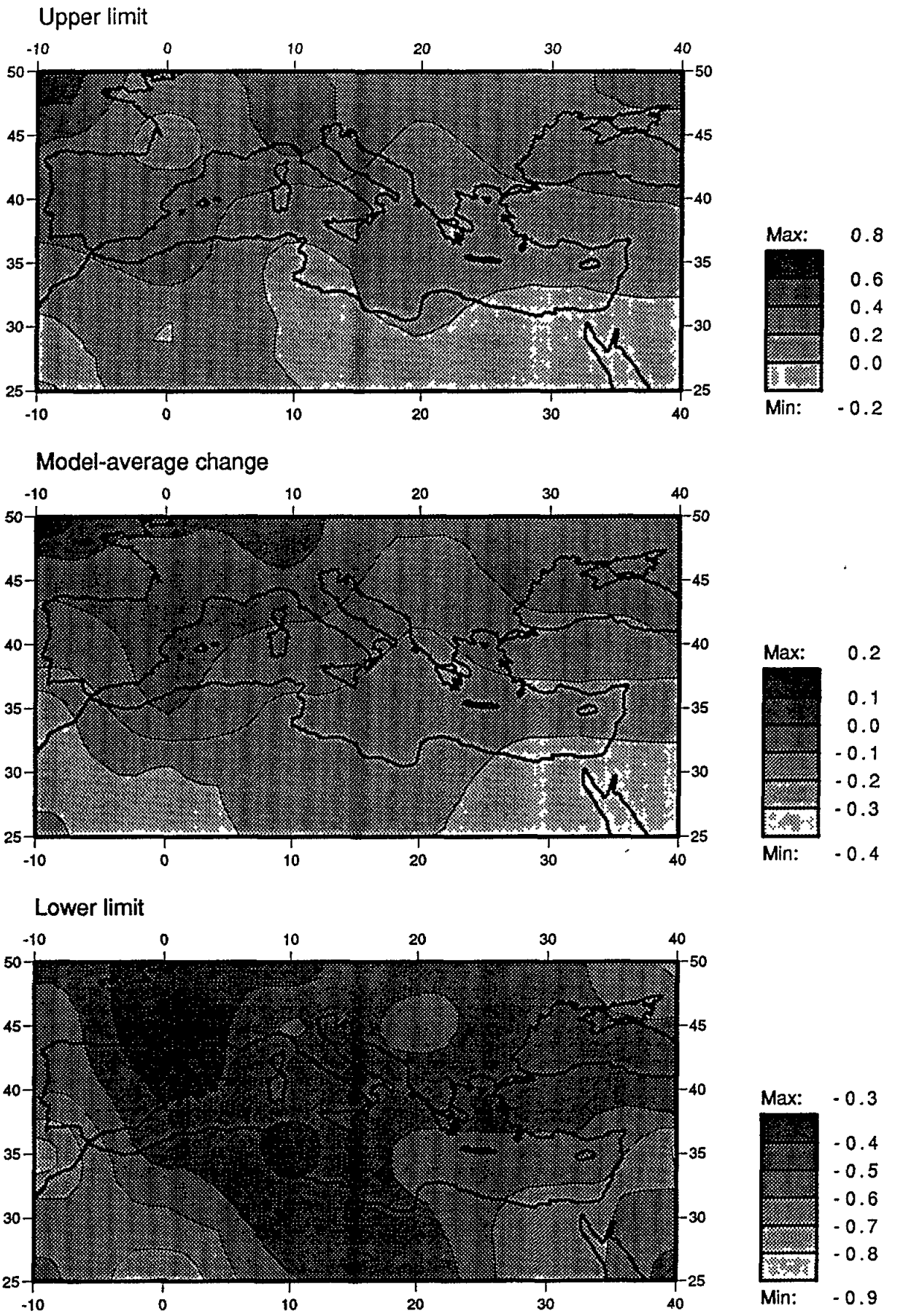

Fig. 3.15 Autumn standardized model-average MSL pressure change per ^{o}C global change, shown with the upper (above) and lower (below) 90% confidence limits (mb)

CHAPTER 4

SUB-GRID-SCALE SCENARIOS

4.1 INTRODUCTION

One problem with the application of GCMs to the study of climate impacts is the coarse resolution of the model grid. The grid scale of the four GCMs used in this study ranges from 4^{o} latitude x 5^{o} longitude (OSU) to 7.83^{o} latitude x 10^{o} longitude (GISS). In Chapter 3, scenarios were developed directly from GCMs, after first interpolating the model output on to a common grid of 5^{o} latitude x 10^{o} longitude. At the latitude of the Mediterranean Basin, the grid intersections are separated by several hundreds of kilometres. This level of resolution is inadequate for many regional climate change studies, especially in areas of high relief. To develop higher resolution scenarios, the problem is to find a statistical link between the large-scale grid point GCM output and the small-scale detail of regional climates.

4.2 SCENARIO CONSTRUCTION

4.2.1 Development of the Method

Kim et al. (1984) looked at the statistical relationship between local and large-scale regionally-averaged values of two meteorological variables: temperature and precipitation. They then used these relationships, developed using principal component analysis techniques, to examine the response of local temperature and precipitation to the predicted change at GCM grid points. The area of study was the state of Oregon. Although the paper contains certain statistical flaws, the underlying idea of statistically relating local and large-scale data is sound.

Methodological flaws in the approach used by Kim et al., were avoided by Wigley et al. (1990). Working with the same Oregon data, these authors employ a much wider range of predictor variables: area-averages of

precipitation and temperature, nearby grid-point values of mean sea-level pressure and the height of the 700mb surface and, for the latter two variables, zonal and meridional gradients across the region between the appropriate grid points. Rather than making use of the seasonal cycle in the data to develop the regression equations, which the Kim et al. study reduces to, Wigley et al. harness the inter-annual variability. Thus, separate regression equations are developed for each month of the year.

Large spatial variations were found in the explained variances, both in calibration and in verification tests made with independent data. When the method is extended to the Mediterranean Basin, we must expect considerable regional variation in the skill of the predictions. For some locations, Wigley et al. found well over 90% of the local temperature variance explained by the large-scale climate in the independent verification. However, in the coastal belt of Oregon where the sea breeze circulation prevails in summer, predictability was rather low. Generally, the relationships for precipitation were weaker than those for temperature. Predictability was found to be highest in the western part of the state, where the orographic influence is strongest. Overall, most of the skill derives from the area-average of the variable which one is trying to predict at the local level.

Wigley et al. used their derived regression equations to illustrate the procedure. However, instead of using actual GCM data they treated the analysis as a sensitivity study, inserting prescribed increases in grid-point temperature (one standard deviation) and precipitation (20%). The contribution of the other variables was ignored. The results show that individual site changes can differ substantially from the grid-point changes.

The two papers, Kim et al. (1984) and Wigley et al. (1990), provide a clear and workable methodology to extract local-to-regional scale climate change information from GCM grid point output.

4.2.2 Application to the Mediterranean Basin

The methods of Kim et al. and Wigley et al. have been modified for application in the Mediterranean region. In particular, we required a general computer program that would be applicable throughout the area and which could be used with meteorological records of variable length and density. After investigating a number of approaches to the problem, we adopted the procedure summarized below:

1. As part of this study, data sets of monthly-mean temperature and total precipitation were compiled for the area surrounding the Mediterranean Basin. Stations in the data sets are listed in Appendix 1. Where possible, each record should be complete for the period 1951-88. Any station with a record length less than 20 years in the period 1951-88 for over six months out of twelve was discarded.

2. Then, for every valid station, the temperature and precipitation anomalies from the long-term (1951-88) mean were calculated. For this part of the work, which is the first step in the construction of the regression equations (the calibration stage), only the data for 1951-80 were used. The 1981-88 data were retained to test the performance of the regression models (the verification stage). For the calculation of the temperature anomaly At_{ij}, the simple difference was used:

$$At_{ij} = t_{ij} - T_j$$

where t_{ij} is the mean temperature of month j in year i, and T_j is the long-term mean for month j. The precipitation anomaly Ap_{ij} was expressed as a ratio of the long-term mean:

$$Ap_{ij} = (p_{ij} - P_j)/P_j$$

where p_{ij} is the monthly total precipitation in month j of year i, and P_j is the long-term mean for that month. If P_j is less than 1mm, then this equation is modified to:

$$Ap_{ij} = (p_{ij} - P_j)/1.0$$

3. The individual station anomalies are then used to calculate regionally-averaged anomalies. The procedures described from here to the end of point 6 are station-specific, and must be repeated for each station in the data set.

   A 5° latitude x 5° longitude square is centred over the station for which regression equations are to be developed (the predicted station). All the stations which fall within this square are used to calculate

the regional averages. If the number of stations is less than three, for temperature, or four, for precipitation, the procedure is halted. For temperature, the anomalies from all stations in the 5° x 5° square are averaged month-by-month to produce an area-average time series. For precipitation, the substantial degree of spatial variability makes it advisable to area-weight the station anomalies before calculating the regional mean for each month. To do this, the 5° x 5° region is divided into 20 x 20 smaller squares. The precipitation anomaly value assigned to a particular square is that of the station nearest to it (with the restriction that the distance separating a square from its nearest station should be no greater than 1° - where the distance is greater the square is ignored). The area average is then the mean of the values in the 400 (or fewer, if any fail the minimum distance criterion) squares. This method is similar to the standard Thiessen polygon method.

4. Regression analyses were performed using station temperature and precipitation anomalies as the predictands. These analyses were carried out on an annual and seasonal basis: winter (December, January, February), spring (March, April, May), summer (June, July, August) and autumn (September, October and November). By considering the monthly values as separate observations within each season, we were able to extend the number of observations and so preserve a high number of degrees of freedom. The predictor variables are the regionally-averaged anomalies of temperature and precipitation.

5. In order to determine the perturbation due to the enhanced greenhouse effect at each station, the results from GCMs were employed. It is assumed that a GCM grid-point temperature or precipitation value is equivalent to a regionally-average value derived from observational data. For each of the four GCMs (GFDL, GISS, OSU and UKMO), the perturbed run and control run grid-point temperature and precipitation values are interpolated to the station position. We then obtain, for temperature:

$$Atm_i = t_i(2 \times CO_2) - t_i(1 \times CO_2)$$

where Atm is the perturbation due to CO_2 or the 'temperature anomaly' for model i and, for precipitation:

$$Ptm_i = [p_i(2 \times CO_2) - p_i(1 \times CO_2)] \times 100/p_i(1 \times CO_2)$$

where Ptm is the standardized perturbation due to CO_2 or the 'precipitation anomaly'.

The values for Atm and Ptm for each GCM are then substituted in the regression equations to obtain a prediction for the station perturbation of temperature (°C) and precipitation (%) due to CO_2.

6. The predicted change in temperature and precipitation for each model is divided by the equilibrium (global mean) temperature change for that model. The results are then averaged across the four GCMs to obtain a composite value.

7. The procedures from points 3 to 6 is repeated for each station throughout the Mediterranean. The results can then be plotted and contoured to obtain a map of the expected patterns of temperature and precipitation change due to the greenhouse effect.

In order to arrive at this procedure, a rigorous investigation of the validity of the method has been carried out. In particular, we have looked at:

- the use of other predictor variables in the regression equations
- performance and verification of the regression equations
- autocorrelation in the data
- multicollinearity in the predictor variables

These aspects are discussed in detail below.

4.2.3 Regression Equation Performance

If the regression equations are to be an effective tool, the predictor variables must explain a high proportion of the variance in the predicted variable both during calibration and verification on independent data. Where the multiple correlation coefficient between the observed and predicted anomalies dropped below 0.8 in the case of temperature (64% of the variance explained) or 0.7 (50% of the variance explained) in the case of precipitation, the station was dropped from the analysis of that variable. Figs. 4.1-4.5 show the variance explained by the annual and seasonal regression equations when used to predict temperature and precipitation. In these cases, only two predictor variables were used: large-scale (i.e. grid point) temperature and precipitation. At the annual level, for temperature, the variance explained exceeds 60% virtually everywhere, and is in excess of 80% for at least half the region. However, for precipitation a much lower percentage of the variance, generally less than 60%, is explained in most areas. This pattern is repeated through the seasons, with the poorest performance in summer.

In addition to using temperature and precipitation as the only predictors, we tested the contribution of a range of pressure variables as additional predictors. Using the MSL pressure data set described in Section 2.1, three anomaly variables were derived: first, the monthly mean

pressure over the station to be predicted, interpolated from the 5° x 10° data set grid, second, the north-south pressure gradient and, third, the west-east pressure gradient over the station. A new set of regression equations was developed with five predictor variables. These were used to calculate the station temperature and precipitation anomalies and then the correlation coefficients between the observed and predicted data sets were calculated. The variances explained (i.e., the square of the correlation coefficients) are shown in Figs. 4.6-4.10. For precipitation, there is an increase in the variance explained when compared with the maps for the regression equations based on temperature and precipitation alone. There is no discernible change in the patterns of temperature prediction.

It is not a sufficient test of regression equation performance to use only the calibration correlation. Verification using an independent data set is required. Data for 1981-88 were excluded at the calibration stage specifically for use in verification. The results of the verification of the regression equations which used only temperature and precipitation anomalies as the predictor variables are shown in Figs. 4.11-15. For temperature, there is a slight shift in the patterns of variance explained. For example, at the annual level, north of the Adriatic Sea the variance drops from over 80% to 60-80%, whereas over western Turkey the reverse occurs. However, these changes are relatively minor. Overall, the temperature regressions show no significant difference in performance between calibration and verification.

The change in the patterns of explained precipitation variance is much more dramatic. At the annual level, there is a considerable decline in the variance explained, to only 0-20% in parts of the eastern Mediterranean. Highest verification values (over 40% of the variance explained) tend to be concentrated in the western Mediterranean. This reduction in variance explained for precipitation persists in the seasonal maps.

Verification of the five-variable regression equations (i.e., including the pressure anomaly variables) was also carried out using the 1981-88 data. The results are shown in Figs. 4.16-4.20. The verification performance of the regression equations with the pressure variables is almost identical to that of the regression equations which use only temperature and precipitation anomalies as the predictors. There is, therefore, no advantage in using the pressure variables. The final sub-grid-scale scenarios were therefore produced from the two-predictor-variable regression equations.

4.2.4 The Contribution of Each Predictor Variable

So far we have looked at five possible predictor variables for inclusion in multiple regression equations to predict station temperature and precipitation anomalies. Of these, three (the pressure variables) have been rejected as making only a trivial additional contribution. We can investigate the basis of this decision more thoroughly by looking at the correlation between the two predicted variables and each of the five potential predictor variables alone.

The results of this analysis are shown in Figs. 4.21-4.25. The first two Figures show the variance explained by the regionally-averaged anomalies of temperature (Fig. 4.21) and precipitation (Fig. 4.22). It is clear that a high proportion of the variance in each station anomaly variable is explained by the regionally-averaged anomaly of the same variable. Wigley et al. (1990) obtained the same result for Oregon State.

The variance explained by the three pressure variables is shown in Figs. 4.23-4.25. In the case of the mean pressure anomaly, the variance explained for both predicted variables is, for most of the region, less than 10%. The maximum variance explained is between 36% and 37%, for precipitation, but this is in the extreme north-west of the study area, away from the main centre of interest. The north-south and west-east

pressure gradient anomalies also explain on average less than 10% of the variance in both predicted variables. The best result is obtained for the prediction of station temperature in the western Mediterranean by the west-east pressure gradient, but even this does not explain more than 25% of the variance. Although some of these relationships are statistically significant, they add little to the multiple regressions because of intercorrelations between the pressure predictor variables and the temperature and precipitation predictors.

4.2.5 The Problem of Multicollinearity

Ideally, the predictor variables in a multiple regression equation should be independent of one another. That is to say, when the correlation between them is calculated, it should effectively be zero. If this is not the case, then the regression coefficients will not be a true estimate of the contribution of each of the predictor variables to the variance in the predicted variable (Gunst and Mason, 1980). We have investigated this problem with regard to the UNEP Mediterranean study region.

The regression equations in this study contain only two predictor variables: regionally-averaged temperature anomalies and regionally-averaged precipitation anomalies. In this situation, it is sufficient to examine the correlation coefficient between these two predictors in order to determine the extent of the multicollinearity. This has been done for two regions: in the western Mediterranean, Spain and Morocco, and in the eastern Mediterranean, Greece and Turkey. The correlations are calculated using the monthly anomalies of area-average temperature and precipitation (sample size 39 years x 12 months = 468).

It was found that the correlation between the temperature and precipitation anomalies was only -0.21 in the western region and only -0.16 in the eastern region. These correlations are sufficiently weak that the problem of multicollinearity can be ignored.

4.2.6 The Problem of Autocorrelation

Regression models which involve time series data (as here) may be biased if the data are autocorrelated. It is a fundamental assumption in linear regression that the error terms have a mean of zero, a constant variance, and are uncorrelated. If not, the regression equation may give a false impression of accuracy, i.e., the multiple correlation coefficient in calibration may seriously overestimate the fidelity of the regression model when used in a predictive sense. We have already seen that the regression equations are effective at predicting station temperature anomalies when tested on the 1981-88 data, but that the results for precipitation are less successful.

In order to assess the effects of autocorrelation, we looked again at two regions: Spain and Morocco in the western Mediterranean and Greece and Turkey in the eastern Mediterranean. The lagged correlation coefficients were computed. The correlation between temperature at time *t* and at time *t-1* is the lag 1 correlation, the correlation between temperature at time *t* and at time *t-2* is the lag 2 correlation, and so on. It is usually sufficient to examine only the first few lag correlations in order to see if autocorrelation is likely to be a problem.

Lagged correlations for the regionally-averaged time series of monthly temperature and precipitation anomalies are shown for the West and East Mediterranean in Tables 4.1 and 4.2. The lagged correlations for precipitation are considerably lower than those for temperature. Although some of these correlations are statistically significant at the 5% level, it appears unlikely that autocorrelation is the cause of the poor performance of the regression models in predicting precipitation in the verification period.

Table 4.1 Autocorrelation in the western Mediterranean

	Temperature	Precipitation
Lag 1	0.19	0.07
Lag 2	0.05	-0.05
Lag 3	0.02	0.02
Lag 4	-0.09	-0.02
Lag 5	-0.07	0.01

Table 4.2 Autocorrelation in the eastern Mediterranean

	Temperature	Precipitation
Lag 1	0.35	0.12
Lag 2	0.16	0.08
Lag 3	0.04	0.04
Lag 4	0.05	0.03
Lag 5	0.06	0.07

4.3 SUB-GRID-SCALE SCENARIOS FOR THE MEDITERRANEAN BASIN

The station network used in the construction of the scenarios is shown in Fig. 4.26. These have at least 20 years of record for six months out of the twelve over the period 1951-88. Station names and attributes (height, position, etc.) are given in Appendix 1. The number of stations available for scenario construction is 248 for temperature and 328 for precipitation. However, not all these stations are used in the final procedure. Some were discarded because they have too few near neighbours for the calculation of the regionally-averaged predictor anomalies, whilst others were discarded because the correlation coefficients between the predicted and observed station anomalies were below 0.8 for temperature or 0.7 for precipitation.

The sub-grid-scale scenarios, constructed according to the method outlined in Section 4.2.2, are shown in Figs. 4.27-4.31. Data sparse and low correlation areas are left blank. The summer precipitation change scenario is the only one where low correlations seriously limit the area over which the procedure can be applied. No prediction for precipitation can be attempted for much of the western Mediterranean in this season.

The annual temperature change scenario shows a variation between +1.6°C and +0.7°C for every °C increase in the global-mean temperature. The northern coast of the Mediterranean Sea marks a zone of rapid transition between low (over the sea) and high (inland) temperature change. The areas of greatest increase (i.e., greatest sensitivity to a change in global mean temperature) are in the south-west and north-east of the study region. The best way to evaluate this map is to compare it with the equivalent scenario based solely on GCM grid-point output (Fig. 3.1). The range of temperature change is larger than that shown by the direct scenario and, of course, the spatial detail is much greater. However, the patterns are broadly the same.

In winter, there are certain differences between the sub-grid-scale (Fig. 4.28) and the direct scenario (Fig. 3.2). This is largely due to the greater resolution of the former. Thus, whereas in the direct scenario the area of high sensitivity in the north-west is shown to dissipate over France, in the sub-grid-scale scenario it wraps round the western Mediterranean Sea into North Africa. In spring, the high sensitivity area again extends further west than in the direct scenario, but this time no further than the Pyrenees.

The summer and autumn sub-grid-scale scenarios show greater divergence from the direct scenarios than is the case in winter and spring. In summer, much of the eastern Mediterranean shows high sensitivity (over +1.3°C) to a 1°Cchange in global-mean temperature, whereas in the direct

scenario the sensitivity over this region is generally less than +1.2°C. Conversely, the area of high sensitivity in the direct scenario over Spain and southern France is not present in the sub-grid-scale scenario. The autumn changes in the sub-grid-scale scenario are larger than those in the direct scenario. This is particularly so over the western Mediterranean, where a sensitivity of over +1.3°C in Fig. 4.31 can be contrasted with an increase of 1.1-1.2°C in Fig. 3.5.

There are two pronounced differences between the direct and sub-grid-scale scenarios of precipitation. The first, and most obvious, is the much greater spatial variability of the latter. This must be expected when we contrast the coarse resolution of the direct scenarios with the high spatial variability of observed precipitation. The high density station network, on which the sub-grid-scale scenarios are based, can reproduce this level of variability. The second is the greater range of sensitivity indicated by the sub-grid-scale scenarios. Thus, the direct annual scenario for precipitation indicates changes of between 4%/month and -1%/month for a 1°C change in global-mean temperature. The sub-grid-scale scenario of Fig. 4.27 has values ranging between +13% and -12%/month.

The annual map indicates that the area expected to experience a decrease in precipitation is slightly greater than the area expected to show an increase. Areas of increase are mainly over the northern part of the study region and over the central Mediterranean between Italy and Tunisia.

In winter (Fig. 4.28), the zone of increased precipitation is larger than that predicted at the annual level. However, the areas affected are much the same: the northern part of the study region and an area extending from Italy and Sardinia south into Tunisia and parts of Algeria and Libya. In spring (Fig. 4.29), the edge of the area of increased rainfall runs along the north coast of the Mediterranean Sea, only extending into North Africa at three spatially-restricted locations. The summer patterns (Fig.

4.30) indicate an increase in precipitation in only four isolated areas. In most places, rainfall is expected to decline. However, because of low correlations, no prediction could be attempted for large parts of Spain, Turkey and North Africa. Autumn precipitation (Fig. 4.31) should decline over the western Mediterranean and increase over much of the central and western Mediterranean.

4.4 CONCLUSIONS

We have applied the methods developed by Kim et al. (1984) and Wigley et al. (1990) to the problem of constructing sub-grid-scale climate change scenarios for the Mediterranean Basin. Regression equations were developed to predict station temperature and precipitation anomalies from regionally-averaged climate anomalies. Of the five predictor variables tested, only temperature and precipitation were found to contribute usefully to the prediction of station values.

After verifying the regression equations (one equation for temperature and one for precipitation for each station and for each season), the equations were used to derive the detailed scenarios. This was done by inserting the appropriate interpolated GCM-derived grid point changes into the regression equation for every station in the data set. The results were contoured to produce a scenario for the Mediterranean Basin.

Annual and seasonal scenarios for both temperature and precipitation change were produced. The temperature scenarios should be a considerable improvement on the direct scenarios developed in Chapter 3. The patterns were broadly similar, but the greater spatial resolution added substantially to our knowledge of the changes indicated by the GCMs for this geographically-complex region. The greatest sensitivity was found in the area to the north of the Mediterranean Sea, with the northern coastline picked out as a zone of rapid transition.

The scenarios for precipitation are much more difficult to evaluate. We showed in Chapter 3 that the direct scenarios for this climate variable are conflicting: where the mean change is suggested to be an increase in precipitation the lower 90% confidence limit is generally negative, and vice versa. Here we have added a second level of uncertainty, since the proportion of the variance in the station precipitation anomalies explained by the regionally-averaged predictor variables is generally small: less than 60% for most of the region and most of the year. Therefore, the confidence that we can place in the sub-grid-scale scenarios of precipitation must be low.

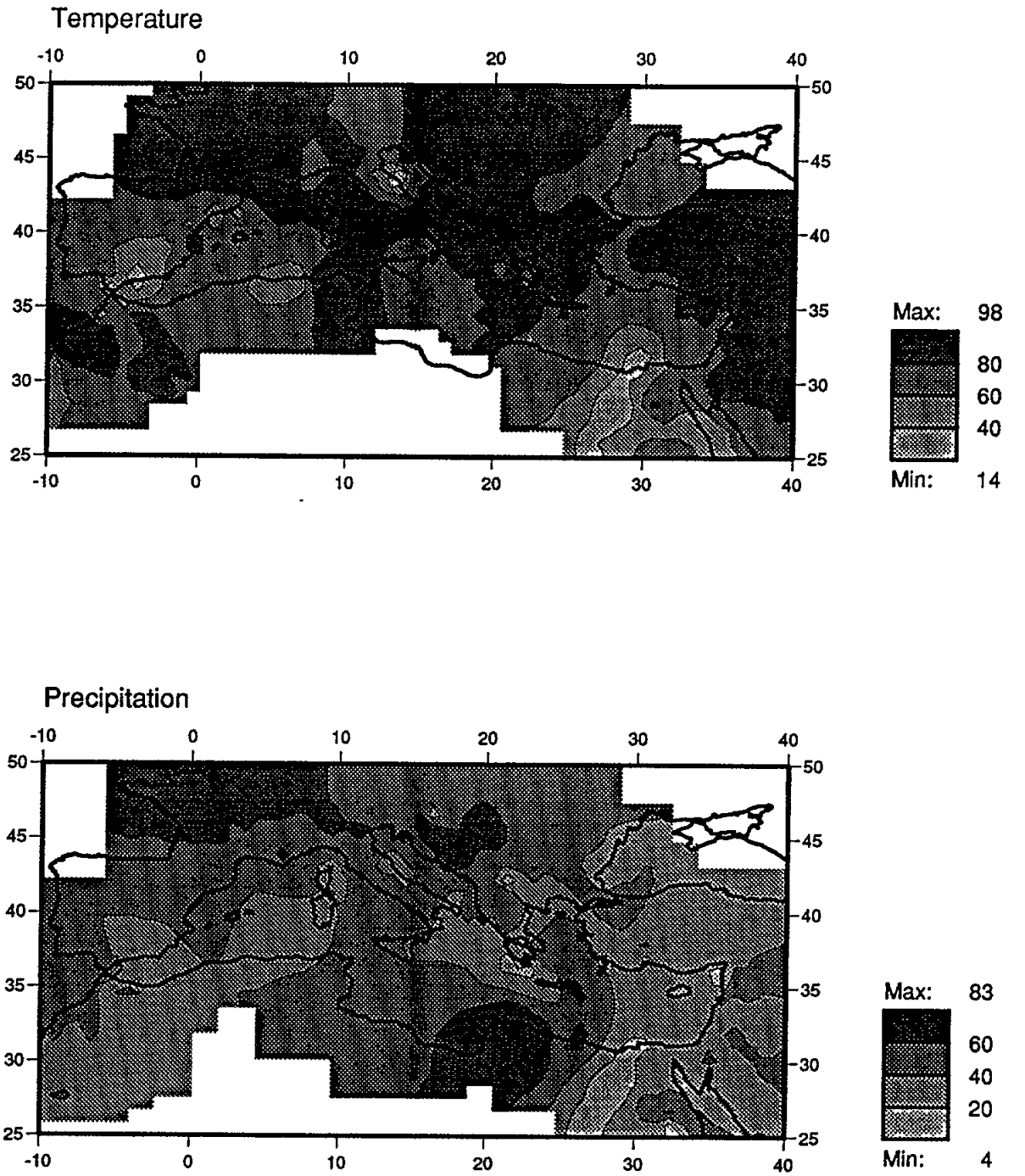

Fig. 4.1 Variance explained (%) by the regression equations estimating annual station temperatures and precipitation in the period 1951-80. Predictor variables temperature and precipitation

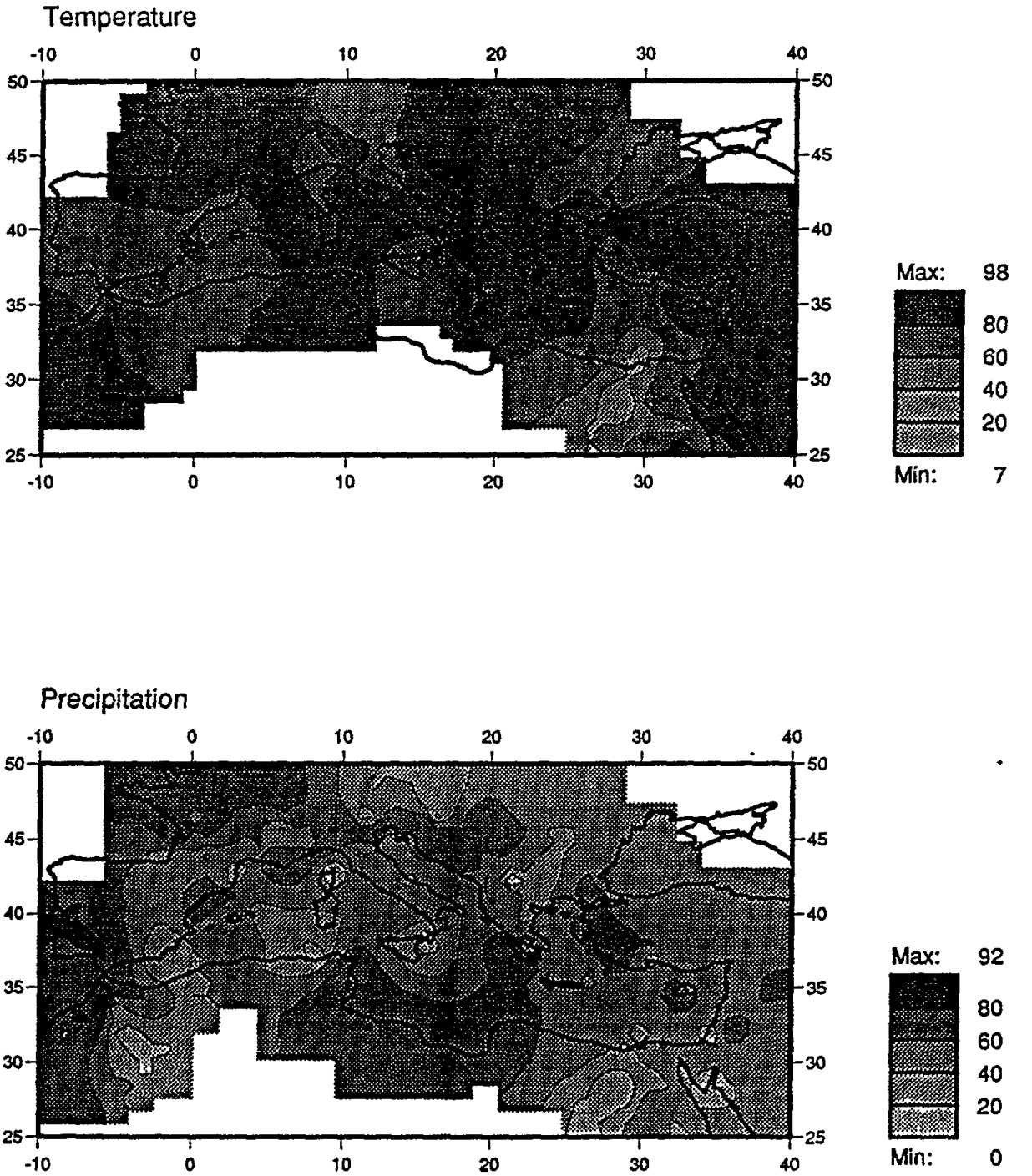

Fig. 4.2 Variance explained (%) by the regression equations estimating winter station temperatures and precipitation in the period 1951-80. Predictor variables temperature and precipitation

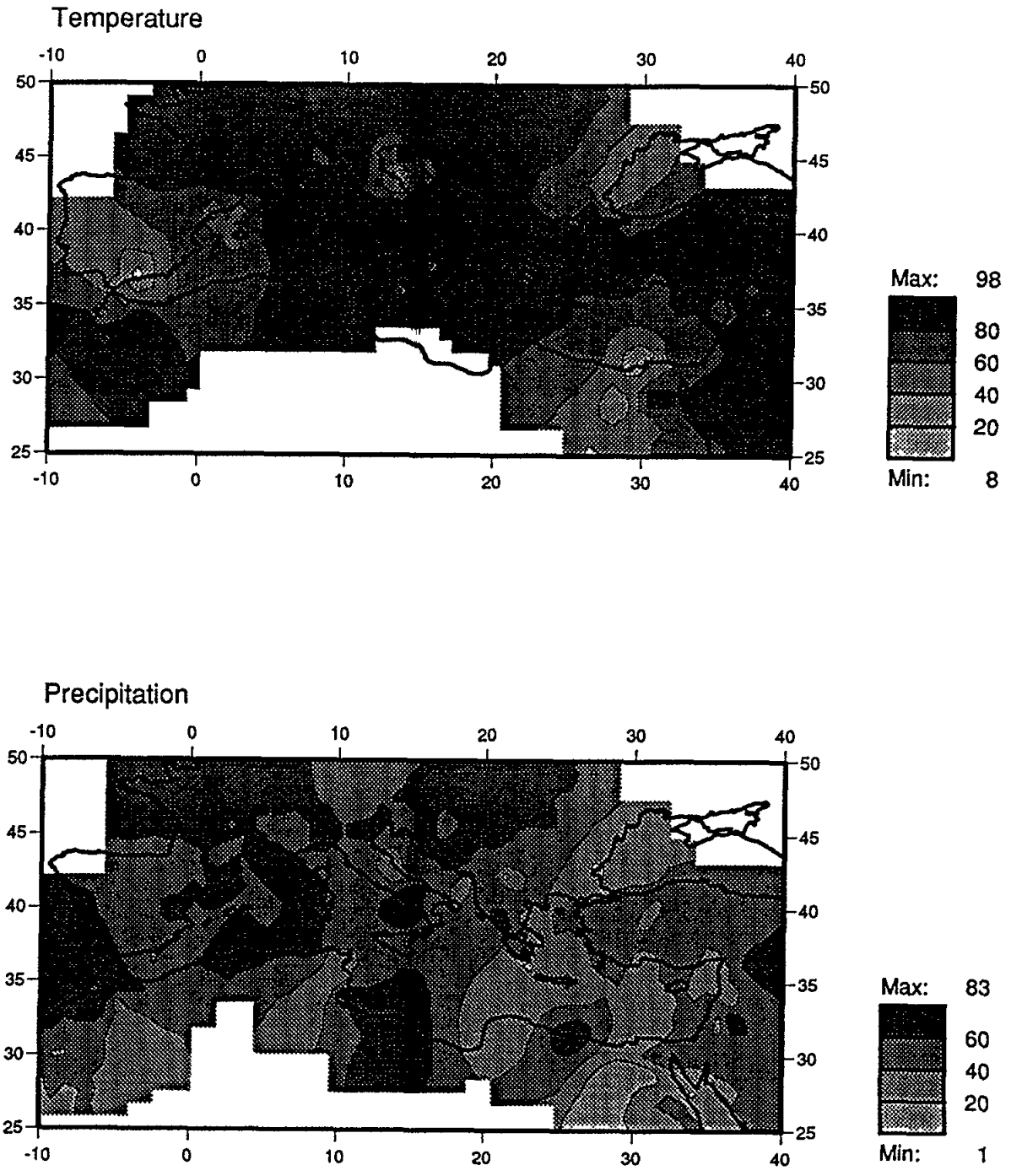

Fig. 4.3 Variance explained (%) by the regression equations estimating spring station temperatures and precipitation in the period 1951-80. Predictor variables temperature and precipitation

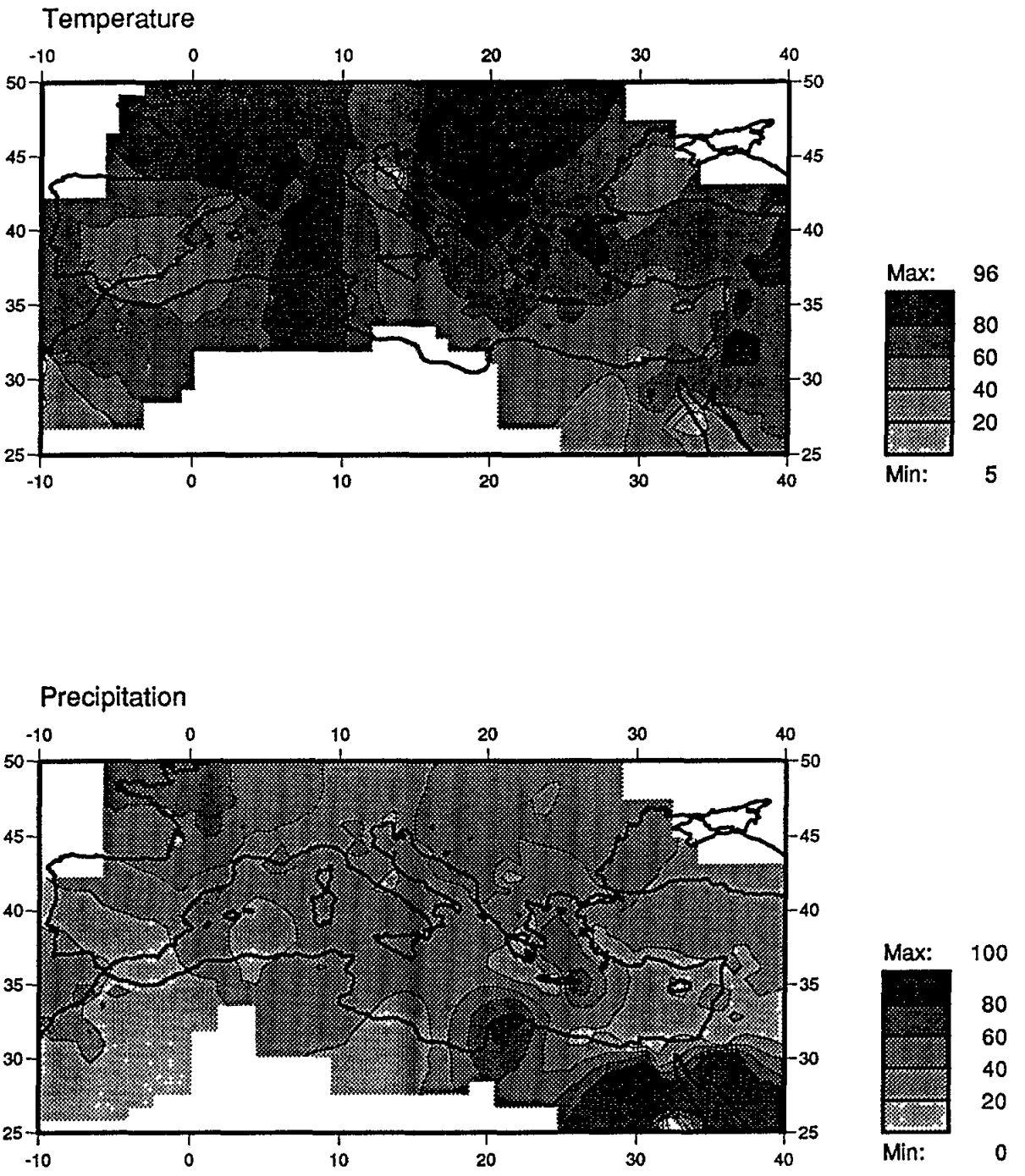

Fig. 4.4 Variance explained (%) by the regression equations estimating summer station temperatures and precipitation in the period 1951-80. Predictor variables temperature and precipitation

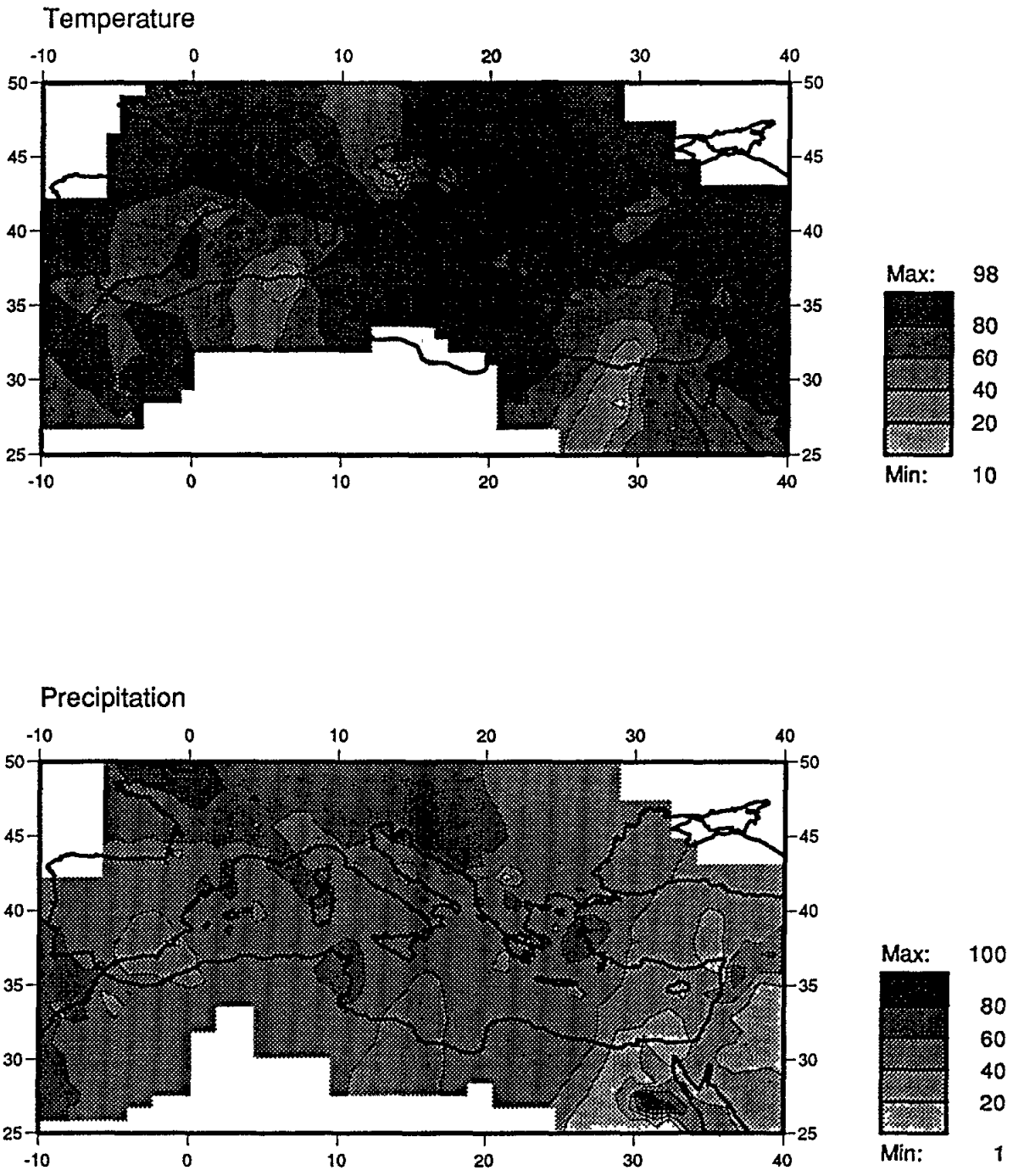

Fig. 4.5 Variance explained (%) by the regression equations estimating autumn station temperatures and precipitation in the period 1951-80. Predictor variables temperature and precipitation

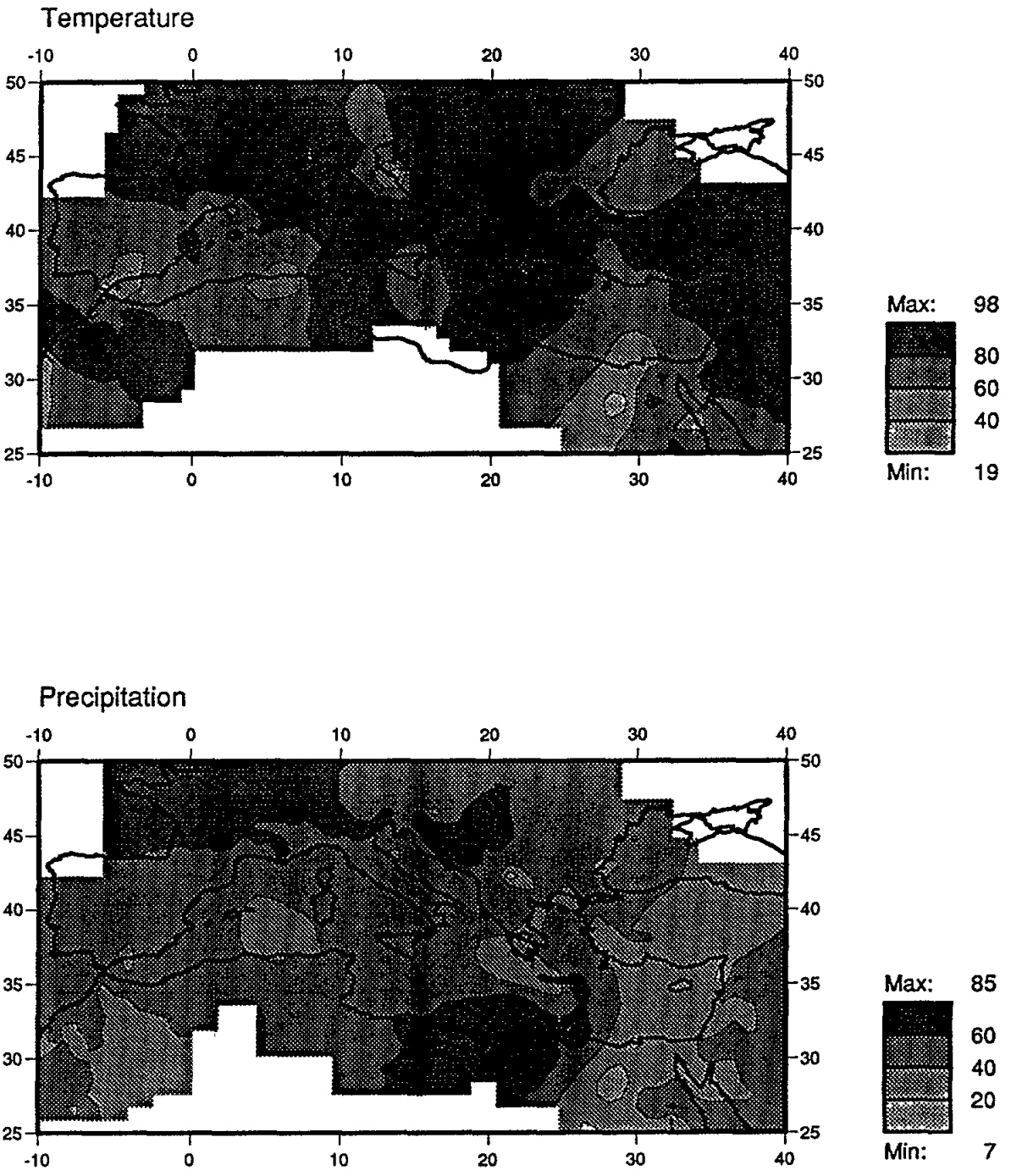

Fig. 4.6 Variance explained (%) by the regression equations estimating annual station temperatures and precipitation, using five predictor variables

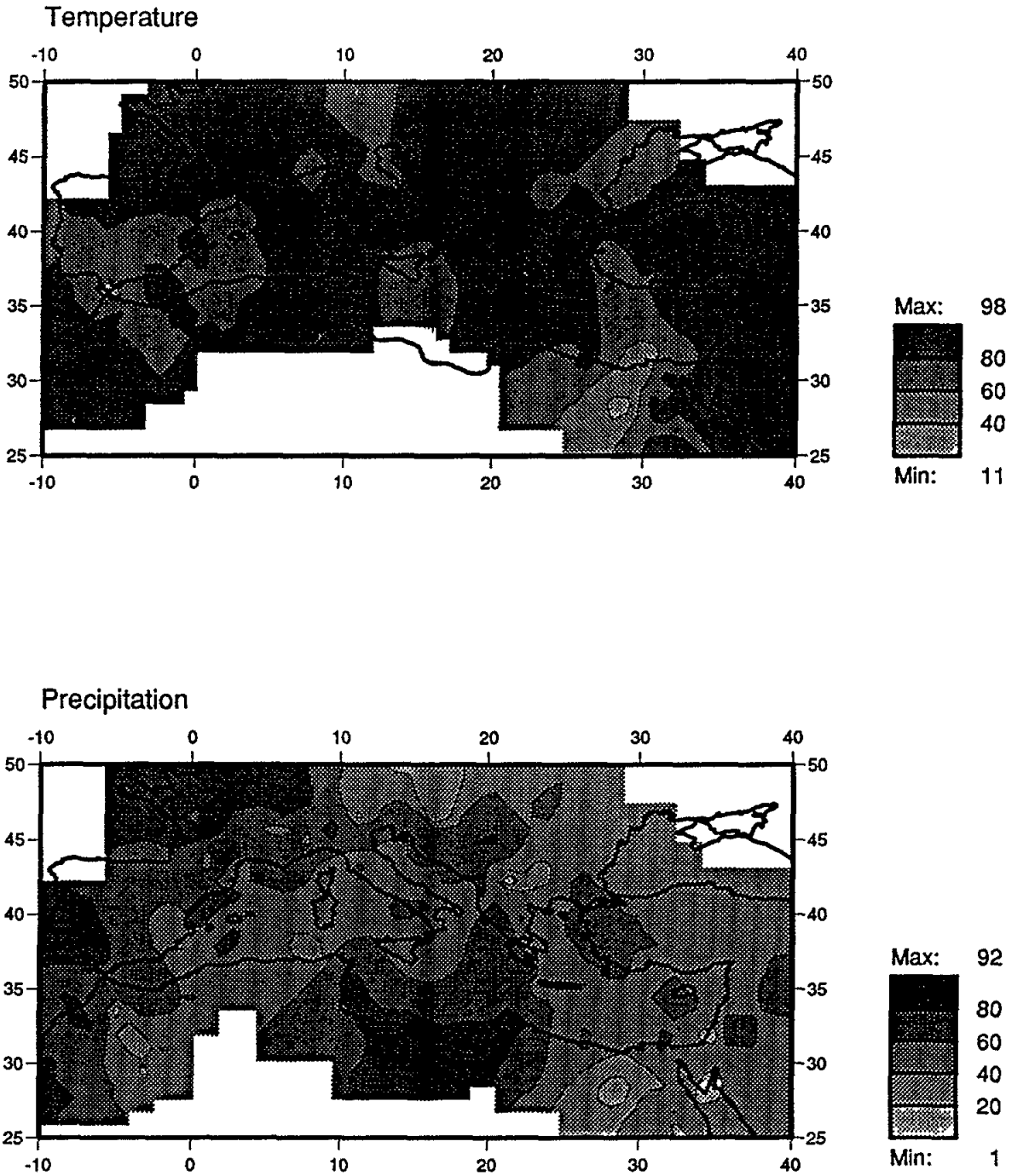

Fig. 4.7 Variance explained (%) by the regression equations estimating winter station temperatures and precipitation, using five predictor variables

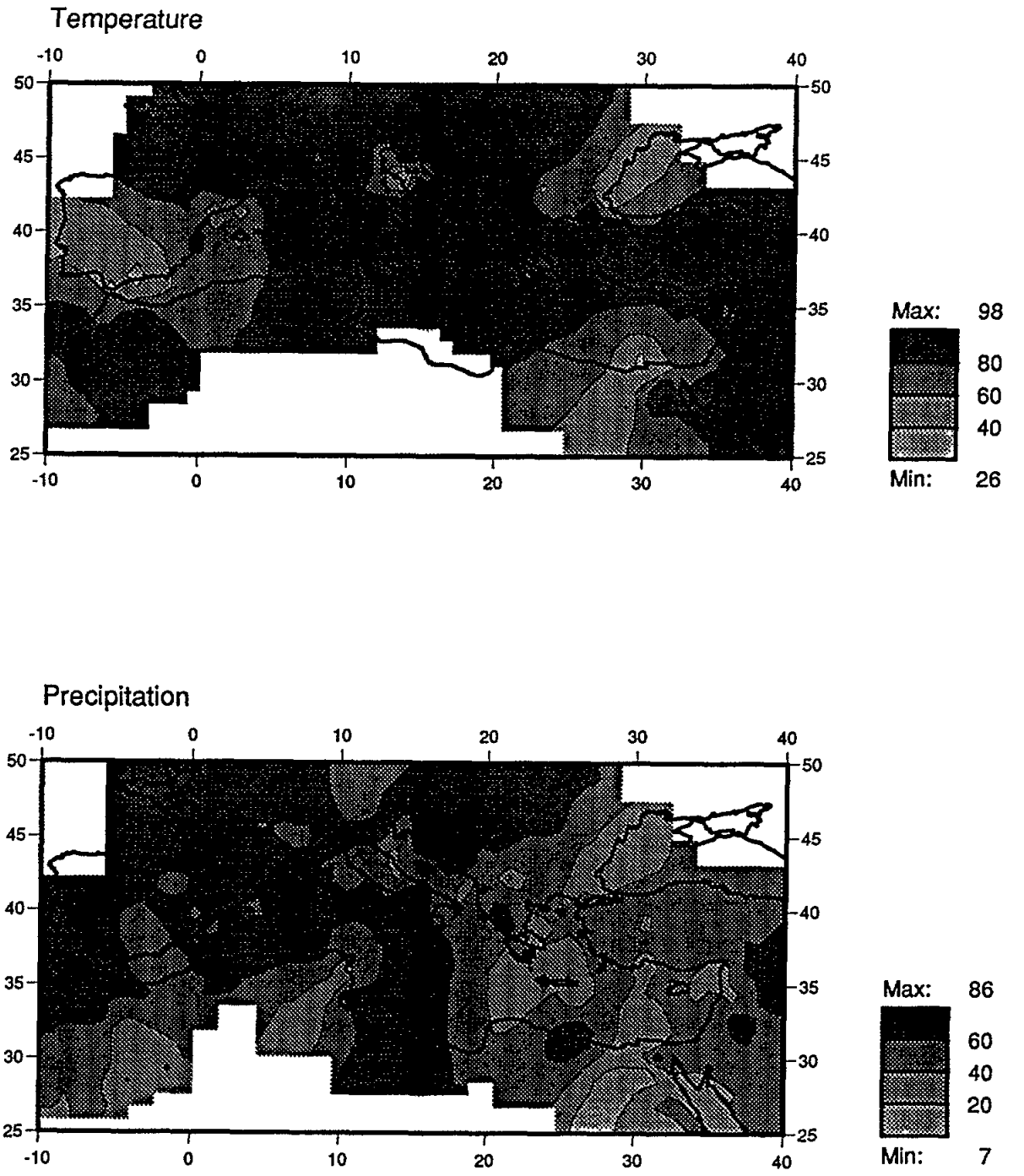

Fig. 4.8 Variance explained (%) by the regression equations estimating spring station temperatures and precipitation, using five predictor variables

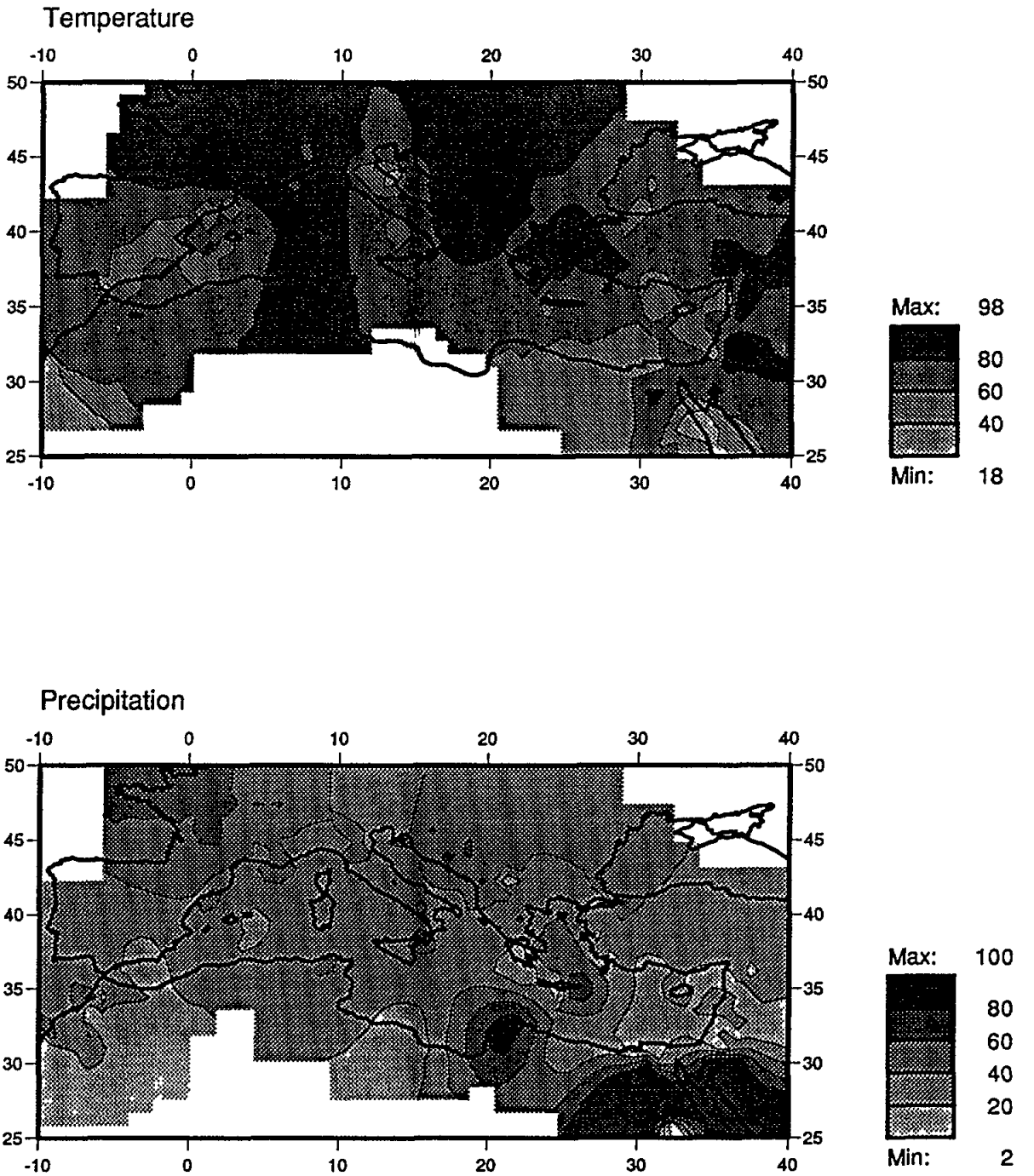

Fig. 4.9 Variance explained (%) by the regression equations estimating summer station temperatures and precipitation, using five predictor variables

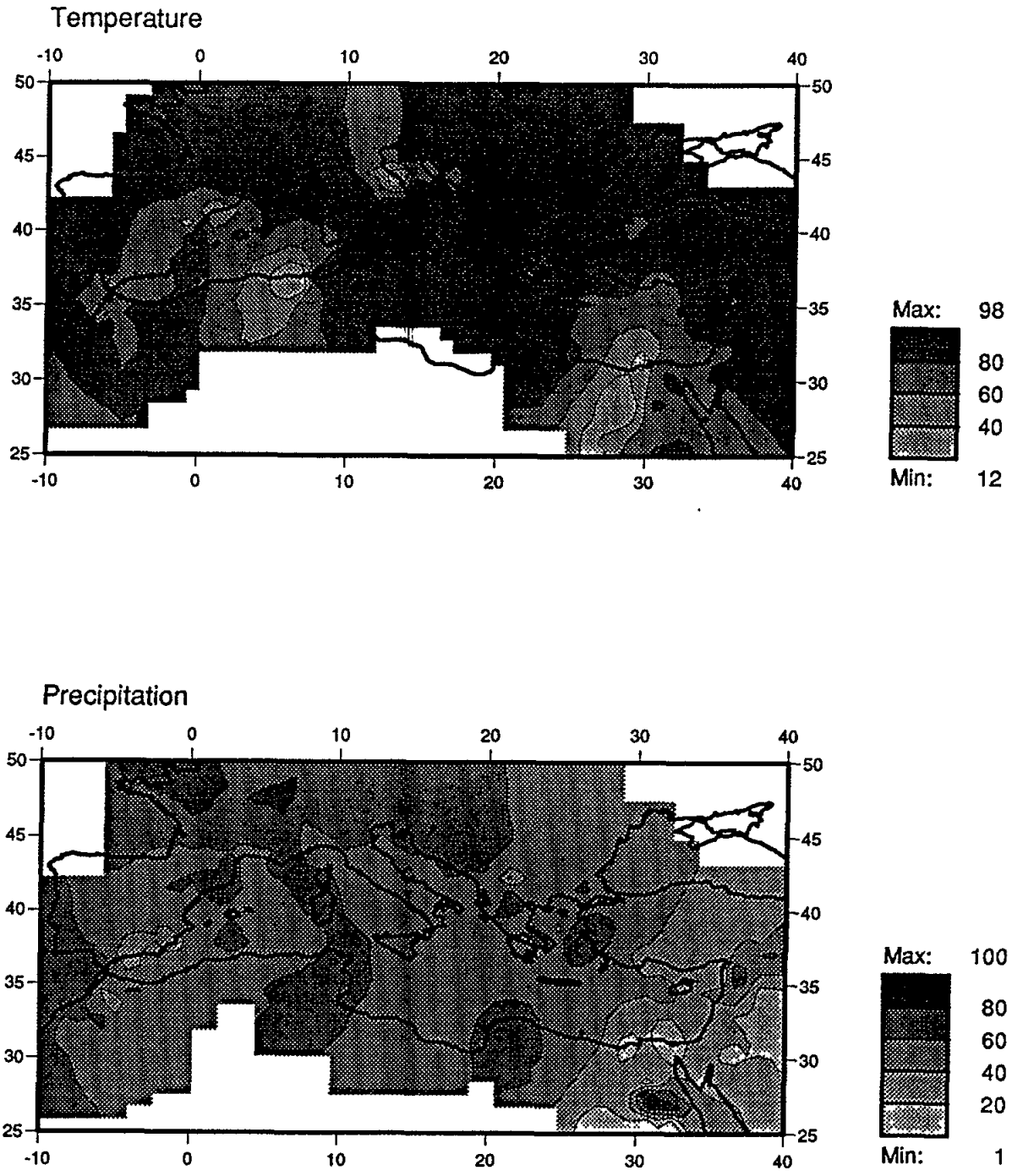

Fig. 4.10 Variance explained (%) by the regression equations estimating autumn station temperatures and precipitation, using five predictor variables

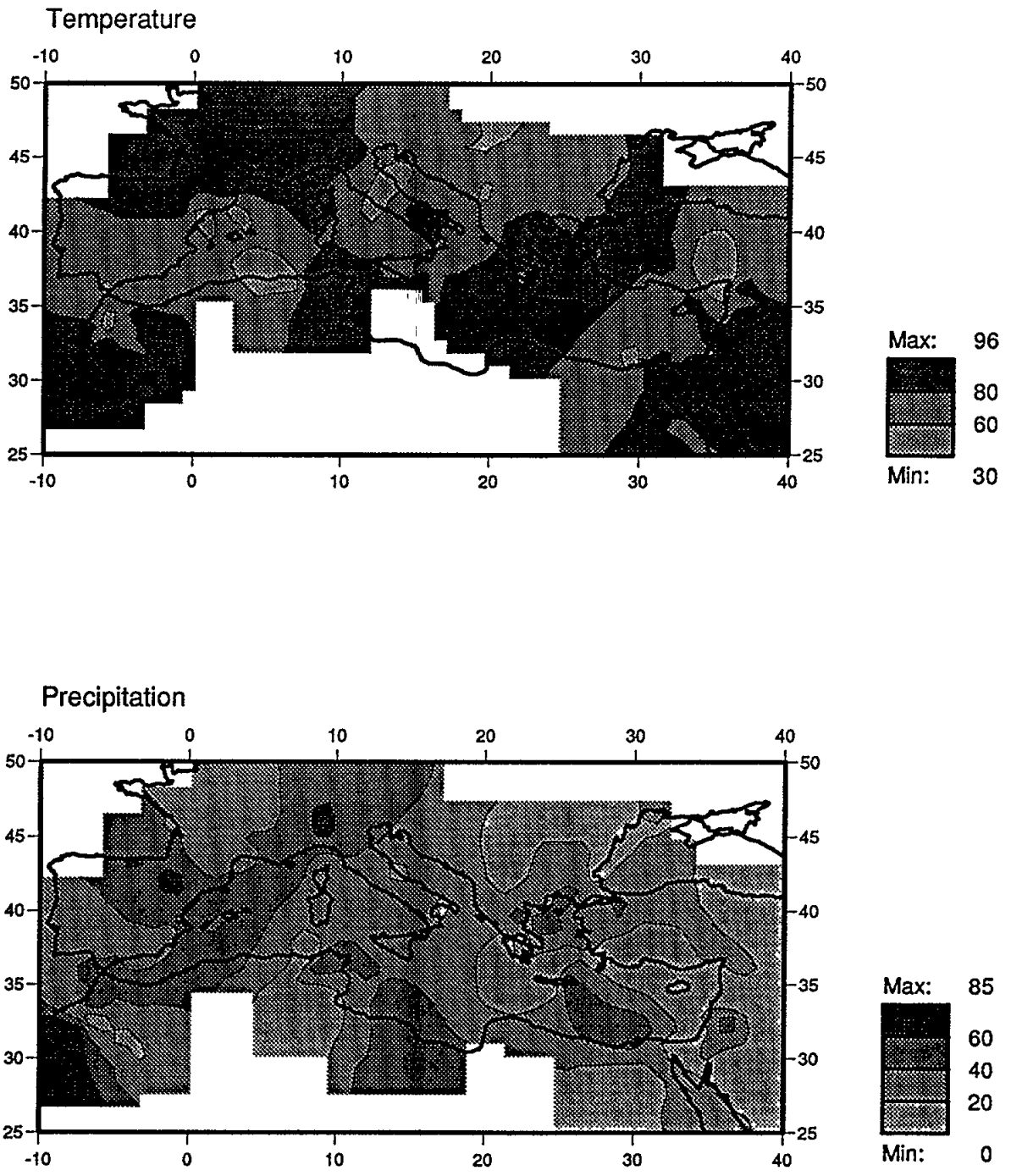

Fig. 4.11 Variance explained (%) by the 2-predictor-variable regression equations estimating annual station temperatures and precipitation in the 1981-88 period

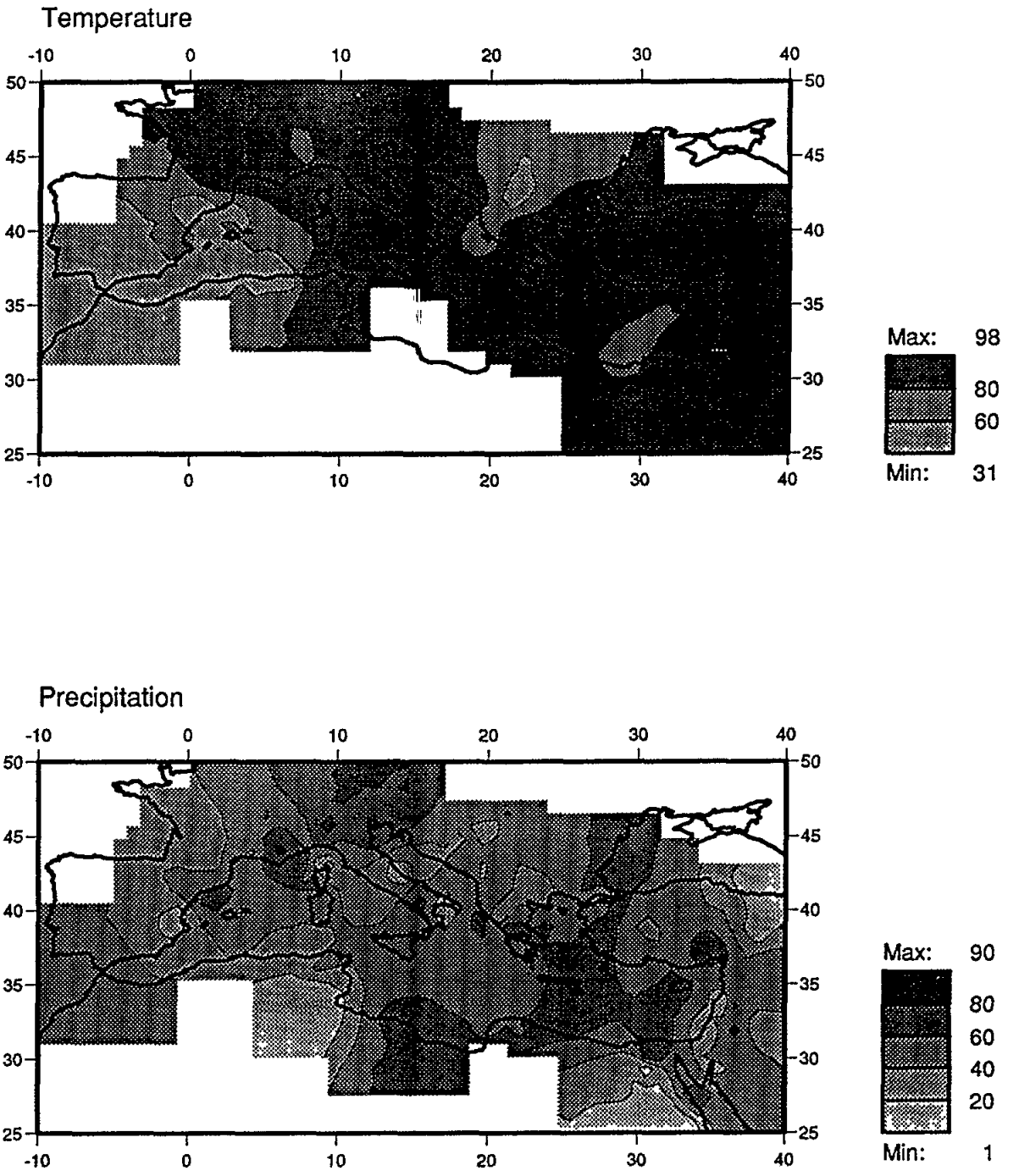

Fig. 4.12 Variance explained (%) by the 2-predictor-variable regression equations estimating winter station temperatures and precipitation in the 1981-88 period

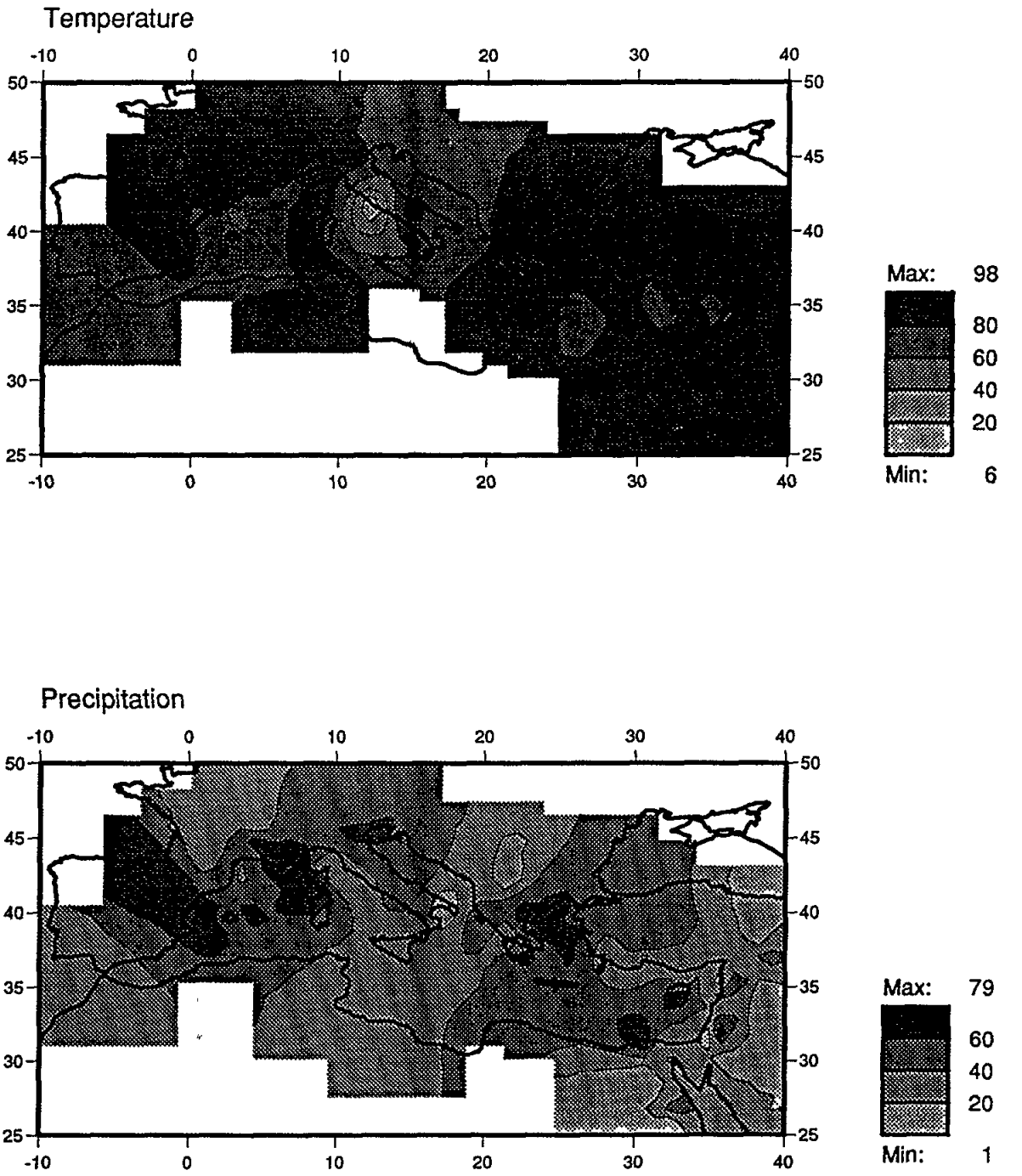

Fig. 4.13 Variance explained (%) by the 2-predictor-variable regression equations estimating spring station temperatures and precipitation in the 1981-88 period

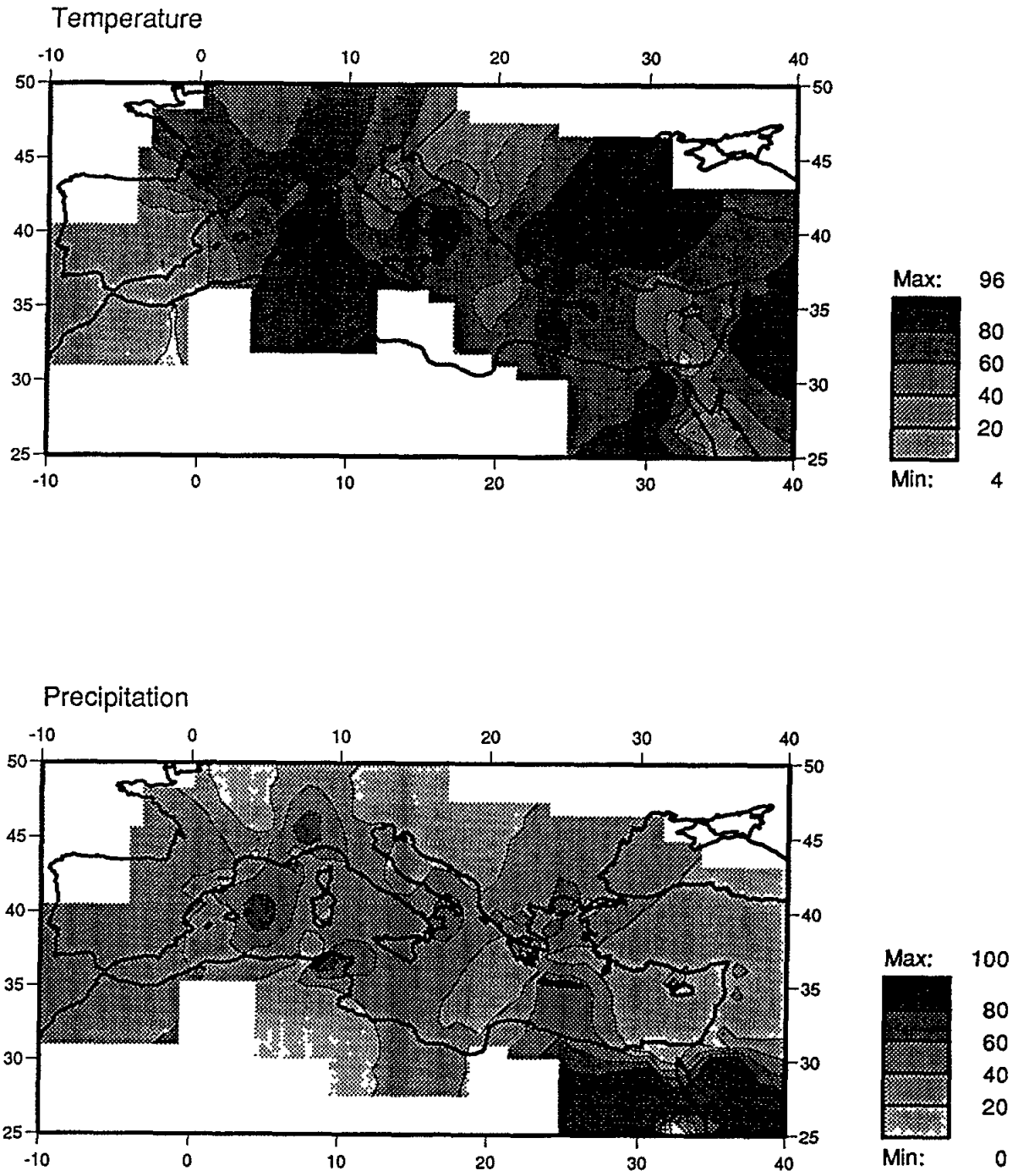

Fig. 4.14 Variance explained (%) by the 2-predictor-variable regression equations estimating summer station temperatures and precipitation in the 1981-88 period

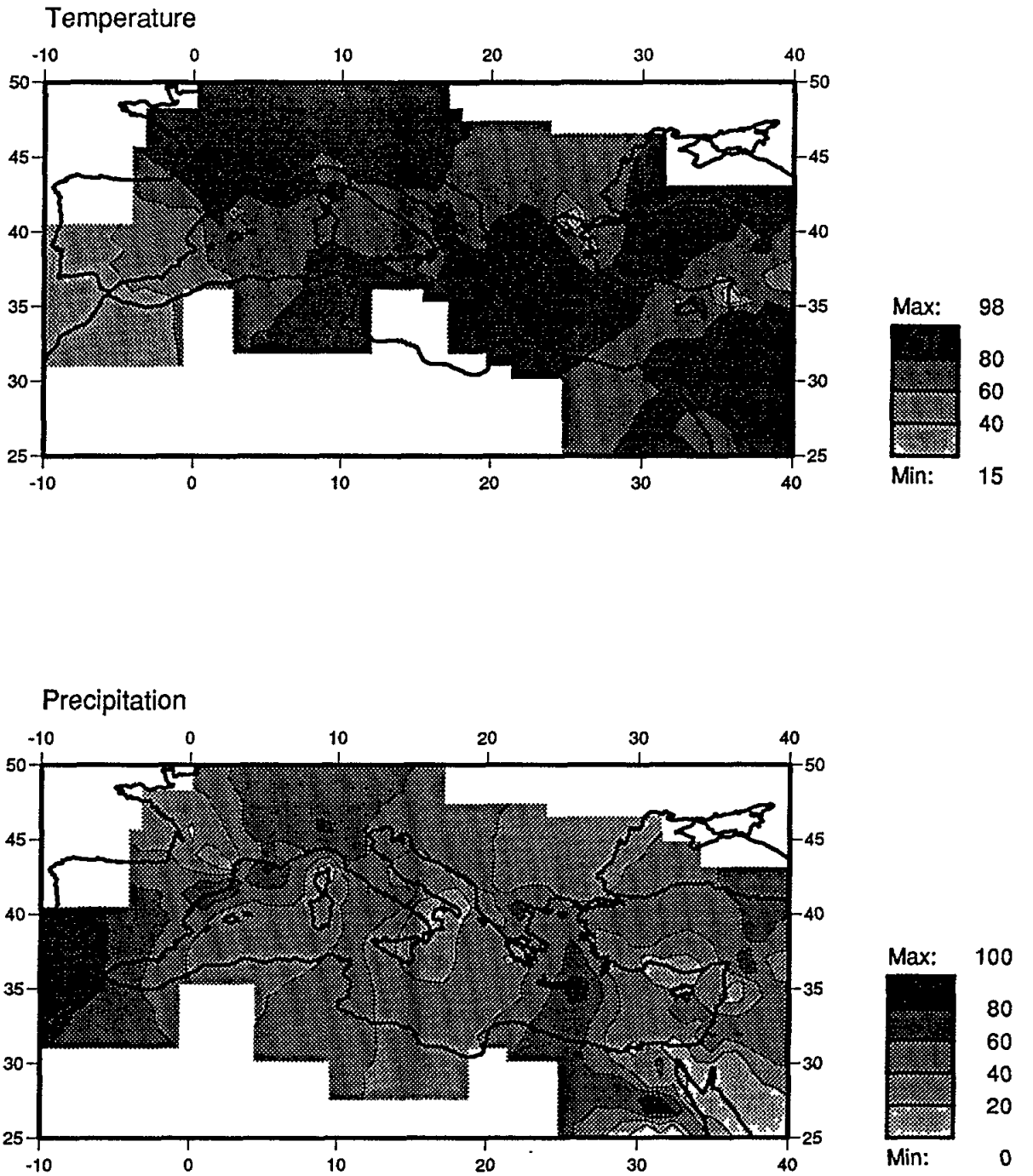

Fig. 4.15 Variance explained (%) by the 2-predictor-variable regression equations estimating autumn station temperatures and precipitation in the 1981-88 period

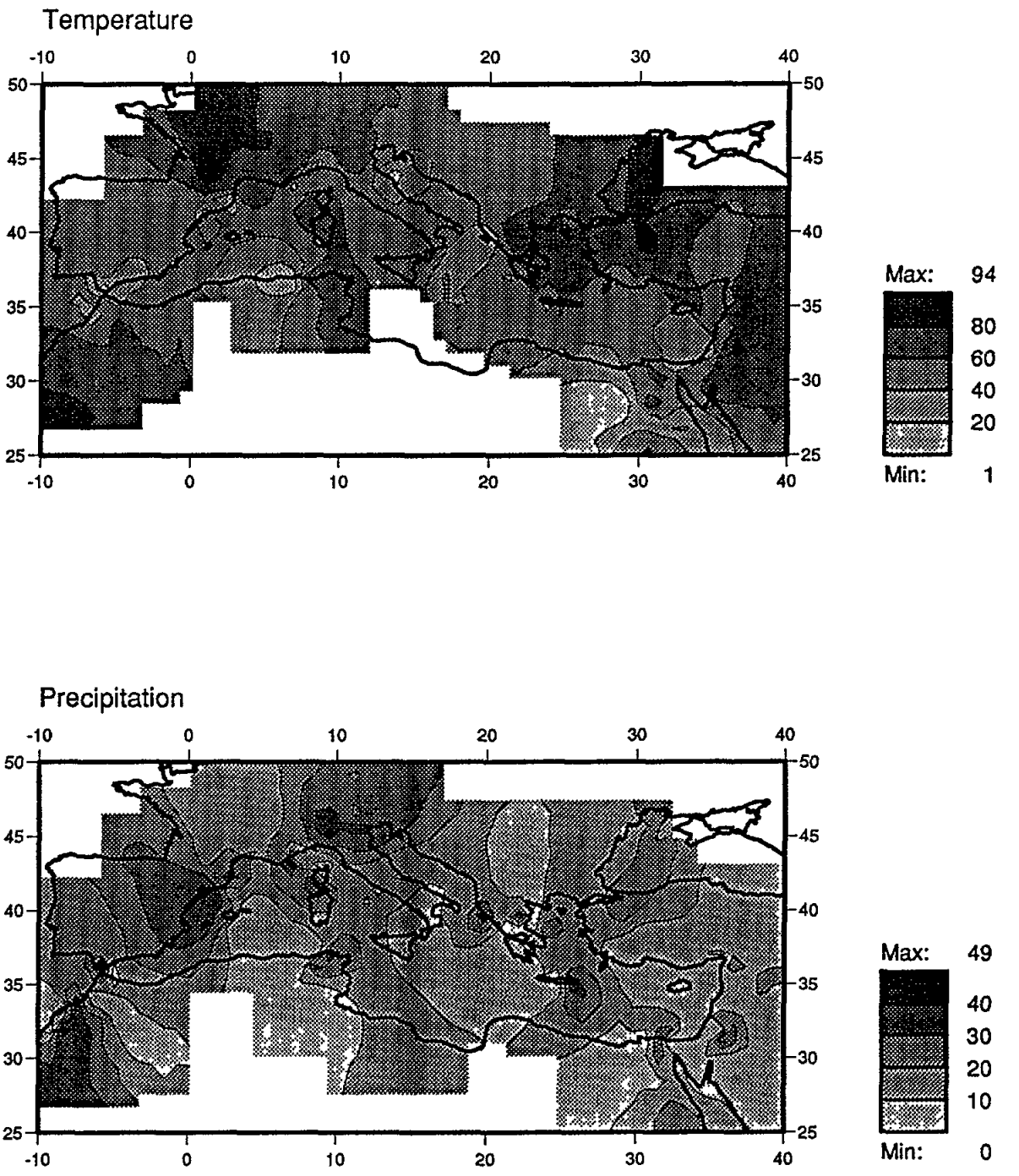

Fig. 4.16 Variance explained (%) by the 5-predictor-variable regression equations estimating annual station temperatures and precipitation in the 1981-88 period

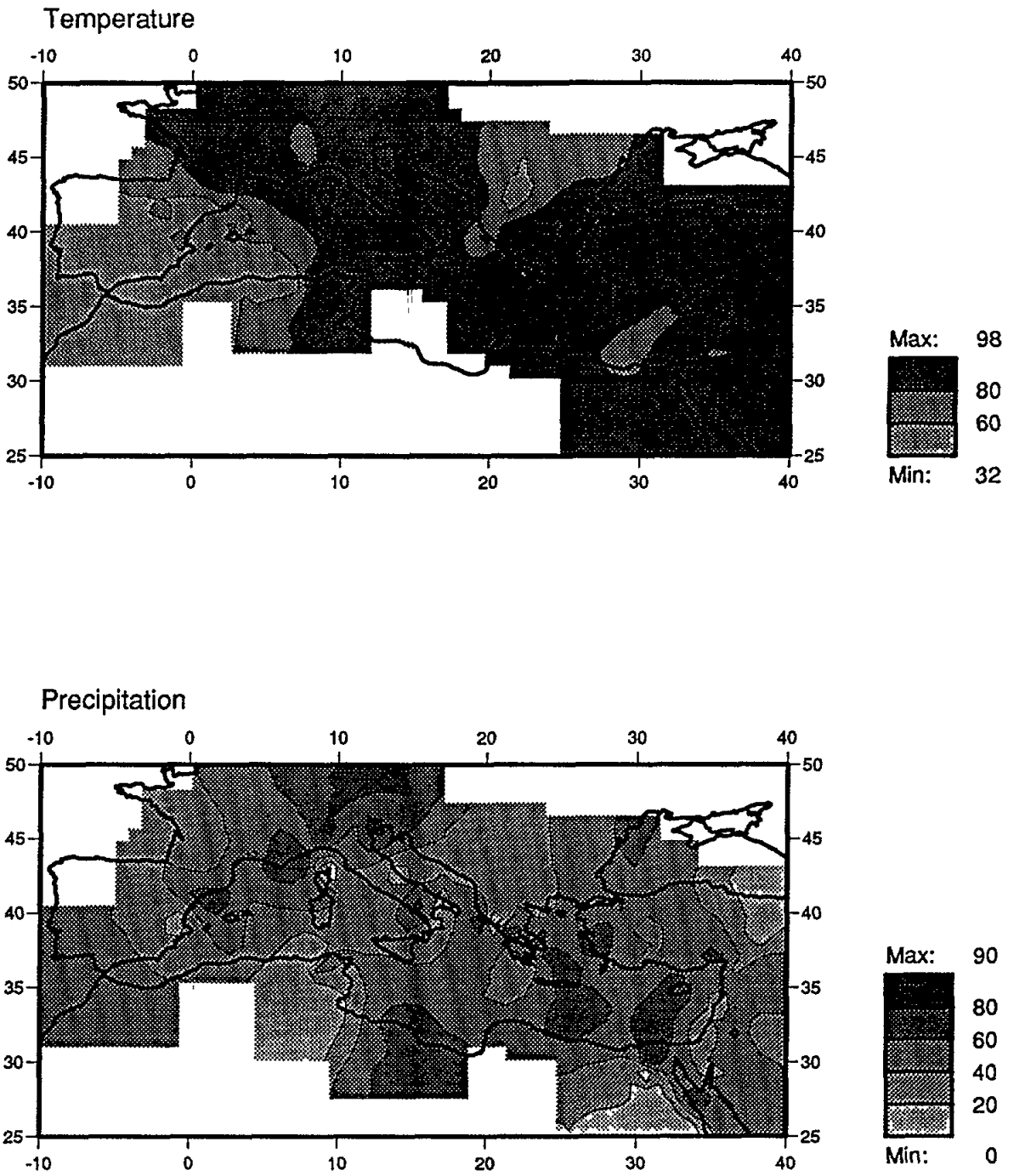

Fig. 4.17 Variance explained (%) by the 5-predictor-variable regression equations estimating winter station temperatures and precipitation in the 1981-88 period

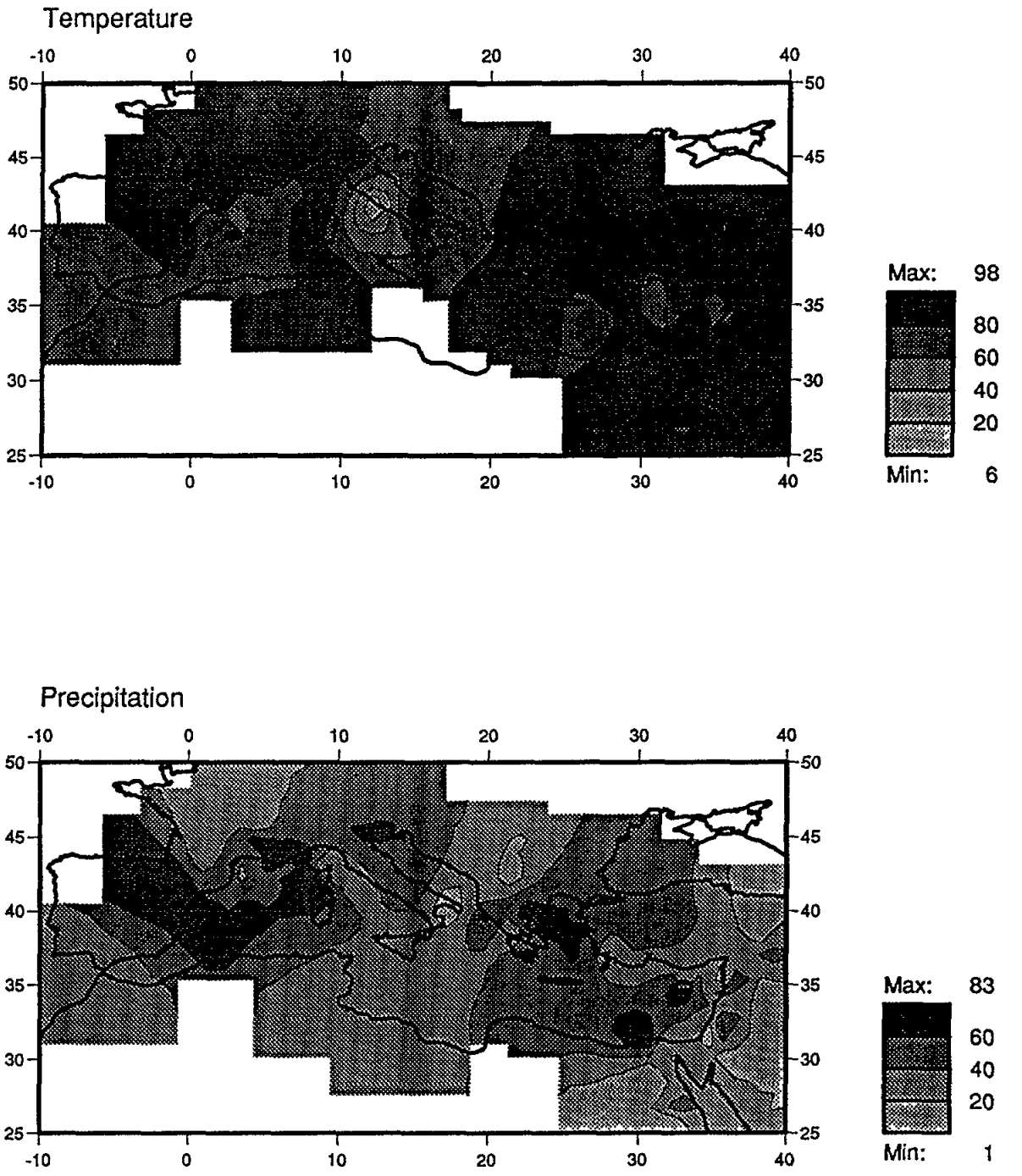

Fig. 4.18 Variance explained (%) by the 5-predictor-variable regression equations estimating spring station temperatures and precipitation in the 1981-88 period

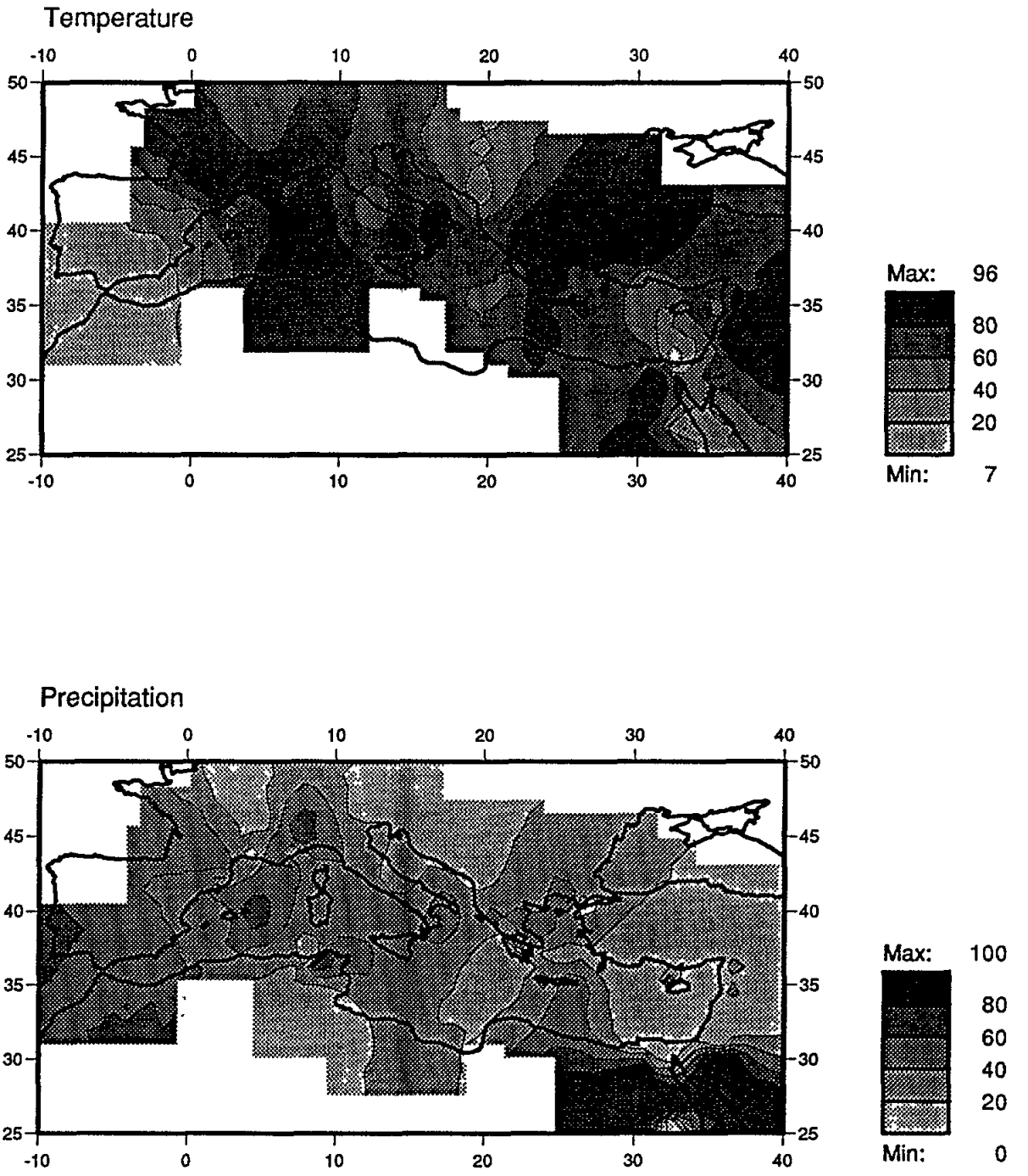

Fig. 4.19 Variance explained (%) by the 5-predictor-variable regression equations estimating summer station temperatures and precipitation in the 1981-88 period

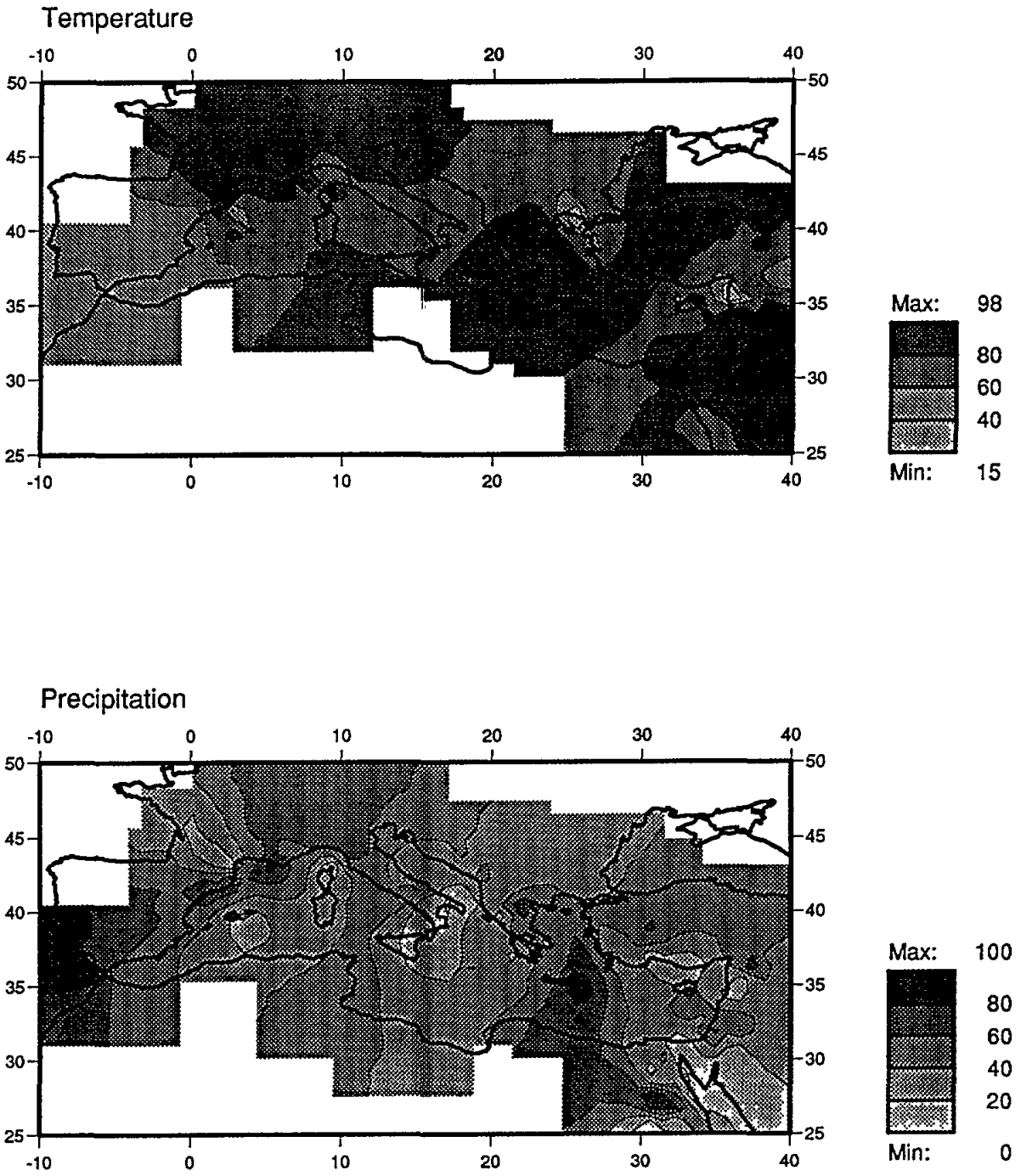

Fig. 4.20 Variance explained (%) by the 5-predictor-variable regression equations estimating autumn station temperatures and precipitation in the 1981-88 period

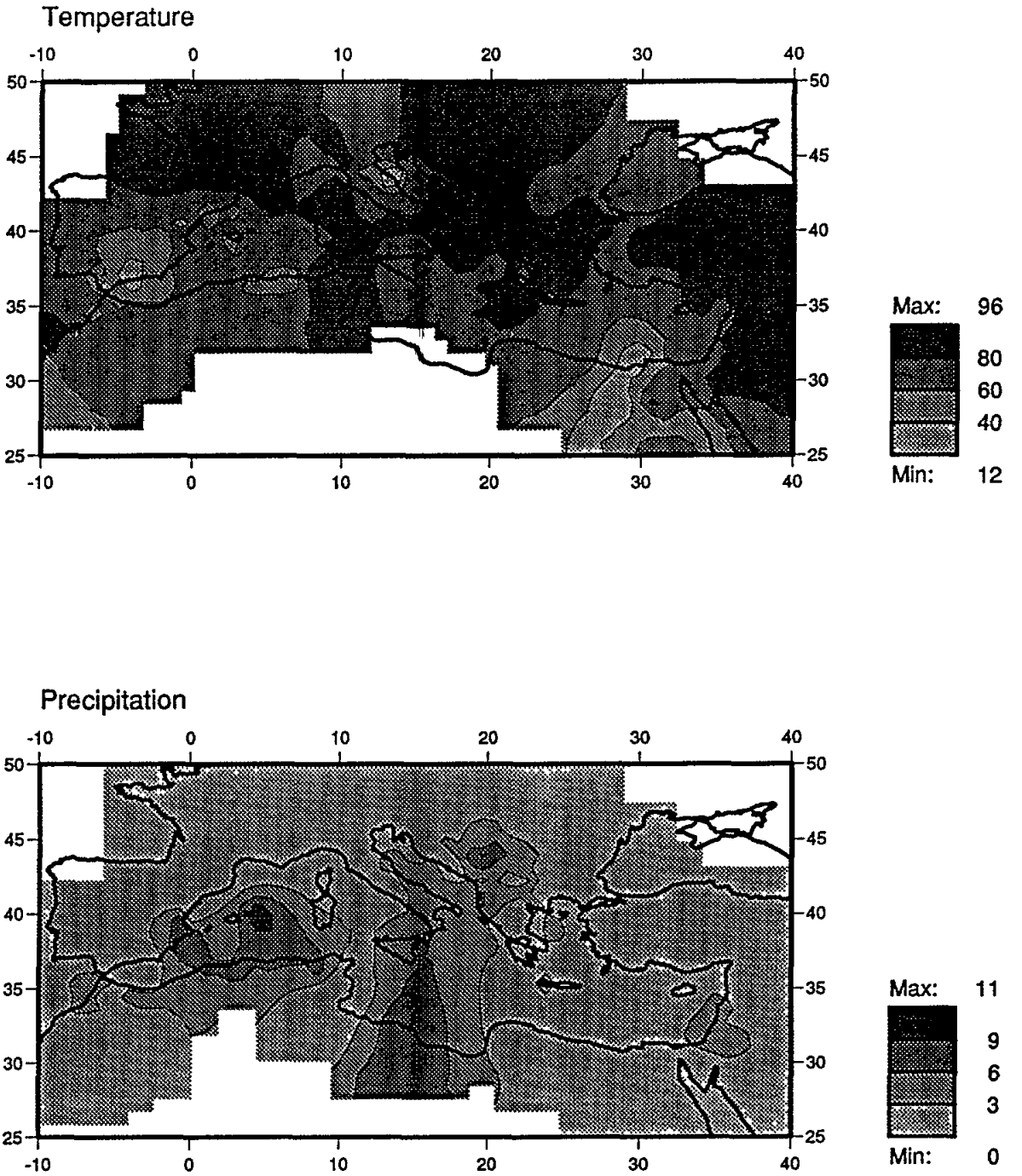

Fig. 4.21 Variance (%) of station temperatures and precipitation explained by regionally-averaged temperature anomalies, 1951-80

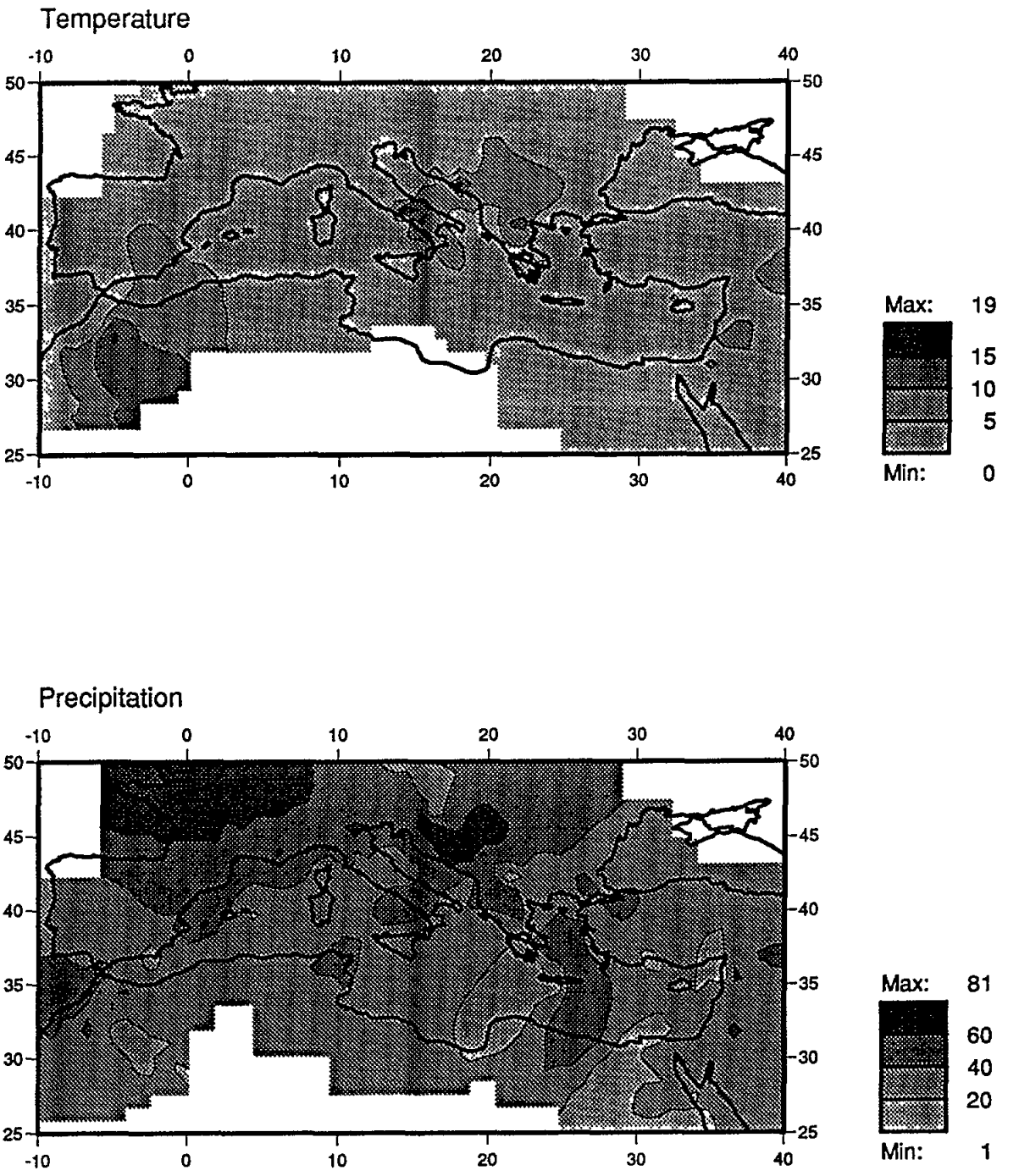

Fig. 4.22 Variance (%) of station temperatures and precipitation explained by regionally-averaged precipitation anomalies, 1951-80

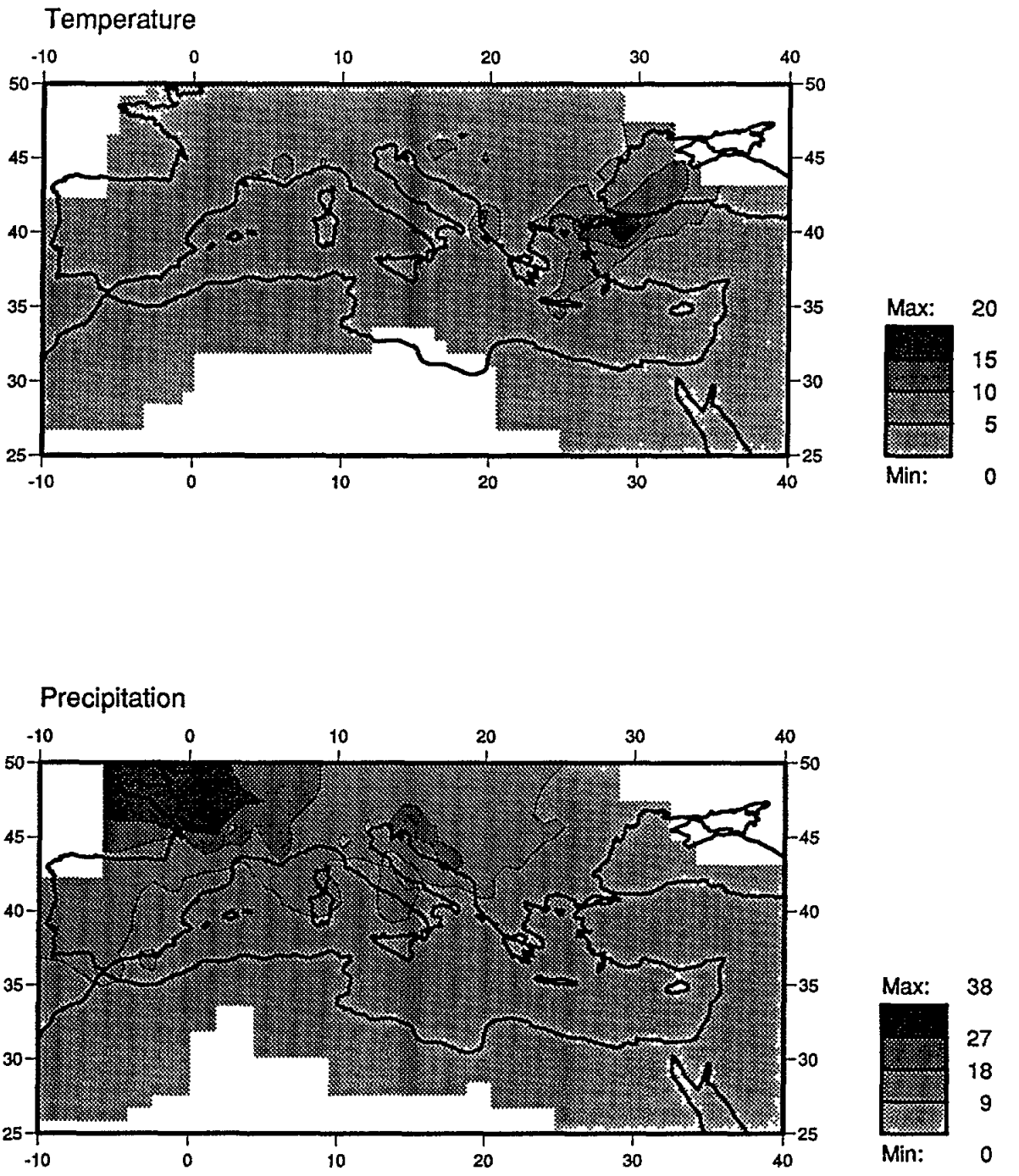

Fig. 4.23 Variance (%) of station temperatures and precipitation explained by regionally-averaged MSL pressure anomalies, 1951-80

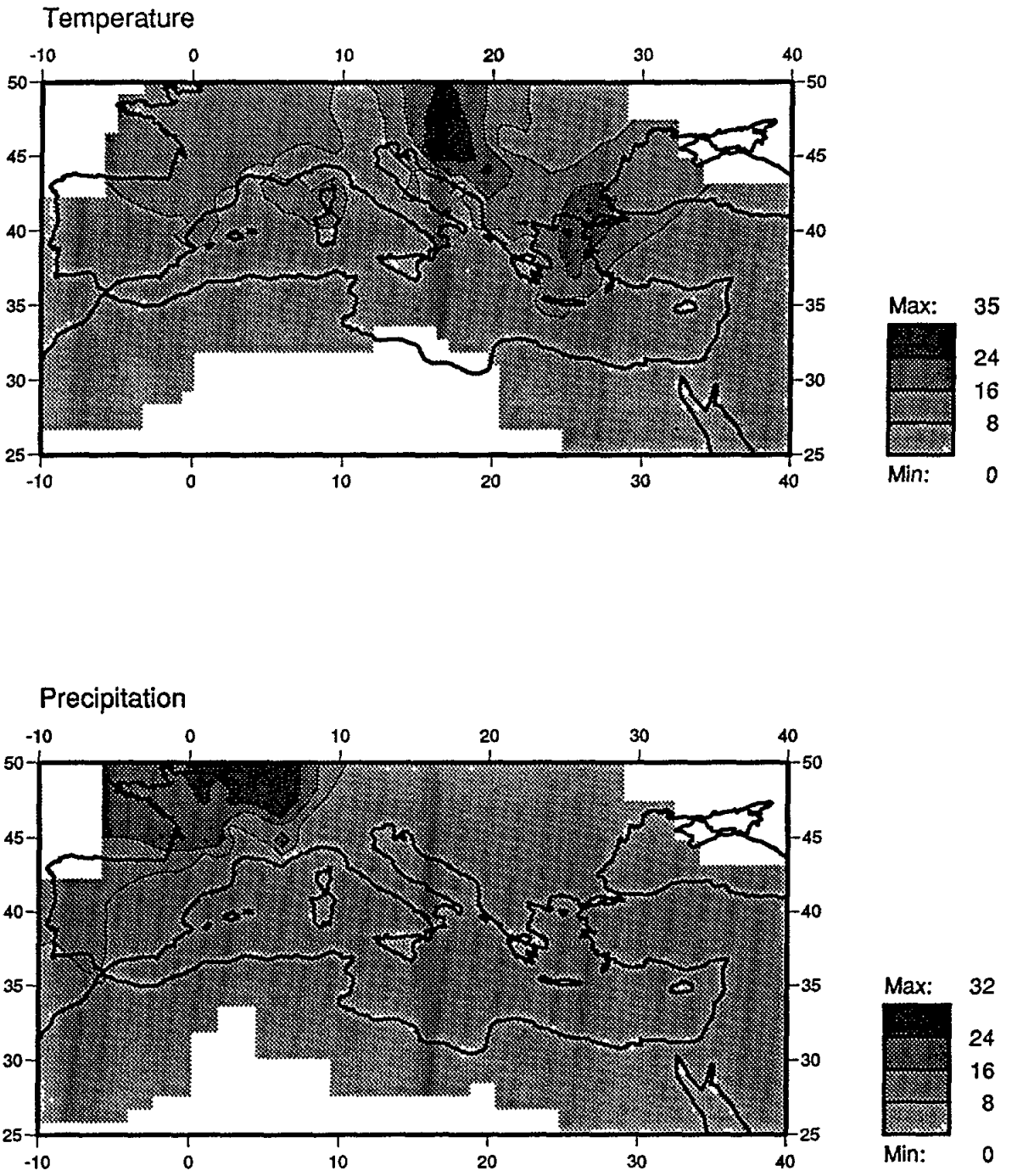

Fig. 4.24 Variance (%) of station temperatures and precipitation explained by regionally-averaged north-south MSL pressure gradient anomalies, 1951-80

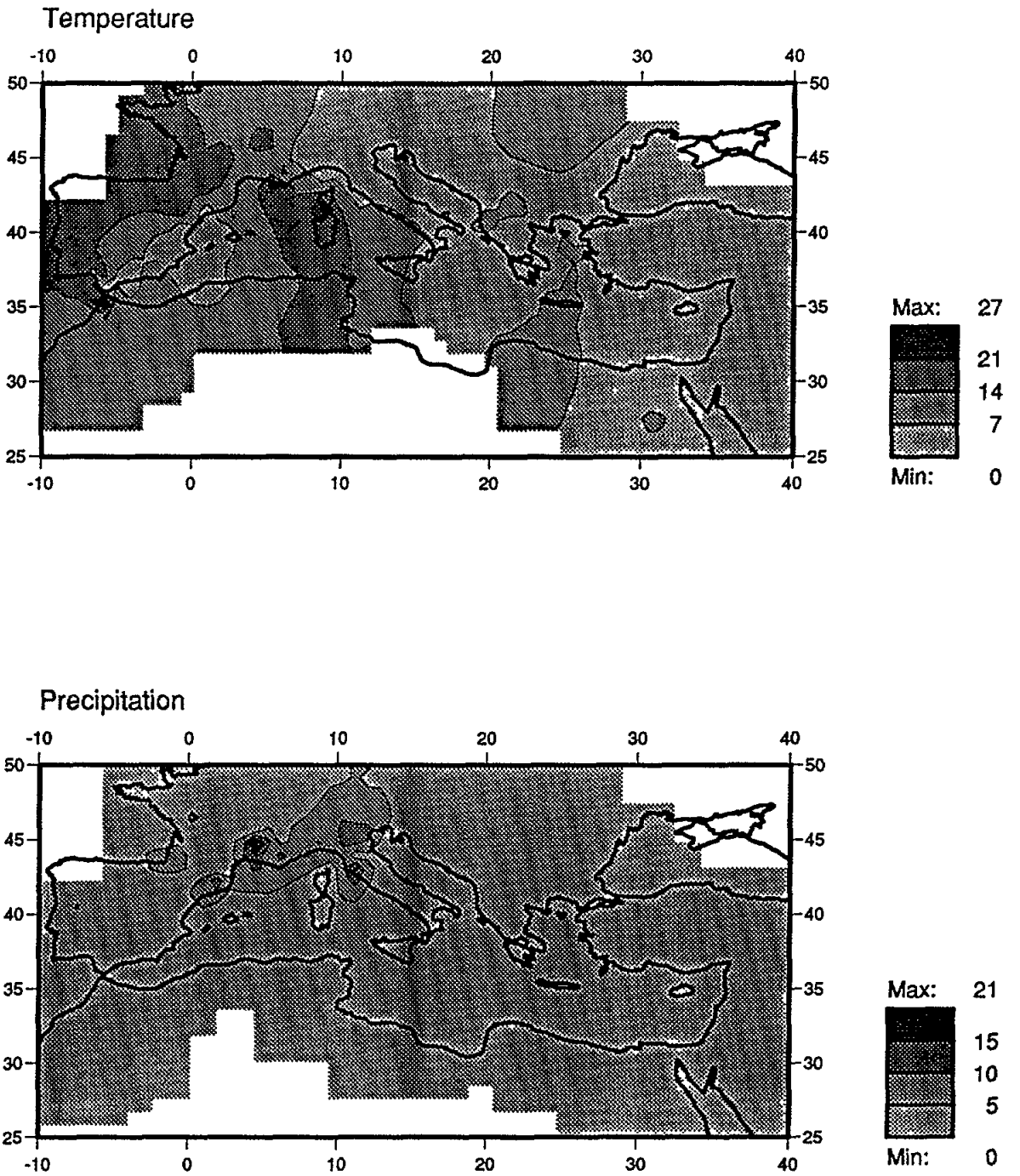

Fig. 4.25 Variance (%) of station temperatures and precipitation explained by regionally-averaged west-east MSL pressure gradient anomalies, 1951-80

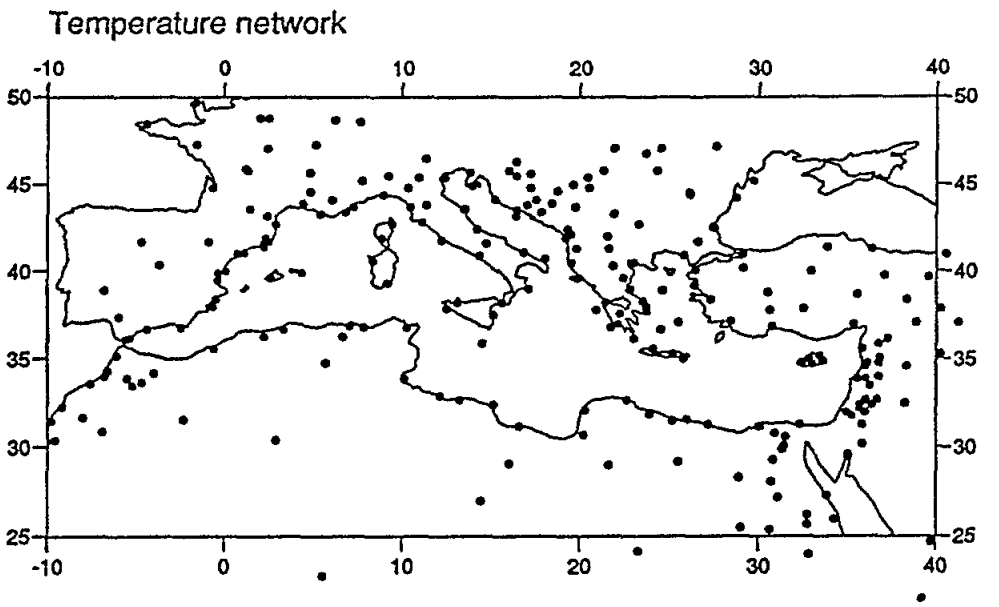

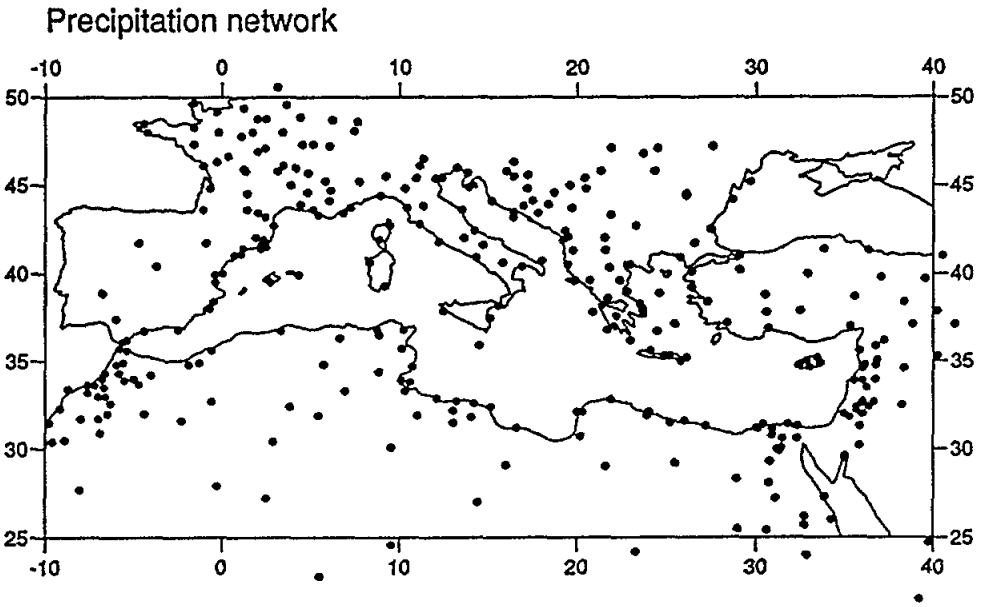

Fig. 4.26 Network of temperature (above) and precipitation (below) measuring stations

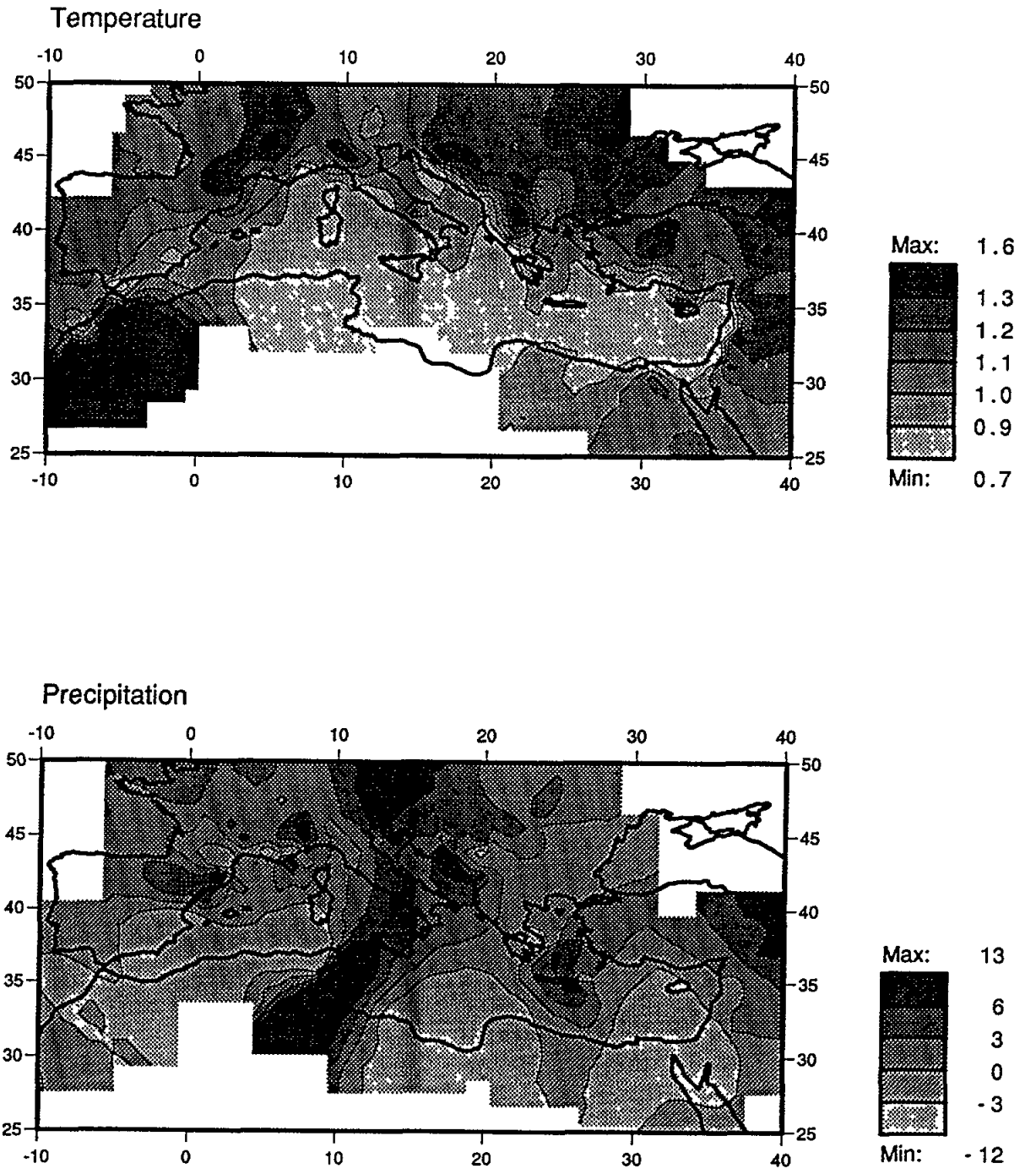

Fig. 4.27 Sub-grid scale scenarios of annual temperature (^{o}C) and precipitation (%) change per ^{o}C change in global-mean temperature

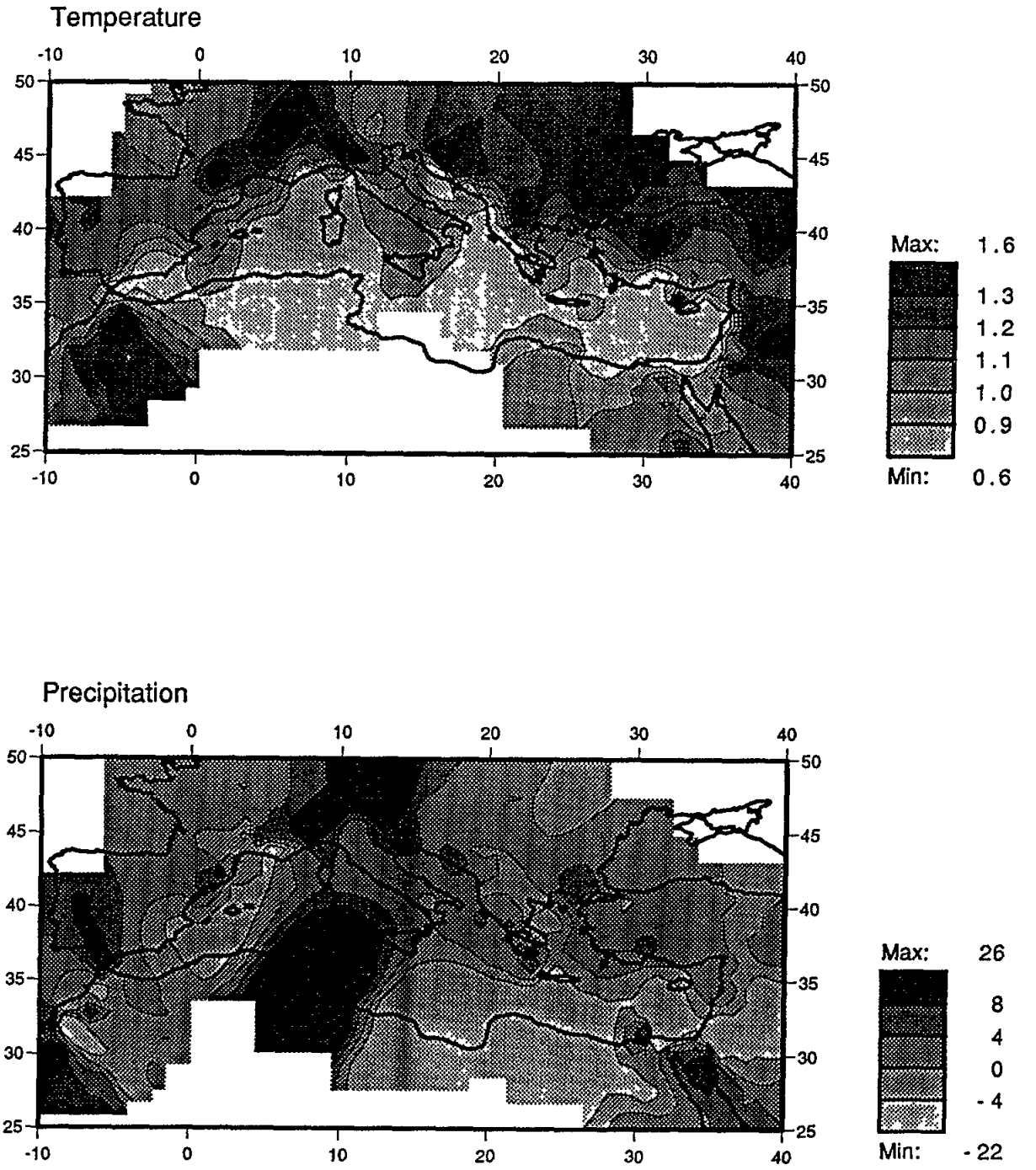

Fig. 4.28 Sub-grid scale scenarios of winter temperature (^{o}C) and precipitation (%) change per ^{o}C change in global-mean temperature

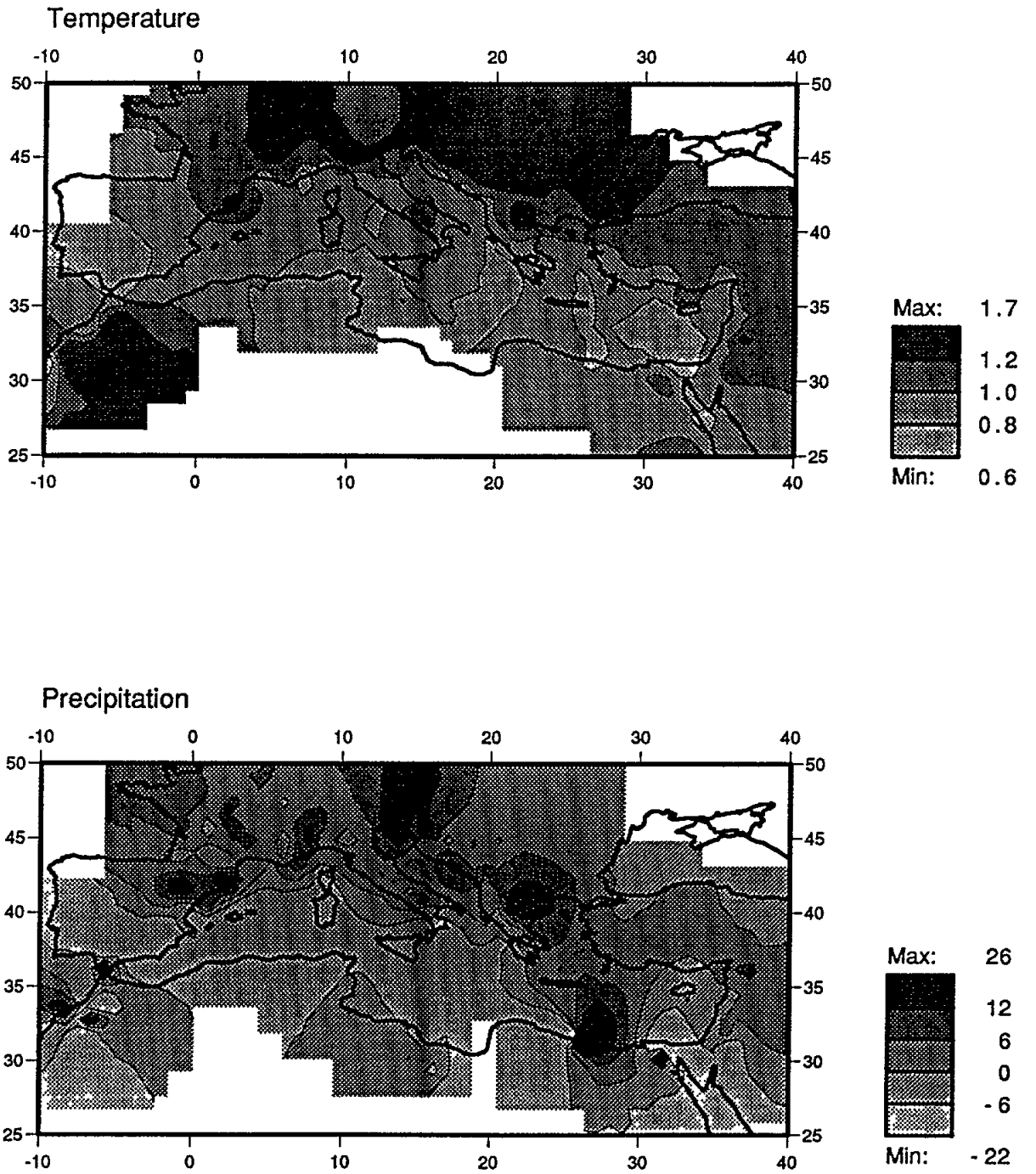

Fig. 4.29 Sub-grid scale scenarios of spring temperature (^{o}C) and precipitation (%) change per ^{o}C change in global-mean temperature

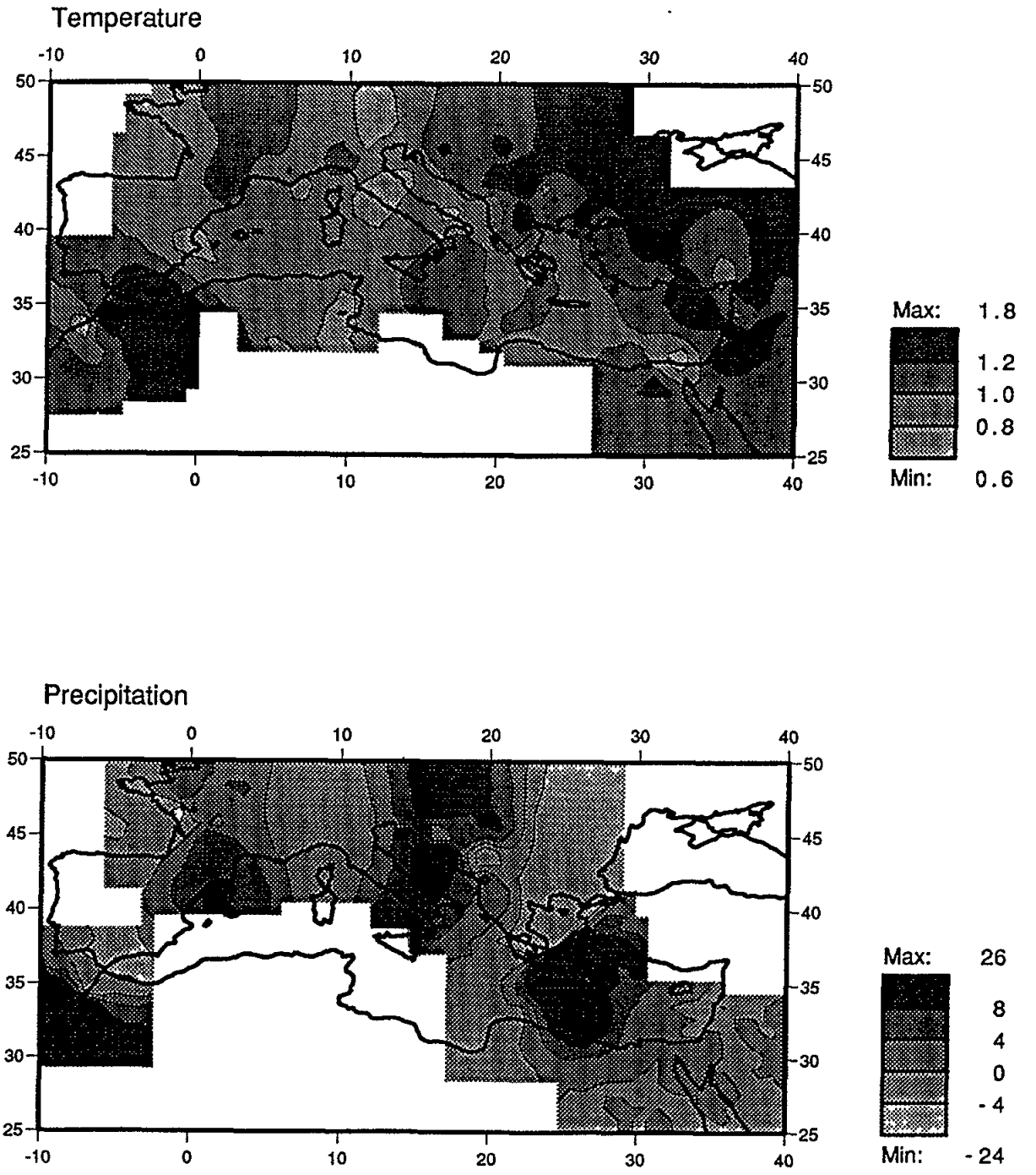

Fig. 4.30 Sub-grid scale scenarios of summer temperature (^{o}C) and precipitation (%) change per ^{o}C change in global-mean temperature

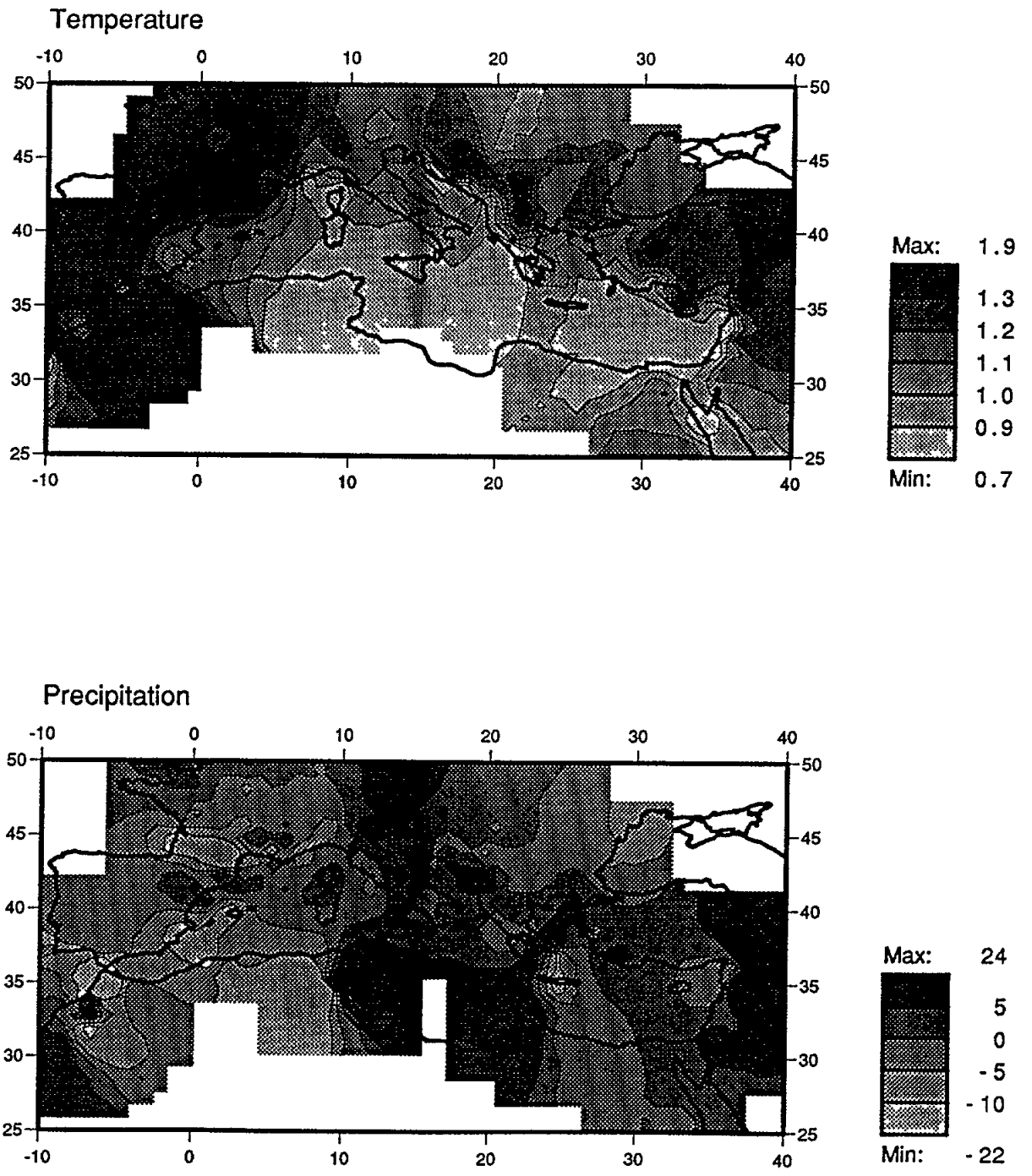

Fig. 4.31 Sub-grid scale scenarios of autumn temperature (^{o}C) and precipitation (%) change per ^{o}C change in global-mean temperature

CHAPTER 5

PRECIPITATION EXTREMES

5.1 INTRODUCTION

We have examined the possible range of impacts of the greenhouse effect on mean precipitation over the Mediterranean Basin. Of equal importance are the implications of such changes in the mean precipitation climatology for extremes - the occurrence of floods and droughts.

Two approaches are possible. The first is to extract extreme-event detail directly from GCM output, as has been done by Wilson and Mitchell (1987) using the UKMO model. The second approach is to model present-day precipitation characteristics statistically and then to perturb the statistical model in a way which corresponds to some assumed and realistic change in the mean climate (as suggested by Waggoner, 1989).

GCM results indicate that mean precipitation amounts should change over the Mediterranean Basin as a result of the greenhouse effect. However, all the evidence presented in this Report so far, indicates that their estimates of the amount, and even the direction of change are very uncertain. Given this uncertainty at the level of the mean, it is unlikely that useful information on the behaviour of extreme events can be extracted from the output of the GCMs used in this study. Nevertheless, in spite of the uncertainty in the predicted changes in the means, it is of interest to see how extremes may change using the statistical approach. This analysis should be considered largely as a sensitivity study, directed at identifying possibly important non-linear relationships between changes in the means and changes in the frequency of extreme events.

5.2 THE METHOD

5.2.1 The models

The statistical characteristics of precipitation are described by two models. The first is a model of the occurrence process, which determines the sequence of wet and dry days, and the second is a model for the amount of precipitation on a wet day. Composite models of this kind are quite common in meteorological and hydrological applications.

A general Markov chain model is used to describe the occurrence process. Wet and dry day sequences are determined by assigning the conditional probability of a wet day given the preceding history of wet and dry days. Here we have considered a first-order chain, where the probability of a wet day depends only on whether the preceding day was wet or dry. The model is fully specified by the probability of a wet day following a wet day (pww), and of a dry day following a dry day (pdd). The probability of a dry day following a wet day is then given by pwd = 1 - pww, and of a wet day following a dry day is given by pdw = 1 - pdd.

The unconditional probability of a wet day (i.e. the expected fraction of wet days) is:

$$pw = (1-pdd)/(2-pdd-pww)$$

and similarly

$$pd = 1 - pw = (1-pww)/(2-pdd-pww)$$

The expected lengths λw, λd of wet and dry spells are:

$$\lambda w = 1/(1-pww) \quad \lambda d = 1/(1-pdd)$$

Other analytical results are given by Gabriel and Neumann (1962).

The amount of precipitation on a wet day is determined by sampling from a probability distribution. Many different types have been used to model the distribution of rainfall amounts: for example, exponential, mixed exponential, gamma and kappa distributions (see, for example, the review by Woolhiser and Roldan, 1982). In this study, the gamma distribution has

been used, following Todorovic and Woolhiser (1975), Katz (1977) and many others.

The probability density function for the gamma distribution is given by:

$$f(x) = (x^{k-1} e^{-x/c})/(c^k \Gamma(k)) \qquad \text{for } x > 0$$

where k and c are the shape and scale parameters respectively. The mean, μ, and variance, σ, of the distribution are then given by:

$$\mu = kc \qquad \sigma^2 = c^2 k$$

In the special case k = 1 the gamma distribution reduces to the exponential. If k < 1, the distribution peaks at x = 0, while if k > 1, it vanishes when x = 0. In the case presented here, where we are modelling the distribution of wet days, k should always exceed one. The mean and variance calculated from c and k apply to the distribution of precipitation on wet days only, not all days. Thus, for instance, μ is not the same as the mean daily rainfall.

The four parameters (pww,pdd,c,k) were evaluated from the daily rainfall records of ten stations with suitable data. The Markov chain parameters are estimated using

$$\text{pww} = \frac{\text{number of wet days followed by a wet day}}{\text{total number of wet days}}$$

and similarly for pdd. A wet day is defined as one where the rainfall is greater than zero. The shape and scale parameters of the Gamma distribution were obtained using the maximum likelihood method (Thom, 1958; Ozturk, 1981). Together, the Markov chain model and the probability distribution model form the overall precipitation model used to investigate the behaviour of extreme events.

Simulations were performed as follows. On each day, a random number x was generated from a uniform distribution on the interval (0,1). The next day was chosen as wet or dry depending on whether x was less or greater than pww (if the current day was wet) or pdw = 1-pdd (if it was dry).

Beginning with an initial wet day, a sequence of 30 days was generated in this way to erase the memory of the initial choice, and the simulation recorded from the 31st day. Whenever a wet day occurred, another random number was selected from the above uniform distribution. This was taken to be the integral of a gamma distribution, which was then inverted to obtain a random gamma-distributed precipitation amount. In this way, a continuous sequence of wet and dry days, with precipitation amounts for the wet days, was simulated.

5.3 THE DATA

The model parameters are derived from observed daily rainfall amounts. The method was applied at ten stations for which daily data are available, as shown in Table 5.1.

For each station, the model parameters were used to simulate time series of the same length as the precipitation record. This was done for each season, and for each month within a season. Then the characteristics of

Table 5.1 Location of daily precipitation stations

	Lat (°N)	Long (°W)	Ht. (m)	Record Length
GREECE				
1. Kerkyra	19.9	39.6	2	1955-1987
3. Naxos	25.5	37.1	9	1955-1987
2. Kytuira	23.0	36.2	n/a	1955-1987
4. Heraklion	25.2	35.3	48	1955-1987
YUGOSLAVIA				
5. Bugojno	17.5	44.1	562	1951-1980
6. Ulcinj	19.2	41.9	30	1951-1980
7. Prilep	21.6	41.3	661	1951-1980
FRANCE				
8. Nimes	4.4	43.9	60	1961-1985
9. St-Raphael	6.8	43.4	n/a	1961-1985
10. Toulouse	1.4	43.6	152	1956-1988

the simulated time series were compared with observations in order to validate the performance of the precipitation model. The results are shown in Table 5.2. In this table, the mean, maximum and minimum daily precipitation, as calculated from the observed and simulated time series, are compared. This is done for both seasonal and monthly time series. The length of the longest wet and dry spells, observed and simulated, are also compared.

Table 5.2 shows that the mean daily precipitation is well simulated, both at the seasonal and monthly level. The error is generally less than 0.05mm. The precipitation model is less effective at reproducing the daily maximum and minimum precipitation. It tends to overestimate the size of the minimum, and underestimate the size of the maximum daily amount. The difference is, however, seldom greater than 1.5mm, and is usually much less. The models also tend to underestimate the length of the longest dry spells. The only exceptions are at Naxos, in summer, when the length is overestimated by eight days, and at Heraklion, where in both seasons the length of the longest dry spell is exaggerated, by nine days in winter and by three days in summer. The simulated longest wet spell in summer is too long at seven of the ten stations. There is a tendency for the modelled longest wet spell in winter to be too short.

5.4 CLIMATIC PERTURBATIONS

In order to investigate the impact of the greenhouse effect on precipitation extremes, it is first necessary to determine the size of the perturbation in the mean and to then estimate consistent perturbations in the statistical model parameters. To do this, we could use the results from GCMs. However, we have already demonstrated that there is a high degree of uncertainty associated with grid-point estimates of precipitation

Table 5.2 Comparison of observed and modelled (control) precipitation parameters

			Seasonal			Monthly				
			Mean	Min	Max	Mean	Min	Max	LW	LD
Kerkyra	Winter	Obs.	486	233	831	162	4	504	15	26
		Con.	490	267	754	163	28	376	13	19
	Summer	Obs.	37	1	127	10	0	71	3	85
		Con.	37	3	95	12	0	68	4	70
Naxos	Winter	Obs.	200	34	429	67	0	234	10	46
		Con.	201	90	329	67	8	182	8	25
	Summer	Obs.	6	0	86	2	0	75	2	77
		Con.	5	0	35	2	0	30	3	85
Kytuira	Winter	Obs.	288	129	523	96	6	333	12	26
		Con.	283	153	435	94	17	214	9	22
	Summer	Obs.	6	0	33	2	0	31	2	90
		Con.	7	0	36	2	0	34	2	86
Heraklion	Wint	Obs.	102	22	271	34	0	152	8	41
		Con.	106	35	210	34	0	128	7	50
	Summer	Obs.	6	0	45	2	0	42	2	82
		Con.	6	0	35	2	0	29	3	85
Bugojno	Winter	Obs.	200	72	315	67	2	218	10	30
		Con.	199	112	321	66	10	161	8	23
	Summer	Obs.	201	72	345	65	13	182	6	31
		Con.	203	99	329	66	9	163	8	26
Ulcinj	Winter	Obs.	480	208	900	160	1	412	11	46
		Con.	475	236	791	158	21	361	15	23
	Summer	Obs.	129	17	315	41	0	186	7	64
		Con.	130	34	293	43	0	166	6	51
Prilep	Winter	Obs.	132	56	279	44	1	124	7	35
		Con.	128	69	219	43	5	112	8	27
	Summer	Obs.	117	39	253	38	0	127	6	48
		Con.	116	48	213	38	1	118	6	38
Nimes	Winter	Obs.	199	79	444	67	0	202	6	49
		Con.	195	80	347	65	6	190	6	32
	Summer	Obs.	115	24	248	38	0	149	4	49
		Con.	118	31	242	39	0	127	6	49
St Raphael	Win	Obs.	272	56	575	91	0	270	8	43
		Con.	279	117	475	93	6	258	8	35
	Summer	Obs.	102	17	292	33	0	221	4	62
		Con.	98	27	206	32	0	123	5	49
Toulouse	Wint.	Obs.	168	64	303	56	3	165	11	37
		Con.	168	93	254	56	11	128	9	20
	Summer	Obs.	157	60	367	51	0	228	7	54
		Con.	155	71	268	51	4	147	8	34

N.B. Precipitation amounts in mm x 10^{-2}
LW = length of the longest wet spell, in days
LD = length of the longest dry spell, in days

amounts. For this reason, it was considered preferable to conduct a sensitivity experiment. The parameters of the two models used to describe precipitation extremes were perturbed arbitrarily, but in some reasonable manner, and the changes in model behaviour were evaluated. It was decided to apply a perturbation equivalent to a change in the mean precipitation of 10% - both an increase and a decrease.

Two experiments were performed. In the first, the perturbation of the mean was only allowed to affect the scale parameter in the gamma distributions. All other model parameters were constrained to remain constant. In the second, the mean wet-day and mean dry-day precipitation amounts were varied, causing pww and pdd to change, whilst the shape and scale parameters were held constant. For the perturbation towards drier conditions, pww was decreased and pdd increased, and vice versa.

5.5 THE RESULTS

Following the perturbation, simulated time series of rainfall were generated from the new model parameters. This was done for each season as a whole, and for the individual months in a season. Again, the length of the simulation in years was the same as that of the initial data set. Thus, a seasonal simulation of a twenty-year record of observations would contain 20 x 90 days.

The results for the two experiments are shown in Table 5.3. In this table, a minus sign indicates a 10% decrease, and a plus sign represents a 10% increase. The perturbation of the mean (and the scale parameter) by 10% is indicated by the letter A. The experiment to perturb pww and pdd to achieve a 10% change in the mean precipitation is designated by the letter M. The table shows the mean, minimum and maximum seasonal and monthly precipitation of the perturbed time series and the standard deviation of the monthly rainfall. Also shown is the length in days of the longest wet

Table 5.3 Results of the experiments to perturb the precipitation models

France

			seasonal			monthly				wet spells		dry spells	
			mean	min	max	mean	min	max	s.d.	long	> 10	long	> 10
Nimes													
DJF	−	M	88	98	91	88	50	91	94	100	0	106	110
DJF	−	A	95	98	92	95	90	91	93	113	100	104	99
DJF	+	M	113	122	115	113	170	109	106	105	0	88	81
DJF	+	A	112	122	109	112	98	106	109	114	0	97	99
MAM	−	M	88	95	89	89	63	90	95	87	0	112	99
MAM	−	A	90	84	104	90	120	96	94	106	200	110	101
MAM	+	M	108	131	101	108	125	108	105	106	100	93	88
MAM	+	A	110	98	112	110	128	122	116	103	200	97	101
JJA	−	M	90	120	90	90	100	102	92	91		94	106
JJA	−	A	93	125	92	93	200	96	90	93		85	100
JJA	+	M	109	121	100	110	550	113	108	102		85	96
JJA	+	A	106	119	112	106	200	118	110	90		88	100
SON	−	M	92	73	104	91	90	100	103	89		105	109
SON	−	A	90	81	94	90	13	86	90	108		97	99
SON	+	M	111	111	116	111	170	104	102	121		100	99
SON	+	A	106	101	107	106	137	109	106	99		99	105
Raphael													
DJF	−	M	87	83	90	87	78	95	95	90	0	97	125
DJF	−	A	88	87	88	89	54	90	89	96	100	105	102
DJF	+	M	109	104	115	109	103	111	112	101	163	88	96
DJF	+	A	105	107	108	105	135	109	106	101	163	96	106
MAM	−	M	86	72	82	86	100	81	86	96		95	126
MAM	−	A	88	80	92	87	93	84	86	97		97	113
MAM	+	M	106	116	98	106	211	92	94	114		91	95
MAM	+	A	108	105	102	107	175	106	100	106		95	102
JJA	−	M	89	73	101	90		108	101	98		129	98
JJA	−	A	90	86	97	91		105	95	96		108	100
JJA	+	M	115	76	115	115		111	111	107		102	103
JJA	+	A	112	86	124	112		121	120	104		105	102
SON	−	M	91	86	108	91	71	113	101	89	100	102	105
SON	−	A	88	97	89	88	124	99	91	96	0	81	103
SON	+	M	111	113	117	111	267	111	106	99	100	77	88
SON	+	A	102	82	113	102	91	97	103	96	100	100	101
Toulouse													
DJF	−	M	90	88	90	90	75	94	97	100	119	120	129
DJF	−	A	90	88	92	90	68	84	94	104	156	132	114
DJF	+	M	110	115	105	110	125	104	101	100	56	97	72
DJF	+	A	110	113	114	110	109	107	112	109	156	127	104
MAM	−	M	87	81	96	87	62	94	98	88	100	128	133
MAM	−	A	89	81	91	89	87	88	87	91	40	114	101
MAM	+	M	108	103	112	108	120	103	104	98	100	96	78
MAM	+	A	109	96	113	109	106	114	115	104	200	113	108
JJA	−	M	91	84	93	91	81	81	89	84	0	93	119
JJA	−	A	90	85	93	90	79	88	90	93	0	91	107
JJA	+	M	112	118	108	111	102	103	101	101	0	84	86
JJA	+	A	110	110	112	110	112	104	106	105	200	82	103
SON	−	M	94	102	87	94	82	93	99	102		104	110
SON	−	A	91	103	89	91	91	95	90	96		89	101
SON	+	M	114	140	108	114	141	105	104	110		88	81
SON	+	A	108	112	105	108	91	104	106	101		107	97

Table 5.3 cont.

Greece

			seasonal			monthly				wet spells		dry spells	
			mean	min	max	mean	min	max	s.d.	long	> 10	long	> 10
Kerkyra													
DJF	−	M	91	84	95	91	71	93	100	102	89	128	126
DJF	−	A	92	92	93	92	89	91	94	94	92	110	96
DJF	+	M	109	115	108	109	167	99	100	101	174	89	63
DJF	+	A	110	106	108	110	148	108	112	102	150	105	83
MAM	−	M	87	60	89	87	52	85	91	91	0	121	116
MAM	−	A	91	92	87	91	83	78	84	83	0	96	97
MAM	+	M	109	118	105	109	127	92	97	98	150	91	87
MAM	+	A	110	113	103	111	112	95	104	93	25	98	94
JJA	−	M	93	26	108	94		100	101	92		110	96
JJA	−	A	90	110	102	90		96	91	95		106	103
JJA	+	M	108	126	111	109		91	101	100		104	104
JJA	+	A	112	123	122	113		107	111	100		103	99
SON	−	M	94	75	104	94	64	105	102	95	83	107	108
SON	−	A	89	86	94	89	85	88	92	102	117	110	106
SON	+	M	113	109	123	113	124	115	116	103	200	112	86
SON	+	A	111	104	120	111	91	118	115	92	167	101	98
Naxos													
DJF	−	M	88	87	92	88	49	86	94	92	0	145	121
DJF	−	A	90	92	88	90	95	82	86	110	200	120	104
DJF	+	M	108	121	104	108	154	93	95	109	200	94	91
DJF	+	A	110	110	106	110	126	103	108	114	433	112	99
MAM	−	M	90	77	87	90		94	91	100		103	109
MAM	−	A	88	98	89	88		97	88	98		100	106
MAM	+	M	108	159	102	108		94	93	109		85	106
MAM	+	A	110	138	97	109		99	107	98		99	105
JJA	−	M	115		127	111		133	129	108		94	93
JJA	−	A	121		118	117		120	121	108		97	109
JJA	+	M	130		147	128		135	140	115		96	98
JJA	+	A	140		143	128		138	135	85		100	112
SON	−	M	100	48	103	99	0	102	103	88	0	108	96
SON	−	A	92	84	84	91	0	93	91	89	0	100	103
SON	+	M	115	67	103	115	0	112	108	97	0	93	102
SON	+	A	109	87	103	108	0	107	110	95	0	103	98

Table 5.3 cont.

Kytuira													
DJF	−	M	91	80	96	91	68	98	100	98	64	114	116
DJF	−	A	92	86	96	92	75	92	96	104	100	96	106
DJF	+	M	108	114	112	108	117	104	106	123	236	90	69
DJF	+	A	110	98	115	110	112	117	117	111	164	100	96
MAM	−	M	92	74	98	93	0	93	95	102		115	102
MAM	−	A	96	100	100	96	75	90	91	103		98	103
MAM	+	M	116	119	118	117	200	108	108	115		110	96
MAM	+	A	110	143	120	111	125	108	111	117		111	102
JJA	−	M	74		78	70		73	74	88		97	85
JJA	−	A	69		71	65		73	70	106		99	79
JJA	+	M	91		94	87		82	86	118		99	94
JJA	+	A	99		111	96		92	91	94		98	98
SON	−	M	94	88	97	94	0	98	95	97		125	103
SON	−	A	89	76	90	89	100	89	88	97		125	99
SON	+	M	112	130	103	112	400	105	100	101		101	97
SON	+	A	108	70	112	108	0	103	106	101		110	99
Hiraklion													
DJF	−	M	92	76	95	92	44	93	94	98	67	110	117
DJF	−	A	90	85	88	90	106	92	90	106	244	98	108
DJF	+	M	112	105	105	112	110	102	105	106	278	85	77
DJF	+	A	110	93	114	110	108	113	111	108	311	104	92
MAM	−	M	86	66	88	86	0	92	93	94		122	103
MAM	−	A	90	76	92	91	300	89	93	100		100	97
MAM	+	M	105	90	113	105	700	90	96	103		94	97
MAM	+	A	105	89	117	105	0	100	106	92		95	102
JJA	−	M	68		90	70		86	81	68		100	79
JJA	−	A	86		72	85		80	81	88		99	98
JJA	+	M	89		83	90		93	94	92		98	97
JJA	+	A	107		101	110		94	104	96		103	101
SON	−	M	88	62	88	88		100	92	104		98	98
SON	−	A	84	90	85	84		91	83	109		96	100
SON	+	M	106	124	102	106		101	98	112		91	98
SON	+	A	105	99	105	105		102	102	102		88	102

Table 5.3 cont.

Yugoslavia

			seasonal			monthly				wet spells		dry spells	
			mean	min	max	mean	min	max	s.d.	long	> 10	long	> 10
Bugojno													
DJF	−	M	89	82	90	89	94	92	99	115		115	132
DJF	−	A	91	89	87	91	66	88	91	115		129	105
DJF	+	M	112	116	103	112	134	106	103	117		105	75
DJF	+	A	112	109	105	112	140	104	111	117		99	94
MAM	−	M	90	95	88	90	84	91	93	92	43	103	122
MAM	−	A	90	85	92	90	85	96	93	107	243	99	103
MAM	+	M	111	128	104	111	121	107	105	115	286	92	75
MAM	+	A	113	122	108	113	129	119	114	114	386	96	82
JJA	−	M	89	83	90	89	62	96	96	105		125	115
JJA	−	A	89	94	88	89	48	89	90	101		106	101
JJA	+	M	107	104	104	107	96	113	104	105		86	81
JJA	+	A	110	102	116	110	70	116	114	103		104	90
SON	−	M	91	92	98	91	59	94	97	98	59	108	118
SON	−	A	90	95	91	90	89	87	90	101	77	95	99
SON	+	M	112	109	108	112	115	98	105	112	177	86	82
SON	+	A	109	117	116	109	93	108	112	105	77	95	96
Ulcinj													
DJF	−	M	94	88	97	94	81	101	100	82	95	116	124
DJF	−	A	92	88	82	93	92	95	92	99	105	100	103
DJF	+	M	111	129	102	111	135	107	104	85	160	101	78
DJF	+	A	109	108	103	109	96	114	108	80	116	100	104
MAM	−	M	91	81	104	92	67	103	105	100	77	107	119
MAM	−	A	89	94	93	90	105	97	94	98	67	99	104
MAM	+	M	109	117	113	110	147	106	107	105	157	85	82
MAM	+	A	109	103	117	109	66	117	115	108	177	92	96
JJA	−	M	89	74	95	89		97	98	91		107	100
JJA	−	A	92	74	85	91		91	97	109		97	100
JJA	+	M	107	110	95	106		98	105	111		104	100
JJA	+	A	108	105	112	107		113	113	102		104	98
SON	−	M	90	97	99	90	80	103	98	112	386	103	111
SON	−	A	91	91	91	91	120	95	93	104	143	102	97
SON	+	M	110	119	113	110	127	113	112	118	429	84	86
SON	+	A	112	124	114	113	82	114	116	128	714	101	97
Prilep													
DJF	−	M	93	80	87	93	71	93	96	93	0	109	125
DJF	−	A	93	79	86	93	104	89	89	92	233	108	99
DJF	+	M	113	107	107	113	141	95	103	107	100	99	83
DJF	+	A	113	109	104	113	149	104	109	111	233	96	89
MAM	−	M	90	75	95	90	80	102	101	100		107	122
MAM	−	A	92	86	92	93	76	95	93	100		102	100
MAM	+	M	115	107	111	115	107	110	109	119		84	71
MAM	+	A	112	105	118	112	96	122	117	112		96	96
JJA	−	M	91	75	93	91	33	94	98	107		111	105
JJA	−	A	90	91	92	89	75	82	89	120		101	100
JJA	+	M	109	112	108	109	292	102	104	115		85	97
JJA	+	A	110	102	115	110	67	117	111	122		110	97
SON	−	M	88	81	86	87	66	95	94	90	100	102	116
SON	−	A	86	76	84	86	66	87	86	91	0	111	108
SON	+	M	109	102	104	109	107	104	105	96	0	93	85
SON	+	A	110	109	107	109	93	106	108	100	333	90	98

and dry spell (designated 'long' in the table), and the average number of spells per year greater than ten days in length (designated >10). All values are expressed in Table 5.3 as a ratio of the control-run amounts. Where the control-run value was zero, no ratio could be calculated and the table location is left blank.

The first point of interest in Table 5.3 is that the response of the model parameters is not always in the expected direction. For example, we would expect that where the perturbation is a decrease in pww and an increase in pdd (-M, corresponding to a 10% decrease in precipitation), then the length of the longest wet spell would decrease in comparison to the control-run value. However, this is not always the case because both pdd and pww were changed. For example, at Bugojno in the winter season, we find that the length increases by 15%.

Information on the change in the statistical distribution of rainfall is given in the first seven columns of Table 5.3. As is to be expected from the way in which the experiments are designed, the mean precipitation per wet day is generally around +/-10% of the control-run value. Exceptions to this rule are mainly in summer, when precipitation amounts are very low. In consequence, a small change can have a very large effect on the perturbed to control run ratio. The effect of the 10% perturbation on the maximum and minimum amount of rainfall per wet day can be very large. To take the example of the -M experiment at Prilep in spring, the mean wet-day precipitation decreases to 90% of the control-run value (as it must), but the minimum (seasonal) value drops to 75%. The greatest effect appears to be on the minimum amount of rainfall per wet day. For the same experiment, this ratio usually changes more than the maximum amount per wet day.

The size of the perturbation is generally greater when the simulation is performed at the monthly level. For example, at Kerkyra in winter for the -M experiment, the minimum precipitation per wet day drops to 71% of the

control-run value for the monthly experiment, but only to 84% for the seasonal experiment.

The final four columns of the table provide information on the changes in wet and dry spell lengths for the two experiments. The greatest risks for the ecologies and economies of the Mediterranean Basin must be associated with an increase in the number and/or length of dry spells and a decrease in the number and/or length of wet spells. We find that a 10% change in the model parameters can lead to a much greater change in the characteristics of the wet and dry spells. For example, at Naxos, the -M perturbation leads to a 45% increase in the length of the longest dry spell, and a 21% increase in the number of dry spells of greater than ten days duration.

5.6 CONCLUSIONS

An important part of any regional impact assessment of the enhanced greenhouse effect must be the investigation of the implications for precipitation extremes - the frequency and severity of droughts and floods. Such information might be obtained from GCMs. However, for the Mediterranean Basin at least, GCM estimates of the amount, and even the direction, of precipitation change are very uncertain. We have therefore adopted an alternative approach based on a two-part statistical model of precipitation. This combines a first-order Markov chain, to describe precipitation occurrence, with a gamma function to describe the distribution of precipitation amounts.

The model was applied to the precipitation records from ten stations in the Mediterranean Basin. Validation was performed by comparing observed characteristics of the records with those derived from model simulation runs. Two groups of experiments were performed using perturbed values of the model parameters. In the first group, the scale parameter of the gamma

distribution function was increased and decreased by 10% In the second, the probability parameters of the Markov chain were altered by plus and minus 10%.

In order to look at the implications for extreme events, we examined the change in the maximum and minimum precipitation amount per wet day, and in the length of wet and dry spells. It was found that the characteristics of extremes changed by a much greater amount than the initial perturbation in the mean. Changes of the order of 20% of the control-run parameters were not unusual. This has particular implications for the Mediterranean Basin, where water supplies are already marginal for many agricultural and industrial activities.

CHAPTER 6

CONCLUSIONS

The enhanced greenhouse effect is expected to lead to substantial changes in climate at the regional level over the next century. The Mediterranean Basin is vulnerable to climate change, particularly through changes in rainfall and water supply and their implications for agriculture and for domestic and industrial water supply. In this study, we have constructed scenarios of climate change due to the enhanced greenhouse effect for the region. The principal features of the scenarios are summarized in Table 6.1 and in the following text.

Table 6.1 Scenarios of climate change over the Mediterranean

Scenario Type	Fig. Nos.	Pages	Variables	Information
Composite GCM	3.1-3.5	75-79	Temperature	Broad patterns of change over the Mediterranean
Composite GCM	3.11-3.15	85-89	Precipitation	Broad patterns of change over the Mediterranean
Sub-grid-scale	4.27-4.31	130-134	Temperature & precipitation	Regional/local patterns of change

The basis of these scenarios is the grid-point output from four General Circulation Models (GCMs): the GFDL, GISS, OSU and UKMO models. The standard approach is to run the model with a nominal "pre-industrial" atmospheric CO_2 concentration (the control run) and then to rerun the model with doubled CO_2 (the perturbed run). The models are allowed to reach equilibrium before the results are recorded. As a test of model accuracy, we compared the control-run results with observations for grid-points in the study region. Two climate variables were examined: mean sea level pressure (MSLP) and precipitation. On the MSLP tests, the most realistic

models were the GISS and UKMO GCMs. However, the GFDL model produced the most accurate simulation of precipitation.

Seasonal and annual scenarios of the regional changes in temperature, precipitation and MSLP, based directly on GCM grid-point output, have been developed. Since no single GCM can be identified as being always the best at simulating current climate, there is little merit in presenting scenarios of climate change based on any single model. We have therefore adopted the approach of Wigley et al. (1992), whereby the information from the four models is combined into a single scenario for each variable. One problem with this approach is that a bias may be introduced by the different equilibrium responses of the individual models. To avoid this, the results are expressed in standardized form, as the change per unit increase in the annual, global-mean equilibrium temperature.

The direct scenarios indicate that the temperature change due to the greenhouse effect for the Mediterranean Basin should be similar to the global response. Precipitation is shown to increase in autumn and winter but decrease in summer and, particularly in the eastern Mediterranean, in spring also. The mean change is, in winter, around +3%/°C and, in summer, around -3%/°C. However, our confidence in the model scenarios of precipitation is low because of the uncertainty associated with the GCM results.

The degree of regional detail in the direct scenarios of climate change is constrained by the coarse resolution of the model grid. This is inadequate for many purposes, especially in areas of high relief. We have adopted the methods developed by Kim et al. (1984) and Wigley et al. (1990) in order to produce a set of high resolution scenarios based on the statistical relationship between grid-point GCM data and observations from surface meteorological stations. Temperature and precipitation scenarios,

based on the combined standardized output from the four GCMs, have been constructed.

The temperature scenarios constructed in this way are likely to be a considerable improvement on the direct scenarios. The patterns were broadly similar, but the greater spatial resolution added substantially to our knowledge of the changes indicated by the GCMs for this geographically-complex region. The greatest sensitivity was found in the area to the north of the Mediterranean Sea, with the northern coastline picked out as a zone of rapid transition. The scenarios of precipitation are more difficult to evaluate. We have already noted the high level of uncertainty associated with the direct scenarios for this variable. Here, we have added a second level of uncertainty, since the relationship between the point precipitation anomalies and the regionally-averaged predictor variables is generally weak: less than 60% of the variance in point precipitation is explained by the predictors over most of the region and most of the year. Therefore, our confidence in the sub-grid-scale scenarios of precipitation must be low.

So far we have discussed regional scenarios of change in the mean value of a climate variable. Of equal importance to the impact analyst, particularly with respect to precipitation, are the implications of these changes for the occurrence of extremes - the frequency and severity of droughts and floods. Such information might be obtained directly from GCMs, but we have already indicated the uncertainties associated with this approach. We have therefore adopted an alternative approach, based on a two-part statistical model of precipitation. This combines a first-order Markov chain, to describe the precipitation occurrence process, with a gamma function to describe the distribution of precipitation amounts on wet days.

The model was applied to the daily precipitation records from ten stations in the region. Validation was performed by comparing observed characteristics with those derived from model simulation runs. Then a perturbation equivalent to a change in the mean precipitation of 10% (both an increase and a decrease) was applied. In order to examine the implications for extreme events, we examined the change in the maximum and minimum precipitation amount per wet day, and in the length of wet and dry spells. It was found that the characteristics of extremes changed by a much greater amount than the initial perturbation of 10%. Changes of the order of 20% were not unusual. This has particular implications for the Mediterranean Basin, where water supplies are already marginal for many agricultural and industrial activities.

The study has demonstrated the wealth of regional detail that can be extracted from coarse resolution GCM grid-point output by synthesizing modelled and observed data. However, the accuracy of any regional scenarios so constructed is constrained by the reliability of GCM results. The GCMs used in the present study are unable to reproduce accurately the characteristics of present-day regional climates, and this must cast doubt on their predictions of the future. Furthermore, the model results used here are derived from equilibrium response predictions, the spatial patterns of which may differ from the changes that will occur in a real, transient response world. For this reason, the scenarios presented in this study can only be taken as an indication of the range of possible changes that might occur as a result of greenhouse warming. However, the construction techniques used here are of general applicability, and the quality of regional scenarios will improve as more accurate GCM predictions become available in the future.

REFERENCES

Chang, J.-H., 1972: *Atmospheric Circulation Systems and Climates.* Oriental Publishing Company, Honolulu.

Cubasch, U. and R.D. Cess, 1990: Processes and modelling. In: *Climate Change: the IPCC Scientific Assessment.* (Eds. Houghton, J.T., Jenkins, G.J. and J.J. Ephraums), Cambridge University Press, Cambridge, 69-91.

Gabriel, K.R. and J. Neumann, 1962: A Markov chain model for daily rainfall occurrence at Tel Aviv. *Quarterly Journal of the Royal Meteorological Society 88,* 90-95.

Gunst, R.F. and R.L. Mason, 1980: *Regression Analysis and its Application.* Marcel Dekker, New York.

Hansen, J.E., Lacis, A., Rind, D. and others, 1984: Climate sensitivity: analysis of feedback mechanisms. In: *Climate Processes and Climate Sensitivity.* (Eds Hansen, J.E. and T. Takahashi), Geophysical Monograph 29, Maurice Ewing Vol. 5. American Geophysical Union, Washington, D.C.

Houghton, J.T., Jenkins, G.J. and J.J. Ephraums, 1990: *Climate Change: the IPCC Scientific Assessment.* Cambridge University Press, Cambridge.

Hulme, M., 1991: A 1951-80 land-based global precipitation climatology for the evaluation of General Circulation Models. Accepted for publication in *Climate Dynamics.*

Jones, P.D., 1987: The early twentieth century Arctic high - fact or fiction? *Climate Dynamics 1,* 63-75.

Jones, P.D., Wigley, T.M.L. and K.R. Briffa, 1987: Monthly mean pressure reconstructions for Europe (back to 1780) and North America (to 1958). *Technical Report DOE/ER/60397-H1,* U.S. Dept. of Energy, Carbon Dioxide Research Division, Washington, D.C.

Katz, R.W., 1977: Precipitation as a chain-dependent process. *Journal of Applied Meteorology 16,* 671-676.

Kim, J.W., Chang, J.T., Baker, N.L. and W.L. Gates, 1984: The statistical problem of climate inversion: determination of the relationship between local and large-scale climate. *Monthly Weather Review 112,* 2069-2077.

Mitchell, J.F.B., Manabe, S., Tokioka, T. and V. Meleshko, 1990: Equilibrium climate change. In: *Climate Change: the IPCC Scientific Assessment.* (Eds. Houghton, J.T., Jenkins, G.J. and J.J. Ephraums), Cambridge University Press, Cambridge, 131-172.

Ozturk, A., 1981: On the study of a probability distribution for precipitation totals. *Journal of Applied Meteorology 20,* 1499-1505.

Santer, B.D. and T.M.L. Wigley, 1990: Regional validation of means, variances, and spatial patterns in General Circulation Model control runs. *Journal of Geophysical Research 95(D1),* 829-850.

Schlesinger, M.E. and Z.-C. Zhao, 1989: Seasonal climate changes induced by doubled CO_2 as simulated by the OSU atmospheric GCM/mixed-layer ocean model. *Journal of Climate 2*, 459-495.

Thom, H.C.S., 1958: A note on the gamma distribution. *Monthly Weather Review 86*, 117-122.

Todorovic, P. and D.A. Woolhiser, 1975: A stochastic model of n-day precipitation. *Journal of Applied Meteorology 14*, 17-24.

Waggoner, P.E., 1989: Anticiptating the frequency distribution of precipitation if climate change alters its mean. *Agricultural and Forest Meteorology 47*, 321-337.

Wetherald, R.T. and S. Manabe, 1986: An investigation of cloud cover change in response to thermal forcing. *Climatic Change 8*, 5-23.

Wigley, T.M.L., Jones, P.D., Briffa, K.R. and G. Smith, 1990: Obtaining sub-grid-scale information from coarse-resolution General Circulation Model output. *Journal of Geophysical Research 95 (D2)*, 1943-1953.

Wigley, T.M.L., Santer, B.D., Schlesinger, M.E. and J.F.B. Mitchell, 1992: Developing climate scenarios from equilibrium GCM results. Submitted to *Climatic Change*.

Wilson, C.A. and J.F.B. Mitchell, 1987: A doubled CO_2 climate sensitivity experiment with a global climate model including a simple ocean. *Journal of Geophysical Research 92(D11)*, 13315-13343.

Woolhiser D.A. and J. Roldan, 1982: Stochastic daily precipitation models. 1: A comparison of distributions of amounts. *Water Resources Research 18*, 1461-1468.

APPENDIX 1

TEMPERATURE AND PRECIPITATION STATIONS USED FOR THE CONSTRUCTION OF THE SUB-GRID-SCALE SCENARIOS

Station	E	N	HT	PRN	TEM	P%	T%
ALBANIA							
1. SHKODRA	19.5	42.1	43	1951-1970	1951-1970	100	100
2. TIRANA	19.8	41.3	89	1951-1970	1951-1970	100	100
3. VLORA	19.5	40.5	1	1951-1970	1951-1970	100	100
ALGERIA							
1. SKIKDA	7.0	36.9	9	1967-1989	1966-1986	52	76
2. ANNABA	7.8	36.8	4	1963-1989	1963-1986	62	94
3. ALGER	3.3	36.7	25	1951-1989	1951-1988	78	81
4. BEJAIA	5.0	36.8	22	1969-1989	1969-1974	38	81
5. CONSTANTINE	6.6	36.3	704	1951-1989	1967-1986	75	100
6. MILIANA	2.2	36.3	722	1951-1989	1951-1986	42	70
7. ORAN	-0.6	35.6	90	1951-1989	1951-1986	74	99
8. BISKRA	5.7	34.8	81	1951-1989	1951-1986	65	88
9. TLEMCEN	-1.3	34.9	805	1951-1989	-	54	0
10. DJELFA	3.3	34.7	1178	1951-1989	1971-1986	33	94
11. LAGHOUAT	2.9	33.8	767	1951-1970	1951-1971	93	90
12. TOUGGOURT	6.0	33.1	85	1951-1989	-	37	0
13. OUED	6.9	33.3	63	1951-1989	-	62	0
14. SEFRA	-0.6	32.7	1058	1951-1989	-	62	0
15. GHARDAIA	3.8	32.4	520	1951-1989	1970-1980	73	40
16. BECHAR	-2.3	31.6	806	1951-1989	1951-1988	79	78
17. OUARGLA	5.4	31.9	141	1951-1972	1963-1971	95	87
18. HASSI-MESSOUD	2.9	31.7	398	1968-1989	1968-1974	45	75
19. GOLEA	2.9	30.4	398	1951-1989	1951-1974	73	96
20. BENI-ABBES	-2.2	30.1	498	1951-1989	1951-1962	36	95
21. TIMIMOUN	0.3	29.3	313	1951-1989	1969-1974	46	81
22. AMENAS	9.6	28.1	562	1963-1989	1963-1974	63	90
23. ADRAR	-0.3	27.9	264	1951-1989	1965-1973	62	86
24. SALAH	2.5	27.2	243	1951-1989	1964-1980	70	58
25. TINDOUF	-8.1	27.7	402	1951-1989	1966-1974	54	74
26. DJANET	9.5	24.6	1054	1951-1989	1965-1980	60	25
27. TAMANRASSET	5.5	22.8	1378	1951-1989	1951-1988	75	76
28. BATNA	6.3	35.6	n/a	1972-1986	1972-1986	100	100
BULGARIA							
1. VRATZA	23.5	43.2	360	1951-1970	1951-1970	92	92
2. LOM	23.2	43.8	33	1961-1989	1961-1979	43	41
3. PLEVEN	24.6	43.4	75	1951-1970	1951-1970	92	92
4. KOLAROVGRAD	26.9	43.3	198	1951-1971	1951-1971	89	90
5. VARNA	27.9	43.2	41	1961-1989	1961-1979	44	39
6. SOFIA	23.3	42.7	564	1951-1989	1951-1979	67	72
7. PLOVDIV	24.8	42.2	160	1951-1970	1951-1970	92	92
8. BOURGAS	27.5	42.5	28	1951-1989	1951-1979	63	70

Station	E	N	HT	PRN	TEM	P%	T%
CYPRUS							
1. PAPHOS	32.4	34.8	10	1951-1989	1951-1989	100	100
2. PRODHROMOS	32.8	35.0	1380	1967-1989	1959-1989	98	99
3. LIMASSOL	33.0	34.7	10	1951-1989	1951-1989	100	98
4. NICOSIA	33.4	35.2	160	1951-1989	1951-1989	100	100
5. LARNACA	33.6	34.9	3	1951-1989	1951-1989	100	100
EGYPT							
1. SALLOUM	25.2	31.5	6	1951-1987	1951-1987	99	89
2. SIDI-BARANI	26.0	31.6	23	1951-1987	1951-1987	100	99
3. MERSA-MATRUH	27.2	31.3	30	1951-1989	1951-1987	99	97
4. NOUZHA	30.0	31.2	7	1951-1987	1951-1975	100	56
5. ROSETTA	30.4	31.4	3	1951-1987	-	74	0
6. DAMIETTA	31.8	31.4	5	1951-1987	-	99	0
7. PORT-SAID	32.3	31.3	6	1951-1987	1951-1987	99	98
8. SAKHA	30.9	31.1	n/a	1951-1987	-	96	0
9. TANTA	30.9	30.8	8	1961-1986	1951-1986	100	100
10. ZAGAZIG	31.5	30.6	13	1961-1986	1951-1986	100	100
11. CAIRO	31.4	30.1	74	1951-1989	1951-1986	99	83
12. GIZA	31.2	30.0	22	1951-1986	1975-1986	100	100
13. HELWAN	31.3	29.9	141	1951-1989	1951-1986	99	96
14. FAYOUM	30.8	29.3	23	1961-1986	1951-1986	100	100
15. MINYA	30.7	28.1	40	1951-1987	1951-1986	100	100
16. ASSUIT	31.1	27.2	70	1951-1986	1951-1986	100	100
17. QENA	32.7	26.2	74	1951-1986	1951-1986	100	100
18. LUXOR	32.7	25.7	88	1951-1986	1951-1986	99	100
19. ASSWAN	32.8	24.0	194	1951-1989	1951-1986	95	100
20. SIWA	25.5	29.2	14	1951-1987	1951-1986	100	100
21. BAHARIA	28.9	28.3	130	1951-1986	1951-1986	100	99
22. DAKHLA	29.0	25.5	112	1951-1989	1951-1986	96	99
23. KHARGA	30.6	25.4	73	1951-1986	1951-1986	100	100
24. ISMAILIA	32.3	30.6	12	1951-1986	1951-1986	64	42
25. TOR	33.6	28.2	3	1955-1986	1956-1986	48	41
26. HURGHADA	33.8	27.3	3	1951-1986	1951-1986	99	100
27. KOSSEIR	34.2	26.0	n/a	1955-1986	1961-1986	88	99
FRANCE							
1. LILLE	3.1	50.6	47	1951-1973	-	100	0
2. CHERBOURG	-1.6	49.7	12	1951-1989	1951-1980	99	99
3. CAEN	-0.3	49.2	64	1951-1973	-	100	0
4. ROUEN	1.2	49.4	155	1951-1973	-	100	0
5. LAON	3.6	49.6	180	1951-1973	-	100	0
6. CHALONS	4.4	48.9	89	1951-1973	-	100	0
7. BREST	-4.4	48.5	103	1951-1989	1951-1988	99	100
8. JOIGNY	3.4	48.0	79	1951-1973	-	100	0
9. FEINS	-1.6	48.3	73	1951-1973	-	100	0
10. TRAPPES	2.0	48.8	168	1951-1986	1951-1986	100	100
11. PARIS	2.5	48.8	50	1951-1989	1951-1988	98	99
12. LAVAL	-0.2	48.0	87	1951-1973	-	100	0
13. NANCY	6.2	48.7	217	1951-1989	1951-1988	99	100
14. STRASBOURG	7.6	48.6	154	1951-1989	1951-1988	99	100
15. COLMAR	7.4	48.1	190	1951-1972	-	100	0
16. QUIMPER	-4.2	48.0	92	1951-1973	-	100	0

Station	E	N	HT	PRN	TEM	P%	T%
17. NANTES	-1.6	47.3	27	1951-1989	1951-1988	99	100
18. ORLEANS	1.7	48.0	125	1951-1973	-	100	0
19. VENDOME	1.1	47.8	79	1951-1973	-	100	0
20. BOURGES	2.4	47.1	162	1951-1989	1951-1980	99	100
21. POUILLY	4.5	47.3	390	1951-1973	-	100	0
22. DIJON	5.1	47.3	227	1951-1989	1951-1988	99	100
23. BESCANCON	6.0	47.2	307	1951-1973	-	100	0
24. ISSOUDUN	2.0	46.9	148	1951-1973	-	100	0
25. LAROCHELLE	-1.1	46.1	1	1951-1973	-	100	0
26. POITIERS	0.3	46.6	117	1951-1973	-	100	0
27. VICHY	3.4	46.1	260	1951-1973	-	100	0
28. NIORT	-0.3	46.3	40	1951-1973	-	100	0
29. ROANNE	4.1	46.0	283	1951-1973	-	100	0
30. BELLEGARDE	1.2	45.9	403	1961-1989	1961-1988	91	92
31. LIMOGES	1.3	45.8	284	1951-1973	1951-1972	100	100
32. CLERMONT	3.1	45.8	403	1951-1973	-	100	0
33. PUY	3.9	45.0	714	1951-1973	-	100	0
34. LYON	4.8	45.7	201	1951-1989	1951-1988	99	100
35. GRENOBLE	5.8	45.2	212	1951-1973	-	100	0
36. BORDEAUX	-0.7	44.8	51	1951-1989	1951-1988	99	99
37. CAHORS	1.4	44.5	124	1951-1973	-	100	0
38. GAP	6.1	44.7	775	1951-1972	-	100	0
39. PEYREHORADE	-1.1	43.6	12	1951-1973	-	100	0
40. TOULOUSE	1.4	43.6	152	1951-1989	1951-1988	99	100
41. REVEL	2.0	43.4	334	1951-1973	-	100	0
42. NIMES	4.4	43.9	60	1951-1989	1951-1988	99	100
43. SALON	5.1	43.6	61	1951-1970	1958-1970	100	100
44. MARSEILLE	5.4	43.3	8	1951-1989	1951-1988	99	100
45. NICE	7.2	43.7	10	1951-1989	1951-1988	98	100
46. PERPIGNAN	2.9	42.7	48	1951-1989	1951-1988	99	100
47. AJACCIO	8.8	41.9	5	1951-1989	1951-1988	99	100
48. MONTELIMAR	4.8	44.6	n/a	1961-1985	1961-1985	100	100
49. ST-RAPHAEL	6.8	43.4	n/a	1961-1985	1961-1985	100	100
50. BASTIA	9.4	42.7	n/a	1961-1985	1961-1985	100	100
51. CARCASSONNE	2.4	43.2	n/a	1961-1985	1961-1985	100	100
52. AUBAN	6.0	44.1	n/a	1961-1985	1961-1985	100	100
GREECE							
1. KERKYRA	19.9	39.6	2	1951-1989	1951-1988	96	96
2. YANENA	20.7	39.6	n/a	1956-1987	-	100	0
3. AGRINION	21.7	38.6	47	1956-1987	-	99	0
4. ARAXOS	21.4	38.2	23	1951-1987	1951-1970	99	100
5. ZAKYNTHOS	20.9	37.8	8	1951-1982	1951-1982	79	79
6. KOZANI	21.8	40.3	627	1955-1987	1955-1987	100	100
7. MIKRA	23.0	40.5	61	1951-1989	1951-1987	96	100
8. LARISSA	22.4	39.6	74	1951-1989	1951-1987	94	97
9. AGXIALO	22.8	39.0	n/a	1956-1987	1956-1987	100	98
10. TRIPOLIS	22.2	37.6	660	1957-1987	1957-1987	100	100
11. KALAMATA	22.1	37.0	5	1951-1989	1951-1988	94	95
12. METHONI	21.7	36.8	34	1951-1987	1951-1987	100	99
13. TANAGRA	23.5	38.3	n/a	1957-1986	1957-1986	99	99
14. ATHENS	23.7	38.0	107	1951-1989	1951-1988	98	97
15. HELLENIKON	23.7	37.9	10	1951-1989	1951-1987	84	80
16. KYTUIRA	23.0	36.2	n/a	1955-1987	1955-1987	100	100
17. SKYROS	24.6	38.9	5	1955-1987	1955-1987	100	100

Station	E	N	HT	PRN	TEM	P%	T%
18. MILOS	24.5	36.7	n/a	1955-1987	1955-1987	99	100
19. ALEXANDROUPOLI	25.8	40.9	3	1951-1987	1951-1987	100	100
20. MITILIA	26.4	39.2	n/a	1955-1987	1957-1987	100	99
21. NAXOS	25.5	37.1	9	1955-1987	1955-1987	100	100
22. SOUDA	24.1	35.6	161	1958-1989	1958-1986	97	97
23. ANOGIA	24.9	35.3	n/a	1951-1985	-	96	0
24. HIRAKLION	25.2	35.3	48	1955-1986	1951-1988	97	97
25. IERPETRA	25.8	35.0	n/a	1956-1987	1956-1987	99	99
26. SITIA	26.1	35.2	28	1951-1985	-	87	0
ISRAEL							
1. LOD	34.9	32.0	49	1951-1989	1951-1988	93	100
2. JERUSALEM	35.2	31.8	809	1951-1989	1951-1980	97	100
3. EILAT	35.0	29.5	11	1951-1989	1951-1988	86	99
ITALY							
1. TRENTO	11.1	46.1	312	1951-1976	-	100	0
2. UDINE	13.2	46.0	92	1967-1989	1967-1980	93	95
3. TORINO	7.7	45.2	301	1951-1985	1961-1985	99	95
4. MILANO	9.2	45.5	103	1951-1987	1951-1986	95	99
5. VERONA	10.9	45.4	67	1961-1989	1961-1985	98	97
6. PADUA	12.0	45.4	13	1951-1974	-	100	0
7. VENEZIA	12.4	45.4	17	1951-1989	1951-1988	98	100
8. TRIESTE	13.8	45.7	20	1951-1989	1951-1988	98	100
9. GENOVA	8.9	44.4	21	1951-1980	1962-1985	100	97
10. PARMA	10.3	44.8	56	1951-1977	1951-1976	100	100
11. BOLOGNA	11.5	44.5	60	1951-1974	1961-1970	100	100
12. PISA	10.4	43.7	2	1961-1989	1961-1980	97	100
13. FLORENCE	11.3	43.8	75	1951-1977	1951-1970	100	100
14. ANCONA	13.5	43.6	104	1951-1978	1951-1978	98	98
15. PESCARA	14.2	42.4	9	1961-1989	1961-1980	97	100
16. ROME	12.2	41.8	2	1951-1989	1951-1988	98	99
17. NAPOLI	14.3	40.9	88	1961-1987	1961-1987	99	99
18. BRINDISI	18.0	40.7	15	1961-1989	1961-1980	98	100
19. MARINA	16.9	40.4	12	1967-1989	1967-1980	96	95
20. MESSINA	15.6	38.2	51	1961-1989	1961-1980	98	100
21. TRAPANI	12.5	37.9	79	1961-1989	1961-1980	98	100
22. CATANIA	15.1	37.5	65	1961-1987	1961-1987	98	99
23. ALGHERO	8.3	40.6	23	1961-1989	1961-1985	79	99
24. CAGLIARI	9.1	39.3	18	1951-1989	1951-1988	98	99
25. AVEZZANO	13.6	42.0	n/a	1951-1970	-	100	0
26. BOLZANO	11.3	46.5	241	1961-1985	1961-1985	99	91
27. GROSSETO	11.1	42.8	5	1961-1985	1961-1985	99	100
28. PERUGIA	12.5	43.1	208	-	1961-1985	0	98
29. FALCONARA	13.4	43.6	12	-	1961-1985	0	97
30. CAMPOBASSO	14.7	41.6	793	1961-1985	1961-1985	99	99
31. BARI	16.8	41.1	34	-	1961-1985	0	99
32. POTENZA	15.8	40.6	823	1961-1985	1961-1973	99	96
33. CROTONE	17.1	39.0	155	-	1961-1985	0	99
34. PALERMO	13.1	38.2	21	-	1961-1985	0	99
MALTA							
1. LUQA	14.5	35.9	80	1951-1989	1951-1988	96	99

Station	E	N	HT	PRN	TEM	P%	T%
JORDAN							
1. IRBID	35.9	32.6	585	1955-1989	1955-1989	100	100
2. RUWASHED	38.2	32.5	686	1960-1989	1961-1989	100	100
3. AMMAN	36.0	32.0	771	1951-1989	1951-1989	100	100
4. DEIR-ALLA	35.6	32.2	-224	1952-1989	1952-1989	100	100
5. MAAN	35.8	30.2	1069	1960-1989	1960-1989	100	100
6. WADI-YABIS	35.6	32.4	-200	1960-1989	1960-1989	96	98
7. MAFRAQ	36.3	32.4	686	1960-1989	1960-1989	100	100
8. ER-RABBAH	35.8	31.3	920	1960-1989	1961-1989	100	95
9. AQABA	35.0	29.6	51	1960-1989	1960-1989	100	100
10. JORDAN-UNIV	35.9	32.0	980	1960-1989	1961-1989	100	90
LEBANON							
1. BEIRUT	35.5	33.9	24	1951-1985	1951-1985	80	84
2. RAYACK	36.0	33.9	921	1951-1984	1951-1985	76	80
3. TRIPOLI	36.0	34.6	10	1951-1982	1951-1980	77	76
LIBYA							
1. NALUT	11.0	31.9	620	1951-1988	1954-1960	98	94
2. BENI-WALID	14.0	31.8	n/a	1951-1989	1951-1960	67	92
3. MIZDA	13.0	31.5	n/a	1951-1988	1951-1960	95	92
4. ZUARA	12.1	32.9	3	1951-1988	1954-1988	98	70
5. GHARIAN	13.0	32.2	n/a	1951-1988	1951-1960	96	94
6. HOMS	14.2	32.6	n/a	1951-1989	1951-1960	92	94
7. TRIPOLI	13.2	32.7	84	1951-1989	1951-1988	90	91
8. MISURATA	15.1	32.4	6	1951-1988	1954-1988	100	93
9. TUMMINA	15.1	32.2	n/a	1951-1989	1951-1960	36	94
10. SIRTE	16.6	31.2	22	1951-1988	1954-1988	98	65
11. BENINA	20.3	32.1	132	1951-1989	1951-1988	85	88
12. BENGHAZI	20.0	32.1	10	1951-1973	1985-1988	100	100
13. AGEDABIA	20.2	30.7	n/a	1951-1988	1954-1988	99	60
14. SHAHAT	21.9	32.8	625	1951-1988	1954-1960	98	94
15. DERNA	22.6	32.7	9	1951-1988	1951-1988	31	50
16. TOBRUQ	24.0	32.1	14	1951-1973	-	100	0
17. ADEM	23.9	31.9	155	1951-1988	1951-1975	96	93
18. SEBHA	14.4	27.0	444	1951-1989	1951-1988	94	90
19. HON	16.0	29.1	261	1954-1988	1954-1988	94	75
20. GIALO	21.6	29.0	62	1951-1988	1964-1988	98	90
21. KUFRA	23.3	24.2	382	1951-1989	1951-1988	86	79
22. GHADAMES	9.5	30.1	n/a	1951-1988	1969-1988	91	96
MALTA							
1. LUQA	14.5	35.9	80	1951-1989	1951-1988	96	99
MOROCCO							
1. TANGIERS	-5.8	35.7	60	1951-1989	1951-1963	87	100
2. TETOUAN	-5.4	35.6	10	1951-1989	1961-1983	83	77
3. LARACHE	-6.1	35.2	n/a	-	1962-1983	0	93
4. HOCEIMA	-4.0	35.1	n/a	-	1963-1983	0	78
5. OUEZZENE	-5.6	34.9	n/a	1951-1981	-	86	0
6. OUJDA	-1.9	34.8	468	1951-1989	1961-1983	86	82

Station	E	N	HT	PRN	TEM	P%	T%
7. SOUK-LARBAT	-6.0	34.8	n/a	1951-1981	-	97	0
8. KENITRA	-6.6	34.3	12	1951-1984	1951-1983	97	96
9. SIDI-KACEM	-5.8	34.3	n/a	1951-1981	-	98	0
10. TAZA	-4.0	34.2	510	1960-1984	1960-1983	97	95
11. RABAT	-6.8	34.0	84	1951-1989	1951-1983	86	86
12. FES	-5.0	34.0	414	1951-1984	1951-1961	97	92
13. MEKNES	-5.5	33.9	549	1951-1989	1951-1988	96	85
14. MIDELT	-4.7	33.7	1515	1951-1989	1951-1983	87	85
15. BEN-SLIMANE	-7.2	33.6	n/a	1951-1982	-	85	0
16. CASABLANCA	-7.6	33.6	58	1951-1989	1951-1988	95	86
17. IFRANE	-5.2	33.5	n/a	-	1958-1983	0	80
18. ROMMANI	-6.7	33.5	n/a	1951-1981	-	59	0
19. JADIDA	-8.7	33.4	n/a	1951-1984	-	81	0
20. SETTAT	-7.6	33.2	n/a	1951-1981	-	97	0
21. KHOURIBGA	-7.0	33.0	n/a	1951-1981	-	98	0
22. OUED-ZEM	-6.6	33.0	n/a	1951-1981	-	99	0
23. KASBA-TADLA	-6.3	32.6	507	1951-1983	1951-1972	58	76
24. SAFI	-9.2	32.3	45	1951-1984	1955-1983	97	85
25. AZILAL	-6.5	32.0	n/a	1951-1981	-	94	0
26. ERRACHIDIA	-4.4	32.0	n/a	1951-1984	-	57	0
27. DEMNATE	-7.0	31.7	n/a	1951-1981	-	98	0
28. MARRAKECH	-8.0	31.7	466	1951-1989	1951-1988	96	85
29. MOGADOR	-9.8	31.5	17	1951-1984	1951-1982	90	81
30. OUARZAZATE	-6.9	30.9	1136	1951-1989	1951-1988	95	83
31. TAROUDANT	-8.9	30.5	n/a	1951-1980	-	89	0
32. AGADIR	-9.6	30.4	19	1951-1989	1951-1988	95	84
ROMANIA							
1. ORADEA	21.9	47.1	135	1951-1970	1951-1970	100	99
2. BISTRITA	24.5	47.1	366	1951-1988	1951-1980	98	99
3. IASI	27.6	47.2	103	1951-1988	1951-1980	98	99
4. CLUJ	23.7	46.8	415	1951-1988	1951-1980	98	99
5. TIMISOARA	21.3	45.8	91	1951-1988	1951-1980	98	99
6. SIBIU	24.3	45.8	452	1951-1988	1951-1980	98	99
7. SULINA	29.7	45.2	9	1951-1988	1951-1980	98	99
8. BANEASA	26.1	44.5	92	1951-1984	1951-1980	78	76
9. FILARET	26.1	44.4	82	1951-1988	1951-1980	74	85
10. CONSTANTA	28.7	44.2	32	1951-1970	1951-1970	100	100
SAUDI ARABIA							
1. TABUK	36.6	28.4	774	1966-1989	1966-1989	59	48
2. HAIL	41.7	27.5	914	1966-1989	1966-1989	61	51
3. WEJH	36.5	26.2	8	1966-1989	1966-1989	60	50
4. MEDINA	39.7	24.7	672	1956-1989	1956-1989	72	68
5. JEDDAH	39.2	21.5	11	1951-1982	1951-1976	73	88
SPAIN							
1. PUIGREIG	1.9	42.0	417	1951-1988	-	89	0
2. BALENYA	2.3	41.9	570	1951-1988	1953-1987	96	93
3. ZARAGOZA	-0.9	41.7	233	1951-1985	1951-1987	95	92
4. SAN-CELONI	2.5	41.7	155	1951-1988	1953-1988	93	91
5. VALLADOLID	-4.7	41.7	715	1951-1989	1951-1988	96	97
6. CALDAS	2.2	41.6	180	1951-1988	1953-1988	93	89

Station	E	N	HT	PRN	TEM	P%	T%
7. ALELLA-COLOMER	2.5	41.5	109	1951-1988	-	96	0
8. SARREAL	1.2	41.4	n/a	1951-1988	1974-1988	94	88
9. BARCELONA	2.2	41.4	95	1951-1985	1951-1987	97	93
10. VILASECA	1.1	41.1	44	1951-1988	1953-1988	95	94
11. TIVISSA	0.7	41.0	310	1951-1988	1953-1988	92	94
12. MADRID	-3.7	40.4	657	1951-1989	1951-1988	97	98
13. CASTELLON	0.0	40.0	47	1931-1980	1951-1988	97	84
14. SEGORBE	-0.4	39.9	364	1951-1987	1951-1987	84	90
15. MAHON	4.3	39.9	59	1951-1989	1951-1980	97	98
16. PALMA	2.6	39.6	17	1951-1989	1951-1980	89	98
17. VALENCIA	-0.4	39.5	11	1951-1989	1951-1970	52	100
18. SON-JUAN	2.7	39.5	4	1951-1989	-	56	0
19. BADAJOZ	-6.8	38.9	192	1951-1989	1951-1980	96	98
20. ALICANTE	-0.5	38.4	82	1951-1989	1951-1980	96	98
21. LAGUNA	-0.7	38.0	1	1951-1988	1953-1988	86	96
22. SEVILLA	-6.0	37.4	13	1951-1989	1951-1988	96	97
23. ALMERIA	-2.5	36.8	7	1951-1981	1951-1986	97	83
24. MALAGA	-4.4	36.7	16	1951-1988	1951-1986	93	83
25. GIBRALTAR	-5.4	36.2	5	1951-1989	1951-1988	99	100
26. ALGECIRAS	-5.6	36.1	100	1951-1988	1951-1988	85	95
SYRIA							
1. KAMISHLI	41.2	37.1	455	1952-1989	1952-1988	97	99
2. ALEPPO	37.2	36.2	393	1951-1989	1952-1988	97	99
3. LATTAKIA	35.8	35.6	9	1952-1989	1952-1988	90	94
4. DEIR-EZZOR	40.2	35.3	212	1951-1989	1952-1988	97	99
5. PALMYRA	38.3	34.6	404	1955-1989	1955-1988	97	99
6. DAMASCUS	36.2	33.5	724	1951-1989	1951-1988	97	99
7. SAFITA	36.1	34.8	n/a	1959-1988	1959-1988	100	100
8. IDLEB	36.7	35.9	n/a	1955-1988	1957-1988	100	100
9. HAMA	36.8	35.1	n/a	1955-1988	1956-1988	100	100
10. HOMUS	36.7	34.8	n/a	1955-1988	1955-1988	100	100
11. NABEK	36.7	34.0	n/a	1955-1988	1959-1988	100	100
12. SUEIDA	36.6	32.7	n/a	1958-1988	1958-1988	100	100
13. TELSHEHAB	36.0	32.7	n/a	1958-1988	1958-1988	100	100
TUNISIA							
1. TUNIS	10.2	36.8	3	1951-1988	1951-1988	100	97
2. JENDOUBA	8.8	36.5	143	1951-1988	1964-1974	100	95
3. KAIROUAN	10.1	35.7	60	1951-1988	1964-1974	100	95
4. GAFSA	8.8	34.4	313	1951-1988	1964-1974	100	93
5. SFAX	10.7	34.7	21	1951-1988	-	100	0
6. GABES	10.1	33.9	4	1951-1988	1951-1974	100	95
7. DJERBA	10.6	33.8	0	1951-1988	-	100	0
8. MEDENINE	10.3	33.3	117	1951-1972	-	100	0
9. AIN-DRAHAM	8.7	36.8	739	1951-1988	-	100	0
TURKEY							
1. EDIRNE	26.6	41.7	48	1951-1989	1951-1988	95	98
2. CANAKKALE	26.4	40.1	3	1951-1989	1951-1988	96	98
3. IZMIR	27.3	38.4	25	1951-1989	1951-1988	96	98
4. MUGLA	28.4	37.2	646	1951-1989	1951-1988	94	96
5. ISTANBUL	29.1	41.0	40	1951-1989	1951-1988	97	98

Station	E	N	HT	PRN	TEM	P%	T%
6. BURSA	29.1	40.2	100	1951-1989	1951-1980	95	97
7. AFYON	30.5	38.8	1034	1951-1989	1951-1988	97	98
8. ISPARTA	30.6	37.8	1043	1951-1989	1951-1988	97	98
9. ANTALYA	30.7	36.9	43	1951-1989	1951-1988	96	98
10. KASTAMONU	33.8	41.4	799	1951-1989	1951-1988	97	98
11. ANKARA	32.9	40.0	894	1951-1989	1951-1988	97	98
12. KONYA	32.5	37.9	1022	1951-1989	1951-1988	93	98
13. KAYSERI	35.5	38.7	1070	1951-1982	1951-1988	97	91
14. ADANA	35.3	37.0	66	1951-1985	1951-1986	95	93
15. SAMSUN	36.3	41.3	44	1951-1989	1951-1988	97	98
16. SIVAS	37.0	39.8	1285	1951-1989	1951-1980	97	100
17. MALATYA	38.3	38.4	998	1951-1989	1951-1988	92	98
18. URFA	38.8	37.1	547	1951-1989	1951-1988	94	96
19. RIZE	40.5	41.0	4	1951-1989	1951-1988	90	96
20. ERZINCAN	39.5	39.7	1215	1951-1989	1951-1988	95	96
21. DIYARBAKIR	40.2	37.9	677	1951-1989	1951-1988	95	98
YUGOSLAVIA							
1. PULA	13.9	44.9	30	1951-1980	1951-1980	100	100
2. ZADAR	15.2	44.1	1	1951-1980	1951-1980	100	100
3. HVAR	16.4	43.2	20	1951-1980	1951-1980	100	100
4. VARAZDIN	16.4	46.3	169	1951-1980	1951-1980	100	100
5. DARUVAR	17.2	45.6	161	1951-1980	1951-1980	100	100
6. BANJA-LUKA	17.2	44.8	160	1951-1980	1951-1980	100	100
7. BUGOJNO	17.5	44.1	562	1951-1980	1951-1980	100	100
8. MOSTAR	17.8	43.4	99	1951-1980	1951-1980	100	100
9. TUZLA	18.7	44.6	305	1951-1980	1951-1980	100	100
10. SREMSKA	19.6	45.0	81	1951-1980	1951-1980	100	100
11. ZRENJANIN	20.4	45.4	82	1951-1980	1951-1980	100	100
12. ZLATIBOR	19.7	43.7	1029	1951-1980	1951-1980	100	100
13. ULCINJ	19.2	41.9	30	1951-1980	1951-1980	100	100
14. NIS	21.9	43.3	196	1951-1980	1951-1980	100	100
15. PRILEP	21.6	41.3	661	1951-1980	1951-1980	100	100
16. ZAGREB	16.0	45.8	163	1951-1989	1951-1988	98	99
17. SISAK	16.4	45.5	98	1951-1970	1951-1970	100	100
18. BEOGRAD	20.5	44.8	132	1951-1989	1951-1988	98	97
19. SPLIT	16.4	43.5	129	1951-1989	1951-1988	98	99
20. LIVNO	17.0	43.8	730	1951-1970	1951-1970	100	100
21. SARAJEVO	18.4	43.9	637	1951-1989	1951-1988	97	99
22. TITOGRAD	19.3	42.4	33	1951-1989	1951-1988	97	98
23. SKOPJE	21.5	42.0	240	1951-1989	1951-1988	97	98

E - latitude
N - longitude
HT - height above sea level (m)
PRN - length of precipitation record
TEM - length of temperature record
P% - percentage of precipitation record present
T% - percentage of temperature record present

PUBLICATIONS OF THE MAP TECHNICAL REPORTS SERIES

1. UNEP/IOC/WMO: Baseline studies and monitoring of oil and petroleum hydrocarbons in marine waters (MED POL I). MAP Technical Reports Series No. 1. UNEP, Athens, 1986 (96 pages) (parts in English, French or Spanish only).

2. UNEP/FAO: Baseline studies and monitoring of metals, particularly mercury and cadmium, in marine organisms (MED POL II). MAP Technical Reports Series No. 2. UNEP, Athens, 1986 (220 pages) (parts in English, French or Spanish only).

3. UNEP/FAO: Baseline studies and monitoring of DDT, PCBs and other chlorinated hydrocarbons in marine organisms (MED POL III). MAP Technical Reports Series No. 3. UNEP, Athens, 1986 (128 pages) (parts in English, French or Spanish only).

4. UNEP/FAO: Research on the effects of pollutants on marine organisms and their populations (MED POL IV). MAP Technical Reports Series No. 4. UNEP, Athens, 1986 (118 pages) (parts in English, French or Spanish only).

5. UNEP/FAO: Research on the effects of pollutants on marine communities and ecosystems (MED POL V). MAP Technical Reports Series No. 5. UNEP, Athens, 1986 (146 pages) (parts in English or French only).

6. UNEP/IOC: Problems of coastal transport of pollutants (MED POL VI). MAP Technical Reports Series No. 6. UNEP, Athens, 1986 (100 pages) (English only).

7. UNEP/WHO: Coastal water quality control (MED POL VII). MAP Technical Reports Series No. 7. UNEP, Athens, 1986 (426 pages) (parts in English or French only).

8. UNEP/IAEA/IOC: Biogeochemical studies of selected pollutants in the open waters of the Mediterranean (MED POL VIII). MAP Technical Reports Series No. 8. UNEP, Athens, 1986 (42 pages) (parts in English or French only).

8. Add. UNEP: Biogeochemical studies of selected pollutants in the open waters of the Mediterranean MED POL VIII) Addendum, Greek Oceanographic Cruise 1980. MAP Technical Reports Series No. 8, Addendum. UNEP, Athens, 1986 (66 pages) (English only).

9. UNEP: Co-ordinated Mediterranean pollution monitoring and research programme (MED POL - PHASE I). Final report, 1975-1980. MAP Technical Reports Series No. 9. UNEP, Athens, 1986 (276 pages) (English only).

10. UNEP: Research on the toxicity, persistence, bioaccumulation, carcinogenicity and mutagenicity of selected substances (Activity G). Final reports on projects dealing with toxicity (1983-85). MAP Technical Reports Series No. 10. UNEP, Athens, 1987 (118 pages) (English only).

11. UNEP: Rehabilitation and reconstruction of Mediterranean historic settlements. Documents produced in the first stage of the Priority Action (1984-1985). MAP Technical Reports Series No. 11. UNEP, Priority Actions Programme, Regional Activity Centre, Split, 1986 (158 pages) (parts in English or French only).

12. UNEP: Water resources development of small Mediterranean islands and isolated coastal areas. Documents produced in the first stage of the Priority Action (1984-1985). MAP Technical Reports Series No 12. UNEP, Priority Actions Programme, Regional Activity Centre, Split, 1987 (162 pages) (parts in English or French only).

13. UNEP: Specific topics related to water resources development of large Mediterranean islands. Documents produced in the second phase of the Priority Action (1985-1986). MAP Technical Reports Series No. 13. UNEP, Priority Actions Programme, Regional Activity Centre, Split, 1987 (162 pages) (parts in English or French only).

14. UNEP: Experience of Mediterranean historic towns in the integrated process of rehabilitation of urban and architectural heritage. Documents produced in the second phase of the Priority Action (1986). MAP Technical Reports Series No. 14. UNEP, Priority Actions Programme, Regional Activity Centre, Split, 1987 (500 pages) (parts in English or French only).

15. UNEP: Environmental aspects of aquaculture development in the Mediterranean region. Documents produced in the period 1985-1987. MAP Technical Reports Series No. 15. UNEP, Priority Actions Programme, Regional Activity Centre, Split, 1987 (101 pages) (English only).

16. UNEP: Promotion of soil protection as an essential component of environmental protection in Mediterranean coastal zones. Selected documents (1985-1987). MAP Technical Reports Series No. 16. UNEP, Priority Actions Programme, Regional Activity Centre, Split, 1987 (424 pages) (parts in English or French only).

17. UNEP: Seismic risk reduction in the Mediterranean region. Selected studies and documents (1985-1987). MAP Technical Reports Series No. 17. UNEP, Priority Actions Programme, Regional Activity Centre, Split, 1987 (247 pages) (parts in English or French only).

18. UNEP/FAO/WHO: Assessment of the state of pollution of the Mediterranean Sea by mercury and mercury compounds. MAP Technical Reports Series No. 18. UNEP, Athens, 1987 (354 pages) (English and French).

19. UNEP/IOC: Assessment of the state of pollution of the Mediterranean Sea by petroleum hydrocarbons. MAP Technical Reports Series No. 19. UNEP, Athens, 1988 (130 pages) (English and French).

20. UNEP/WHO: Epidemiological studies related to environmental quality criteria for bathing waters, shellfish-growing waters and edible marine organisms (Activity D). Final report on project on relationship between microbial quality of coastal seawater and health effects (1983-86). MAP Technical Reports Series No. 20. UNEP, Athens, 1988 (156 pages) (English only).

21. UNEP/UNESCO/FAO: Eutrophication in the Mediterranean Sea: Receiving capacity and monitoring of long-term effects. MAP Technical Reports Series No. 21. UNEP, Athens, 1988 (200 pages) (parts in English or French only).

22. UNEP/FAO: Study of ecosystem modifications in areas influenced by pollutants (Activity I). MAP Technical Reports Series No. 22. UNEP, Athens, 1988 (146 pages) (parts in English or French only).

23. UNEP: National monitoring programme of Yugoslavia, Report for 1983-1986. MAP Technical Reports Series No. 23. UNEP, Athens, 1988 (223 pages) (English only).

24. UNEP/FAO: Toxicity, persistence and bioaccumulation of selected substances to marine organisms (Activity G). MAP Technical Reports Series No. 24. UNEP, Athens, 1988 (122 pages) (parts in English or French only).

25. UNEP: The Mediterranean Action Plan in a functional perspective: A quest for law and policy. MAP Technical Reports Series No. 25. UNEP, Athens, 1988 (105 pages) (English only).

26. UNEP/IUCN: Directory of marine and coastal protected areas in the Mediterranean Region. Part I - Sites of biological and ecological value. MAP Technical Reports Series No. 26. UNEP, Athens, 1989 (196 pages) (English only).

27. UNEP: Implications of expected climate changes in the Mediterranean Region: An overview. MAP Technical Reports Series No. 27. UNEP, Athens, 1989 (52 pages) (English only).

28. UNEP: State of the Mediterranean marine environment. MAP Technical Reports Series No. 28. UNEP, Athens, 1989 (225 pages) (English only).

29. UNEP: Bibliography on effects of climatic change and related topics. MAP Technical Reports Series No. 29. UNEP, Athens, 1989 (143 pages) (English only).

30. UNEP: Meteorological and climatological data from surface and upper measurements for the assessment of atmospheric transport and deposition of pollutants in the Mediterranean Basin: A review. MAP Technical Reports Series No. 30. UNEP, Athens, 1989 (137 pages) (English only).

31. UNEP/WMO: Airborne pollution of the Mediterranean Sea. Report and proceedings of a WMO/UNEP Workshop. MAP Technical Reports Series No. 31. UNEP, Athens, 1989 (247 pages) (parts in English or French only).

32. UNEP/FAO: Biogeochemical cycles of specific pollutants (Activity K). MAP Technical Reports Series No. 32. UNEP, Athens, 1989 (139 pages) (parts in English or French only).

33. UNEP/FAO/WHO/IAEA: Assessment of organotin compounds as marine pollutants in the Mediterranean. MAP Technical Reports Series No. 33. UNEP, Athens, 1989 (185 pages) (English and French).

34. UNEP/FAO/WHO: Assessment of the state of pollution of the Mediterranean Sea by cadmium and cadmium compounds. MAP Technical Reports Series No. 34. UNEP, Athens, 1989 (175 pages) (English and French).

35. UNEP. Bibliography on marine pollution by organotin compounds. MAP Technical Reports Series No. 35. UNEP, Athens, 1989 (92 pages) (English only).

36. UNEP/IUCN: Directory of marine and coastal protected areas in the Mediterranean region. Part I - Sites of biological and ecological value. MAP Technical Reports Series No. 36. UNEP, Athens, 1990 (198 pages) (French only).

37. UNEP/FAO: Final reports on research projects dealing with eutrophication and plankton blooms (Activity H). MAP Technical Reports Series No. 37. UNEP, Athens, 1990 (74 pages) (parts in English or French only).

38. UNEP: Common measures adopted by the Contracting Parties to the Convention for the Protection of the Mediterranean Sea against pollution. MAP Technical Reports Series No. 38. UNEP, Athens, 1990 (100 pages) (English, French, Spanish and Arabic).

39. UNEP/FAO/WHO/IAEA: Assessment of the state of pollution of the Mediterranean Sea by organohalogen compounds. MAP Technical Reports Series No. 39. UNEP, Athens, 1990 (224 pages) (English and French).

40. UNEP/FAO: Final reports on research projects (Activities H,I and J). MAP Technical Reports Series No. 40. UNEP, Athens, 1990 (125 pages) (English and French).

41. UNEP: Wastewater reuse for irrigation in the Mediterranean region. MAP Technical Reports Series No. 41. UNEP, Priority Actions Programme, Regional Activity Centre, Split, 1990 (330 pages) (English and French).

42. UNEP/IUCN: Report on the status of Mediterranean marine turtles. MAP Technical Reports Series No. 42 UNEP, Athens, 1990 (204 pages) (English and French).

43. UNEP/IUCN/GIS Posidonia: Red Book "Gérard Vuignier", marine plants, populations and landscapes threatened in the Mediterranean. MAP Technical Reports Series No. 43. UNEP, Athens, 1990 (250 pages) (French only).

44. UNEP: Bibliography on aquatic pollution by organophosphorus compounds. MAP Technical Reports Series No. 44. UNEP, Athens, 1990 (98 pages) (English only).

45. UNEP/IAEA: Transport of pollutants by sedimentation: Collected papers from the first Mediterranean Workshop (Villefranche-sur-Mer, France, 10-12 December 1987). MAP Technical Reports Series No. 45. UNEP, Athens, 1990 (302 pages) (English only).

46. UNEP/WHO: Epidemiological studies related to environmental quality criteria for bathing waters, shellfish-growing waters and edible marine organisms (Activity D). Final report on project on relationship between microbial quality of coastal seawater and rotarus-induced gastroenterities among bathers (1986-88). MAP Technical Reports Series No.46, UNEP, Athens, 1991 (64 pages) (English only).

47. UNEP: Jellyfish blooms in the Mediterranean. Proceedings of the II workshop on jellyfish in the Mediterranean Sea. MAP Technical Reports Series No.47. UNEP, Athens, 1991 (320 pages) (parts in English or French only).

48. UNEP/FAO: Final reports on research projects (Activity G). MAP Technical Reports Series No. 48. UNEP, Athens, 1991 (126 pages) (parts in English or French only).

49. UNEP/WHO: Biogeochemical cycles of specific pollutants. Survival of pathogens. Final reports on research projects (Activity K). MAP Technical Reports Series No. 49. UNEP, Athens, 1991 (71 pages) (parts in English or French only).

50. UNEP: Bibliography on marine litter. MAP Technical Reports Series No. 50. UNEP, Athens, 1991 (62 pages) (English only).

51. UNEP/FAO: Final reports on research projects dealing with mercury, toxicity and analytical techniques. MAP Technical Reports Series No. 51. UNEP, Athens, 1991 (166 pages) (parts in English or French only).

52. UNEP/FAO: Final reports on research projects dealing with bioaccumulation and toxicity of chemical pollutants. MAP Technical Reports Series No. 52. UNEP, Athens, 1991 (86 pages) (parts in English or French only).

53. UNEP/WHO: Epidemiological studies related to environmental quality criteria for bathing waters, shellfish-growing waters and edible marine organisms (Activity D). Final report on epidemiological study on bathers from selected beaches in Malaga, Spain (1988-1989). MAP Technical Reports Series No. 53. UNEP, Athens, 1991 (127 pages) (English only).

54. UNEP/WHO: Development and testing of sampling and analytical techniques for monitoring of marine pollutants (Activity A): Final reports on selected microbiological projects. MAP Technical Reports Series No. 54. UNEP, Athens, 1991 (83 pages) (English only).

55. UNEP/WHO: Biogeochemical cycles of specific pollutants (Activity K): Final report on project on survival of pathogenic organisms in seawater. MAP Technical Reports Series No. 55. UNEP, Athens, 1991 (95 pages) (English only).

56. UNEP/IOC/FAO: Assessment of the state of pollution of the Mediterranean Sea by persistent synthetic materials which may float, sink or remain in suspension. MAP Technical Reports Series No. 56. UNEP, Athens, 1991 (113 pages) (English and French).

57. UNEP/WHO: Research on the toxicity, persistence, bioaccumulation, carcinogenicity and mutagenicity of selected substances (Activity G): Final reports on projects dealing with carcinogenicity and mutagenicity. MAP Technical Reports Series No. 57. UNEP, Athens, 1991 (59 pages) (English only).

58. UNEP/FAO/WHO/IAEA: Assessment of the state of pollution of the Mediterranean Sea by organophosphorus compounds. MAP Technical Reports Series No. 58. UNEP, Athens, 1991 (122 pages) (English and French).

59. UNEP/FAO/IAEA: Proceedings of the FAO/UNEP/IAEA Consultation Meeting on the Accumulation and Transformation of Chemical contaminants by Biotic and Abiotic Processes in the Marine Environment (La Spezia, Italy, 24-28 September 1990), edited by G.P. Gabrielides. MAP Technical Reports Series No. 59. UNEP, Athens, 1991 (392 pages) (English only).

60. UNEP/WHO: Development and testing of sampling and analytical techniques for monitoring of marine pollutants (Activity A): Final reports on selected microbiological projects (1987-1990). MAP Technical Reports Series No. 60. UNEP, Athens, 1991 (76 pages) (parts in English or French only).

61. UNEP: Integrated Planning and Management of the Mediterranean Coastal Zones. Documents produced in the first and second stage of the Priority Action (1985-1986). MAP Technical Reports Series No. 61. UNEP, Priority Actions Programme, Regional Activity Centre, Split, 1991 (437 pages) (parts in English or French only).

62. UNEP/IAEA: Assessment of the State of Pollution of the Mediterranean Sea by Radioactive Substances. MAP Technical Reports Series No. 62, UNEP, Athens, 1992 (133 pages) (English and French).

63. UNEP/WHO: Biogeochimical cycles of specific pollutants (Activity K) - Survival of Pathogens - Final reports on Research Projects (1989-1991). MAP Technical Reports Series No. 63, UNEP, Athens, 1992 (86 pages) (French only).

64. UNEP/WMO: Airborne Pollution of the Mediterranean Sea. Report and Proceedings of the Second WMO/UNEP Workshop. MAP Technical Reports Series No. 64, UNEP, Athens, 1992 (246 pages) (English only).

65. UNEP: Directory of Mediterranean Marine Environmental Centres. MAP Technical Reports Series No. 65, UNEP, Athens, 1992 (351 pages) (English and French).

PUBLICATIONS "MAP TECHNICAL REPORTS SERIES"

1. PNUE/COI/OMM: Etudes de base et surveillance continue du pétrole et des hydrocarbures contenus dans les eaux de la mer (MED POL I). MAP Technical Reports Series No. 1. UNEP, Athens, 1986 (96 pages) (parties en anglais, français ou espagnol seulement).

2. PNUE/FAO: Etudes de base et surveillance continue des métaux, notamment du mercure et du cadmium, dans les organismes marins (MED POL II). MAP Technical Reports Series No. 2. UNEP, Athens, 1986 (220 pages) (parties en anglais, français ou espagnol seulement).

3. PNUE/FAO: Etudes de base et surveillance continue du DDT, des PCB et des autres hydrocarbures chlorés contenus dans les organismes marins (MED POL III). MAP Technical Reports Series No. 3. UNEP, Athens, 1986 (128 pages) (parties en anglais, français ou espagnol seulement).

4. PNUE/FAO: Recherche sur les effets des polluants sur les organismes marins et leurs peuplements (MED POL IV). MAP Technical Reports Series No. 4. UNEP, Athens, 1986 (118 pages) (parties en anglais, français ou espagnol seulement).

5. PNUE/FAO: Recherche sur les effets des polluants sur les communautés et écosystèmes marins (MED POL V). MAP Technical Reports Series No. 5. UNEP, Athens, 1986 (146 pages) (parties en anglais ou français seulement).

6. PNUE/COI: Problèmes du transfert des polluants le long des côtes (MED POL VI). MAP Technical Reports Series No. 6. UNEP, Athens, 1986 (100 pages) (anglais seulement).

7. PNUE/OMS: Contrôle de la qualité des eaux côtières (MED POL VII). MAP Technical Reports Series No. 7. UNEP, Athens, 1986 (426 pages) (parties en anglais ou français seulement).

8. PNUE/AIEA/COI: Etudes biogéochimiques de certains polluants au large de la Méditerranée (MED POL VIII). MAP Technical Reports Series No. 8. UNEP, Athens, 1986 (42 pages) (parties en anglais ou français seulement).

8. Add. PNUE: Etudes biogéochimiques de certains polluants au large de la Méditerranée (MED POL VIII). Addendum, Croisière Océanographique de la Grèce 1980. MAP Technical Reports Series No. 8, Addendum. UNEP, Athens, 1986 (66 pages) (anglais seulement).

9. PNUE: Programme coordonné de surveillance continue et de recherche en matière de pollution dans la Méditerranée (MED POL -PHASE I). Rapport final, 1975-1980. MAP Technical Reports Series No. 9. UNEP, Athens, 1986 (276 pages) (anglais seulement).

10. PNUE: Recherches sur la toxicité, la persistance, la bioaccumulation, la cancérogénicité et la mutagénicité de certaines substances (Activité G). Rapports finaux sur les projets ayant trait à la toxicité (1983-85). MAP Technical Reports Series No. 10. UNEP, Athens, 1987 (118 pages) (anglais seulement).

11. PNUE: Réhabilitation et reconstruction des établissements historiques méditerranéens. Textes rédigés au cours de la première phase de l'action prioritaire (1984-1985). MAP Technical Reports Series No. 11. UNEP, Priority Actions Programme, Regional Activity Centre, Split, 1986 (158 pages) (parties en anglais ou français seulement).

12. PNUE: Développement des ressources en eau des petites îles et des zones côtières isolées méditerranéennes. Textes rédigés au cours de la première phase de l'action prioritaire (1984-1985). MAP Technical Reports Series No. 12. UNEP, Priority Actions Programme, Regional Activity Centre, Split, 1987 (162 pages) (parties en anglais ou français seulement).

13. PNUE: Thèmes spécifiques concernant le développement des ressources en eau des grandes îles méditerranéennes. Textes rédigés au cours de la deuxième phase de l'action prioritaire (1985-1986). MAP Technical Reports Series No. 13. UNEP, Priority Actions Programme, Regional Activity Centre, Split, 1987 (162 pages) (parties en anglais ou français seulement).

14. PNUE: L'expérience des villes historiques de la Méditerranée dans le processus intégré de réhabilitation du patrimoine urbain et architectural. Documents établis lors de la seconde phase de l'Action prioritaire (1986). MAP Technical Reports Series No. 14. UNEP, Priority Actions Programme, Regional Activity Centre, Split, 1987 (500 pages) (parties en anglais ou français seulement).

15. PNUE: Aspects environnementaux du développement de l'aquaculture dans la région méditerranéenne. Documents établis pendant la période 1985-1987. MAP Technical Reports Series No. 15. UNEP, Priority Actions Programme, Regional Activity Centre, Split, 1987 (101 pages) (anglais seulement).

16. PNUE: Promotion de la protection des sols comme élément essentiel de la protection de l'environnement dans les zones côtières méditerranéennes. Documents sélectionnés (1985-1987). MAP Technical Reports Series No. 16. UNEP, Priority Actions Programme, Regional Activity Centre, Split, 1987 (424 pages) (parties en anglais ou français seulement).

17. PNUE: Réduction des risques sismiques dans la région méditerranéenne. Documents et études sélectionnés (1985-1987). MAP Technical Reports Series No. 17. UNEP, Priority Actions Programme, Regional Activity Centre, Split, 1987 (247 pages) (parties en anglais ou français seulement).

18. PNUE/FAO/OMS: Evaluation de l'état de la pollution de la mer Méditerranée par le mercure et les composés mercuriels. MAP Technical Reports Series No. 18. UNEP, Athens, 1987 (354 pages) (anglais et français).

19. PNUE/COI: Evaluation de l'état de la pollution de la mer Méditerranée par les hydrocarbures de pétrole MAP Technical Reports Series No. 19. UNEP, Athens, 1988 (130 pages) (anglais et français).

20. PNUE/OMS: Etudes épidémiologiques relatives aux critères de la qualité de l'environnement pour les eaux servant à la baignade, à la culture de coquillages et à l'élevage d'autres organismes marins comestibles (Activité D). Rapport final sur le projet sur la relation entre la qualité microbienne des eaux marines côtières et les effets sur la santé (1983-86). MAP Technical Reports Series No. 20. UNEP, Athens, 1988 (156 pages) (anglais seulement).

21. PNUE/UNESCO/FAO: Eutrophisation dans la mer Méditerranée: capacité réceptrice et surveillance continue des effets à long terme. MAP Technical Reports Series No. 21. UNEP, Athens, 1988 (200 pages) (parties en anglais ou français seulement).

22. PNUE/FAO: Etude des modifications de l'écosystème dans les zones soumises à l'influence des polluants (Activité I). MAP Technical Reports Series No. 22. UNEP, Athens, 1988 (146 pages) (parties en anglais ou français seulement).

23. PNUE: Programme national de surveillance continue pour la Yougoslavie, Rapport pour 1983-1986. MAP Technical Reports Series No. 23. UNEP, Athens, 1988 (223 pages) (anglais seulement).

24. PNUE/FAO. Toxicité, persistance et bioaccumulation de certaines substances vis-à-vis des organismes marins (Activité G). MAP Technical Reports Series No. 24. UNEP, Athens, 1988 (122 pages) (parties en anglais ou français seulement).

25. PNUE: Le Plan d'action pour la Méditerranée, perspective fonctionnelle; une recherche juridique et politique. MAP Technical Reports Series No. 25. UNEP, Athens, 1988 (105 pages) (anglais seulement).

26. PNUE/UICN: Répertoire des aires marines et côtières protégées de la Méditerranée. Première partie - Sites d'importance biologique et écologique. MAP Technical Reports Series No. 26. UNEP, Athens, 1989 (196 pages) (anglais seulement).

27. PNUE: Implications des modifications climatiques prévues dans la région méditerranéenne: une vue d'ensemble. MAP Technical Reports Series No. 27. UNEP, Athens, 1989 (52 pages) (anglais seulement).

28. PNUE: Etat du milieu marin en Méditerranée. MAP Technical Reports Series No. 28. UNEP, Athens, 1989 (225 pages) (anglais seulement).

29. PNUE: Bibliographie sur les effets des modifications climatiques et sujets connexes. MAP Technical Reports Series No. 29. UNEP, Athens, 1989 (143 pages) (anglais seulement).

30. PNUE: Données météorologiques et climatologiques provenant de mesures effectuées dans l'air en surface et en altitude en vue de l'évaluation du transfert et du dépôt atmosphériques des polluants dans le bassin méditerranéen: un compte rendu. MAP Technical Reports Series No. 30. UNEP, Athens, 1989 (137 pages) (anglais seulement).

31. PNUE/OMM: Pollution par voie atmosphérique de la mer Méditerranée. Rapport et actes des Journées d'étude OMM/PNUE. MAP Technical Reports Series No. 31. UNEP, Athens, 1989 (247 pages) (parties en anglais ou français seulement).

32. PNUE/FAO: Cycles biogéochimiques de polluants spécifiques (Activité K). MAP Technical Reports Series No. 32. UNEP, Athens, 1989 (139 pages) (parties en anglais ou français seulement).

33. PNUE/FAO/OMS/AIEA: Evaluation des composés organostanniques en tant que polluants du milieu marin en Méditerranée. MAP Technical Reports Series No. 33. UNEP, Athens, 1989 (185 pages) (anglais et français).

34. PNUE/FAO/OMS: Evaluation de l'état de la pollution de la mer Méditerranée par le cadmium et les composés de cadmium. MAP Technical Reports Seri es No. 34. UNEP, Athens, 1989 (175 pages) (anglais et français).

35. PNUE: Bibliographie sur la pollution marine par les composés organostanniques. MAP Technical Reports Series No. 35. UNEP, Athens, 1989 (92 pages) (anglais seulement).

36. PNUE/UICN: Répertoire des aires marines et côtières protégées de la Méditerranée. Première partie - Sites d'importance biologique et écologique. MAP Technical Reports Series No. 36. UNEP, Athens, 1990 (198 pages) (français seulement).

37. PNUE/FAO: Rapports finaux sur les projets de recherche consacrés à l'eutrophisation et aux efflorescences de plancton (Activité H). MAP Technical Reports Series No. 37. UNEP, Athens, 1990 (74 pages) (parties en anglais ou français seulement).

38. PNUE: Mesures communes adoptées par les Parties Contractantes à la Convention pour la protection de la mer Méditerranée contre la pollution. MAP Technical Reports Series No. 38. UNEP, Athens, 1990 (100 pages) (anglains, français, espagnol et arabe).

39. PNUE/FAO/OMS/AIEA: Evaluation de l'état de la pollution par les composés organohalogénés MAP Technical Reports Series No. 39 UNEP, Athens, 1990 (224 pages) (anglais et français).

40. PNUE/FAO: Rapports finaux sur les projets de recherche (Activités H, I et J). MAP Technical Reports Series No. 40. UNEP, Athens, 1990 (125 pages) (anglais et français).

41. PNUE: Réutilisation agricole des eaux usées dans la région méditerranéenne. MAP Technical Reports Series No. 41. UNEP, Priority Actions Programme, Regional Activity Centre, Split, 1990 (330 pages) (anglais et français).

42. PNUE/UICN: Rapport sur le statut des tortues marines de Méditerranée. MAP Technical Reports Series No. 42. UNEP, Athens, 1990 (204 pages) (anglais et français).

43. PNUE/UICN/GIS Posidonie: Livre rouge "Gérard Vuignier" des végétaux, peuplements et paysages marins menacés de Méditerranée. MAP Technical Reports Series No. 43. UNEP, Athens, 1990 (250 pages) (français seulement).

44. PNUE: Bibliographie sur la pollution aquatique par les composés organophosphorés. MAP Technical Reports Series No. 44. UNEP, Athens, 1990 (98 pages) (anglais seulement).

45. PNUE/AIEA: Transfert des polluants par sédimentation: Recueil des communications présentées aux premières journées d'études méditerranéennes (Villefranche-sur- Mer, France, 10-12 décembre 1987) MAP Technical Reports Series No. 45. UNEP, Athens, 1990 (302 pages) (anglais seulement).

46. PNUE/OMS: Etudes épidémiologiques relatives aux critères de la qualité de l'environnement pour les eaux servant à la baignade, à la culture de coquillages et à l'élevage d'autres organismes marins comestibles (Activité D). Rapport final sur le projet sur la relation entre la qualité microbienne des eaux marines côtières et la gastroentérite provoquée par le rotavirus entre les baigneurs (1986-88). MAP Technical Reports Series No.46. UNEP, Athens, 1991 (64 pages) (anglais seulement).

47. PNUE: Les proliférations de méduses en Méditerannée. Actes des IIèmes journées d'étude sur les méduses en mer Méditerranée. MAP Technical Reports Series No.47. UNEP, Athens, 1991 (320 pages) (parties en anglais ou français seulement).

48. PNUE/FAO: Rapports finaux sur les projets de recherche (Activité G). MAP Technical Reports Series No. 48. UNEP, Athens, 1991 (126 pages) (parties en anglais ou français seulement).

49. PNUE/OMS: Cycles biogéochimiques de polluants spécifiques. Survie des Pathogènes. Rapports finaux sur les projets de recherche (activité K). MAP Technical Reports Series No. 49. UNEP, Athens, 1991 (71 pages) (parties en anglais ou français seulement).

50. PNUE: Bibliographie sur les déchets marins. MAP Technical Reports Series No. 50. UNEP, Athens, 1991 (62 pages) (anglais seulement).

51. PNUE/FAO: Rapports finaux sur les projets de recherche traitant du mercure, de la toxicité et des techniques analytiques. MAP Technical Reports Series No. 51. UNEP, Athens, 1991 (166 pages) (parties en anglais ou français seulement).

52. PNUE/FAO: Rapports finaux sur les projets de recherche traitant de la bioaccumulation et de la toxicité des polluants chimiques. MAP Technical Reports Series No. 52. UNEP, Athens, 1991 (86 pages) (parties en anglais ou français seulement).

53. PNUE/OMS: Etudes épidémiologiques relatives aux critères de la qualité de l'environnement pour les eaux servant à la baignade, à la culture de coquillages et à l'élevage d'autres organismes marins comestibles (Activité D). Rapport final sur l'étude épidémiologique menée parmi les baigneurs de certaines plages à Malaga, Espagne (1988-1989). MAP Technical Reports Series No. 53. UNEP, Athens, 1991 (127 pages) (anglais seulement).

54. PNUE/OMS: Mise au point et essai des techniques d'échantillonnage et d'analyse pour la surveillance continue des polluants marins (Activité A): Rapports finaux sur certains projets de nature microbiologique. MAP Technical Reports Series No. 54. UNEP, Athens, 1991 (83 pages) (anglais seulement).

55. PNUE/OMS: Cycles biogéochimiques de polluants spécifiques (Activité K): Rapport final sur le projet sur la survie des microorganismes pathogènes dans l'eau de mer. MAP Technical Reports Series No. 55. UNEP, Athens, 1991 (95 pages) (anglais seulement).

56. PNUE/COI/FAO: Evaluation de l'état de la pollution de la mer Méditerranée par les matières synthétiques persistantes qui peuvent flotter, couler ou rester en suspension. MAP Technical Reports Series No. 56. UNEP, Athens, 1991 (113 pages) (anglais et français).

57. PNUE/OMS: Recherches sur la toxicité, la persistance, la bioaccumulation, la cancérogénicité et la mutagénicité de certaines substances (Activité G). Rapports finaux sur les projets ayant trait à la cancérogénicité et la mutagénicité. MAP Technical Reports Series No. 57. UNEP, Athens, 1991 (59 pages) (anglais seulement).

58. PNUE/FAO/OMS/AIEA: Evaluation de l'état de la pollution de la mer Méditerranée par les composés organophosphorés. MAP Technical Reports Series No. 58. UNEP, Athens, 1991 (122 pages) (anglais et français).

59. PNUE/FAO/AIEA: Actes de la réunion consultative FAO/PNUE/AIEA sur l'accumulation et la transformation des contaminants chimiques par les processus biotiques et abiotiques dans le milieu marin (La Spezia, Italie, 24-28 septembre 1990), publié sous la direction de G.P. Gabrielides. MAP Technical Reports Series No. 59. UNEP, Athens, 1991 (392 pages) (anglais seulement).

60. PNUE/OMS: Mise au point et essai des techniques d'échantillonnage et d'analyse pour la surveillance continue des polluants marins (Activité A): Rapports finaux sur certains projets de nature microbiologique (1987-1990). MAP Technical Reports Series No. 60. UNEP, Athens, 1991 (76 pages) (parties en anglais ou français seulement).

61. PNUE: Planification intégrée et gestion des zones côtières méditerranéennes. Textes rédigés au cours de la première et de la deuxième phase de l'action prioritaire (1985-1986). MAP Technical Reports Series No. 61. UNEP, Priority Actions Programme, Regional Activity Centre, Split, 1991 (437 pages) (parties en anglais ou français seulement).

62. PNUE/AIEA: Evaluation de l'état de la pollution de la mer Méditerranée par les substances radioactives. MAP Technical Reports Series No. 62, UNEP, Athens, 1992 (133 pages) (anglais et français).

63. PNUE/OMS: Cycles biogéochimiques de polluants spécifiques (Activité K) - Survie des pathogènes - Rapports finaux sur les projets de recherche (1989-1991). MAP Technical Reports Series No. 63, UNEP, Athens, 1992 (86 pages) (français seulement).

64. PNUE/OMM: Pollution par voie atmosphérique de la mer Méditerranée. Rapport et actes des deuxièmes journées d'études OMM/PNUE. MAP Technical Reports Series No. 64, UNEP, Athens, 1992 (246 pages) (anglais seulement).

65. PNUE: Répertoire des centres relatifs au milieu marin en Méditerranée. MAP Technical Reports Series No. 65, UNEP, Athens, 1992 (351 pages) (anglais et français).

Issued and printed by:

Mediterranean Action Plan
United Nations Environment Programme

Additional copies of this and other publications issued by
the Mediterranean Action Plan of UNEP can be obtained from:

Co-ordinating Unit for the Mediterranean Action Plan
United Nations Environment Programme
Leoforos Vassileos Konstantinou, 48
116 35 Athens
GREECE

Publié et imprimé par:

Plan d'action pour la Méditerranée
Programme des Nations Unies pour l'Environnement

Des exemplaires de ce document ainsi que d'autres
publications du Plan d'action pour la Méditerranée
du PNUE peuvent être obtenus de:

Unité de coordination du Plan d'action pour la Méditerranée
Programme des Nations Unies pour l'Environnement
Leoforos Vassileos Konstantinou, 48
116 35 Athènes
GRECE